Amyloid Protein Binding Partners in Alzheimer's Disease and Other Neurodegenerative Disorders

Helen Felicity Stanyon

A thesis submitted to

QUEEN MARY, UNIVERSITY OF LONDON

for the degree of

DOCTOR OF PHILOSOPHY

School of Biological and Chemical Sciences

Queen Mary, University of London

February 2015

I, Helen Felicity Stanyon, confirm that the research included within this thesis is my own work or that where it has been carried out in collaboration with, or supported by others, that this is duly acknowledged below and my contribution indicated. Previously published material is also acknowledged below.

I attest that I have exercised reasonable care to ensure that the work is original, and does not to the best of my knowledge break any UK law, infringe any third party's copyright or other Intellectual Property Right, or contain any confidential material.

I accept that the College has the right to use plagiarism detection software to check the electronic version of the thesis.

I confirm that this thesis has not been previously submitted for the award of a degree by this or any other university.

The copyright of this thesis rests with the author and no quotation from it or information derived from it may be published without the prior written consent of the author.

Signature:

Date:

Details of Collaboration and Publications:

Publications:

Stanyon, H. F., Cong, X., Chen, Y., Shahidullah, N., Rossetti, G., Dreyer, J., Papamokos, G., Carloni, P. and Viles, J. H. (2014). "Developing Predictive Rules for Coordination Geometry from Visible Circular Dichroism of Copper(II) and Nickel(II) Ions in Histidine and Amide Main-Chain Complexes." *Febs Journal* **281**(17): 3945-3954.

Stanyon, H. F., Patel, K., Begum, N. and Viles, J. H. (2014). "Copper(II) Sequentially Loads onto the N-Terminal Amino Group of the Cellular Prion Protein before the Individual Octarepeats." *Biochemistry* **53**(24): 3934-3939.

Stanyon, H. F. and Viles, J. H. (2012). "Human Serum Albumin Can Regulate Amyloid-B Peptide Fiber Growth in the Brain Interstitium: Implications for Alzheimer Disease." *Journal of Biological Chemistry* **287**(33): 28163-28168.

Collaborations:

The experimental Visible Circular Dichroism data presented in Chapter 6A was complemented by the computer simulations of spectra carried out by Dr Xiaojing Cong, Dr Giulia Rossetti, Dr Jens Dreyer, Dr George Papamokos and Prof Paolo Carloni from the German Research School for Simulation Sciences.

All mass spectrometry acquisition was in collaboration with Dr Susan E. Slade and Prof Jim Scrivens from the University of Warwick.

All Electron Paramagnetic Resonance studies were carried out in collaboration with Dr Maxie Roessler from Queen Mary, University of London.

ABSTRACT

Many neurodegenerative disorders are characterised by protein misfolding and subsequent amyloid fibrillisation and deposition. Amyloid-beta peptide (Aβ) was found to be the main constituent of the extracellular amyloid plaques of Alzheimer's disease (AD) in the 1980s. What triggers amyloid formation or inhibits it are of particular interest. This thesis focuses on the effect of endogenous proteins and molecules on amyloid fibrillisation.

In Chapter 3, I show that at physiological micromolar levels found in the cerebrospinal fluid, human serum albumin inhibits the rate of Aβ fibrillisation. Indeed *in vitro* the amount of amyloid fibres generated directly correlates to the proportion of Aβ not competitively bound to albumin. Albumin binds cholesterol and fatty acids *in vivo*, both of which have been linked with an increased risk of developing AD. In Chapter 4, I show Aβ competes with these molecules for albumin binding, so disrupting albumin's ability to inhibit Aβ fibrillisation. My observations suggest a significant role for albumin regulating Aβ fibril growth.

Albumin also binds Cu^{2+} *in vivo* with a tight picomolar affinity. Animal models suggest disrupted Cu^{2+} homeostasis potentiate AD phenotype. In Chapter 5, I show that regardless of Aβ alloform or fibrillisation stage, the affinity for Cu^{2+} is in the ~20 picomolar range but weaker than albumin.

Circular Dichroism spectroscopy in the visible region (Vis-CD) is a powerful technique to study metal-protein interactions. In Chapter 6, I develop a set of empirical rules that relates the appearance of particular Vis-CD spectral features to the conformation of the

complex. These rules are used to gain insight into Cu^{2+}-protein complexes in Prion disease and Parkinson's disease. I show the N-terminal amino group of cellular prion protein (PrP^C) has a tighter affinity for Cu^{2+} than the individual octa-repeat binding sites present within PrP^C and show for the first time that Cu^{2+} loads on to the N-terminal amino group before the single octa-repeat binding sites. I determine the affinity of Cu^{2+} for model N-terminal peptides of alpha-synuclein of Parkinson's disease and show that side-chain coordination stabilises the complex and increases the affinity for copper compared to main-chain coordination only.

This thesis highlights the importance of overlapping interactions with endogenous proteins and molecules in the development of neurodegenerative disease. Indeed, the amyloid protein binding partners studied here are all co-localised at the synapse thus future *in vitro* studies of neurodegenerative disease should consider the complex nature of interactions possible *in situ*.

ACKNOWLEDGEMENTS

My sincere appreciation is extended to the Biotechnology and Biological Sciences Research Council for funding this project and Queen Mary University of London for hosting my PhD.

I would like to express my deepest gratitude to my supervisor, Dr John H. Viles, for giving me this wonderful opportunity and also for all his support and guidance throughout my research project.

I would also like to extend my appreciation to my research panel members, Dr Caroline Brennan and Dr Ewan Main.

There are many individuals who have my special thanks for help with the acquisition of data presented in this thesis. All mass spectrometry data presented in this thesis (Chapter 4) was acquired in collaboration with Prof Jim Scrivens at the University of Warwick and the technical assistance of Dr Susan E. Slade at the Mass Spectrometry Facility. Thanks must also go to my collaborators from the German Research School for Simulation Sciences; Dr Xiaojing Cong, Dr Giulia Rossetti, Dr Jens Dreyer, Dr George Papamokos and Prof Paolo Carloni, for their work on simulating visible circular dichroism spectra, presented in Chapter 6 Part A, which complements my experimental data to create a more complete picture of copper-peptide complexes and visible CD. For all of their help with electron paramagnetic resonance, I am indebted to Dr Maxie Roessler and Dr Ray Burton-Smith. Finally, for his initial assistance with using the transmission electron microscope, I thank Graham McPhail.

I have been fortunate enough to supervise a number of very talented undergraduate students throughout my PhD, who have contributed to projects I have worked on, acquiring data of a very high standard. Thus for some of the EPR data in Chapter 5, in collaboration with Dr Maxie Roessler, I would like to thank Nicholas Dev-Pillay. I am grateful to my very first undergraduate students, Yan Chen and Nabeela Shahidullah, for their hard work on visible circular dichroism of Cu^{2+}- and Ni^{2+}- peptide complexes, contributing to the data presented in Chapter 6, Part A. For their diligence and hard work on the binding of Cu^{2+} to the N-terminal of the prion protein (Chapter 6, Part B), I extend my gratitude to Khushbu Patel and Nadia Begum. Finally, I thank Pelak Patel and Uroosa Mayet for their thoroughness and contributions towards the study of Cu^{2+} binding to the N-terminal of alpha-synuclein (Chapter 6, Part C).

Special thanks go to the entire Dr Viles group; Dr Nadine D. Younan, Mr Christian Matheou, Mr Miao Gu and Mr Joseph Barritt for their continuous support throughout my PhD; but especially to Dr Nadine D. Younan for her assistance at the start of the project. One must not forget to mention the wonderful tea times and group outings we had.

I would also like to thank every member of the Prof Richard Pickersgill group; Miss Yumiko Tashiro, Dr Shuang Gu, Dr Allan Pang, Dr Saima Rehman, Mr Piers Rycroft and Miss Junyi Qiu for all their help and support but also for the enjoyable and fun times at work.

Last but not least, I am grateful to all of my family and friends for their continual support over these past four years.

CONTENTS

TABLE OF FIGURES

LIST OF TABLES

ABBREVIATIONS

Aβ	–	Amyloid Beta
AβO	–	Aβ Oligomers
Abs K_a	–	Absolute Association Constant
αCTF	–	α-Secretase Cleaved APP C-terminal fragment
AD	–	Alzheimer's Disease
ADDL	–	Aβ-Derived Diffusible Ligands
AFM	–	Atomic Force Microscopy
AFU	–	Arbitary Fluorescence Units
AICD	–	APP Intracellular Domain
AMPAR	–	α-Amino-3-Hydroxy-5-Methyl-4-Isoxazolepropionic Acid Receptor
amu	–	Atomic Mass Units
ANOVA	–	Analysis of Variance
APP	–	Amyloid Precursor Protein
App K_a	–	Apparent Association Constant
αSyn	–	Alpha-Synuclein
BACE1	–	β-Site APP Cleaving Enzyme 1
BBB	–	Blood Brain Barrier
βCTF	–	β-Secretase Cleaved APP C-Terminal Fragment
CC	–	Cystatin C
CD	–	Circular Dichroism Spectroscopy
CNS	–	Central Nervous System
CPCM	–	Conductor-Polarised Continuum Solvent Model
CSF	–	Cerebrospinal Fluid
Δε	–	Molar Ellipticity
DFT	–	Density Functional Theory
DMSO	–	Dimethyl Sulfoxide
EM	–	N-Ethylmorpholine
EPR	–	Electron Paramagnetic Resonance
Fmoc	–	*N*-(9-fluorenyl)methoxycarbonyl

FTIR	–	Fourier Transform Infrared Spectroscopy
GWAS	–	Genome-Wide Association Study
HEPES	–	2-[4-(hydroxyethyl)piperazin-1-yl] ethanesulfonic acid
HFIP	–	Hexafluoroisopropanol
HSA	–	Human Serum Albumin
HSE	–	Heyd-Scuseria-Ernzerhof
IAPP	–	Islet Amyloid Polypeptide
K_a	–	Association Constant
k_{app}	–	Apparent Rate of Fibre Elongation
K_d	–	Dissociation Constant
LDL	–	Low Density Lipoprotein
LMW Aβ	–	Low Molecular Weight Aβ Oligomers
LTD	–	Long-Term Depression
LTP	–	Long-Term Potentitaion
LUV	–	Large Unilamellar Vesicle
MA	–	Myristic Acid
MS	–	Mass Spectrometry
NAC	–	Non-Amyloid β Component
NMDAR	–	N-Methyl-D Aspartate Receptor
NMR	–	Nuclear Magnetic Resonance Spectroscopy
NTA	–	Nitrilotriacetic Acid
PA	–	Palmitic Acid
PD	–	Parkinson's Disease
PrP	–	Prion Protein
PrP^C	–	Cellular Prion Protein
PS1	–	Presenilin 1
PS2	–	Presenilin 2
PTA	–	Phosphotungstic Acid
SAP	–	Serum Amyloid P Component
sAPPα	–	Soluble α-Secretase Cleaved APP N-terminal fragment
sAPPβ	–	Soluble β-Secretase Cleaved APP N-terminal fragment
sd	–	Standard Deviation

SDS	–	Sodium Dodecyl Sulphate
SEC	–	Size Exclusion Chromatography
t_{50}	–	Time Taken to Reach Half Maximal Fluorescence Intensity
TD-DFT	–	Time-Dependent Density Functional Theory
TEM	–	Transmission Electron Microscopy
TFA	–	Trifluoroacetic Acid
TFE	–	Trifluoroethanol
TGN	–	Trans Golgi Network
ThT	–	Thioflavin T
TIP	–	Temperature-Independent pH
t_{lag}	–	Lag Time
TSE	–	Transmissible Spongiform Encephalopathy
TTR	–	Transthyretin
UV	–	Ultra-Violet
Vis	–	Visible
Vis-CD	–	Visible Circular Dichroism Spectroscopy

CHAPTER ONE:

INTRODUCTION

1.1. ALZHEIMER'S DISEASE (AD)

Alzheimer's disease (AD) was first described by Alois Alzheimer at the beginning of the 20th century (Alzheimer 1907). It is the most common form of dementia, playing a role in almost three quarters of all dementia patients. AD is predominantly a stand-alone dementia but mixed dementia, a combination of AD with vascular dementia, also accounts for 10 % of all dementia cases (Alzheimer's Society 2014).

1.1.1. The Social and Economic Impact of AD

Dementia is an ever growing burden to the population, particularly in the developed world as the average life expectancy is increasing and the proportion of the population over 65 is expanding. One in three people over the age of 65 will develop dementia (Alzheimer's Society 2014) and it is the fourth leading cause of death in women in England and Wales after heart disease, stroke and cancer (Office for National Statistics 2011). Currently there are approximately 800,000 people in the UK with dementia and this is predicted to double over the next 40 years (Alzheimer's Society 2014). The cost of dementia in the UK was estimated to be £23 billion last year (Alzheimer's Society 2014) thus research into the cause and ultimately cure of AD is extremely important. It is estimated there are 45 million people with AD worldwide (Alzheimer's Disease International 2009).

1.1.2. Symptoms, Pathology and Diagnosis

AD, like other dementias, is caused by the loss of neurons and synapses triggering memory loss and other cognitive deficits. Neurodegeneration is predominantly within the hippocampus and the cerebral cortex, particularly the parietal lobe, temporal lobe, regions of the frontal lobe and the cingulate gyrus. These areas play an important role in memory formation, language and navigation thus neuron loss here leads to the typical AD

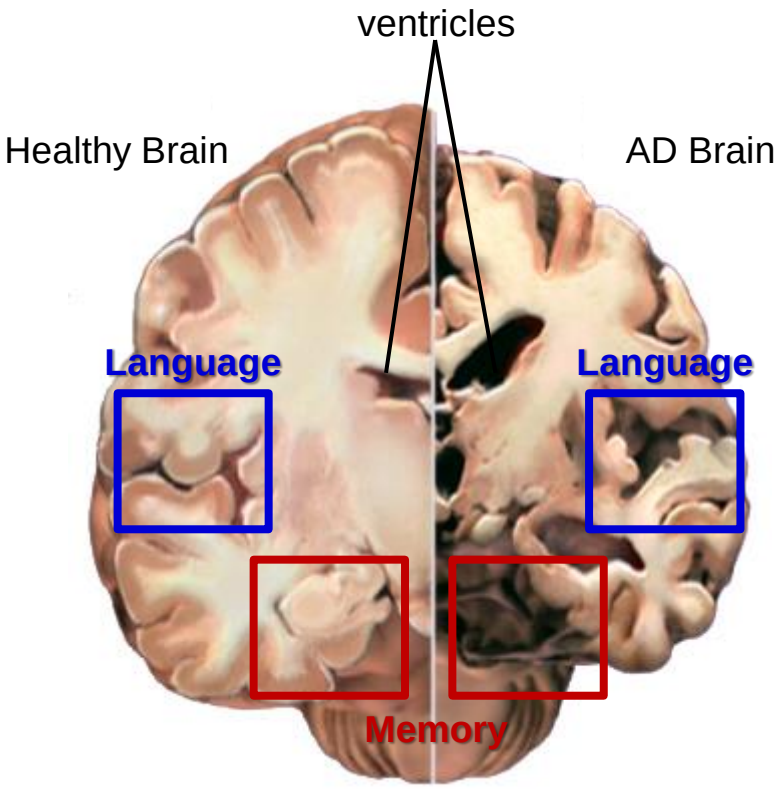

Figure 1.01. The Location of Neurodegeneration in AD.

AD causes neurodegeneration throughout the cerebral cortex and hippocampus, particularly in areas responsible for memory and language, causing enlargement of the ventricles and shrinkage of the grey matter. Modified from alz.org.

symptoms of memory loss, disorientation and problems with communication. A schematic of the extent of shrinkage in the AD brain compared to that of a normal brain can be seen in Figure 1.01. The neurodegeneration in the cortex affecting the memory and language areas is particularly apparent, as is the increased ventricle size. The diagnosis of AD is defined by the localisation of neurodegeneration and the presence of two types of protein accumulation, extracellular amyloid plaques in the cortical interstitium and cerebro-vasculature and secondly intracellular neurofibrillary tangles in the brain post-mortem (Figure 1.02).

1.2. AMYLOID-BETA PEPTIDE (Aβ)

The amyloid plaques observed extracellularly in AD brains are mainly comprised of the peptide amyloid beta (Aβ) first characterised by Masters *et al*. in the 1980s (Masters *et al.* 1985).

1.2.1. Aβ Sequence

Aβ is a short peptide of typically 39-43 amino acid residues in length. The most common alloforms are Aβ(1-40) and Aβ(1-42). The sequence of Aβ(1-42) is shown below:

5 10 15 20 25 30 35 40

DAEFR HDSGY EVHHQ KLVFF AEDVG SNKGA IIGLM VGGVV IA

Blue denotes the hydrophilic residues, while red denotes the hydrophobic residues. It is clear that the N-terminal is mainly hydrophilic and there are two distinct hydrophobic regions; the central hydrophobic cluster (residues 17-21) and the C-terminal (residues 29-42). Many of these hydrophobic residues have large bulky side chains and therefore have a high propensity to form beta-sheets.

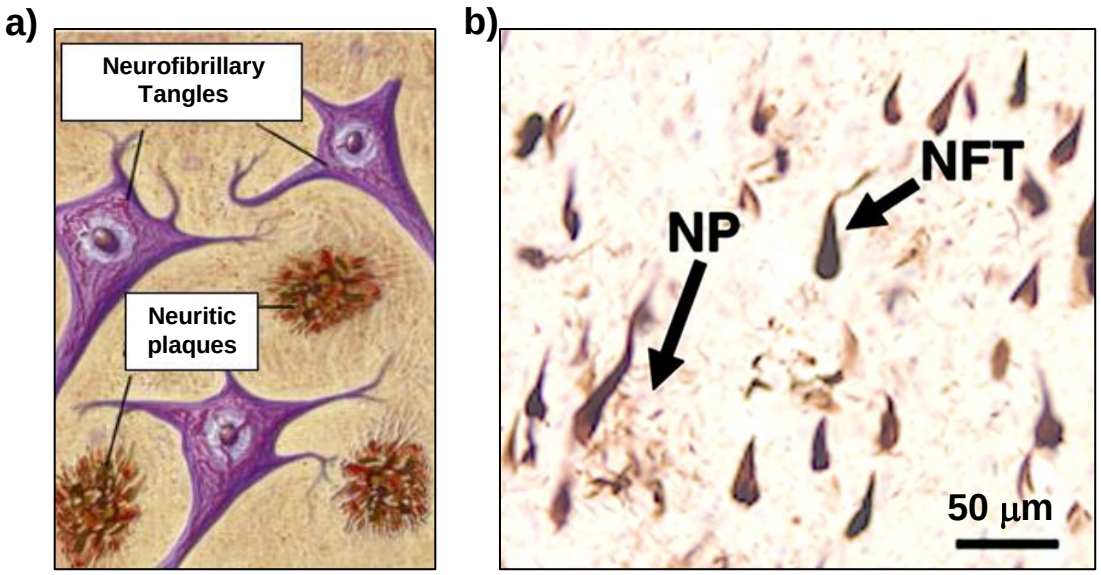

Figure 1.02. Neuritic Plaques and Neurofibrillary Tangles are Hallmarks of AD.

a) A diagram showing the extracellular neuritic plaques and intracellular neurofibrillary tangles associated with AD. b) An immunohistochemically stained hippocampal region from an AD patient showing the neuritic plaques (NP) and neurofibrillary tangles (NFT). Adapted from (Gamblin *et al.* 2003, Mahdi *et al.* 2010).

1.2.2. Amyloid Precursor Protein

Aβ is produced from the Amyloid Precursor Protein (APP), an integral transmembrane glycoprotein whose expression is concentrated in the neurons. Its function is unknown but it has been suggested to play a role in synapse formation and neuronal plasticity (Priller *et al.* 2006, Turner *et al.* 2003). The gene encoding APP is located on chromosome 21 in humans (Kang *et al.* 1987). Three main isoforms exist that are 695, 751 and 770 residues in length. The principal form in neurons is the 695 isoform, while the other two are predominantly expressed elsewhere in the body (Kang *et al.* 1987, Kitaguchi *et al.* 1988, Ponte *et al.* 1988, Tanzi *et al.* 1988). APP can be processed through two distinct pathways; the amyloidogenic pathway and the non-amyloidogenic pathway, as shown in Figure 1.03.

Amyloidogenic Processing Pathway

The amyloidogenic pathway is the processing pathway which produces Aβ through cleavage of APP by a series of secretases (Haass 2004). First, the extracellular domain is cleaved by β-secretase between residues 671 and 672 of the 770 isoform, which corresponds to residues 596 and 597 of the 695 isoform, leaving the C-terminal fragment (βCTF) anchored in the membrane and releasing the soluble N-terminal fragment (sAPPβ). The βCTF is then cleaved by γ-secretase within the transmembrane domain to produce Aβ. γ-secretase can cleave the βCTF at multiple points, which results in the variance in the length of Aβ. Once cleaved, the Aβ is released extracellularly or into the lumen of vesicles.

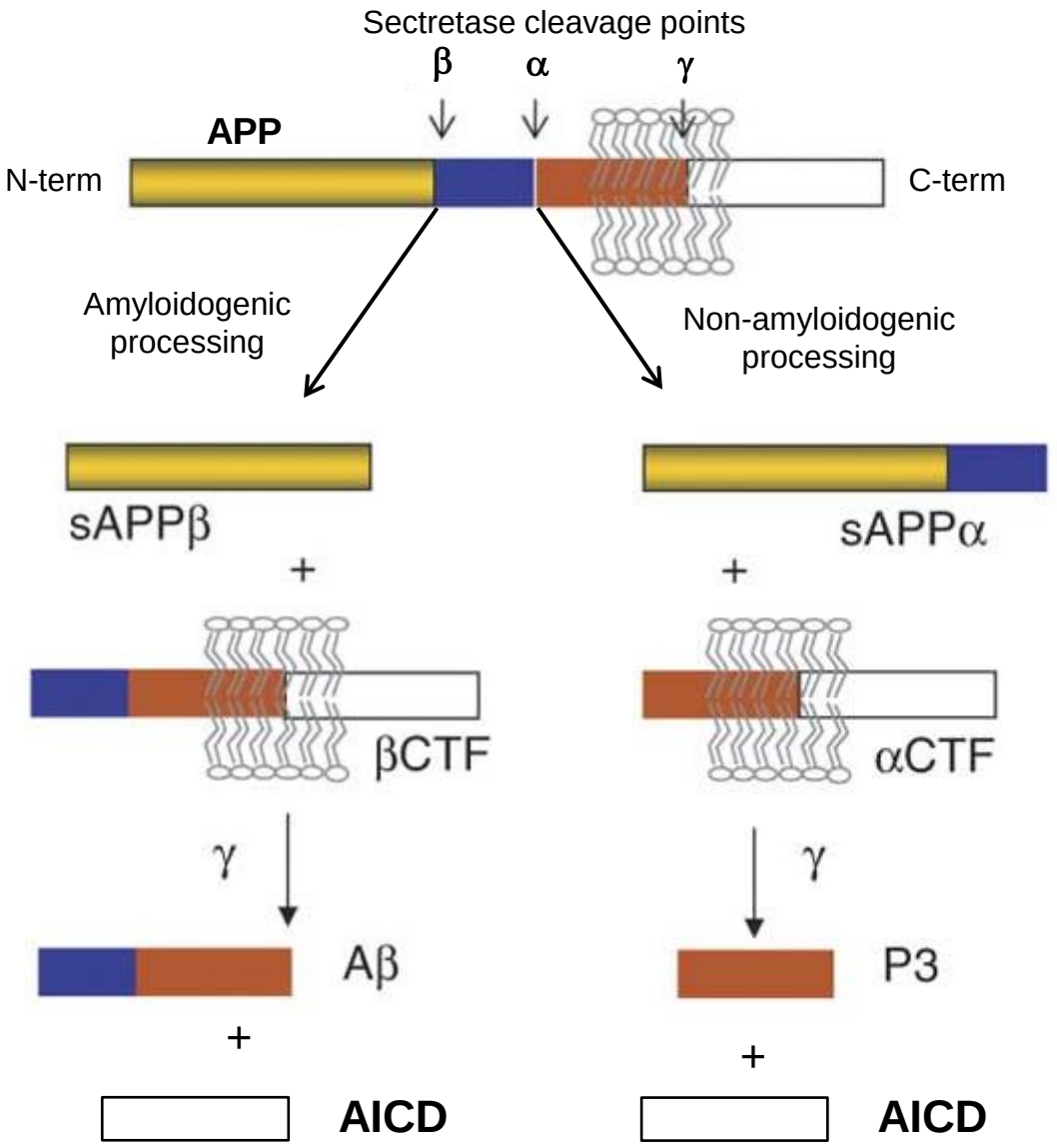

Figure 1.03. Processing of APP.

APP either goes through amyloidogenic processing that results in Aβ production or non-amyloidogenic processing to produce the P3 peptide. Modified from (Tian *et al.* 2010)

Non-Amyloidogenic Processing Pathway

The non-amyloidogenic processing pathway of APP also involves cleavage by a series of secretases. The extracellular domain of APP is cleaved by α-secretase between residues 687 and 688 of the 770 isoform, which corresponds to Lys^{16} and Leu^{17} of Aβ . This releases the soluble N-terminal fragment sAPPα and the C-terminal fragment (αCTF) anchored in the membrane. The αCTF fragment, like the βCTF fragment, is cleaved by γ-secretase. In this case, the P3 fragment (Aβ(17-42)) is released extracellularly and the APP intracellular domain (AICD) is released into the cytoplasm, see Figure 1.03.

1.2.3. APP Location and Trafficking

After synthesis APP can be trafficked from the endoplasmic reticulum to the plasma membrane or locate to the trans-Golgi network (TGN). Only a small fraction reaches the cell surface and is quickly internalised due to its "YENPTY" motif near the C-terminus (Haass *et al.* 2012, Lai *et al.* 1995, Marquez-Sterling *et al.* 1997). Once internalised, APP is delivered to endosomes, where a fraction is recycled to the cell surface. A fraction of internalised APP is also degraded in lysosomes (Haass *et al.* 1992). Mutations in the YENPTY motif inhibit APP internalisation and decrease Aβ production (Perez *et al.* 1999). The non-amyloidogenic pathway of APP processing occurs predominantly at the cell surface as this is the location of the α-secretase complex (Haass *et al.* 2012, Sisodia 1992). The mature γ-secretase complex is located both at the cell surface and in the endosomal system (Dries *et al.* 2008, Kaether *et al.* 2006, Nixon 2007, Pasternak *et al.* 2004).

The location of Aβ production from APP is dependent on the location of the β-secretase complex. The β-secretase enzyme BACE1 (β-site APP cleaving enzyme 1) is enriched in

lipid rafts in the plasma membrane (Cordy *et al.* 2003, Riddell *et al.* 2001) but also undergoes internalisation to endosomes (Huse *et al.* 2000, Pastorino *et al.* 2002). BACE1 is an aspartyl protease and thus optimum activity occurs at an acidic pH (~ pH 4.5) (Vassar *et al.* 1999), which is consistent with major activity in endosomes. However, β-secretase cleavage does not occur exclusively in endosomes (Haass *et al.* 2012). Figure 1.04 depicts these trafficking pathways of APP in a non-polarised mammalian cell.

In neuronal cells, APP is transported to axons and dendrites in post-Golgi transport vesicles after leaving the TGN (Kins *et al.* 2006). Axonal delivery uses the fast axonal transport system (Koo *et al.* 1990), and surprisingly, travels unidirectionally continuously (Kaether *et al.* 2000). Major secretion sites of Aβ are distal axons and synapses (Lazarov *et al.* 2002, Sheng *et al.* 2002). It has been suggested that APP transported in the axonal vesicles are processed by β- and γ-secretase, producing Aβ in these vesicles (Kamal *et al.* 2001).

Regions of the brain where Aβ plaques are most abundant are regions that exhibit the highest baseline of metabolic activity, an indicator of high neuronal and synaptic activity (Buckner *et al.* 2005, Gusnard *et al.* 2001, Raichle *et al.* 2001). Stimulation of N-methyl-D-aspartate receptors (NMDARs) inhibits long term potentiation (LTP) and increases APP expression, promoting Aβ production (Lesné *et al.* 2005). Increased Aβ leads to long-term depression (LTD) (Kamenetz *et al.* 2003). APP overexpression and Aβ generation also decreases the number of α-amino-3-hydroxy-5-methylisoxazole-4-propionic acid receptors (AMPARs) and NMDARs at the cell surface (Hsieh *et al.* 2006, Snyder *et al.* 2005). This forms a negative feedback loop: increased neuronal activity

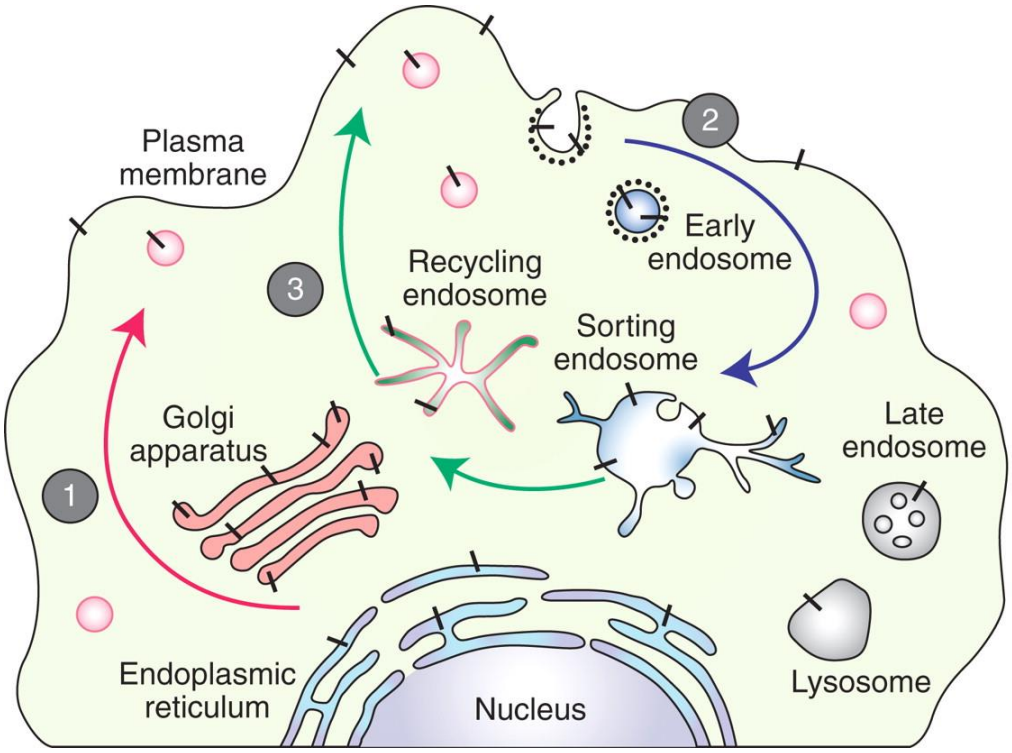

Figure 1.04. Intracellular APP Trafficking.

APP molecules (black bars) mature through the constitutive secretory pathway (1). Once APP reaches the cell surface, it is rapidly internalized (2) and subsequently trafficked through endocytic and recycling organelles to the TGN or the cell surface (3). Adopted from (Haass *et al.* 2012).

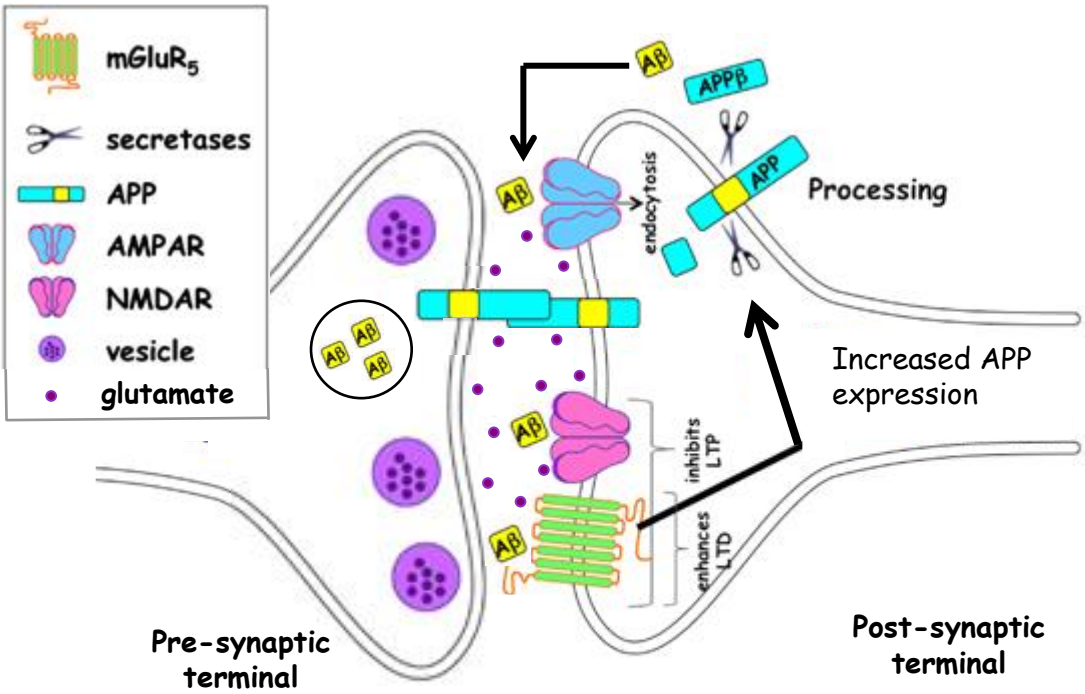

Figure 1.05. Negative Feedback of Aβ at the Glutamatergic Synapse.

Neuronal activity leads to Aβ release at the synapse, which binds to receptors on the post-synaptic terminal, causing increased APP expression, enhanced LTD, LTP inhibition and AMPAR reduction, which decrease neuronal activity. Modified from (Westmark 2013).

produces more Aβ which depresses synaptic function thus decreasing neuronal activity (Haass *et al.* 2012). This feedback loop is depicted in Figure 1.05.

1.2.4. Mutations Found in Familial AD

Familial early-onset AD represents approximately 5 % of all AD cases. Familial AD patients have been found to have mutations in APP or within key proteins in the γ-secretase complex; presenilin 1 (PS1) or presenilin 2 (PS2). Interestingly, the majority of people with Down's syndrome will develop early-onset AD. Down's syndrome is the result of a trisomy of chromosome 21, which is the location for the gene encoding APP, thus the production of APP is dramatically elevated. As many as 25 mutations have been identified in APP and over 150 in PS1 of the γ-secretase complex (Tabaton *et al.* 2007). Mutations in the γ-secretase complex promote Aβ(1-42) production over Aβ(1-40) (Scheuner *et al.* 1996, Thinakaran *et al.* 1996). A summary of common mutants of APP are shown in Figure 1.06. These mutations can result in increased Aβ production, such as the Flemish mutation (A692G), which inhibits α-secretase cleavage, or the Swedish mutation (K670N/M671L) which increases production through potentiation of γ-secretase cleavage (Hardy 1997). Alternatively, the point mutations can promote Aβ(1-42) production over Aβ(1-40), such as the Florida (I716V) and London (V717I) mutations which alter the site of γ-secretase cleavage (Hardy 1997). Point mutations in APP that are within the sequence of Aβ itself can increase the amyloidogenic properties of Aβ. The majority of Aβ point mutations are clustered around residues 21-23 (residues 692-694 in full-length APP770) (Murakami *et al.* 2002). These either result in the loss of a negative charge (e.g. the Dutch mutation E22Q), which increases the pI of Aβ closer to physiological pH making Aβ less soluble, or the introduction of a glycine, which may promote misfolding. Indeed the Arctic mutation (E22G) will have both of these effects.

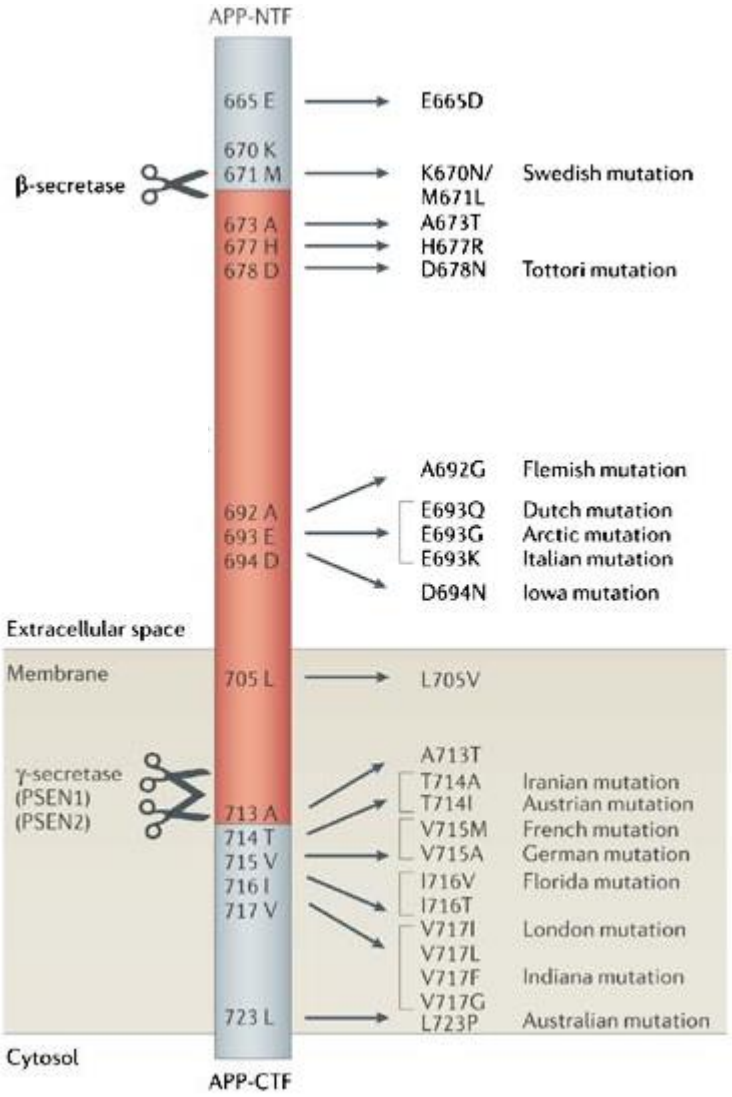

Figure 1.06. Common Point mutations of APP Found in Familial AD.

The point mutations shown either influence APP cleavage by β and γ secretases or are within the sequence of Aβ itself. Modified from (Van Dam *et al.* 2006).

1.3. Aβ STRUCTURE

1.3.1. Monomeric Aβ Structure

Monomeric Aβ is natively unstructured in water but has the ability to transiently form both alpha-helical and beta-sheet structures (Zhang *et al.* 2000). In a membrane mimicking environment, using sodium dodecyl sulphate (SDS), Aβ has been shown to form α-helices from residues 17-24 and 28-36 (Barrow *et al.* 1992, Soto *et al.* 1995). Amyloidogenesis requires Aβ to form a β-sheet fold.

1.3.2. Fibrillar Aβ Structure

Aβ forms amyloid fibres that are approximately 10 nm in diameter and of indeterminate length, up to microns, and can exhibit periodical twists. Variability in periodicity and the number of protofilaments that form a fibre can occur within a single sample (Figure 1.07) (Meinhardt *et al.* 2009), known as fibril polymorphism. Much work has been done to elucidate the structure of Aβ fibres, using a variety of techniques. The information gleamed from some of these techniques is discussed.

X-Ray Diffraction

X-ray diffraction data of Aβ(11-25) fibrils over full-length Aβ fibrils has been used to examine the internal structure of fibre protofilaments as X-ray diffraction data is less detailed with full-length Aβ (Makin *et al.* 2005). The Aβ monomers form an extended β-strand and associate to form cross-β ribbons, where the chains run perpendicular to the fibre axis (Sikorski *et al.* 2003). The fibres form with an intersheet distance of approximately 10 Å and an interstrand distance of 4.7 Å (Sikorski *et al.* 2003), producing a characteristic X-ray fibre diffraction pattern, shown in Figure 1.08a,b.

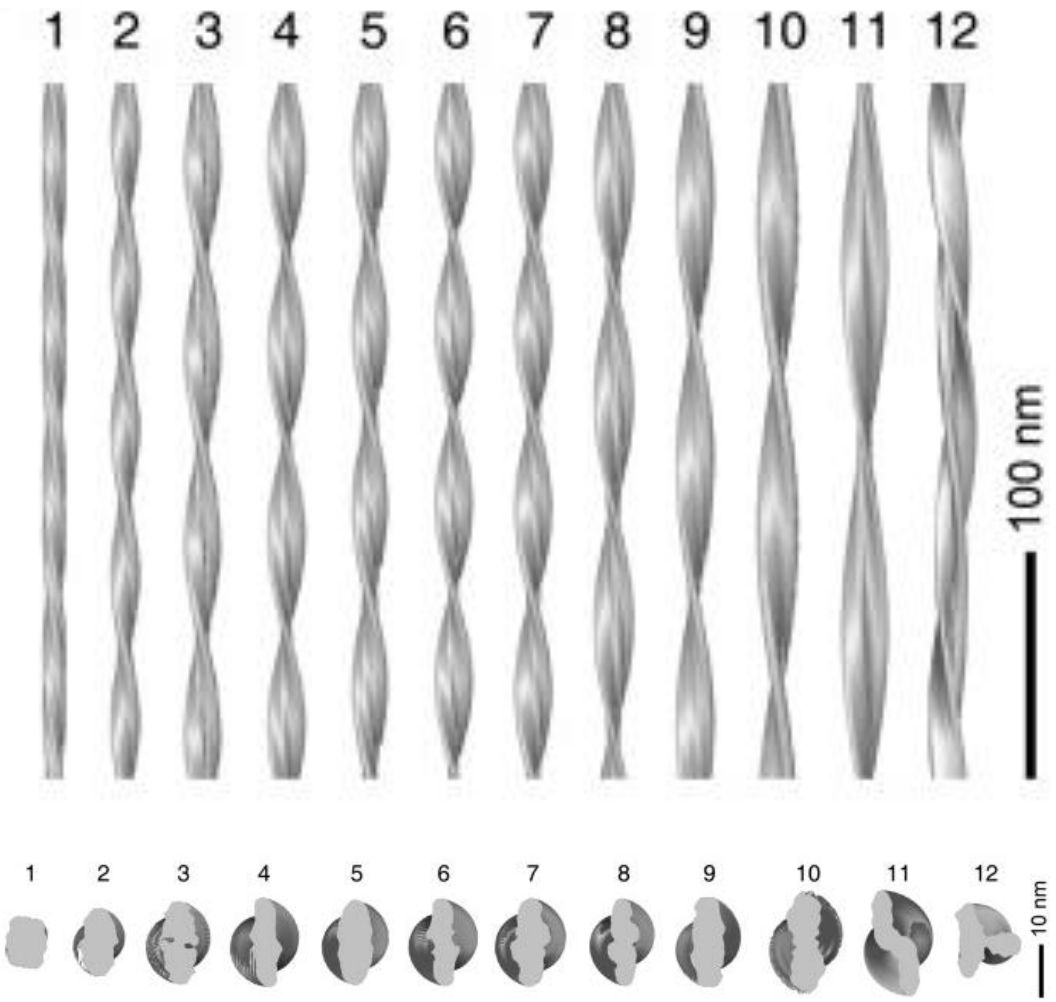

Figure 1.07. Aβ Fibres have Periodical Twists.

The periodicity of fibres can vary within a single sample. Adapted from (Meinhardt *et al.* 2009).

Solid-State Nuclear Magnetic Resonance

Solid-state nuclear magnetic resonance (NMR) has proven to be a particularly useful technique for the elucidation of amyloid fibre structure. This is because solid-state NMR can provide constraints on inter-atomic distances and torsion angles at a site-specific level. Indeed, the measure of inter-atomic distance of ^{13}C up to 6 Å is possible, with standard error of only 0.1-0.2 Å (Tycko 2000). Tycko and colleagues have created structural models of Aβ fibrils (Figure 1.08c,d) predominantly through the use of solid-state NMR measurements, specifically of ^{13}C-^{13}C dipole-dipole couplings, chemical shifts of ^{13}C and ^{15}N and intramolecular correlations of backbone carbonyl group orientations, but also in conjunction with transmission electron microscopy (TEM) (Antzutkin *et al.* 2002, Paravastu *et al.* 2008, Petkova *et al.* 2002, Tycko 2006). The models are consistent with the X-ray diffraction data. Aβ forms two β-strands per monomer in a β-turn-β fold, a hair-pin-like structure, such that the central hydrophobic core and the hydrophobic C-terminal domain side chains are packed together and hydrophobic interactions stabilise the structure. The structure is also stabilised by a salt bridge between Asp^{23} and Lys^{28}. The N-terminus (residues 1-10) is disordered. Solid-state NMR can also be used to establish the supramolecular structure. It has been revealed that both Aβ(1-40) and Aβ(1-42) fibres contain in-register, parallel β-sheets (Antzutkin *et al.* 2002, Balbach *et al.* 2002, Benzinger *et al.* 1998).

Electron Paramagnetic Resonance

The location and contacts of β-strand segments within fibres can be elucidated using electron paramagnetic resonance (EPR) spectroscopy. This involves introduction of cysteine residues with nitroxide spin labels. EPR measurements on both Aβ(1-40) and Aβ(1-42) fibres indicate the greatest side-chain mobility in the N-terminal and central

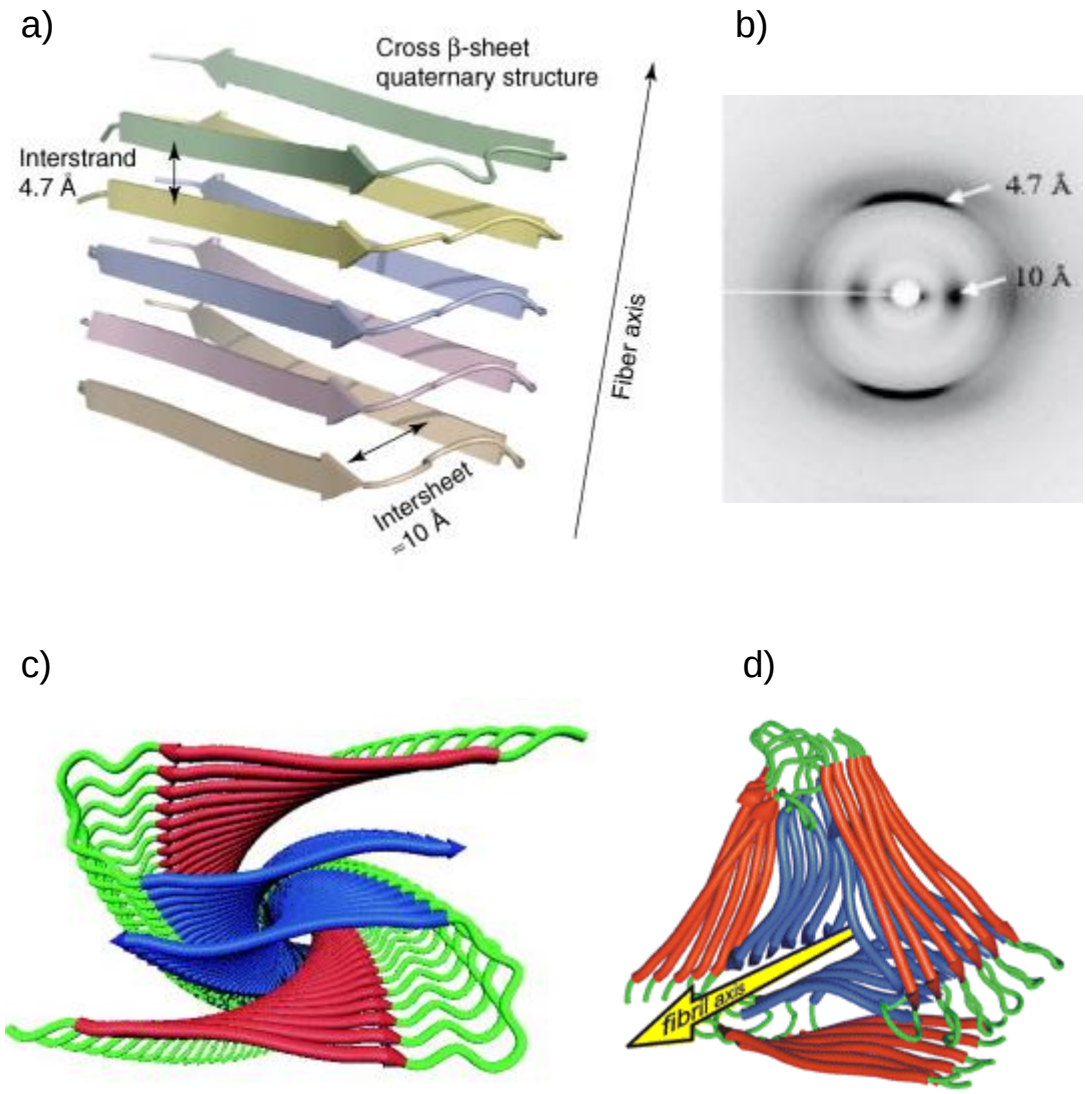

Figure 1.08. Aβ Fibril Structure.

a) Aβ monomers polymerise to form protofibrils with a cross β-sheet structure that have constant interstrand and intersheet distances. b) The characteristic X-ray diffraction pattern observed for amyloid fibrils. c) and d) show possible fibre structures achieved by the association of protofibrils. Adapted from (Fowler *et al.* 2007, Paravastu *et al.* 2008, Tycko 2006).

segments of Aβ (Török *et al.* 2002), consistent with the structurally disordered regions in the Tycko model. The EPR supports the in-register, parallel alignment of the peptide chain within the cross-β motif (Török *et al.* 2002).

Hydrogen/Deuterium Exchange

The molecular structure of fibres can also be probed indirectly through the use of hydrogen/deuterium (H/D) exchange. Based upon the availability of backbone amide protons to exchange, information about the fold of the protein can be inferred; protons on the surface will be readily exchanged whereas protons buried from the solvent or involved in hydrogen bonds will exchange slowly, if at all. Between 48 and 55 % of backbone amide protons have been reported to be highly protected from H/D exchange in Aβ(1-40) fibres (Kheterpal *et al.* 2003). This is consistent with the Tycko model, where approximately half of the residues form the two β-strands and the other residues are disordered.

Fibre Polymorphisms

In vitro fibre formation has shown that there can be many different polymorphisms within a single sample formed (Meinhardt *et al.* 2009, Petkova *et al.* 2005). However, fibres with a specific molecular structure will be dominant depending on the conditions in which the fibres are formed. For example, fibres with 2-fold symmetry shown in Figure 1.07c dominate in quiescent (no agitation) conditions whereas fibres with 3-fold symmetry (Figure 1.07d) dominate with agitation despite the growth conditions being otherwise identical in peptide concentration, pH, temperature, ionic strength and buffer composition (Paravastu *et al.* 2008). It has been shown that fibres grown from seeds of a specific molecular structure will take or "inherit" the same structure as the seeds irrespective of the fibril growth conditions (Paravastu *et al.* 2008, Petkova *et al.* 2005). Interestingly, a

recent study has isolated Aβ fibril fragments from the brains of AD patients and seeded *in vitro* Aβ fibre growth (Lu *et al.* 2013). The resultant daughter fibres were homogeneous in structure demonstrating that the seeds must all have had the same molecular structure. It is surprising that the brain-derived Aβ fibres are not polymorphic and suggests that differences in fibril structure may correlate with differences in disease development (Lu *et al.* 2013). Clearly this behaviour has many parallels with different prion strains in transmissible spongiform encephalopathies.

1.3.3. Oligomeric Aβ Structure

Oligomeric Aβ has been suggested to be the most toxic form of Aβ, however there are many different oligomeric species reported in the literature. Oligomers can either be off-pathway or on-pathway to fibril formation and many oligomers exist in dynamic equilibrium with monomers, other oligomeric assemblies, protofibrils and fibres (Figure 1.09). These have been studied from both *ex vivo* and *in vitro* sources.

Aβ-Derived Diffusible Ligands (ADDLs)

Aβ-derived diffusible ligands (ADDLs) are a group of Aβ oligomers whose molecular mass ranges between 17-42 kDa, with a major species at 27 kDa and 17 kDa (Lambert *et al.* 1998).

*Aβ*56*

Aβ*56 is the only oligomeric species of a definite size (56 kDa) that has been isolated so far and was isolated from transgenic mice brains. This soluble oligomer is larger than the size range of the ADDLs (Lesné *et al.* 2006).

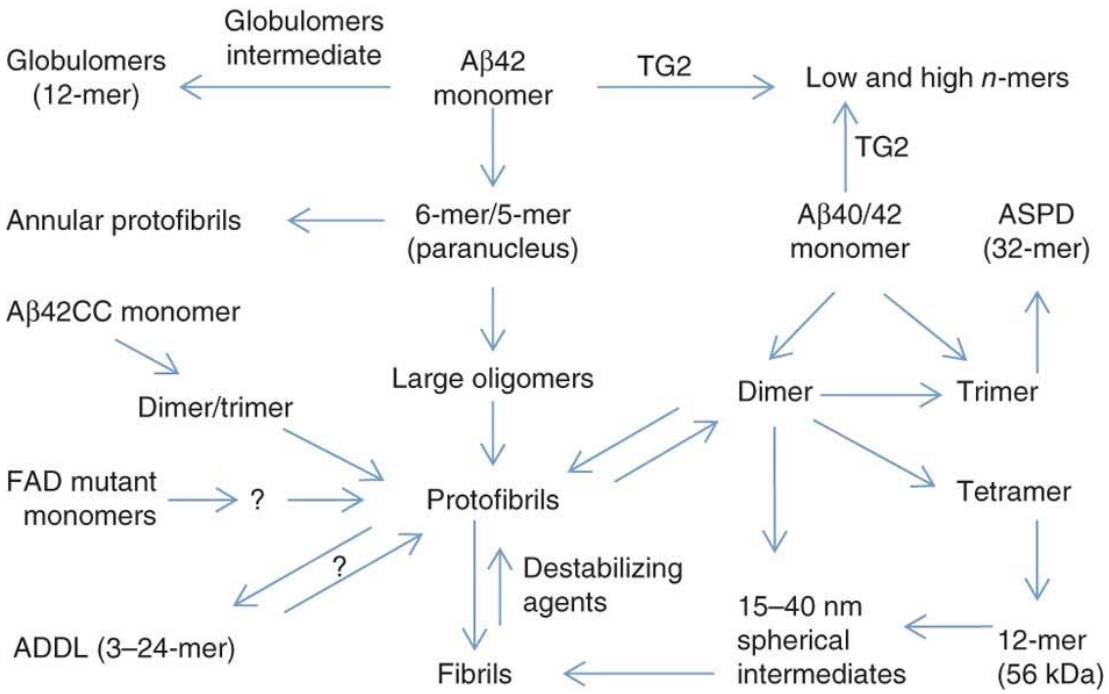

Figure 1.09. Interconversion Between Different Aβ Assemblies.

Proposed interconversion between naturally and synthetically-derived Aβ assemblies based on pathways described in the literature. Reproduced from (Benilova *et al.* 2012).

Low Molecular Weight Aβ Oligomers (LMW Aβ)

Low molecular weight oligomers (LMW Aβ) encompass dimers and trimers thus are 6-12-kDa assemblies. They have no detectable secondary structure (Walsh *et al.* 1999, Walsh *et al.* 1997).

Aβ Oligomers (AβO)

These are high molecular weight Aβ oligomers that measure 2–5 nm in height with atomic force microscopy, indicating a size of 10-100 kDa (Dahlgren *et al.* 2002).

Protofibrils

Protofibrils are appear to be composed of beaded chains with a beading periodicity of 3-6 nm (Walsh *et al.* 1999). They are sometimes described as flexible and curved and have a length of less than 200 nm and a diameter of ~ 8 nm (Hartley *et al.* 1999, Walsh *et al.* 1997). Protofibrils have a β-sheet structure but a high level of random coil also exists in protofibrillar samples (Walsh *et al.* 1999).

Annular Protofibrils

Annular protofibrils, unlike the protofibrils described above, are off-pathway to fibre formation (Lasagna-Reeves *et al.* 2011). They form pores with an outer diameter of 7–12 nm and an inner diameter of 1.5-2.5 nm (Lashuel *et al.* 2002, Lashuel *et al.* 2003). They are formed of 40-60 Aβ monomers (Lashuel *et al.* 2002) and contain substantial β-sheet character (Kayed *et al.* 2009). It has been proposed that annular protofibrils are formed from six hexamers coming together to form the pore (Shafrir *et al.* 2010).

Amylospheroids

Amylospheroids are perfectly spherical Aβ assemblies that are 10–15-nm in diameter (Hoshi *et al.* 2003, Matsumura *et al.* 2011). They are composed of 32–150 monomers (Noguchi *et al.* 2009).

1.4. Aβ FIBRILLISATION

1.4.1. Kinetics of Fibre Formation

The progress of Aβ monomer to Aβ fibres follows a characteristic growth curve that has distinct stages; nucleation, elongation and a plateau phase (Nilsson 2004), as shown in Figure 1.10.

The nucleation stage of Aβ fibrillisation is the rate limiting step of fibre formation. During this lag phase the native-state Aβ monomers must undergo misfolding, which allows for amyloidogenic aggregation. At this stage the monomers must polymerise to form a nucleating seed, which is typically a small oligomer of Aβ. The addition of preformed seeds to a monomeric Aβ sample will remove the nucleation stage and fibrillisation will enter the elongation stage directly.

The elongation phase of fibrillisation is the rapid addition of Aβ monomers to the ends of existing fibrils. Fragmentation of amyloid fibres has a profound influence on the rate of fibre formation. Fragmentation of fibres generates many nucleating ends so as to accelerate fibre fragmentation. Elongation continues until a plateau stage is reached. This is the point of maximal fibril formation.

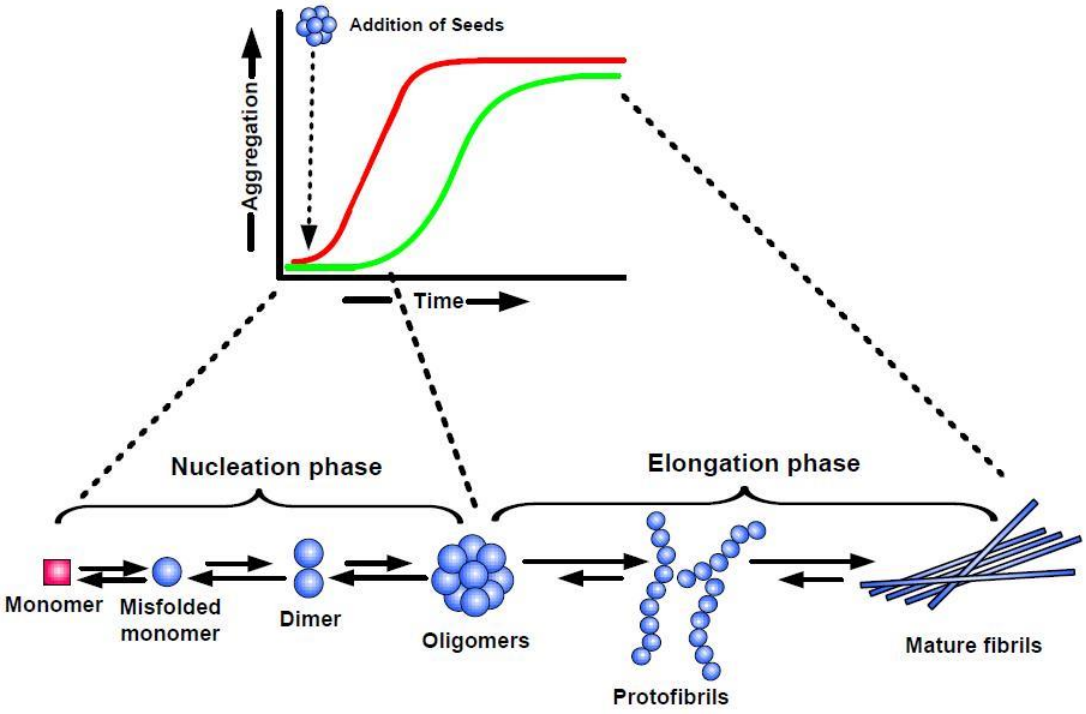

Figure 1.10. Stages of Aβ Fibril Formation.

Aβ fibril growth follows a characteristic sigmoidal growth curve. During the nucleation phase, a seed forms from which protofibrils and fibres can develop during the elongation phase. Reproduced from (Kumar *et al.* 2011).

The transition of Aβ monomers to fibres is not a strict linear progression as each step is in dynamic equilibrium with its previous and following steps. For example, protofibrils can become either mature fibres or disassemble to become oligomers.

1.4.2. Fibril Detection

There are several different methods used to detect amyloid fibrils. This can be through direct visualisation or through characterisation of features specific to amyloid fibres.

Microscopy

TEM and Atomic Force Microscopy (AFM) are excellent methods for visualising amyloid fibres. The resolution of these types of microscopy means that not just fibres can be imaged but also protofilaments and oligomeric assemblies as structures on a nanometre scale are visible. However, microscopy is a qualitative technique so the differences in the number of fibres generated between samples cannot be readily calculated.

Thioflavin T Fluorescence

Thioflavin T (ThT) is a benzothiazole dye that binds to amyloid fibres with high specificity. Upon binding to amyloid fibres, ThT will fluoresce at an emission maximum of 490 nm when excited at 440 nm (LeVine 1993). Free ThT will not fluoresce thus the progression of fibrillisation in the presence of ThT will produce the characteristic growth curve seen in Figure 1.10. This is an effective quantitative method for detecting fibres and has therefore been used throughout this thesis to monitor Aβ fibrillisation. The use of ThT as a detection method is described in more detail in Chapter 2.

Congo Red

Congo red is a secondary azo dye that binds to amyloid fibres and is often used as an amyloid stain in histopathology. Congo red exhibits birefringence upon binding fibres, changing from red to yellow/green. This method was popular for detection but has recently been shown to stabilise the native protein monomers, disturbing the amyloid formation pathway (Frid *et al.* 2007).

β-Sheet Detection

The switch in secondary structure from α-helical or random coil to β-sheet is a hallmark of amyloid assembly thus determination of secondary structure using circular dichroism (CD) or Fourier-transform infrared (FTIR) spectroscopy is employed in fibre detection. However, this is not completely indicative of amyloidogenic fibre formation as other types of aggregates (amorphous) may also display β-sheet structure. These techniques should therefore be utilised concomitantly with other fibre detection techniques.

1.5. THE NATURE AND MECHANISM OF THE TOXIC Aβ SPECIES

1.5.1. The Toxic Aβ Species

The nature of the toxic Aβ species is highly debated. The plaques were first thought to be the most toxic species but the lack of correlation between the deposition of plaques and neuronal loss contradicts this view (Yankner *et al.* 2008). However, there is still some strong evidence for plaques acting as a toxic species from *in vivo* studies in transgenic mice. A study using multiphoton microscopy established a direct causal relationship between plaques and neurodegeneration, showing that plaque formation was followed by neurodegeneration, not the other way round, (Meyer-Luehmann *et al.* 2008). Others have shown that neuronal loss only occurs in the vicinity of plaques (Urbanc *et al.* 2002).

The toxic oligomer hypothesis suggests oligomers are the toxic species of Aβ aggregates (Lambert *et al.* 1998). The multitude of different Aβ oligomers described in the literature (see section 1.3.3) complicates this view with different structures being identified as the toxic Aβ species in AD. ADDLs were identified as the toxic species by Lambert *et al.* (Lambert *et al.* 1998), which was subsequently supported by a study showing their concentration is increased in AD patients by approximately 70-fold compared to non-sufferers (Gong *et al.* 2003). ADDLs have been shown to inhibit long term potentiation in hippocampal neurons (Walsh *et al.* 2002). Aβ*56 was identified as the toxic species by its correlation with decreased mouse performance in a Morris water maze test and injection of Aβ*56 decreasing the spatial memory of four month old rats (Lesné *et al.* 2006). AβOs have been identified to be 40 times more toxic than monomeric Aβ and 10 times more toxic than fibres (Dahlgren *et al.* 2002). Protofibrils have been identified to be toxic in a number of studies (Hartley *et al.* 1999, Walsh *et al.* 1999). Amylospheroids have also been identified as toxic in a number of studies (Hoshi *et al.* 2003, Matsumura *et al.* 2011, Noguchi *et al.* 2009). The toxicity of Aβ oligomers may therefore not be due to one particular species but rather various oligomers acting in non-specific ways to cause toxicity (Benilova *et al.* 2012). Identifying the toxic species is hampered by the heterogeneity of oligomeric preparations.

1.5.2. The Mechanism of Toxicity

Not only is the Aβ species responsible for toxicity still not clear, the mechanism by which Aβ causes toxicity is also disputed. The proposed mechanisms can be broadly divided into three categories; membrane alterations, oxidative stress and modulation of postsynaptic receptor activity.

Membrane Alterations

This may include the formation of annular protofibrils in the membrane, which have been proposed to cause toxicity either by non-specific leakage or as a Ca^{2+} channel (Arispe *et al.* 2007, Arispe *et al.* 1993, Jang *et al.* 2010). Alternatively membrane alterations can occur through contact with the hydrophobic ends of amyloid fibrils. Indeed, work with large unilamellar vesicles (LUVs) as a model for cell membranes has shown that the ends of amyloid fibrils can distort the shape of vesicles, puncture the vesicles and cause the formation of bubbles in the outer membrane (Milanesi *et al.* 2012). Aβ has also been shown to increase the conductance of the lipid bilayer, either through localised structural defects or indirect thinning of the membrane (Sokolov *et al.* 2006).

Oxidative Stress

Increased levels of oxidative damage are observed in AD brains. Oxidative stress has been detected prior to the formation of amyloid plaques (Nunomura *et al.* 2006). Methionine at position 35 of Aβ is found oxidised in Aβ isolated from plaques (Dong *et al.* 2003). It has been suggested that Aβ produces reactive oxygen species through Fenton/Haber-Weiss reactions in the presence of transition metals, specifically copper or iron (Huang *et al.* 1999).

Modulation of Postsynaptic Receptor Activity

Increasing evidence points to Aβ disrupting normal postsynaptic receptor activity. NMDAR-dependent toxicity has been reported by a number of studies, as has LTP impairment and increased LTD, which are NMDAR-mediated processes (Alberdi *et al.* 2010, Chen *et al.* 2002, Cullen *et al.* 1996, Decker *et al.* 2010, Domingues *et al.* 2007, Ferreira *et al.* 2012, He *et al.* 2011, Li *et al.* 2009, Li *et al.* 2011a, Rammes *et al.* 2011, Rönicke *et al.* 2011, Shankar *et al.* 2007, Tackenberg *et al.* 2013, Texidó *et al.* 2011, Wu

et al. 1995, You *et al.* 2012). The direct interaction between Aβ and NMDARs is discussed in section 1.8.1.

It is possible the theories are closely interconnected and the toxicity of Aβ is not due to one single mechanism. Indeed, there is evidence for an interconnection between oxidative stress and NMDAR activity modulation to cause neurotoxicity (He *et al.* 2011).

1.6. AMYLOID CASCADE HYPOTHESIS

The most widely supported theory for the process of AD development is the amyloid cascade hypothesis, shown in Figure 1.11 (Hardy *et al.* 1992). In this hypothesis, increased Aβ production and deposition occurs first causing synaptic dysfunction and altered kinase/phosphatase activity, which leads to the hyper-phosphorylation of tau. Formation of tau neurofibrillary tangles are therefore a product of increased Aβ accumulation with this hypothesis and have been thought to play a secondary role in Aβ neurotoxicity. However, tau mediates Aβ toxicity (Ittner *et al.* 2011), exemplified by tau deficiency being protective against Aβ-induced cell death in mice models and neuronal cultures (Ittner *et al.* 2010, Rapoport *et al.* 2002). Evidence suggests that tau hyperphosphorylation is not simply a by-product of Aβ accumulation and there may be a direct interaction between Aβ and tau (Guo *et al.* 2006).

The amyloid cascade hypothesis is not infallible with two main issues. Firstly, neurodegeneration can present before amyloid plaque deposition and the severity of AD does not necessarily correlate with the extent of deposition (Yankner *et al.* 2008). This can be resolved by the evidence that the toxic species of Aβ is a soluble oligomer rather than the plaques. Secondly, APP and Aβ are expressed ubiquitously in the human body

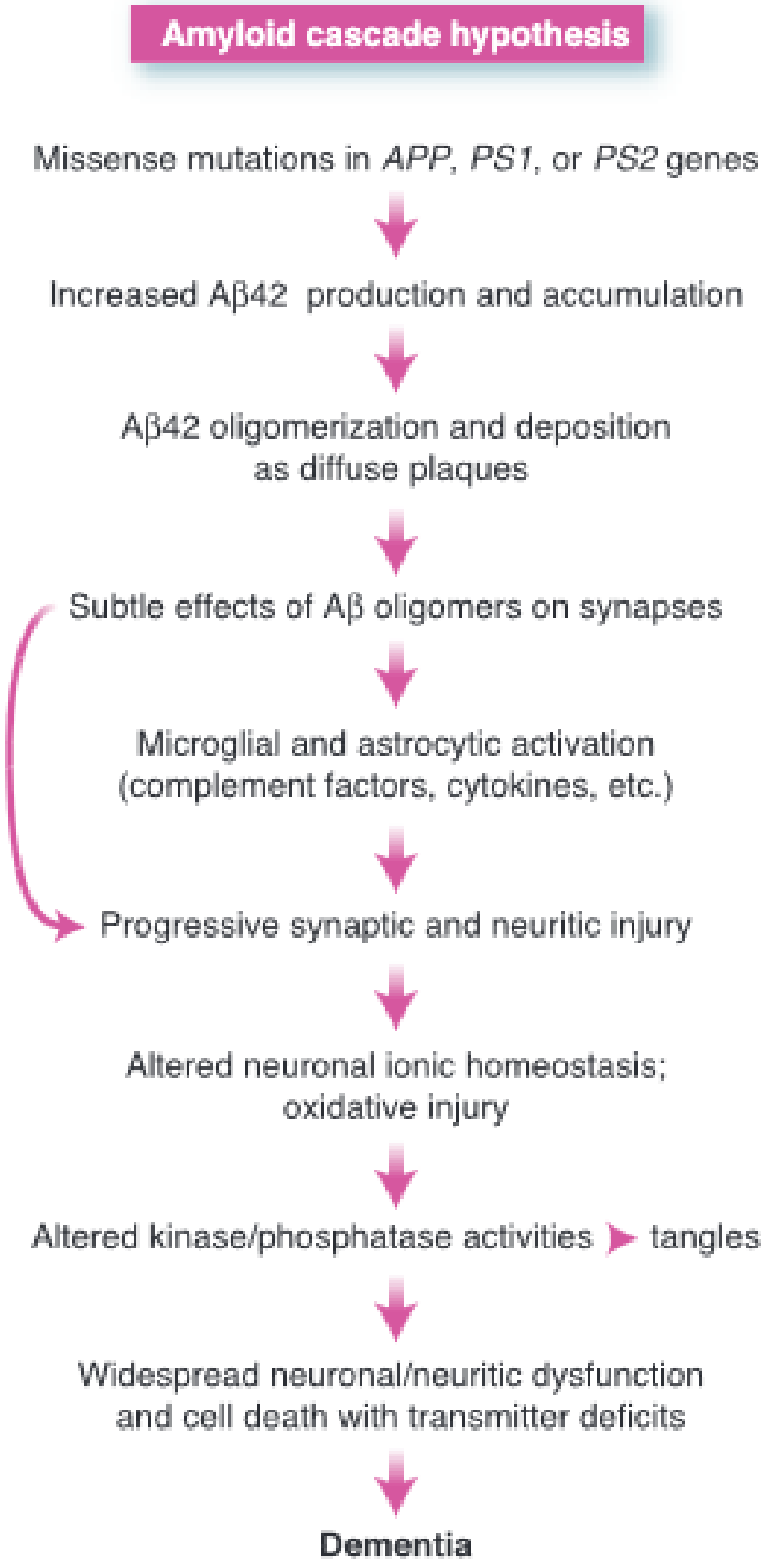

Figure 1.11. The Amyloid Cascade Hypothesis.

Reproduced from (Hardy *et al.* 2002).

throughout their lifetime but AD manifests at old-age and only affects specific regions in the brain.

1.7. AD RISK FACTORS

1.7.1. Genetic Risk Factors

In addition to the genetic mutations that cause familial AD (discussed in section 1.2.4), there are genetic variants that increase the risk of developing sporadic AD. A number of these have been identified using genome-wide association studies (GWAS). The most significant gene identified is the *APOE ε4* allele. This encodes apolipoprotein E, a protein that conjugates with cholesterol and other fats to transport them through the blood plasma. Those heterozygous for *APOE ε4* are up to four times more likely to develop AD and homozygotes have an eight-fold increased risk (Corder *et al.* 1993).

Other genes identified using GWAS include *ABCA7*, *BIN1*, *CD2AP*, *CLU*, *CR1*, *EPHA1*, *MS4*, *PICALM* and *SORL1*. The majority of genes that have been identified can be divided into four distinct categories; cholesterol metabolism, ubiquitination, endocytosis and immunity (Lambert *et al.* 2013).

1.7.2. Environmental Risk Factors

An increased risk of developing AD is not exclusive to genetic factors but environment can also play a role. Like genetic risk factors, some of these risks are unavoidable, however, others can be controlled.

Age has the highest impact on AD, more than doubling the risk of development at the age of 80 compared to age 65. AD is more prevalent in women than men but the risk

associated with gender is likely to be due to age as women have a greater average life expectancy.

Existing medical conditions can also increase the risk of developing AD. An increased risk is associated with cardiovascular disease, diabetes and traumatic brain injury (Biessels *et al.* 2006, Kivipelto *et al.* 2002, Kivipelto *et al.* 2001, Roberts *et al.* 1994). A risk associated with the development of cardiovascular disease and AD is high levels of serum cholesterol (Kivipelto *et al.* 2002).

Finally, diet and general health can also influence the risk of developing AD. It has been shown that obesity and a diet high in saturated fat increase the risk, while exercise and diets low in saturated fats and higher in omega 3 and 6 fats reduce the risk (Morris *et al.* 2003).

1.8. Aβ BINDING PARTNERS

The interactions Aβ establishes within the body is an important factor for understanding the mechanisms behind the development of AD. Aβ has been shown to interact with a variety of proteins and metal ions. These have either been found co-localised with Aβ in amyloid plaques, are thought to be implicit in cell surface interactions or bind extracellular soluble Aβ, as is the case for albumin (Luo *et al.* 2014, Stanyon *et al.* 2012)

1.8.1. Proteins

Proteins with which Aβ interacts can broadly be split into three categories; membrane associated proteins and receptors, intracellular or extracellular chaperones, and other amyloid proteins.

N-Methyl-D Aspartate Receptors (NMDARs)

Excessive NMDAR activation has been implicated in the pathophysiology of AD (Snyder *et al.* 2005). NMDARs are activated by Aβ oligomers (Brito-Moreira *et al.* 2011). Oligomeric Aβ binding NMDAR results in synaptic depression through conformational changes rather than changes in ion flow through its channel (Kessels *et al.* 2013). Aβ promotes the endocytosis of NMDARs (Snyder *et al.* 2005).

Prion Protein (PrP)

The cellular prion protein (PrP^C) is a membrane anchored protein that has been identified as a cell surface receptor for Aβ. It was identified through a screening that involved over 200,000 proteins, using an unbiased cDNA library (Laurén *et al.* 2009).

Aβ does not interact with PrP^C in monomeric form and it is not until Aβ misfolds and forms oligomers that the interaction occurs. It has been shown that PrP^C binds oligomers of Aβ of approximately 20 monomers in size (Younan *et al.* 2013). A nanomolar affinity of the oligomers for PrP has been consistently reported (Balducci *et al.* 2010, Calella *et al.* 2010, Chen *et al.* 2010, Gunther *et al.* 2010, Laurén *et al.* 2009). Binding of Aβ to PrP^C halts the Aβ fibrillisation pathway such that the Aβ is arrested in oligomeric form and does not form fibres (Younan *et al.* 2013). PrP^C is also able to disassemble mature fibres into oligomers (Younan *et al.* 2013). This ability to trap Aβ in oligomeric form suggests a mechanism of increased neurotoxicity *in vivo*. Indeed, an *in vivo* model has shown that PrP is crucial for the neurotoxicity observed in AD. An AD mouse model with a PrP knock-out was shown to develop Aβ plaques but no neurotoxicity was exhibited (Gimbel *et al.* 2010). In addition, in normal mice expressing PrP^C the interaction between Aβ oligomers and PrP^C has been shown to inhibit long term potentiation in hippocampal

slices (Laurén *et al.* 2009). Interestingly, PrP can mediate excessive NMDAR activity when in a copper-loaded state (You *et al.* 2012).

Clusterin

A link between developing AD and the protein clusterin has been identified from GWAS (Sleegers *et al.* 2010). Clusterin (also known as Apolipoprotein J) is part of a family of extracellular protein-folding chaperones, which have been shown to stabilise proteins and prevent their aggregation *in vitro* (Humphreys *et al.* 1999, Narayan *et al.* 2012a, Narayan *et al.* 2012b, Wyatt *et al.* 2009, Yerbury *et al.* 2007). Clusterin forms long-lived stable complexes with oligomers of Aβ ranging from dimers to 50-mers (Narayan *et al.* 2012b). Clusterin is a predominant Aβ-binding protein in CSF (Ghiso *et al.* 1993). An estimated K_d of the clusterin-Aβ interaction has been calculated to be 4.8 nM (Hammad *et al.* 1997). Clusterin is found co-localised with Aβ in extracellular amyloid deposits (Yerbury *et al.* 2007). It has been suggested that clusterin binds to small Aβ oligomers *in vivo* in order to keep the aggregates soluble, prevent their further formation into toxic aggregates, and facilitate their uptake and degradation via receptor-mediated endocytosis (Wyatt *et al.* 2011). Clusterin interacts with the cell surface receptor megalin, which mediates clusterin-Aβ uptake (Hammad *et al.* 1997).

Cystatin C (CC)

Cystatin C (CC) is a protein found in all body fluids and tissues. Cystatins are inhibitors of cysteine proteinases and CC has a broad spectrum of biological roles (Bobek *et al.* 1992). Within the brain CC has been implicated in the repair of the nervous system and in the response to neurodegeneration (Levy *et al.* 2006). There is evidence that neuronal cells are protected directly by CC against a variety of toxic insults, including Aβ induced

toxicity. CC is itself prone to amyloid formation upon formation of domain-swapped dimers (Janowski *et al.* 2001, Staniforth *et al.* 2001).

CC has been shown to co-localise with Aβ plaque deposits in animal models (Steinhoff *et al.* 2001, Uchida *et al.* 1997, Wei *et al.* 1996). CC predominantly co-localises with Aβ in the brains of AD patients in senile plaque cores (Maruyama *et al.* 1990, Vinters *et al.* 1990) and amyloid-laden vascular walls (Bobek *et al.* 1992).

CC binds to soluble Aβ to inhibit Aβ fibrillisation and oligomerisation in a concentration dependent manner (Sastre *et al.* 2004, Selenica *et al.* 2007). The interaction involves residues 101-117 of CC (Juszczyk *et al.* 2009) and the N-terminal domain of Aβ (residues 1-17) with a K_d in the low nanomolar range (Sastre *et al.* 2004). This inhibitory effect has been observed *in vivo* in mice over-expressing both CC and APP (Kaeser *et al.* 2007, Mi *et al.* 2007). CC concentrations found endogenously do not seem to be sufficient to inhibit Aβ deposition in AD. Moreover, reduced levels of CC have been observed in AD patients (Hansson *et al.* 2009). A polymorphism of the CC gene (*CST3*), which reduces CC secretion, has been identified to increase the risk of developing AD (Finckh *et al.* 2000). Additionally, two PS2 mutations associated with AD cause reduced CC secretion and alter CC trafficking (Ghidoni *et al.* 2007).

Serum Amyloid P Component (SAP)

Serum amyloid P component (SAP) is a member of the pentraxin family of proteins, which are characterised by their homo-pentameric disc-like structure. SAP monomers are 25 kDa in size and rich in anti-parallel β-strands (Emsley *et al.* 1994, Wood *et al.* 1988). SAP is synthesised and catabolised in the liver (Hutchinson *et al.* 1994) and is present in

the CSF at concentrations of approximately 8.5 ng/ml (Hawkins *et al.* 1994). SAP is universally found in all amyloid deposits, including AD plaques (Coria *et al.* 1988, Pepys *et al.* 1982). SAP is found especially in plaques with fibrillar Aβ deposits but not in diffuse plaques (Veerhuis *et al.* 2003).

The interaction of SAP with Aβ is Ca^{2+}-dependent and has a K_d of 6 nM at pH 7.5 (Hamazaki 1995b). SAP will promote the aggregation of Aβ at physiological CSF concentrations (Hamazaki 1995a). The SAP-Aβ interaction depends on the degree of Aβ fibril formation. SAP will bind to mature fibres, covering the surface of the fibres, but not protofibrils (Nielsen *et al.* 2000).

SAP inhibits the degradation of amyloid fibrils by proteases. It has been suggested that SAP binding to Aβ fibres *in vivo* masks their fibrillar conformation, inhibiting their degradation (Tennent *et al.* 1995).

Islet Amyloid Polypeptide (IAPP)

Islet amyloid polypeptide (IAPP) is a 37 residue peptide hormone. It is mainly produced and secreted by β-cells in the pancreas (Westermark *et al.* 1987). IAPP shares a high degree of sequence identity (25 %) and similarity (50 %) with Aβ (O'Nuallain *et al.* 2004). IAPP is also prone to formation of amyloid fibrils and its deposition in the pancreatic islets are a characteristic of type II diabetes.

In vitro studies have shown that early nonfibrillar and nontoxic Aβ and IAPP species bind each other with high affinity forming soluble, nonfibrillar, and nontoxic heteroligomers. The cytotoxic self-association and amyloidogenesis of both Aβ and IAPP are delayed by

this interaction (Yan *et al.* 2007). However, preformed IAPP or Aβ fibrils are able to seed Aβ-IAPP oligomers to further aggregate into hetero-fibrillar cytotoxic assemblies (Yan *et al.* 2014). Short peptide sequences of Aβ and IAPP have been identified as 'hot regions' of the Aβ-IAPP interaction, which are the shortest sequences that are able to cross-interact with a high affinity. These sequences are also involved in the self-association of the peptides (Andreetto *et al.* 2010).

There is a positive association between IAPP and Aβ levels in the serum of AD patients (Qiu *et al.* 2014). Injection of IAPP into AD mouse models reduces the amyloid burden and Aβ levels in the brain, improving their learning and memory. Injection causes the translocation of Aβ from the brain into the CSF and plasma (Zhu *et al.* 2014). These results suggest a protective effect of IAPP in AD. However, IAPP deposition has been witnessed in the brain parenchyma and blood vessels of late-onset AD patients without clinically apparent diabetes. IAPP deposition co-localised with Aβ deposition was only occasional (Jackson *et al.* 2013) raising the possibility that IAPP can also contribute to AD aetiology.

Human Serum Albumin (HSA)

In the blood plasma 90-95 % of Aβ is directly bound to HSA (Biere *et al.* 1996, Kuo *et al.* 2000). The interaction between Aβ and HSA is investigated and discussed in detail in Chapters 3 and 4.

Transthyretin (TTR)

Transthyretin (TTR), also known as prealbumin, is a 55 kDa tetrameric protein synthesised predominantly in the liver. It is a thyroid hormone carrier and vitamin A

transporter (Andrea *et al.* 1980, Monaco 2002, Raz *et al.* 1969). It is found in the serum and CSF at concentrations of 3-7 μM and 0.1-0.36 μM, respectively (Vatassery *et al.* 1991). TTR is a major Aβ-binding protein in CSF and decreased CSF TTR concentrations have been reported in AD patients (Hansson *et al.* 2009, Riisøen 1988, Serot *et al.* 1997). Aβ added to CSF is quickly sequestered by TTR into stable complexes (Schwarzman *et al.* 1994).

TTR has been shown to bind Aβ *in vitro* and inhibit Aβ fibrillisation (Schwarzman *et al.* 1994, Schwarzman *et al.* 2004, Yang *et al.* 2013). TTR binds to all forms of Aβ; monomers, oligomers and fibrils (Buxbaum *et al.* 2008, Costa *et al.* 2008, Giunta *et al.* 2005, Liu *et al.* 2006). However, it binds Aβ aggregates better than monomeric Aβ (Buxbaum *et al.* 2008, Du *et al.* 2010, Liu *et al.* 2006). There is also preference for Aβ alloform, binding Aβ(1-42) better than Aβ(1-40) (Buxbaum *et al.* 2008). Binding is dependent on the quaternary structure of TTR, with TTR monomers binding better than tetramers (Du *et al.* 2010). The stoichiometry and affinity of binding are difficult to establish with very different K_ds published of 430 μM and 28 nM (Costa *et al.* 2008, Liu *et al.* 2006).

Aβ-TTR complexes have been isolated from brains of transgenic mouse models of AD and human AD brains (Buxbaum *et al.* 2008, Li *et al.* 2011b). Crossing the APP23 AD mouse model with a mouse over-expressing TTR normalised cognitive function and decreased the amount of Aβ deposited normally observed with the APP23 model (Buxbaum *et al.* 2008). Additionally, TTR knock-out APP23 mice develop Aβ deposits sooner than APP23 mice (Buxbaum *et al.* 2008).

Peptides derived from the Aβ-binding domain in TTR are also able to bind Aβ and inhibits its toxicity (Cho *et al.* 2014).

Tau

Phosphorylated tau has been found to interact with monomeric and oligomeric Aβ in damaged neurons in both mouse AD models and AD patients (Manczak *et al.* 2013). The levels of Aβ-tau complexes in the CSF are decreased in AD patients compared to other types of dementia and non-demented controls (Kristofikova *et al.* 2014). Aβ binds tau with an affinity in the low nanomolar range, which is tighter than the affinity of tau for itself (Guo *et al.* 2006). Formation of the stable Aβ-tau complex enhances phosphorylation of tau, which promotes dissociation of the complex (Guo *et al.* 2006).

A very recent study has shown that amyloidogenic regions of the two peptides, Aβ(25-35) and tau(273-284), will cross-interact and polymerise to form heteroligomers. The incorporation of tau into Aβ(25-35) reduces the propensity of Aβ(25-35) to fibrillise. However, this incorporation also promotes the advancement of tau monomers and dimers to larger oligomers and aggregates (Do *et al.* 2014).

1.8.2. Metal Ions

Some transition metal ions are found concentrated in AD plaques, in particular Cu^{2+}, Zn^{2+}, and Fe^{3+} (Lovell *et al.* 1998, Miller *et al.* 2006). These transition metal ions can interact with Aβ and affect its fibrillisation. The interaction of Aβ with Cu^{2+} has been studied most extensively and is discussed in detail in Chapter 5.

Zn^{2+} ions completely inhibit Aβ fibrillisation, even at low concentrations of both Aβ and Zn^{2+} (Chen *et al.* 2011, Noy *et al.* 2008, Sarell *et al.* 2010). Zn^{2+} can form an inter-molecular complex with Aβ, cross-linking histidine residues on multiple Aβ molecules (Faller *et al.* 2009, Miller *et al.* 2010, Minicozzi *et al.* 2008, Syme *et al.* 2006), which likely inhibits fibrillisation by interfering with the cross-β assembly (Viles 2012). Aβ loaded with Zn^{2+} has also been shown to form annular pore-like oligomers (Chen *et al.* 2011).

The affinity of Fe^{3+} for Aβ is relatively weak (Garzon-Rodriguez *et al.* 1999, Valensin *et al.* 2011) yet iron dysregulation of iron has been shown to exacerbate the AD phenotype in fly and mice models (Grossi *et al.* 2009, Liu *et al.* 2011, Rival *et al.* 2009). Fe^{3+} inhibits the rate of Aβ fibrillisation (Chen *et al.* 2011, Liu *et al.* 2011), influencing fibre morphology such that shorter, more curved fibres are generated. This altered morphology may be what influences Aβ toxicity (Liu *et al.* 2011).

1.9. HUMAN SERUM ALBUMIN

The HSA-Aβ interaction is of particular interest in this thesis and is investigated in Chapters 3 and 4. In this section an overview of the role and structure of HSA is given.

1.9.1. Location and Function

HSA synthesis takes place in the liver. The gene is located on chromosome 4 and undergoes post-translational cleavage in the rough endoplasmic reticulum and Golgi vesicles before it is secreted into the blood stream (Putnam 1975). HSA is the most abundant protein in the blood plasma at a concentration of ~ 640 μM. It has many functions, mainly as a transport protein but it also maintains oncotic pressure and pH in

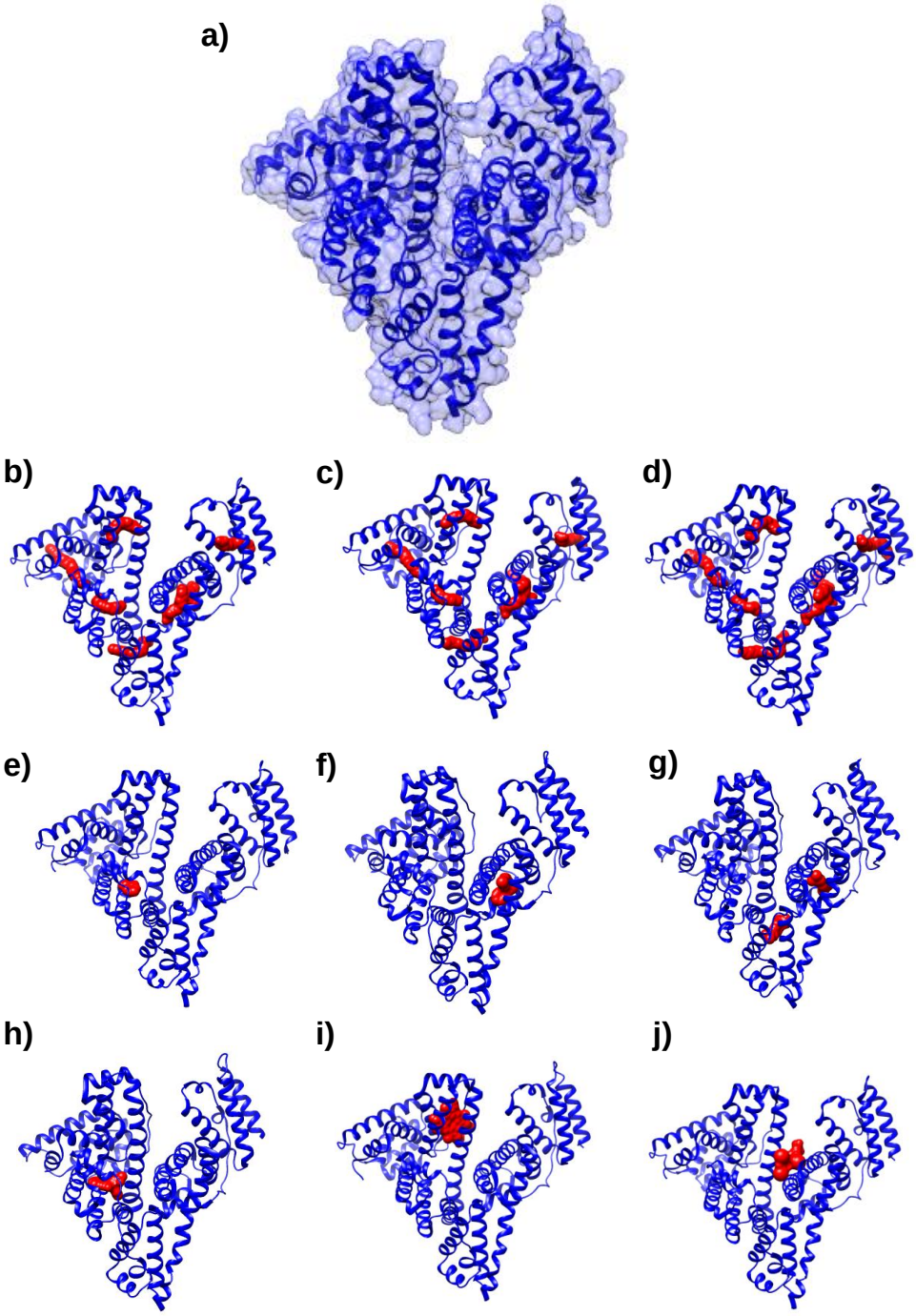

Figure 1.12. The Crystal Structure of HSA and Ligand Binding Sites.

a) The crystal structure of HSA with no ligands bound (1AO6). b-j) The crystal structure of HSA with common ligands bound shown as red space fill structures. b) myristic acid (1E7G), c) palmitic acid (1E7H), d) stearic acid (1E7I) e) aspirin (2I2Z), f) diazepam (2BXF), g) ibuprofen (2BXG), h) warfarin (2BXD), i) heme (1N5U), j) thyroxine (1HK4). The four-character code in brackets denotes the assigned code in the RCSB protein data bank from which the images were generated in UCSF Chimera.

the blood plasma. HSA is also the most abundant protein in the CSF but its concentration is much reduced compared to the blood plasma at ~ 3 μM (Stevens *et al.* 1979).

1.9.2. Structure

Monomeric HSA is 585 residues in length with a molecular mass of approximately 66 kDa. HSA is a largely alpha helical globular protein with 67 % of the residues forming helices. The remainder is mainly formed form extended peptide chains with 10 % forming β-loops. The crystal structure is shown in Figure 1.12a (Carter *et al.* 1994). It comprises three domains that are in turn divided into two subdomains, which together form a heart-like shape. It contains 35 cysteines, which form 17 disulphide bridges that stabilise the fold. A dimer of HSA can form that is joined by a disulphide bridge between the free thiol from Cys^{34} in each monomer. HSA has many hydrophobic pockets that bind a variety of hydrophobic molecules.

1.9.3. Common Ligands

HSA binds a wide variety of ligands including fatty acids, thyroid hormones, metal ions and pharmaceuticals. The crystal structures of many ligands binding to HSA have been deposited in the RCSB Protein Data Bank. The majority of these are for different chain length fatty acids, such as myristic acid, palmitic acid, and stearic acid (Figure 1.12 b-d) (Bhattacharya *et al.* 2000). However, crystal structures of HSA complexed with common pharmaceuticals (Ghuman *et al.* 2005, Yang *et al.* 2007), heme (Wardell *et al.* 2002) and the thyroid hormone thyroxine (Petitpas *et al.* 2003) have also been resolved (Figure 1.12e-j). It is clear that, with the exception of thyroxine, all of these ligands bind in one or more of seven hydrophobic pockets on HSA.

In addition to HSA binding hydrophobic ligands, HSA is also a Cu^{2+} transport protein. The site of Cu^{2+} binding has been identified to involve the N-terminal residues DAH (Patel *et al.* 1993). The affinity of the Cu^{2+}-albumin is extremely tight with a K_d of 1 pM (Rózga *et al.* 2007).

1.10. AIMS OF THIS THESIS

Although a great deal of progress has been made since Aβ was first isolated in the 1980s, many important details relating to its interaction with endogenous proteins and metal ions are missing. The main aims of this thesis are outlined below, but more detailed aims are within each of the results chapters, chapters 3 to 6.

I. Compare the fibril formation of Aβ in the presence and absence of HSA at CSF concentrations, to establish the influence of HSA on Aβ self-association (Chapter 3).
II. Determine the nature of the interaction between Aβ and HSA in terms of the size of the Aβ species and location of binding as well as the influence of cholesterol and other endogenous albumin binding molecules (Chapter 4).
III. Determine the affinity of monomeric, oligomeric and fibrillar Aβ to ascertain if Aβ has a high enough affinity for Cu^{2+} to compete with HSA for Cu^{2+} and be physiologically relevant (Chapter 5).
IV. Develop predictive rules for Cu^{2+}-peptide coordination geometry using visible CD and use these to investigate the coordination and affinity of Cu^{2+} for other amyloid peptides, specifically the prion protein and alpha-synuclein (Chapter 6).

CHAPTER TWO:

MATERIALS, METHODS AND THEORY

In this chapter I first outline a little of the basic theory behind some of the techniques employed in this thesis. This is followed by materials and methods. Methods used in a single chapter can be found in the individual chapters.

2.1 THEORY

2.1.1 Absorbance (UV-Vis) Spectroscopy

This technique uses the ultraviolet (UV), 180 to 400 nm, and visible (Vis) spectrum, 400 to 800 nm. The basis of absorbance spectroscopy is that the energy from UV-Vis radiation can excite peripheral electrons from a ground state to a higher energy level. The wavelength (energy) of light absorbed depends on the energy difference between the two electronic orbitals and is therefore a characteristic of the particular molecule. The more energy required, the shorter the wavelength at which absorbance will occur. Transition metals have electrons in their d-orbitals, the energy difference between d-orbitals is small and so typically occur in the visible region. π-orbital transitions found in, for example, aromatic rings, such as those in the side chains of the amino acids tryptophan and tyrosine, require more energy giving an absorption spectrum close to 280 nm.

UV-Vis spectroscopy is a particularly useful approach to determine the concentration of proteins. The absorbance of tryptophan and tyrosine side-chains, along with disulphide bonds at 280 nm can be used as concentration monitors of proteins. The Beer-Lambert law (eq 2.01) highlights the linear relationship between absorbance and concentration of a protein:

$$A = \varepsilon . c . l \qquad \text{(eq 2.01)}$$

Rearrangement of this equation to make concentration the product is demonstrated by eq 2.02:

$$c = \frac{A}{\varepsilon . l} \qquad \text{(eq 2.02)}$$

where A is the absorbance, c is the molar concentration of a protein, ε is the extinction coefficient of the side chains and l is the pathlength in centimetres (cm). To calculate the concentration of a protein in a 1 cm pathlength cuvette using the absorbance at 280 nm, the following equation (eq 2.03) would be used to account for the contribution of each Trp and Tyr residue and each disulphide bond:

$$c = \frac{A_{280}}{\varepsilon^{Trp}.N_{Trp} + \varepsilon^{Tyr}.N_{Tyr} + \varepsilon^{S\text{-}S}.N_{S\text{-}S}} \qquad \text{(eq 2.03)}$$

where ε^x is the extinction coefficient and N_x is the number of the chromophores (Gill *et al.* 1989). Substituting in the extinction coefficients of each of the chromophores at 280 nm gives equation 2.04:

$$c = \frac{A_{280}}{5690.N_{Trp} + 1280.N_{Tyr} + 120.N_{S\text{-}S}} \qquad \text{(eq 2.04)}$$

When measuring the concentration of proteins, any light scatter present due to aggregates in solution must be taken into account to avoid an overestimate of the A_{280}. The effect of light scattering is determined at longer wavelengths prior to the onset of the absorption at 280 nm, specifically over the wavelength range 320-350 nm. The absorption intensity at 280 nm that is due to light scatter is calculated from equation 2.05:

$$A_{scatter,280} = 10^{(2.5\log A_{320} - 1.5\log A_{350})} \qquad \text{(eq 2.05)}$$

The equation used for determination of the concentration of a protein in a 1 cm pathlength cuvette, accounting for light scatter, therefore becomes equation 2.06:

$$c = \frac{A_{280} - 10^{(2.5\log A_{320} - 1.5\log A_{350})}}{5690.N_{Trp} + 1280.N_{Tyr} + 120.N_{S\text{-}S}} \qquad \text{(eq 2.06)}$$

Only absorbance measurements between 0.1-1 are used (ideally at 0.8) because it is inaccurate to determine concentration outside this range of absorbance values. Quartz glass cuvettes are used because quartz does not absorb light in the UV- or the Vis-regions.

For further information on absorbance spectroscopy, Chapters 12 and 13 by Alex Drake in "Methods in Molecular Biology" volume 22 are an excellent guide (Drake 1994a, Drake 1994b).

2.1.2 Fluorescence Spectroscopy

Electrons that have been excited to a higher state, as described for absorption spectroscopy, emit energy when they return to their ground state. This energy may be emitted as heat or occasionally as light radiation. Fluorescence spectroscopy measures this light radiation after excitation. The emitted light will have less energy than the excitation energy due to energy lost from collisions and heat thus will emit light at a longer wavelength, known as the Stokes shift (Figure 2.01). Substances that exhibit fluorescence typically have delocalised electrons, in the form of conjugated double bonds and are referred to as fluorophores.

Despite the intensity of a fluorescence signal potentially being proportional to the concentration of the fluorophore, assuming there is no self-absorption or quenching, values obtained from fluorescence spectroscopy cannot be compared between machines. This is because the amount of fluorescence detected from a system is not consistent with instrumentation. Fluorescence units are therefore described as arbitrary fluorescence units (AFU).

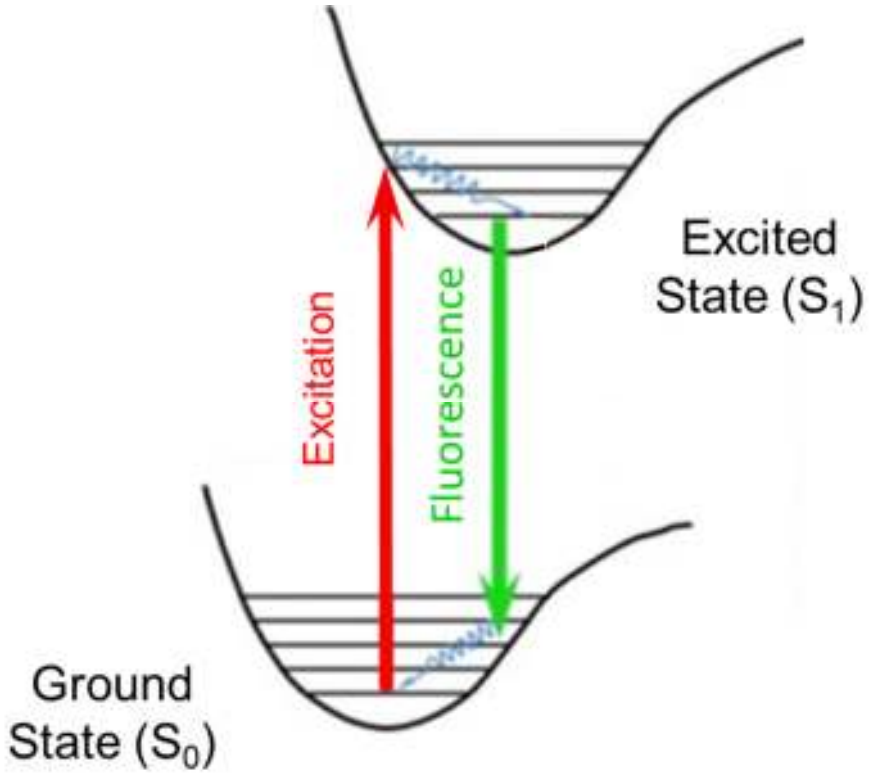

Figure 2.01. State Diagram of Fluorescence.

Electrons are excited to a high energy state at one wavelength and emit fluorescence at a lower energy wavelength due to energy lost through heat and collisions. Adapted from (Wei *et al.* 2012).

For further information on the theory of fluorescence, refer to "Principles of Fluorescence Spectroscopy" (Lakowicz 1999) and Chapter 15 of "Methods in Molecular Biology" volume 22 (Varley 1994)

Two different types of instrumentation have been used in this thesis to detect fluorescence; single-cell spectrophotometers and multi-well fluorescence readers.

Single Cell Fluorescence

A fluorescence spectrophotometer uses a xenon lamp to produce a light beam, which is converged on to the entrance slit of the excitation monochromator through two lenses. After monochromation the excitation beam is converged on to the sample cell. The emitted fluorescence is detected at 90^{o} to the excitation beam through the emission slit, which is then directed to the computer resulting in a fluorescence spectrum (see Figure 2.02a).

The advantage of using a single-cell spectrophotometer is that the monochromator allows any excitation wavelength to be used and an emission spectrum sweeping a large range of wavelengths to be collected.

Multi-Well Fluorescence

A multi-well spectrometer can hold multi-well plates that allow for many fluorescence experiments to be run concomitantly under identical conditions (e.g. temperature or agitation). Rather than containing a monochromator like the single-cell spectrophotometer, the excitation and emission wavelengths are controlled by filters in a multi-well fluorescence reader. The fluorescence detected is therefore at a wavelength specific to the emission filter used, not a spectrum. An outline of the set-up of a multi-

a)

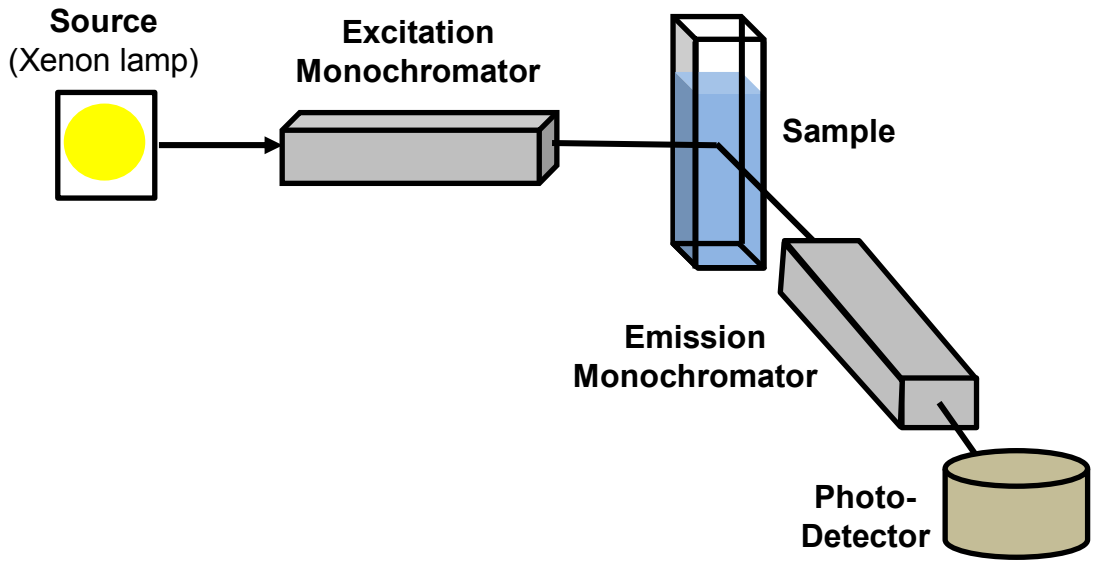

b)

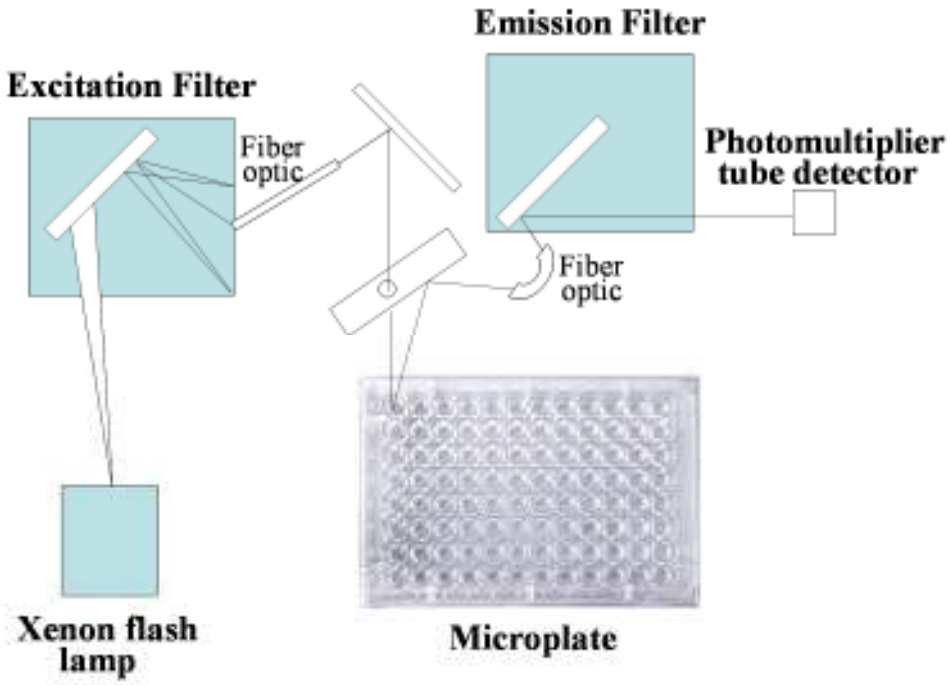

Figure 2.02. Schematics of Typical Fluorescence Reader Systems.

The typical set up of a) a single-cell fluorescence spectrometer, and b) a multi-well fluorescence reader Adapted from (Lakowicz 1999).

well plate fluorescence reader is shown in Figure 2.02b. The multi-well fluorescence reader used throughout this thesis (BMG Fluostar Galaxy) allows for orbital shaking of the multi-well plate in addition to temperature control. The fluorescence emission can be detected from above or below the plate.

Two types of fluorophore exist; intrinsic fluorophores and extrinsic fluorophores. Intrinsic fluorophores include the side chains of aromatic amino acids, such as tyrosine and tryptophan. Extrinsic fluorescence requires the addition of a fluorescent probe to a sample, such as Thioflavin T (ThT) in the case of amyloid fibre detection.

ThT Fluorescence

ThT fluorescence was used in this thesis to study Aβ fibre formation. ThT is a fluorescent dye that interacts with amyloids (Sunde *et al.* 1997). The structure of ThT is shown in Figure 2.03. It has a K_d of ~ 1 μM for Aβ amyloids and the interaction is not affected by salts, such as NaCl (LeVine 1993). ThT will only fluoresce once bound to amyloid fibrils. Fluorescence is observed at ~ 490 nm when excited at 440 nm. The stoichiometric ratio used in this thesis is 1:2 Aβ:ThT.

Intrinsic Tyrosine Fluorescence

Intrinsic tyrosine fluorescence was used in establishing the affinity of Aβ for Cu^2. Aβ contains a tyrosine at position 10, which when excited at 280 nm will emit fluorescence at ~ 310 nm. The intrinsic tyrosine fluorescence of Aβ can be quenched by binding of Cu^{2+} close to the fluorophore. The tyrosine fluorescence will return when the Cu^{2+} is no longer bound to Aβ, which can be achieved through the use of a competing ligand with a known affinity for Cu^{2+}.

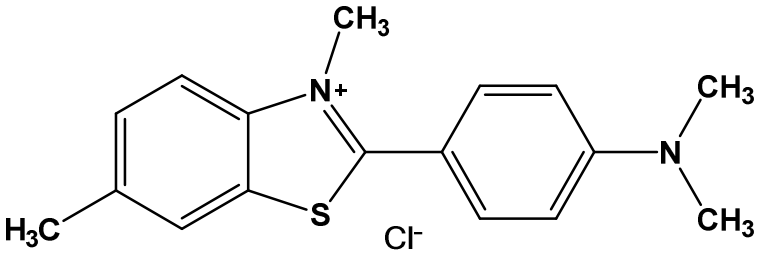

Figure 2.03. The Structure of Thioflavin T.

2.1.3 Circular Dichroism Spectroscopy

Circular dichroism (CD) spectroscopy is a form of absorption spectroscopy that uses circularly polarised light. Circularly polarised light can rotate clockwise (right) and anti-clockwise (left). The difference in absorption (ΔA) between the left (A_L) and right (A_R) circularly polarised light by a chromophore results in a CD spectrum. A difference between the absorption depends on the chirality of the chromophore thus a non-chiral molecule will absorb left and right circularly polarised light to the same extent, resulting in no CD signal. A diagram of the main features of a CD instrument is shown in Figure 2.04.

The difference in absorption can be related to the molar extinction coefficient using the Beer-Lambert law (eq 2.07):

$$\Delta\varepsilon = \frac{\Delta A}{c.l} \qquad \text{(eq 2.07)}$$

where $\Delta\varepsilon$ is the difference in molar extinction coefficient, or molar ellipticity, ΔA is the difference in absorbance, c is the molar concentration and l is the pathlength of the sample in centimetres.

The relationship between the direct CD measurements, θ (mdeg) and ΔA is shown in equation 2.08.

$$\theta = \Delta A \,.\, 33{,}000 \qquad \text{(eq 2.08)}$$

Therefore, the direct CD measurements can be converted to molar ellipticity ($\Delta\varepsilon$) with units of $M^{-1}cm^{-1}$ through the combination of equations 2.07 and 2.08 (eq 2.09).

$$\Delta\varepsilon = \frac{\theta}{33000.c.l} \qquad \text{(eq 2.09)}$$

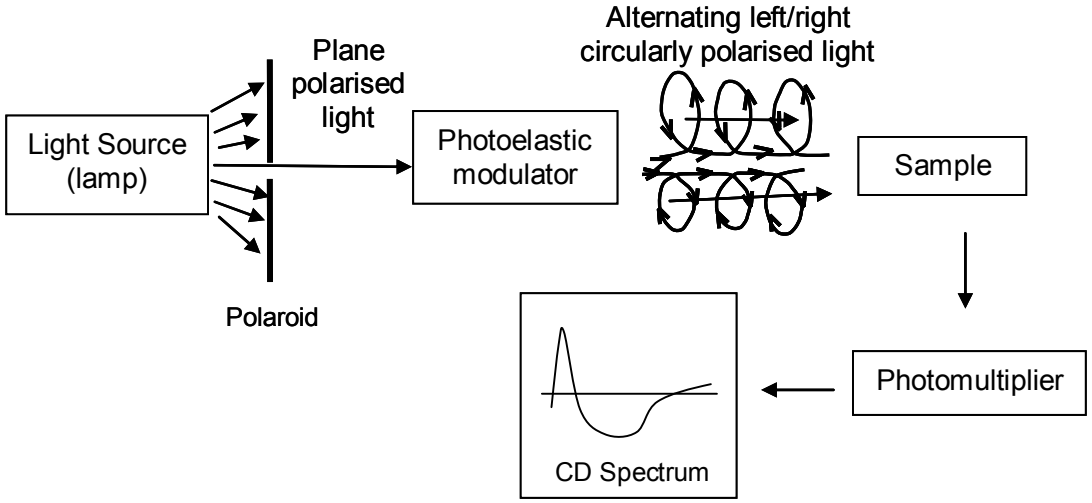

Figure 2.04. Schematic of the Basic Components of a CD Spectrometer.

Adapted from (Drake 1994c).

Visible CD

Visible CD (Vis-CD) utilises wavelengths 300 to 800 nm of the light spectrum. Therefore, like visible absorbance spectroscopy, it is useful for observing d-d transitions of metal ions. As Vis-CD requires a chiral chromophore, the metal ion typically forms a complex with a ligand to be chirally active. There are three particular effects which contribute to the activity of a metal–ligand complex, these are:

- The configurational effect. This occurs when the distribution of donor atoms coordinating the metal ion are asymmetrical.

- The conformational effect. This is due to ring puckering and is less applicable to complexes with planar coordination geometry of Cu^{2+} and Ni^{2+} complexes studied in this thesis.

- The vicinal effect. This effect is observed when a chiral carbon atom is in the backbone of a ring between two chelated donor atoms, typically main chain amides. This effect is the main determinant of optical activity in metal-peptide complexes studied in this thesis.

These effects mean that in addition to free metal ions, metal ions bound to non-chiral molecules, such as glycine, also have no optical activity and are CD silent. This was exploited in calculating an affinity for peptide-Cu^{2+} complexes in Chapter 6.

For more information on the theory of circular dichroism (CD), refer to Chapter 16 of "Methods in Molecular Biology", Volume 22 (Drake 1994c) and Chapter 10 of "Biophysical Tools for Biologists", Volume 1 (Martin *et al.* 2008).

2.1.4 Electron Paramagnetic Resonance

Electron paramagnetic resonance (EPR), also known as electron spin resonance, studies the resonant transitions between energy levels of electron magnetic dipole moments. Every electron has a magnetic dipole moment, which can either align parallel (low energy state) or anti-parallel (high energy state) to an applied external magnetic field. The magnetic field is scanned such that the energy of the applied electromagnetic radiation matches the gap between these low and high energy states, thus allowing the electrons to move between their two states. The EPR spectrum is converted from the net absorption of energy that occurs due to more electrons being in the low energy state.

The spin, which is the intrinsic angular momentum of an electron, is another vector of EPR. All elementary particles of a given kind have the same unitless spin quantum number. For example, the copper nucleus has a spin of 3/2 and an electron has a spin of 1/2. Only species which contain unpaired electrons, such as Cu^{2+} which has one unpaired electron in its outer shell, have the spin necessary to interact with the applied electromagnetic field.

A simple energy level diagram for an electron with spin 1/2 is shown in Figure 2.05. The energy level separation can be changed by varying the applied magnetic field, B. Resonant absorption occurs if the frequency is adjusted so that $\Delta E = h\nu$. The separation between the low energy state and the high energy state is $\Delta E = g\mu_B B_z$. Therefore, this can be written as equation 2.10. The two states are described by the g-factor (g), the Bohr Magneton (μ_B) and the strength of the experimental magnetic field (B_z) in gauss.

$$\Delta E = h\nu = g\mu_B B_z \qquad \text{(eq 2.10)}$$

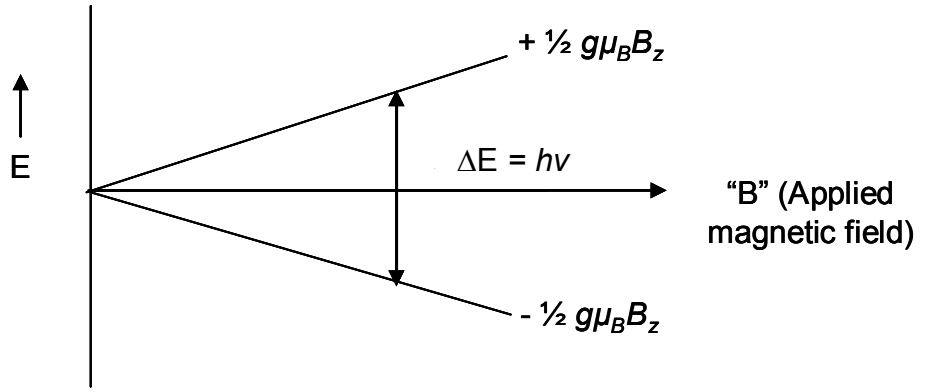

Figure 2.05. Energy Level Diagram for an Electron with Spin 1/2.

An unpaired electron moves between the two energy levels by either emitting or absorbing electromagnetic radiation (-1/2 $g\mu_B B_z$ and +1/2 $g\mu_B B_z$, respectively) such that $h\nu=\Delta E$. The 2 states are described by the g-factor (g), the Bohr Magneton (μ_B) and the strength of the magnetic field (B_z) in gauss. Adapted from (Weil *et al.* 2007).

Experimentally, it is easier to vary the magnetic field by small increments than vary the frequency of the radiation. The position of the line in an EPR spectrum is indicated by the value of the magnetic field at which the sample has absorbed energy. g-factors are used to denote line position instead of field or frequency due to differences in EPR spectrometers and experimental conditions.

The g-factor

The g-factor (g) is a dimensionless quantity, which can be used to identify the electronic structure of the paramagnetic centre. Comparisons between the g-factor for an electron in an experimental system (calculated using equation 2.10) and the g-factor for a free electron in a vacuum ($g_e = 2.002319$) can be used to obtain information on the nature of the atomic or molecular orbital containing the unpaired electron. This is particularly relevant for studies with transition metal ions, such as in this thesis, where the g-factors can be drastically affected by interactions between the electron spin and orbitals.

The only cause of the deviations of the g-factors from 2.002319 are the magnetic interactions involving the orbital angular momentum of the unpaired electron, which depends on its chemical environment. There are two interactions that involve the orbital angular momentum; its interaction with the external magnetic field and spin-orbit coupling. The spin-orbit coupling results from the nucleus "orbiting" around the electron (from the electron's point of view), which generates a magnetic field at the electron due to the motion of the positive charge.

The orbital motion of the electron is quenched when the electron is orbiting close to nuclei because of the electrostatic effect between the negatively charged electron and the nuclei. The orbital motion of the electron will be affected differently depending on whether the

electrostatic effect is equal along all the axes. Some examples of potential molecular geometries for peptide-Cu^{2+} complexes and the resulting EPR spectra are shown in Figure 2.06. Octahedral geometry is isotropic for all rotations (Figure 2.06a), whereas tetrahedral geometry is anisotropic for all rotations (Figure 2.06c). Axial square-planar geometry has linear rotational symmetry thus anisotropy is observable except when the applied magnetic field is in the plane perpendicular to the axis of symmetry (Figure 2.06b). Cu^{2+}-EPR is usually of the axial type (Figure 2.06b). Two components of the EPR spectrum shown are the g_{II} (the parallel g factor) and $g_{\perp}$ (the perpendicular g-factor), which are the g-factors appropriate to the magnitudes of the applied magnetic field when it is parallel or perpendicular to the system's symmetry axis, respectively. Figure 2.06b shows a major absorption at $g_{\perp}$ (high field) and a lesser absorption at g_{II} (low field).

Hyperfine Splitting

After unpaired electrons are placed in a magnetic field, the number of energy levels are increased from one to two ($E = + \frac{1}{2} g\mu_B B_z$ and $E = - \frac{1}{2} g\mu_B B_z$), as shown in Figure 2.05. This increase in the number of energy levels through exposing the electrons to a magnetic field is called splitting. Further splitting in energy levels, known as hyperfine splitting, arises from the interactions between the electrons and the nucleus. The magnetic moment of the nucleus is restricted to a few particular orientations relative to the external magnetic field. For example, the copper nucleus has a spin of 3/2, and thus has nuclear spin orientations of +3/2, +1/2, -1/2 and -3/2. The nuclear magnetic moment's orientation affects the magnetic energy of the electron meaning absorption lines are obtained over a range of magnetic field values from what would otherwise be the one resonance absorption line. The EPR spectrum therefore consists of a number of bands rather than just one (see Figure 2.07). As well as the anisotropy in g there may be an anisotropy in the hyperfine splittings (A) as well. Typically for Cu^{2+}-EPR, the hyperfine splitting $A_{\perp}$

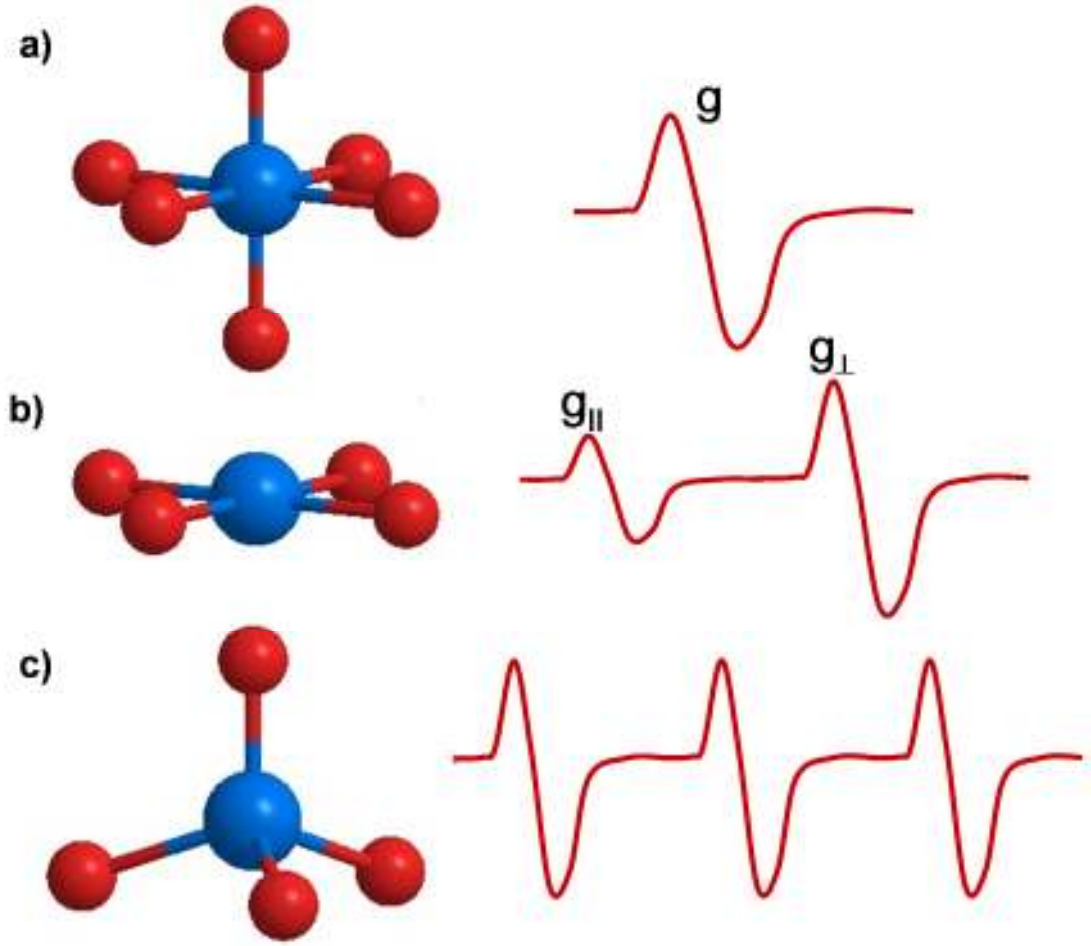

Figure 2.06. Typical EPR Spectra for Different Cu^{2+} Coordination Geometries.

The typical EPR spectra observed for Cu^{2+}-peptide complexes with a) octahedral, b) square-planar, and c) tetrahedral coordination geometries. Adapted from (Sarell 2010).

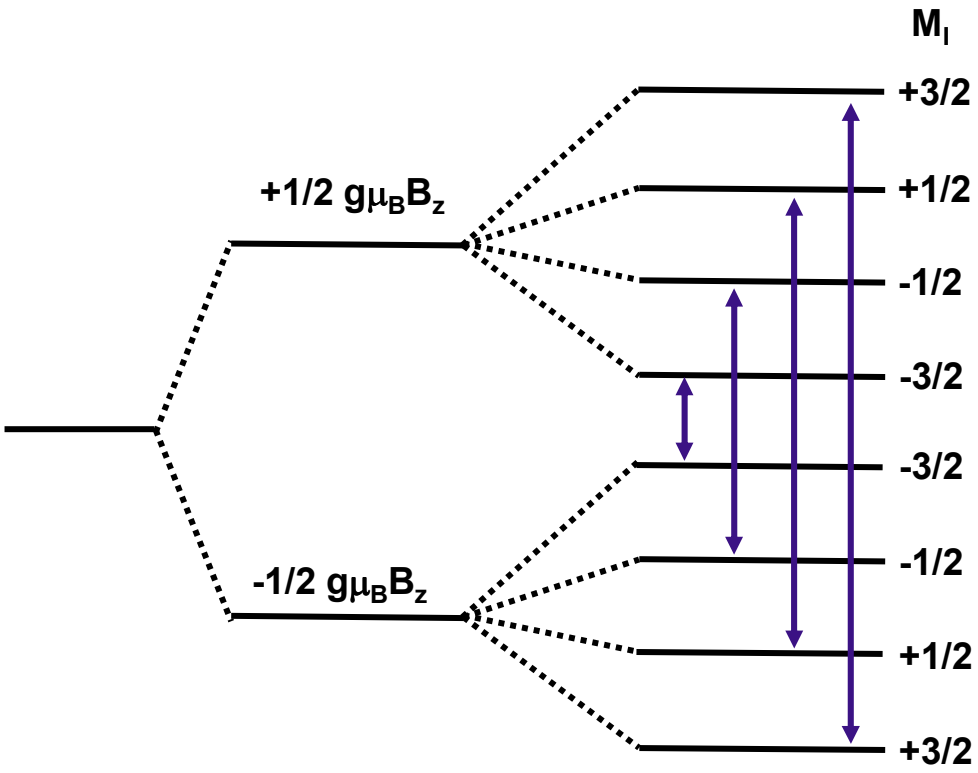

Figure 2.07. Hyperfine Splitting of the Cu^{2+} Electron

Four transitions are allowed from the ground state to the excited state based on the orientation of the nuclear angular momentum vector (M_I) shown by the purple arrows, which results in four splittings. If the magnetic field is kept constant, the smaller the difference between energy states, the lower the frequency is at which they occur.

(the hyperfine splitting at $g_{\perp}$) is poorly resolved, while the A_{II} (the hyperfine splitting at g_{II}) is much larger, with the four features at g_{II} resolved.

An idealised Cu^{2+}-peptide EPR spectrum is shown in Figure 2.08 with its two component parts arising from the axial coordination of Cu^{2+}, meaning anisotropy of the g-factor is exhibited, resulting in parallel (low field) and perpendicular (high field) components. The hyperfine splitting (A) results in four splittings within both components of the spectra. The g value is reported as the centre of the multiplet and A is measured as the field between splittings.

Using EPR to Identify Coordination Ligands

An influential paper by Peisach and Blumberg describes how EPR spectra of Cu^{2+} tetragonal complexes can be used to infer the identity of the ligands in the equatorial plane (Peisach *et al.* 1974). Using different classes of model compounds, they studied the relationship between the A_{II} and g_{II} values and produced a guide that can be used to suggest binding ligands in the complex, see Figure 2.09. The A_{II} values are obtained in gauss (ΔH) from the EPR spectrum but are converted to millikaysers (mK) for the Peisach-Blumberg plot using equation 2.11:

$$A = 0.046686 * g * \Delta H \qquad \text{(Eq 2.11)}$$

where g is the free electron g-factor (2.002319).

For more information on the theory of EPR, please refer to "Electron Paramagnetic Resonance: Elementary Theory and Practical Applications" (Weil *et al.* 2007).

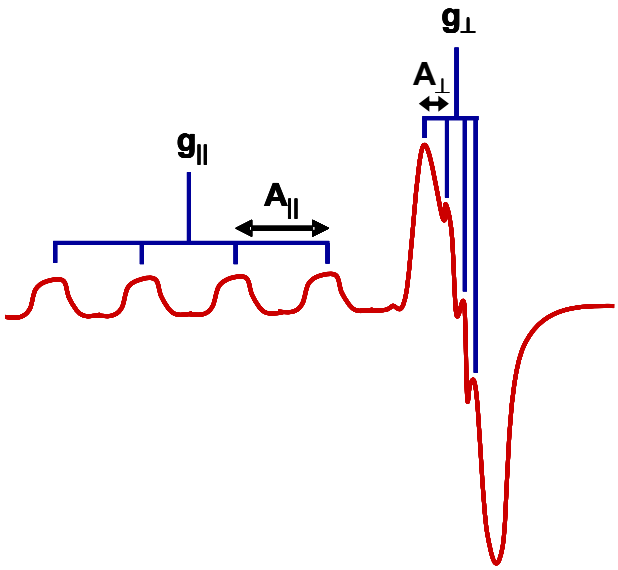

Figure 2.08. A Model EPR Spectrum for Cu^{2+}-Peptide Complexes

Cu^{2+} shows a square-planar geometry in the Cu^{2+}-peptide complex, giving g-parallel (g_{II}) and g-perpendicular ($g_{\perp}$) bands. There is clearly resolved hyperfine splitting of these bands (A_{II} and $A_{\perp}$) due to the orientation of the copper nucleus, which has spin of 3/2. Adapted from (Sarell 2010).

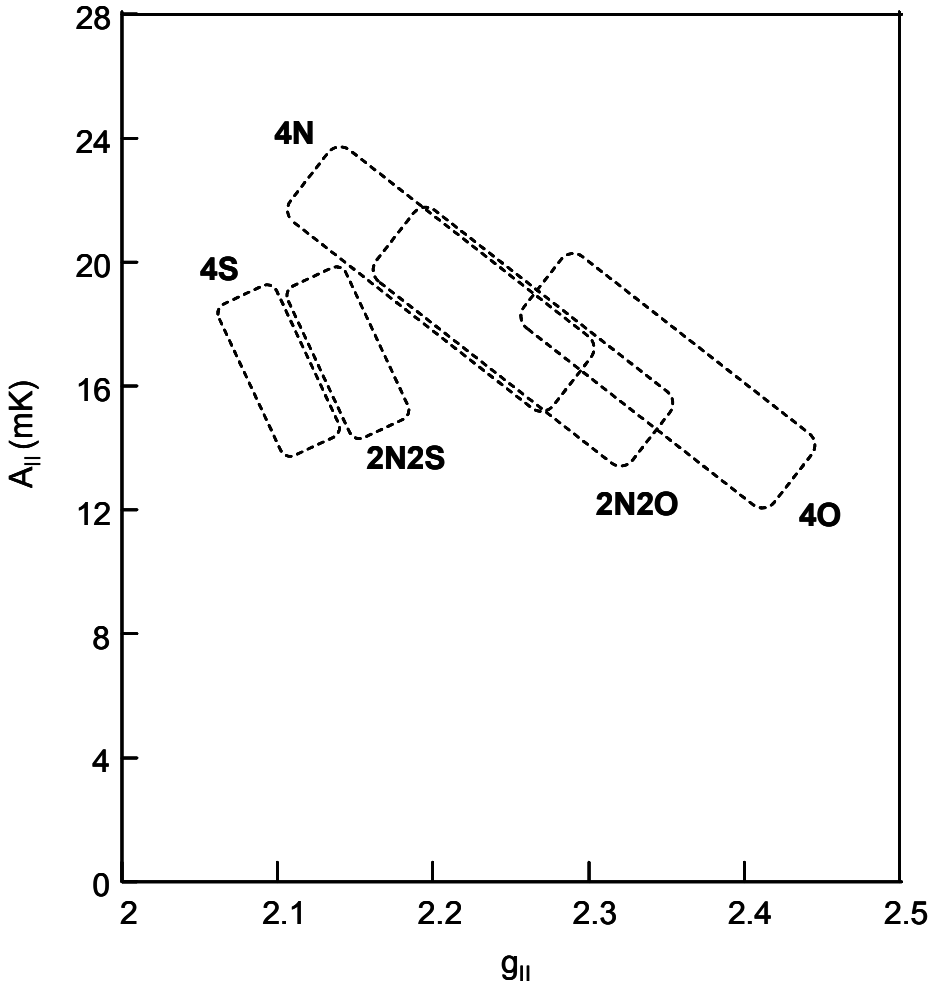

Figure 2.09. Peisach-Blumberg Plot

The Peisach-Blumberg plot can be used to predict the coordinating ligands (Nitrogen, Oxygen, Sulphur) of a Cu^{2+}-peptide complex with square-planar geometry from the relationship between the A_{II} and g_{II} obtained from an EPR spectrum. Adapted from (Peisach *et al.* 1974)

2.1.5 Affinity

The Principles of Affinity

Any reaction or binding event can be thought of as an equilibrium between the reactants and products. In the case of a protein (P) binding to a ligand (L) in a one to one ratio to form a protein-ligand complex (PL) then:

$$P+L \rightleftharpoons PL \qquad \text{(eq 2.11)}$$

The association constant (K_a) for this binding event is given by the ratio of the products formed relative to the reactants remaining (eq 2.12) and has units of $Molar^{-1}$.

$$K_a = \frac{[Product]}{[Reactants]} = \frac{[PL]}{[P][L]} \qquad \text{(eq 2.12)}$$

The reverse reaction, where the metal dissociates from the ligand, is inversely proportional to the K_a. The dissociation constant (K_d) is given by equation 2.13 and has units in Molar concentrations.

$$K_d = \frac{[P][L]}{[PL]} \qquad \text{(eq 2.13)}$$

The smaller the dissociation constant, and accordingly the bigger the association constant, the higher the affinity between the two components of the complex. The dissociation constant, K_d, is useful as it indicates at what concentration of ligand half of the protein's binding site will be occupied by the ligand. For example, for a complex with a K_d of 1 nM, at a ligand concentration of 1 nM, half of the available protein binding sites will be occupied. If the concentration of ligand is sub-nanomolar, then only a small amount of the ligand will be bound to the protein, even if the ligand is in excess relative to the protein. Alternatively, ligand concentrations much greater than 1 nM, will result in ligand occupying all available protein binding sites.

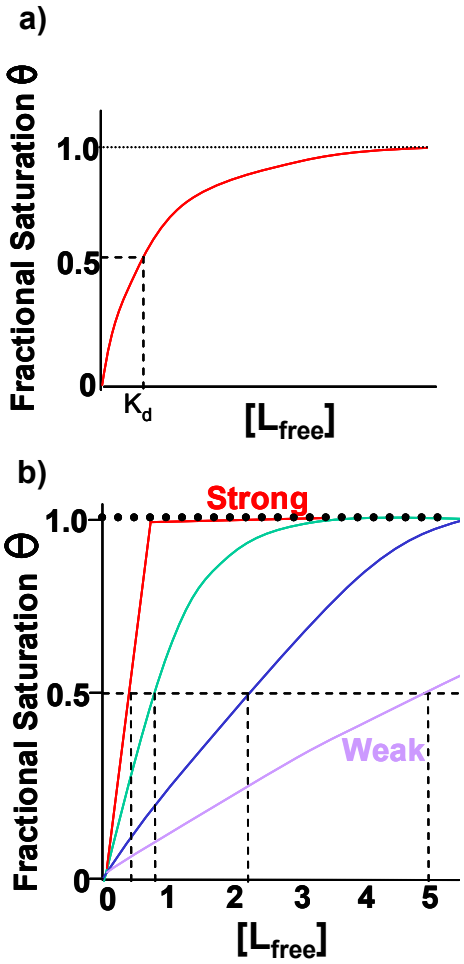

Figure 2.10. Ligand Binding Curves.

a) Shows a typical binding curve with saturation of the binding site (θ) on the y axis and free ligand concentration ($[L_{free}]$) on the x axis. The K_d is calculated at 50 % binding site saturation. b) Illustrates different binding curves seen for strong through to weak binding.

Effect of pH and Temperature

Stability constants can either be expressed as the 'absolute' affinity, a value which is pH-independent or the 'apparent affinity', a value which is pH-dependent. In this thesis the experimentally measured affinity of Cu^{2+}-peptide complexes is the apparent affinity. It is more useful to know the affinity at a particular pH, e.g. at physiological pH 7.4, as the affinity of Cu^{2+} for a peptide can be strongly influenced by pH. This is because H^+ ions can compete with Cu^{2+} ions for binding sites. Thus the affinity can be much tighter in alkaline conditions compared to acidic conditions.

The affinity of a peptide for a ligand is strongly influenced by its surroundings. Affinity is temperature dependent; the K_d increases with increasing temperature for exothermic reactions but decreases for endothermic reactions.

Methods of Calculating Affinity

There are multiple different ways the affinity of a complex can be determined, with any technique that can quantitatively measure the levels of products or reactants present potentially able to measure the affinity. In this thesis spectroscopic techniques, specifically Vis-CD, intrinsic tyrosine fluorescence and EPR, are employed.

A common method of presenting affinity data is as a binding curve. Binding curves are graphs of ligand concentration on the x axis against the saturation of the binding site (θ) on the y axis (see Figure 2.10a). The shape of the binding curve gives information of the strength of binding between the peptide and ligand, examples shown in Figure 2.10b. The dissociation constant K_d can be calculated when $\theta = 0.5$, i.e. half the ligand is bound and half is not. However, if the binding curve exhibits tight binding, it can only be determined that the K_d is stronger than the concentrations of peptide and ligand used. For tight

binding, all of the added ligand binds to the peptide, as it is titrated in, and no detectable free ligand remains in solution.

In this thesis, the equipment used to measure affinity requires micromolar concentrations of peptide and Cu^{2+} ions, which results in tight binding curves. The K_d therefore cannot be calculated directly. Consequently, competitive chelators with a known affinity for Cu^{2+} ions were used to generate an observed equilibrium between free Cu^{2+}, chelator-bound Cu^{2+} and peptide-bound Cu^{2+}.

Affinity Calculations

The absolute affinities (Abs K_a) of Cu^{2+} chelators commonly used in determining the affinity of Cu^{2+}-peptide complexes, glycine and nitrilotriacetic acid (NTA), are quoted at 25-30 °C at ionic strengths between 0.01 to 0.5 in "Data for Biochemical Research" (Dawson 1986). From this, the apparent stability constants (App K_a) at pH 7.4 can be calculated using equations 2.14 and 2.15. The Abs K_a, App K_a and App K_d for $Cu^{2+}(Gly)_2$, and Cu^{2+}(NTA) are shown in Table 2.01**.**

$$\log \alpha = pK_a - pH \qquad \text{(eq 2.14)}$$

$$\log \text{App } K_a = \log \text{Abs} K_a - \log \alpha \qquad \text{(eq 2.15)}$$

Table 2.01. The Affinities of Competing Cu^{2+} Chelators.

Copper Chelator		Log Abs K_a	Log App K_a at pH 7.4	App K_a at pH 7.4 (M^{-1})	App K_d at pH 7.4 (M)
NTA		13.1	10.7	$5.0 * 10^{10}$	$1.99 * 10^{-11}$
Glycine	K_{a1}	8.1	5.87	$7.4 * 10^{5}$	$1.35 * 10^{-6}$
	K_{a2}	7.1	4.87	$7.4 * 10^{4}$	$1.35 * 10^{-5}$

For example, the pK_a of NTA is 9.8 and the absolute affinity of NTA for Cu^{2+} is 13.1 (Dawson 1986) so using equations 2.14 and 2.15**,** the apparent affinity at pH 7.4 can be calculated:

$\log \alpha = 9.8\text{-}7.4 = 2.4$

$\log$ App K_a at pH 7.4 = 13.1 – 2.4 = 10.7

This gives an apparent affinity at pH 7.4 of $5.0 * 10^{10}$ M^{-1} or a dissociation constant of 19.9 pM.

Calculating the Affinity of Cu^{2+} for Peptides

At equilibrium, where the concentrations of Cu^{2+} bound to the peptide and Cu^{2+} bound to the competing chelator are evenly distributed, the K_d is equal to the concentration of free Cu^{2+}. For chelators that bind Cu^{2+} in a 1:1 complex, equation 2.16 can be used to calculate the K_d:

$$K_d = [Cu^{2+}_{free}] = \frac{[Cu^{2+}_{total}] - [Cu^{2+}_{bound\ to\ peptide}]}{1 + AppK_a[Competitor_{free}]} \quad \text{(eq 2.16)}$$

Where, $[Cu^{2+}_{bound\ to\ peptide}]$ is equal to half the Cu^{2+} concentration, $AppK_a$ is the apparent K_a of the competing chelator and $[Competitor_{free}] = [Competitor_{total}] - [Cu^{2+}_{bound\ to\ peptide}]$. Alternatively, the K_d can also be calculated from the observed K_d in the presence of the competing ligand by using equation 2.17 (Wells *et al.* 2006).

$$K_d = ObsK_d \cdot \frac{AppK_d}{[Competitor_{free}]} \quad \text{(eq 2.17)}$$

Where, $ObsK_d$ is the observed Kd and is equal to $[Cu^{2+}_{bound\ to\ peptide}]$ and the $AppK_d$ is the apparent K_d of the competing chelator.

Worked Example for Calculating Cu^{2+} Affinity for Aβ Using NTA as a Competing Chelator

Below is a worked example of calculating the affinity of Aβ(1-42) for Cu^{2+} using NTA as a competing Cu^{2+} chelator. The experimental specifics are taken from one of the fluorescence experiments in Chapter 5 (Figure 5.02a):

$[A\beta \text{ total}] = 10 * 10^{-6}$ M

$[Cu^{2+} \text{ total}] = 4 * 10^{-6}$ M

$[Cu^{2+}{}_{\text{bound to A}\beta}] = 2 * 10^{-6}$ M

Apparent K_a at pH 7.4 for NTA = $5.0 * 10^{10}$ M^{-1}

Apparent K_d at pH 7.4 for NTA = $2.0 * 10^{-11}$ M

$[NTA_{total}] = 6 * 10^{-6}$ M

$[NTA_{free}] = 6 * 10^{-6} - 2 * 10^{-6} = 4 * 10^{-6}$ M

Using equation 2.16:

$$K_d = \frac{(4*10^{-6})-(2*10^{-6})}{1+(5.0*10^{10})(4*10^{-6})}$$

$$K_d = \frac{2*10^{-6}}{200001}$$

$K_d = 9.99995 * 10^{-12}$ M = 10 pM

Similarly, using equation 2.17:

$$K_d = 2*10^{-6} . \frac{2*10^{-11}}{4*10^{-6}}$$

$K_d = (2 * 10^{-6})(5 * 10^{-6})$

$K_d = 10 * 10^{-12}$ M = 10 pM

Calculating the Affinity of Cu^{2+}-Peptide Complexes using Glycine as a Competing Chelator

Calculating the affinity of Cu^{2+}-peptide complexes using glycine, as I have in Chapter 6, is more complicated than using NTA. This is because glycine can form either a Cu(Gly) or $Cu(Gly)_2$ complex, thus their affinity is given by K_{a1} and K_{a2} (Dawson 1986), see Table 2.01. The equation used to calculate the K_d is similar to equation 2.16 but takes into account the two binding modes of Cu^{2+} to glycine:

$$K_d=\left[Cu^{2+}{}_{free}\right]=\frac{[Cu^{2+}{}_{total}]-[Cu^{2+}{}_{bound\ to\ peptide}]}{1+\ AppK_{a1}[Gly_{free}]+AppK_{a1}AppK_{a2}[Gly_{free}]^2} \qquad \text{(eq 2.18)}$$

If the Cu^{2+}-peptide complex has an affinity much tighter than the Cu(Gly) complex (at least three orders of magnitude), it can be assumed that all Cu^{2+} not bound to peptide forms a $Cu(Gly)_2$ complex. However, if the affinity of the Cu^{2+}-peptide complex is similar to glycine then the distribution of Cu^{2+} between the two complexes must be calculated to determine the concentration of free glycine.

It is known that:

$$[Gly_{free}] = [Gly_{total}] - [Cu(Gly)] - 2[Cu(Gly)_2] \qquad \text{(eq 2.19)}$$

where, [Cu(Gly)] and $[Cu(Gly)_2]$ are the concentrations of Cu^{2+} in the respective glycine complexes.

It is also known that:

$$\frac{[Cu(Gly)_2]}{[Cu(Gly)]}=AppKa_2\left[Gly_{free}\right] \qquad \text{(eq 2.20)}$$

Therefore, equations 2.19 and 2.20 can be combined to give equation 2.21:

$$\frac{[Cu(Gly)_2]}{[Cu(Gly)]}=AppKa_2([Gly_{total}] - [Cu(Gly)] - 2[Cu(Gly)_2]) \qquad \text{(eq 2.21)}$$

It is known that the concentration of Cu^{2+} bound to glycine is equal to the concentration of Cu^{2+} bound to peptide at equilibrium, thus equation 2.22 can be substituted into equation 2.21 and simplified to give equation 2.23.

$$[Cu(Gly)_2] = [Cu^{2+}_{\text{bound to peptide}}] - [Cu(Gly)] \quad \text{(eq 2.22)}$$

$$[Cu^{2+}_{\text{bound to peptide}}]\text{-}[Cu(Gly)] = AppK_{a2}[Gly_{total}][Cu(Gly)] + AppKa_2[Cu(Gly)]^2 - 2AppK_{a2}[Cu^{2+}_{\text{bound to peptide}}][Cu(Gly)] \quad \text{(eq 2.23)}$$

When all known values are substituted into equation 2.23, the resulting equation will be in the form $ax^2 + bx + c = 0$, where x is [Cu(Gly)]. [Cu(Gly)] can therefore be calculated using the quadratic formula (eq 2.24). Of course, a quadratic equation shows two solutions for x but as [Cu(Gly)] is constrained by $[Cu^{2+}_{total}]$, only the value for x that is lower than $[Cu^{2+}_{total}]$ is relevant.

$$x = \frac{-b \pm \sqrt{b^2-4ac}}{2a} \quad \text{(eq 2.24)}$$

Once the value of [Cu(Gly)] is known, equation 2.22 can be used to calculate the value of $[Cu(Gly)_2]$. From this, equation 2.19 can be used to determine $[Gly_{free}]$. Finally, once $[Gly_{free}]$ has been calculated, the K_d can be determined using equation 2.18.

Worked Example for Calculating Cu^{2+} Affinity for PrP^C using Glycine as a Competing Chelator

Below is a worked example of calculating the affinity of the first three N-terminal residues of PrP^C (KKR) for Cu^{2+} using glycine as a competing Cu^{2+} chelator. The experimental specifics are taken from one of the Vis-CD experiments in Chapter 6B (Figure 6B.02a):

$[PrP_{total}] = 200 * 10^{-6}$ M

$[Cu^{2+}_{total}] = 200 * 10^{-6}$ M

$[Cu^{2+}_{\text{bound to PrP}}] = 100 * 10^{-6}$ M

$[Gly_{total}] = 267 * 10^{-6}$ M

Apparent K_{a1} at pH 7.4 for Gly = $7.4 * 10^{5}$ M^{-1}

Apparent K_{a2} at pH 7.4 for Gly = $7.4 * 10^{4}$ M^{-1}

First [Cu(Gly)] (x) is calculated from equation 2.23 followed by equation 2.24:

$$100*10^{-6} - x = (7.4*10^{4} * 267*10^{-6}*x) + 7.4*10^{4}x^{2} - (2 * 7.4*10^{4} * 100*10^{-6} * x)$$

$$7.4*10^{4}x^{2} + 5.958x - 100*10^{-6} = 0$$

$$x=\frac{-5.958\pm\sqrt{5.958^{2}-4(7.4*10^{4})(-100*10^{-6})}}{2(7.4*10^{4})}$$

$x = 1.42589 * 10^{-5}$ M

$[Cu(Gly)_2]$ is then calculated using equation 2.22:

$[Cu(Gly)_2] = 100*10^{-6} - 1.42589*10^{-5} = 8.57411 * 10^{-5}$ M

$[Gly_{free}]$ can then be calculated using equation 2.19:

$[Gly_{free}] = 267*10^{-6} - 1.42589*10^{-5} - 2(8.57411*10^{-5})$

$[Gly_{free}] = 81*10^{-6}$ M

Finally, the K_d can be determined using equation 2.18:

$$K_d=\frac{(200*10^{-6})-(100*10^{-6})}{1+(7.4*10^{5})(81*10^{-6})+(7.4*10^{5})(7.4*10^{4})(81*10^{-6})^{2}}$$

$$K_d = \frac{100*10^{-6}}{420.2}$$

$K_d = 2.3798 * 10^{-7}$ M = 240 nM

In the original paper published (Stanyon *et al.* 2014), the concentration of the free glycine at $\theta = 0.5$ calculated did not take into account the distribution of Cu^{2+} between the two binding modes of glycine. This caused an over-estimation of the K_d calculated, for example in the case illustrated above, 61 nM rather than 240 nM was obtained. This over-estimation of affinities does not affect the conclusions within the paper.

For an excellent review on calculating affinity see Xiao *et al.* (Xiao *et al.* 2010).

2.1.6 Aβ Solubilisation

There are several different methods currently used for the solubilisation of Aβ. Organic cosolvents, usually hexafluoroisopropanol (HFIP) or trifluoroethanol (TFE) (Chen *et al.* 2001, Zagorski *et al.* 1992) are common in the literature. The use of chaotropic agents such as dimethylsulfoxide (DMSO) (Stine *et al.* 2003) and organic acids such as trifluoroacetic acid (TFA) (Zagorski *et al.* 1999) are also used. Alternatively basic conditions, such as using dilute sodium hydroxide (NaOH) to obtain a pH of ~10.5 have also been shown to effectively solubilise Aβ (Fezoui *et al.* 2000) and is used extensively.

A problem with using organic solvents such as HFIP is that they influence fibrillogenesis and cytotoxicity and might not be fully removed. This adds to the variability that is already a major problem in fibril growth studies (Shen *et al.* 1995). Residual presence of these organic solvents from data collected *in vitro* presents the problem of whether the

results are physiologically relevant. Using dilute sodium hydroxide for solubilisation avoids these problems.

An additional advantage of using high pH solubilisation conditions is that it avoids Aβ being near its isoelectric point. Aβ synthetically produced using Fmoc (*N*-(9-fluorenyl)methoxycarbonyl) chemistry contains bound trifluoroacetate, which will create an acidic environment when Aβ is solubilised. When Aβ is subsequently added to buffer at a neutral pH the solution passes through the isoelectric point of Aβ (pH 5.3), where the potential for Aβ aggregation and precipitation is maximised. This can result in highly variable kinetic behaviour and fibril morphologies (Wood *et al.* 1996). The use of basic conditions to solubilise Aβ avoids the transition from low pH via its pI to physiological pH, preventing the problems associated with Aβ being at its pI (Fezoui *et al.* 2000, Teplow 2006).

The NaOH method has been shown to be as effective as three other commonly used methods; the HFIP method, the DMSO/water/Tris method, and the $NaCl/PO_4$ method (Hortschansky *et al.* 2005, Lashuel *et al.* 2003). Furthermore, NaOH pretreatment has been shown to result in fewer aggregates and diminish variability (Fezoui *et al.* 2000). Because of this, dilute NaOH was used to solubilise lyophilised Aβ in the studies in this thesis, although these other solubilisation methods were explored.

2.2 MATERIALS

2.2.1 Chemicals

The chemicals used in this thesis are listed in Table 2.02 with details of the supplier, purity and molecular weight.

Table 2.02. Chemicals Used in this Thesis.

Chemicals	Supplier	Molecular Weight (g/mol)	Purity / Grade
Hydrochloric Acid (HCl)	BDH Biochemical	36.46	Spectroscopy grade 1.18
Sodium Hydroxide (NaOH)	BDH Biochemical	40.00	≥ 99 %
Copper (II) Chloride Dihydrate ($CuCl_2 \cdot 2H_2O$)	Sigma - Aldrich	170.48	≥ 99.99 %
Nickel (II) Chloride Hexahydrate ($NiCl_2 \cdot 6H_2O$)	BDH Biochemical	237.69	≥ 98 %
Sodium Chloride (NaCl)	Sigma - Aldrich	58.44	≥ 98 %
N-ethylmorpholine (EM)	Sigma - Aldrich	115.20	~ 99 %
2-[4-(hydroxyethyl)piperazin-1-yl] ethanesulfonic Acid (HEPES)	Sigma - Aldrich	238.30	≥ 99.5 %
Potassium Phosphate Monobasic (KH_2PO_4) 1 M solution	Sigma - Aldrich	-	-
Potassium Phosphate Dibasic (K_2HPO_4) 1 M solution	Sigma - Aldrich	-	-
Thioflavin T (ThT)	Sigma - Aldrich	318.87	
Glycine	BDH Biochemical	75.07	
Nitrilotriacetic acid (NTA)	Sigma - Aldrich	191.1	≥ 99 %
Phosphotungstic acid (PTA)	Sigma - Aldrich	2880.05	Microscopy grade
Cholesterol	Sigma - Aldrich	386.66	≥ 99 %
Palmitic Acid	Sigma - Aldrich	256.42	≥ 99 %
Dimethylsulfoxide (DMSO)	Sigma - Aldrich	78.13	≥ 99.9 %

2.2.2 Peptides and Proteins

Amyloid-Beta

All Aβ peptides were purchased commercially from Zinsser Analytic and Cambridge Research Biochemicals and supplied as lyophilised powder. Aβ peptides were synthesised using solid-phase Fmoc chemistry. After removal from the resin and de-protection, the peptides were purified using reverse-phase HPLC and characterised using mass-spectrometry. The sequence of Aβ peptides used throughout this thesis were based on the human sequence of Aβ. Aβ(1-40) and Aβ(1-42) were designed with the native amino and carboxyl groups at the N-terminus and C-terminus, respectively. The truncated Aβ(1-16) was utilised for some studies as it is missing the residues responsible for fibrillisation but still contain the Cu^{2+} binding residues. This is not a native sequence thus the C-terminus was amidated to mimic the continuation of the peptide sequence. The sequences of the peptides are listed below:

Aβ(1-40):

DAEFRHDSGYEVHHQKLVFFAEDVGSNKGAIIGLMVGGVV

Aβ(1-42):

DAEFRHDSGYEVHHQKLVFFAEDVGSNKGAIIGLMVGGVVIA

Aβ(1-16)

DAEFRHDSGYEVHHQK-Amide

Human Serum Albumin

Human serum albumin used throughout this thesis was essentially fatty acid and globulin free and was purchased from Sigma-Aldrich as a lyophilised powder.

2.2.3 Equipment And Software

The details of all instruments used to collect data in this thesis are given in their respective individual method sections. The software used to process the data presented is this thesis is listed below in Table 2.03.

Table 2.03. The Software Used in this Thesis to Present Data.

Software	Manufacturer	Version
Pro-Data Suite	Applied PhotoPhysics	4.2.0
KaleidaGraph	Synergy Software	4.01
Chimera	University of California, San Francisco	1.9

2.3 METHODS

2.3.1 General Methods

pH and Buffers

Ultra-high quality water (10^{-18} $\Omega^{-1}cm^{-1}$ resistivity) was used throughout. Typically experiments were carried out at pH 7.4, unless otherwise specified, to recreate physiological conditions. The pH was adjusted to within 0.05 pH units of the desired pH using small aliquots of 10-100 mM NaOH or HCl when needed. The pH was measured using a Thermo Electron Orion 3 Star pH benchtop meter with an electrode with a 3 mm stem diameter to allow the pH of samples to be read whilst in 1 cm path length quartz cuvettes. Buffers used included HEPES, EM and Phosphate Buffer, a mixture of mono- and dibasic potassium phosphate.

Aβ Solubilisation

Lyophilised full length Aβ(1-40) or Aβ(1-42) was solubilised at 0.7 mg/mL in dilute NaOH in water at pH ~10.5 and gently rocked at 5 °C for 48 – 72 hours. Prior to use, the solubilised Aβ was centrifuged at 16,100 x *g* at 5 ºC for 5 minutes.

Determining Protein Concentration

For proteins containing tryptophan and tyrosine residues, the concentration was determined from UV-Vis absorption at 280 nm using equation 2.06. UV-Vis absorption spectra were obtained with a Hitachi U-3010 double beam spectrophotometer, using a 1 cm path length quartz cuvette (Hellma).

2.3.2 Aβ Fibrillisation

Thioflavin T Fluorescence

The kinetics of amyloid formation was monitored by the binding of ThT. The ThT measurements were conducted on a BMG Galaxy Fluostar 96 well plate fluorescence reader. Readings were obtained using an excitation wavelength of 440 nm and emission wavelength of 490 nm. Readings were taken every 30 minutes for approximately 400 hours with the well plates being subjected to 30 seconds of orbital shaking prior to each measurement. 10 μM Aβ was incubated with 20 μM ThT at 30 ºC in 160 mM NaCl. 30 mM HEPES buffer was used throughout to maintain pH at 7.4.

Curve Fitting

As discussed in Chapter 1, Aβ fibrillisation follows a characteristic growth curve. The data obtained from ThT fluorescence over time can be fitted to the growth curve using equation 2.24 (Uversky *et al.* 2001).

$$Y=(y_i+m_ix)+\frac{(y_f+m_fx)}{1+e^{-(x-x_0)/\tau}} \quad \text{(eq 2.24)}$$

where, Y is the ThT fluorescence intensity, x is the time, x_0 is the time at half height of fluorescence (t_{50}) and τ is a time constant. The initial and final fluorescence are given by the straight lines $y_i + m_ix$ and $y_f + m_fx$, respectively.

A number of empirical parameters relating to the kinetics of fibrillisation can be extracted from this curve. In addition to the t_{50}, the time taken for nucleation or lag time (t_{lag}), and the apparent rate of elongation (k_{app}) can also be determined from equations 2.25 and 2.26, respectively.

$$t_{lag} = x_0-2\tau \quad \text{(eq 2.25)}$$

$$k_{app} = 1/\tau \quad \text{(eq 2.26)}$$

Kinetic Parameter Statistical Analysis

Kinetic parameters have been extracted from typically 6 or more raw traces and the mean values and standard errors calculated. Analysis of variance (ANOVA) was used to compare the kinetic parameters extracted from curve fitting under different conditions, such as in the presence of different concentrations of HSA (Chapter 3). One-way ANOVA with Tukey-HSD post-hoc tests were used to reveal significant differences at $\alpha = 0.05$.

2.3.3 Visible Circular Dichroism

Typically, Visible CD spectra were recorded at 25° C on an Applied Photophysics Chirascan instrument between 260 and 800 nm, with sampling points every 2 nm, using a 1 cm pathlength quartz cell (Hellma). Typically, three scans were recorded and averaged, the baseline spectrum (three scans averaged) subtracted from each spectrum

followed by smoothing using a window of 6 nm. The molar ellipticity, $\Delta\varepsilon$ ($M^{-1}cm^{-1}$), spectra were obtained through conversion of the direct CD measurements, (θ, in millidegrees), using equation 2.09.

Small aliquots of fresh aqueous solutions were used to add metal ions (Cu^{2+} as $CuCl_2.2H_2O$, Ni^{2+} as $NiCl_2.6H_2O$) and glycine for titrations. Titrations carried out at pH 7.4 were in the presence of 20 mM ethylmorpholine buffer whereas titrations carried out at pH 9.5 were in the absence of buffers. The pH was measured before and after acquiring each spectrum.

2.3.4 Electron Paramagnetic Resonance (EPR)

EPR spectra were recorded at 10 K on a Bruker E580 X-band EPR spectrometer equipped with a super high Q continuous wave cavity and Oxford Instruments ESR900 continuous flow LHe cryostat. Spectra were obtained at an X-band microwave frequency of 9.38 GHz, using a microwave power of 0.5 mW across a sweep width of 2000 G, centred at 3000 G with a modulation amplitude of 10 G and modulation frequency of 100 KHz. Typically, two scans were recorded and averaged then baseline spectrum subtracted. Samples were loaded into an EPR quartz tube with an outside diameter of 4 mm and inside diameter of 3 mm (Wilmad Lab Glass). Samples were run in 50 mM temperature-independent pH (TIP) buffer composed of 60 % HEPES and 40 % phosphate buffer (Sieracki *et al*. 2008). TIP buffer was at pH 7.5, unless stated otherwise.

CHAPTER THREE:

HUMAN SERUM ALBUMIN CAN REGULATE AMYLOID-BETA PEPTIDE FIBRE GROWTH IN THE BRAIN INTERSTITIUM. IMPLICATIONS FOR ALZHEIMER'S DISEASE

3.1. ABSTRACT

Alzheimer's disease (AD) is a neurodegenerative disorder characterised by extracellular accumulation of amyloid-beta peptide (Aβ) in the brain interstitium. Human serum albumin (HSA) binds 95 % of Aβ in blood plasma and is thought to inhibit plaque formation in peripheral tissue. However, albumin's role in binding Aβ in the cerebrospinal fluid (CSF) has been largely overlooked. Here I investigate the effect of HSA on both Aβ(1-40) and Aβ(1-42) fibril growth. I show that at micromolar CSF levels, HSA inhibits the kinetics of Aβ fibrillisation, significantly increasing the lag-time and decreasing the total amount of fibrils produced. Furthermore, I show that the amount of amyloid fibres generated directly correlates to the proportion of Aβ not competitively bound to albumin. My observations suggest a significant role for HSA regulating Aβ fibril growth in the brain interstitium.

The work presented in this chapter forms the basis of work published in J Biol Chem 2012 (Stanyon *et al.* 2012).

3.2. INTRODUCTION

Interestingly, unlike systemic amyloid related diseases, although Aβ is found in the blood plasma at 0.1 – 0.5 nM concentrations (Seubert *et al.* 1992), similar to Aβ levels found in the cerebrospinal fluid (CSF) (Lame *et al.* 2011), Aβ amyloid deposits are largely found in the interstitium within the brain. Human serum albumin (HSA) binds 90-95 % of the Aβ found in blood plasma (Biere *et al.* 1996, Kuo *et al.* 2000). HSA is the most abundant protein in blood serum, at a concentration of ~640 μM (Carter *et al.* 1994), but has a markedly reduced concentration in the CSF of typically 3 μM (Stevens *et al.* 1979). This may explain why Aβ plaques are only observed in the extracellular space of the brain and not the peripheral tissue.

The affinity of monomeric Aβ for HSA has been determined and a dissociation constant (K_d) of 5-10 μM, for both Aβ(1-40) and Aβ(1-42), based upon a 1:1 stoichiometry has been consistently reported by a number of groups (Bohrmann *et al.* 1999, Kuo *et al.* 2000, Rózga *et al.* 2007). Indeed, with 640 μM concentration of albumin in blood plasma, a K_d of only 30 μM would be sufficiently tight to bind more than 95 % of physiological Aβ.

The level of HSA in the CSF (3 μM) and a micromolar affinity (K_d = 5-10 μM) for Aβ suggests that although the majority of Aβ is bound to HSA in the blood, the capacity of albumin to bind Aβ in the brain interstitium will be quite sensitive to changes in HSA levels. Therefore, variations in the capacity of HSA to bind Aβ, through decreased HSA concentration or competition for the Aβ binding site, could play a role in the build-up of toxic Aβ oligomers and fibres within the brain.

There is some debate over whether HSA binds to Aβ monomers or oligomers. Milojevic *et al* have performed a series of experiments that have produced results consistent with HSA binding to oligomers but not monomers or fibrils (Milojevic *et al.* 2007, Milojevic *et al.* 2011, Milojevic *et al.* 2009). Similarly it has been suggested that HSA traps Aβ in an oligomeric form (Reyes Barcelo *et al.* 2009). Others have suggested HSA binds monomers of Aβ (Kuo *et al.* 2000, Rózga *et al.* 2007). A study using immobilised Aβ polymers and biotin labelling indicates HSA can inhibit soluble Aβ addition to immobilized Aβ seeds, suggesting Aβ polymerisation inhibition (Bohrmann *et al.* 1999).

As HSA interacts with Aβ, I was interested in how HSA might affect the kinetics of fibril formation; fibre nucleation and elongation. Although it is has been suggested albumin inhibits fibre formation (Bohrmann *et al.* 1999, Reyes Barcelo *et al.* 2009), I know of no direct study of the kinetics of amyloid formation in the presence of CSF levels of albumin. Here I study inhibition of Aβ-fibril growth in detail.

3.3. AIM

To understand fibre formation and kinetics *in vivo* I monitor fibril growth rates using physiologically relevant (1-10 μM) and substoichiometric concentrations of HSA to determine the concentration dependent inhibition of Aβ fibril formation.

3.4. EXPERIMENTAL

3.4.1. ThT Fluorescence

Fibre growth was followed using ThT fluorescence, as described in Chapter 2.

3.4.2. Transmission Electron Microscopy (TEM)

Glow-discharged carbon-coated 300-mesh copper grids (SPI supplies, PA, USA), were prepared using the droplet method, where 5 µl aliquots of samples from the fibre growth assay were adsorbed for 1 minute followed by 5 µl of 2% (w/v) of phosphotungstic acid adjusted to pH 7.4, to negatively stain the sample. Images were recorded on a JEOL JEM-1230 electron microscope (Tokyo, Japan) operated at 80 kV.

3.4.3. Affinity Calculations

The albumin-Aβ complex is in equilibrium with free Aβ with a dissociation constant of 5 µM.

$$\left[\begin{matrix}\text{Albumin-A}\beta \\ \text{(1:1 complex)}\end{matrix}\right] \rightleftharpoons \left[\begin{matrix}\text{A}\beta\text{ (free)} \\ \text{(A}\beta\text{ monomers} \rightleftharpoons \text{A}\beta\text{ fibrils)}\end{matrix}\right] + \left[\text{HSA (free)}\right]$$

$$K_d = \frac{[\text{HSA free}]\left[\begin{matrix}\text{A}\beta\text{ free} \\ \text{(monomeric or fibrillar)}\end{matrix}\right]}{[\text{HSA-A}\beta\text{ complex}]} \qquad \text{(eq 3.01)}$$

This can be rewritten as:

$$K_d = \frac{([\text{Total HSA}]-[\text{Bound HSA}])([\text{Total A}\beta]-[\text{Bound A}\beta])}{[\text{Bound HSA-A}\beta]} \qquad \text{(eq 3.02)}$$

As the bound concentration is unknown, this becomes x:

$$K_d = \frac{([\text{Total HSA}]-x)\ ([\text{Total A}\beta]-x)}{x} \qquad \text{(eq 3.04)}$$

When the appropriate values are submitted within the above equation, a quadratic equation is produced. Therefore, x is solved using the following quadratic formula (eq 2.23).

Example Worked Calculation

For total Aβ concentration of 10 μM and total HSA concentration of 10 μM:

$$5\ \mu M = \frac{(10\ \mu M - x)(10\ \mu M - x)}{x}$$

$$5x = x^2 - 20x + 100$$

$$x^2 - 25x + 100 = 0$$

$$x = \frac{25 \pm \sqrt{25^2 - (4 \times 1 \times 100)}}{2 \times 1}$$

$x = 5$, $x = 20$.

However, as the concentration bound must be lower than the total concentration, $x = 5\ \mu M$.

$$\textbf{\% A}\beta_{\text{bound}} = \frac{5\ \mu M \times 100}{10\ \mu M} = \textbf{50 \%}$$

3.5. RESULTS

3.5.1. HSA inhibits the kinetics of Aβ(1-40) fibre formation

The kinetics of Aβ fibril formation were monitored using Thioflavin T (ThT), a dye that fluoresces upon binding to amyloid fibrils. The rate of fibre formation of Aβ(1-40) was monitored over time in the presence and absence of increasing concentrations of HSA, using a 96 well-plate fluorescence reader. A characteristic fibrillisation growth curve is obtained, which has a lag-phase and growth-phase, due to nucleation and fibril elongation respectively.

In Figure 3.01 I show the fibrillisation growth curves obtained from 10 μM Aβ(1-40) in the presence of 0, 3, 5 and 10 μM HSA. Typically 6 individual traces were obtained at each albumin concentration and key kinetic parameters, including the t_{50}, t_{lag} and $k_{app,}$ extracted through fitting the characteristic sigmoidal growth curves (Uversky *et al.* 2001). For comparison, the average t_{50} of Aβ fibrillisation in the absence of albumin is depicted as a dashed line on each trace. It is clear from Figure 3.01 that fibril growth is delayed by all three substoichiometric concentrations of HSA as the elongation phase of the growth curves are all past the average t_{50} for Aβ(1-40) alone.

There was some variation in the fibril growth kinetics and so essentially the identical experiment was repeated on three other separate occasions, an example of which is shown in Figure 3.02. The fibril growth kinetics from these four separate experiments, for Aβ(1-40) fibrillisation in the presence of increasing concentrations of HSA were averaged together to generate large n numbers (n = 24), and the standard errors calculated, as shown in Figure 3.03. Variation in the kinetic parameters for fibril growth recorded on separate days was comparable to variation for individual fibre growth experiments. One way ANOVA with Tukey-HSD post-hoc tests was performed on this data; HSA increases the t_{50} of Aβ(1-40) fibril growth but this was only significant ($P < 0.05$) at half a molar equivalent of HSA (5 μM) and higher. Analysis of the t_{lag} and k_{app} indicates HSA prolongs the lag-phase of Aβ fibril formation with as little as 1 μM HSA but has no significant effect on the rate of elongation of fibres (k_{app}) once nucleation has taken place. This means the effect on the t_{50}s is exclusively due to the inhibition of fibre nucleation, measured as the lag-time (t_{lag}). It is clear that substoichiometric amounts of HSA at concentrations found in the CSF increase the lag time of Aβ(1-40) fibre formation.

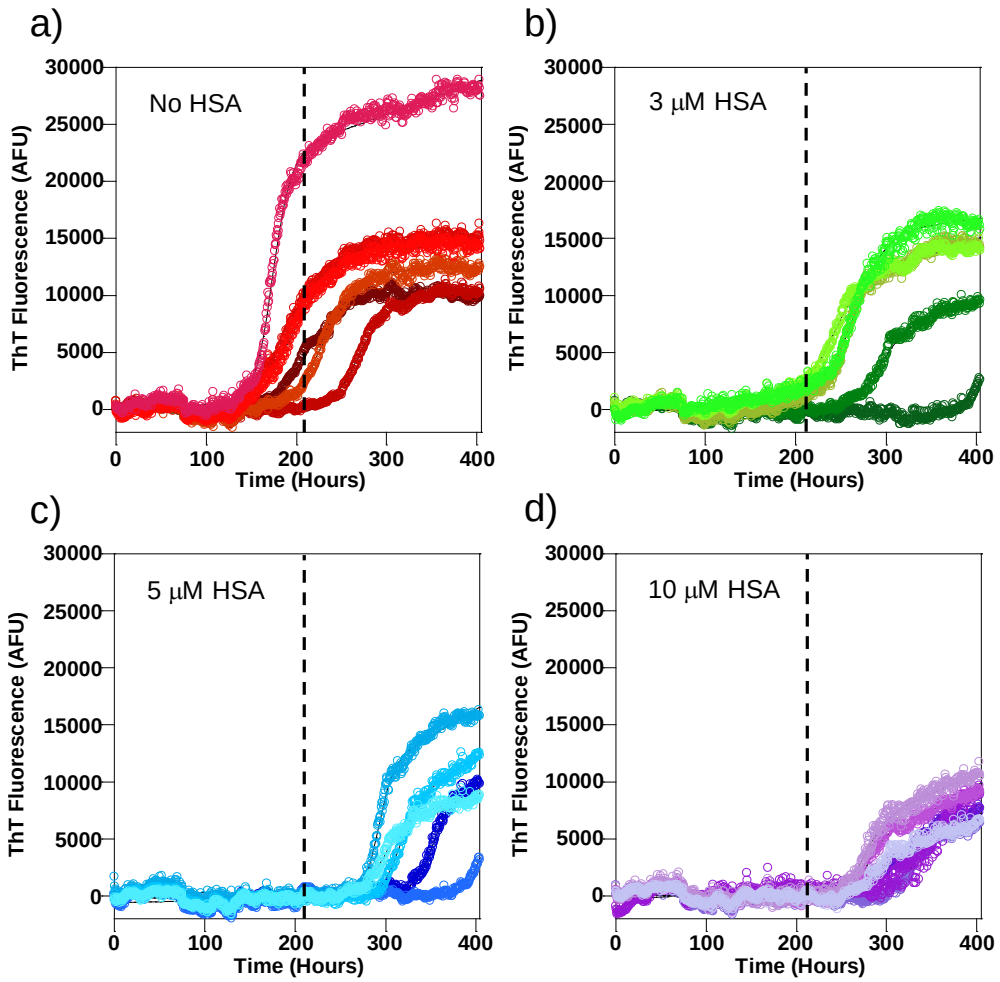

Figure 3.01. Aβ(1-40) Fibril Growth in the Presence of Albumin.

Fibrillisation of 10 μM Aβ(1-40) was monitored using ThT fluorescence. Concentrations of albumin found in the CSF inhibit fibre formation. Here individual traces of a) Aβ alone, and Aβ in the presence of b) 3 μM, c) 5 μM, and d) 10 μM HSA are shown. The mean t_{50} for Aβ alone is shown on traces a-d as a dashed line.

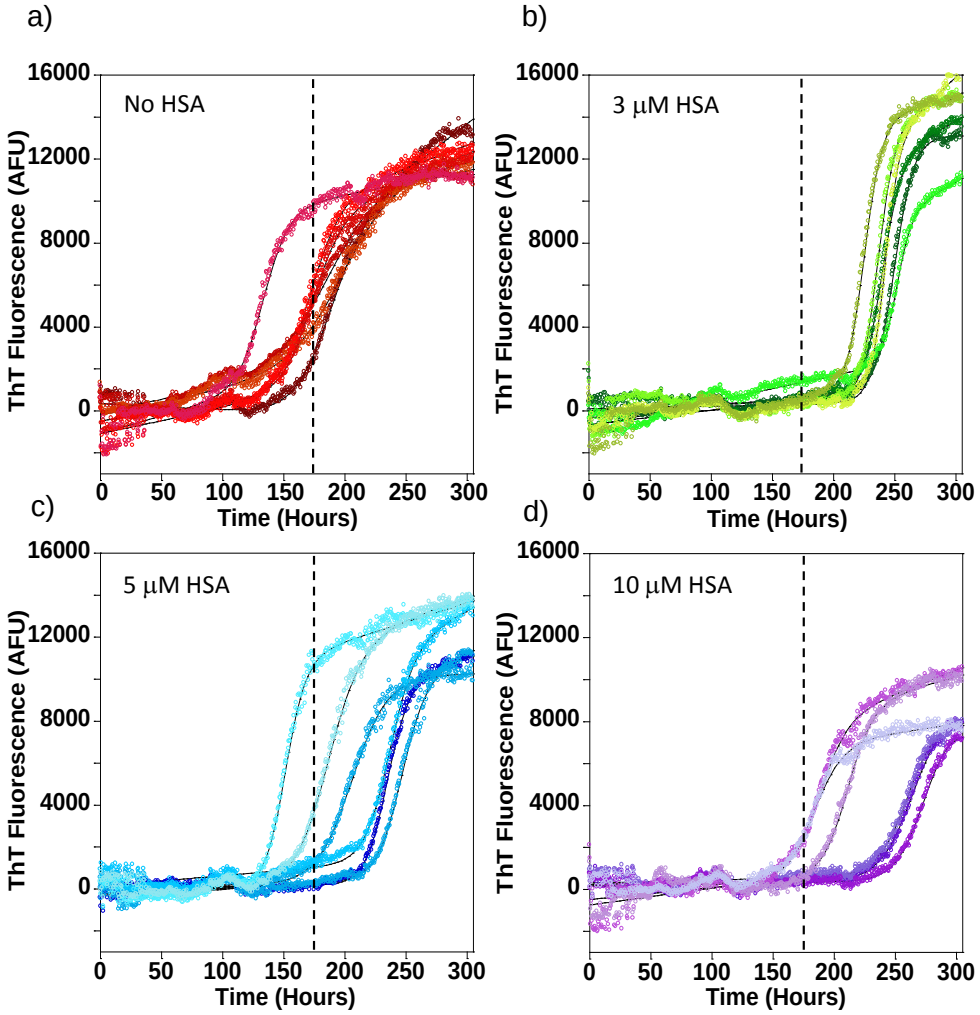

Figure 3.02. Aβ(1-40) Fibril growth in the Presence of HSA. (One of 4 Repeat Experiments)

Fibrillisation of 10 μM Aβ(1-40) in 30 mM HEPES and 160 mM NaCl at pH 7.4 at 30 °C was monitored using ThT fluorescence. Here individual traces of a) Aβ alone, and Aβ in the presence of b) 3 μM, c) 5 μM, and d) 10 μM HSA are shown. The average t_{50} for Aβ alone is shown on traces a-d as a dashed line. This is a repeat of the experiment shown in Figure 3.01.

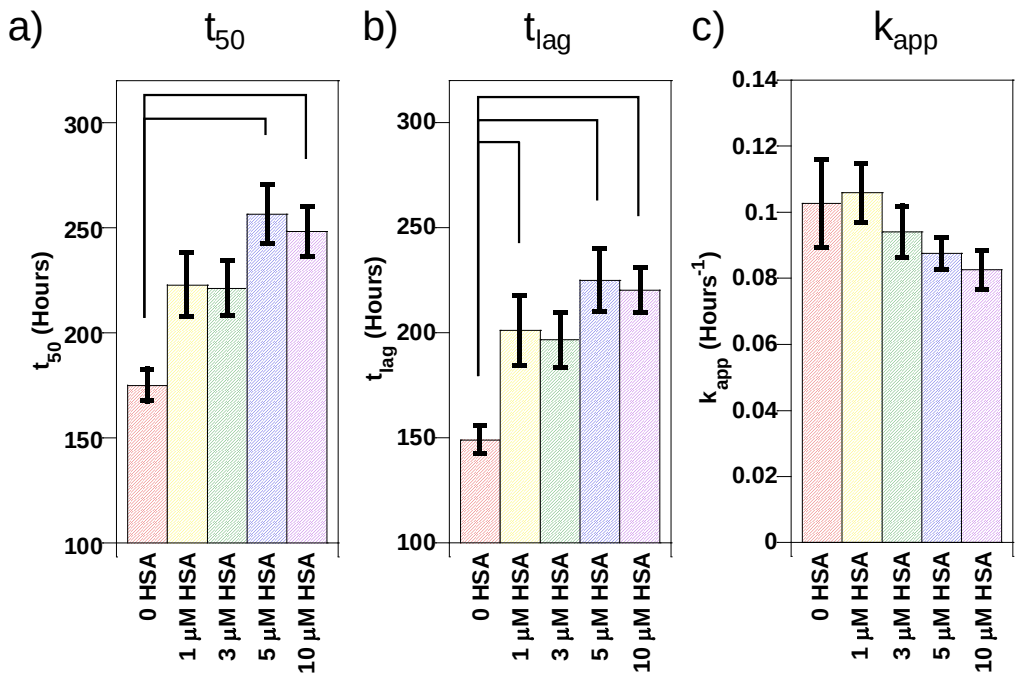

Figure 3.03. Kinetic Parameters for Aβ(1-40) Fibril Growth Experiments in the Presence of Increasing HSA.

The mean a) t_{50}, b) t_{lag}, and c) k_{app} values pooled from 4 separate experiments are shown, with their standard errors (n =24). Significant differences are shown by connecting lines at $\alpha = 0.05$. These have been calculated using one-way ANOVA, with Tukey HSD post-hoc tests. The rate of nucleation of fibre formation is significantly reduced by albumin.

3.5.2. HSA reduces the total number of fibres generated

There is also a reduction in the total amount of fibres generated as indicated by the maximal fluorescence signal produced after more than 400 hours. From Figure 3.01 it is clear that the ThT fluorescence signal for 10 μM HSA present is approximately half the intensity relative to Aβ(1-40) in the absence of HSA. The mean maximum fluorescence intensities and the associated standard errors from the four repeat experiments of Aβ(1-40) fibrillisation were also calculated and are shown in Figure 3.04a. The trend that can be observed from this is that the maximum fluorescence intensity, or total amount of fibres generated, decreases as the concentration of HSA present increases. This closely agrees with what is known about the K_d of HSA for Aβ. With a K_d of 5 μM and an equimolar mixture of Aβ and HSA (at 10 μM) then 50 % of the Aβ molecules will bind to HSA (see example calculation in Section 3.4.3.). Interestingly, at this level of HSA there is exactly a 50 % reduction in total fibres generated for Aβ(1-40). Using the known dissociation constant between Aβ and HSA (K_d = 5 μM), it is possible to calculate the amount of free and bound Aβ for any concentration of Aβ and HSA by solving simple quadratic equations derived from the equation for the dissociation constant, see Section 3.4.3 and Table 3.01.

Table 3.01. The Proportion of 10 μM Aβ Bound to HSA Based on a K_d of 5 μM

Total HSA (μM)	Aβ Bound to HSA (μM)	Aβ Free (μM)	Aβ Free (%)
10	5.00	5.00	50.0
5	2.93	7.07	70.7
3	1.86	8.14	81.4
1	0.65	9.35	93.5

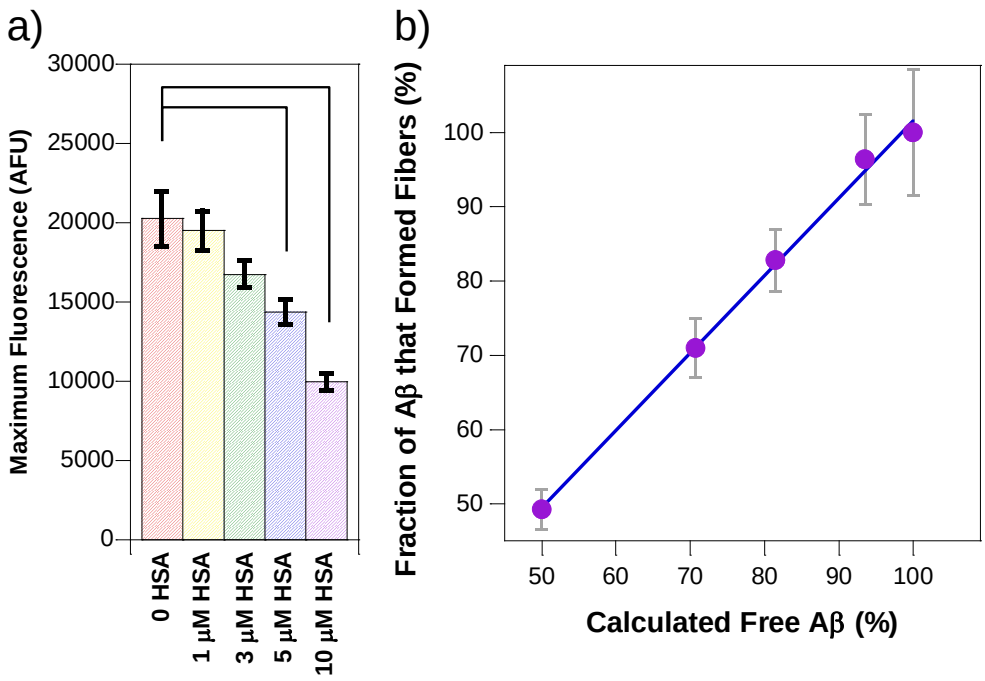

Figure 3.04. Competitive Effects of Albumin on Total Aβ Fibrils Generated.

a) The average maximum fluorescence values pooled from 4 separate experiments of Aβ(1-40) with increasing concentrations of albumin are shown, with their standard errors. Significant differences from Aβ alone are shown by connecting lines at $\alpha = 0.05$. b) The correlation between fraction of fibres generated and the calculated fraction of Aβ free to form fibres (not bound to increasing concentrations of HSA). Based upon a K_d of 5 µM. There is a strong correlation (R = 0.998) between the percentage of fibres generated and the predicted fraction of Aβ not bound to albumin (gradient = 1.04).

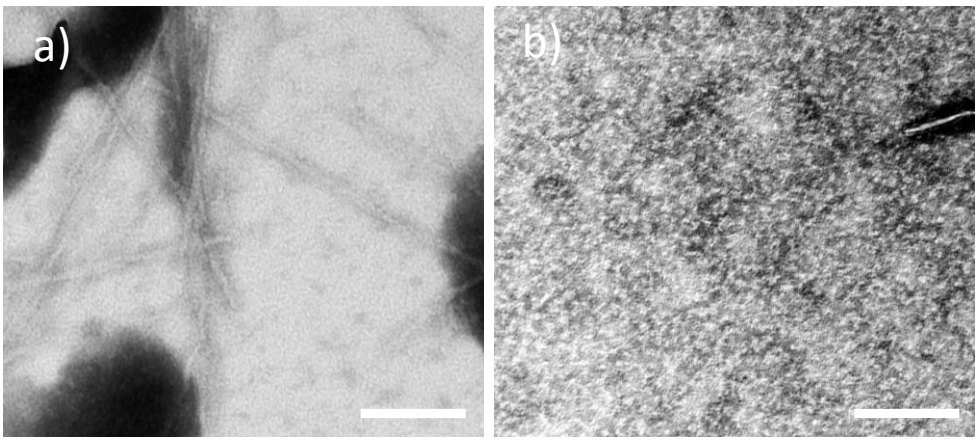

Figure 3.05. TEM of Aβ(1-40) Fibril Growth in a) the Absence and b) the Presence of Albumin.

Aβ forms many long, twisted fibres alone but very few are formed with HSA present. The scale bar is 100 nm. 10 μM Aβ(1-40) in the presence and absence of 10 μM HSA in 30 mM HEPES and 10 mM NaCl at pH 7.4 was incubated for 400 hours at 30 ^{o}C with intermittent agitation. Samples are negatively stained with phosphotungstic acid.

The strong correlation between the total amount of fibres generated and the predicted amount of available Aβ (not bound to HSA) is striking, as shown in Figure 3.04b. In particular the linear regression gives an R value of 0.998 and gradient of 1.0.

To confirm that albumin has indeed inhibited fibre formation a second detection method was used. Aβ(1-40) was incubated with 10 μM HSA for 400 hours as before (Figure 3.01) and TEM images obtained. In the absence of albumin typical fibre morphology is observed with numerous fibres generated (Figure 3.05a). In the presence of albumin almost no fibres or oligomers could be observed after searching many squares per grid (Figure 3.05b).

3.5.3. Albumin has the same effect on Aβ(1-42)

Next I wanted to investigate the effect of albumin on Aβ(1-42), the more amyloidogenic Aβ peptide found in plaques. Aβ(1-42) shows similar fibril growth kinetics to Aβ(1-40), as shown in Figure 3.06, with all traces in the presence of 5 and 10 μM HSA showing delays in fibre formation relative to Aβ alone. One-way ANOVA with Tukey-HSD post-hoc tests showed that HSA significantly ($P < 0.05$) increased the lag phase and t_{50} of Aβ(1-42) fibril growth at concentrations over 5 μM (Figure 3.07). Once again it can be observed that the maximal ThT fluorescence intensity for the fibril growth is reduced in the presence of albumin, indicating that as well as increasing the time required for fibrils to form, the total concentration of fibres formed is also reduced.

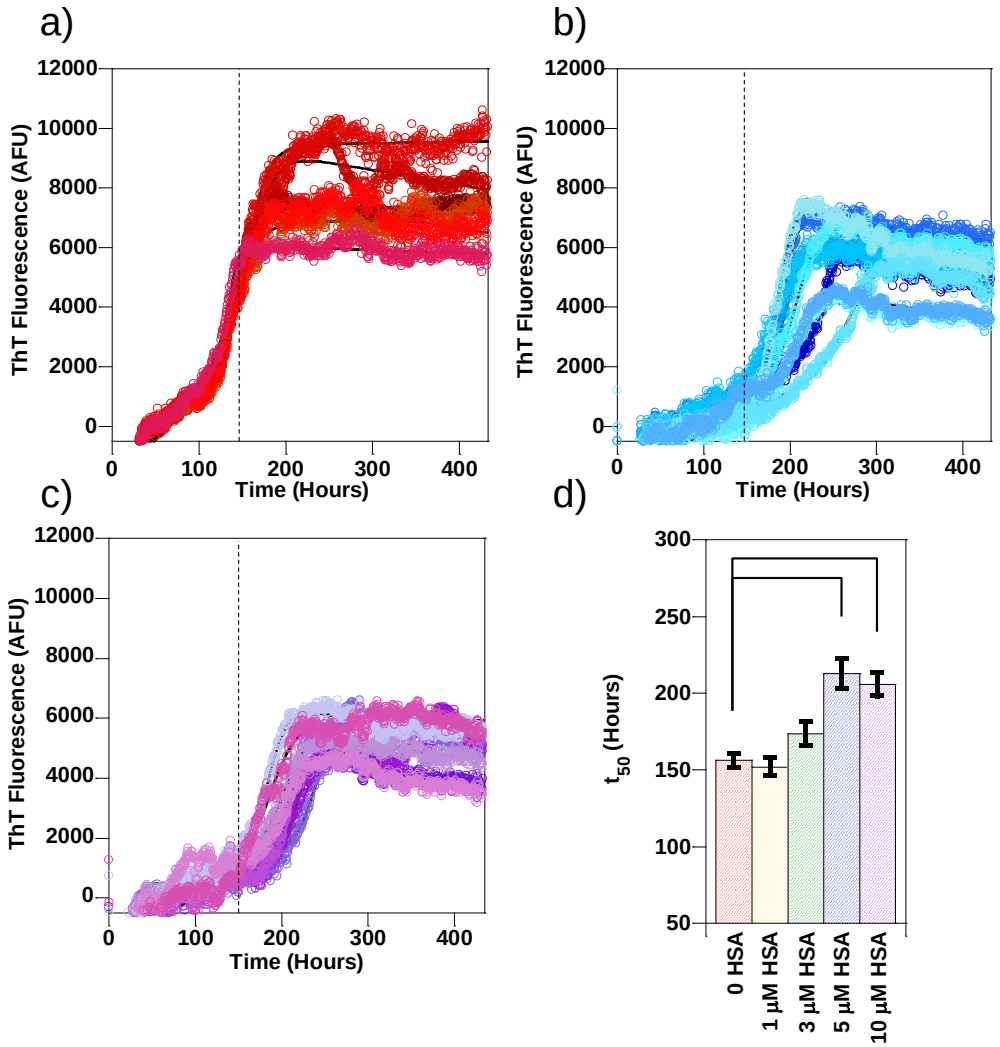

Figure 3.06. Aβ(1-42) Fibril Growth in the Presence of HSA.

Fibrillisation of 10 μM Aβ(1-42) was monitored using ThT fluorescence. Here individual traces of a) Aβ alone, and Aβ in the presence of b) 5 μM, and c) 10 μM HSA are shown. The average t_{50} for Aβ alone is shown on traces a-c as a dashed line. d) The average t_{50} values for each concentration of HSA with their standard errors. Significant differences from Aβ alone are shown by connecting lines at $\alpha = 0.05$. Physiologically relevant micromolar levels of albumin inhibits Aβ(1-42) fibre formation.

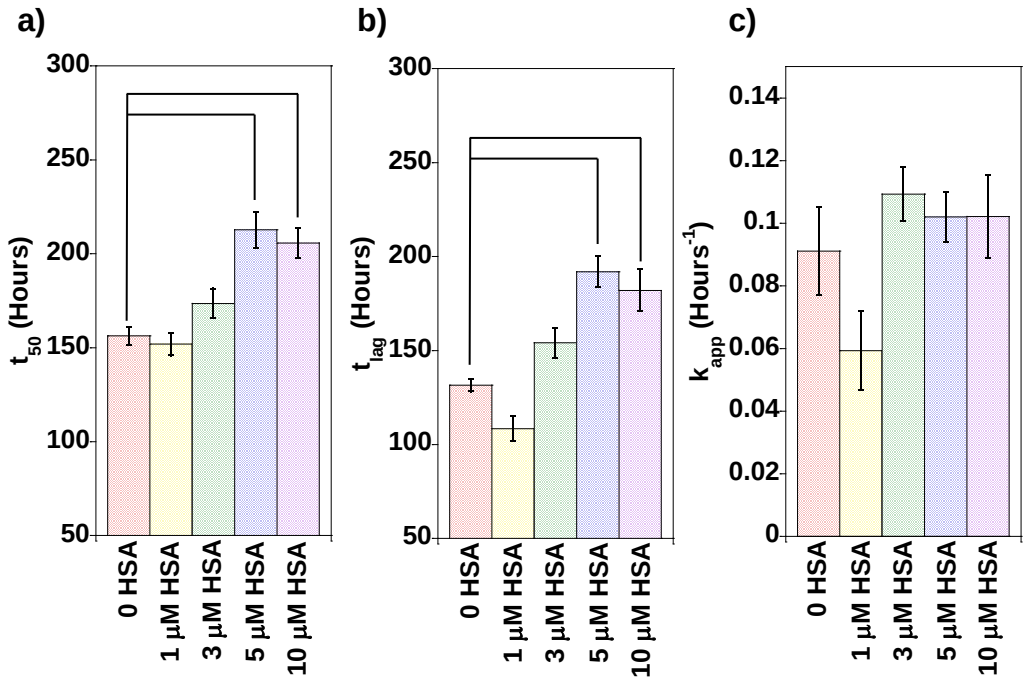

Figure 3.07. Kinetic Parameters for Mean Fibril Growth of Aβ(1-42) in the Presence of Varying Concentrations of HSA.

Fibrillisation of 10 µM Aβ(1-42) in 30 mM HEPES and 160 mM NaCl at pH 7.4 at 30 °C was monitored using ThT fluorescence. Here the a) t_{50}, b) t_{lag}, and c) k_{app}, with their standard errors are shown. Significant differences between Aβ alone and albumin concentrations are shown by connecting lines, typically observed for 5 and 10 µM HSA.

3.6. DISCUSSION

Perhaps because levels of albumin are so much lower in the CSF than the blood plasma a role for HSA interacting with extracellular Aβ in the brain interstitium has largely been overlooked. However, 3 μM concentration of albumin still represents the major protein component of the CSF. Furthermore, even though the affinity of Aβ for HSA is quite modest (K_d = 5 μM), it is clear ~ 40 % of Aβ within the CSF will be bound to HSA. My results show that at physiological levels of albumin the rate at which fibre formation is nucleated for both Aβ(1-40) and Aβ(1-42) is significantly inhibited. Moreover the total concentration of fibre generated is reduced by HSA, this suggests that HSA binds to Aβ molecules and traps them in a non-fibrillar form so they are not available to form fibres.

In the presence of physiological micromolar levels of albumin, some but not all Aβ is trapped in a non-fibrillar form of Aβ. Indeed, the total concentration of fibres generated with increasing levels of HSA (Figure 3.04) shows a remarkably close agreement with the amount of free and albumin bound Aβ that would be expected for a K_d of 5 μM. The predicted percentage of free Aβ based on HSA's affinity for Aβ is shown in Figure 3.04b. HSA can bind to Aβ in a non-fibrillar form as the final amount of fibres produced is reduced by the presence of HSA. My data strongly supports HSA interacting with monomeric Aβ to form a 1:1 complex with a K_d of 5 μM. Although binding oligomers of Aβ cannot be ruled out, they must be small, less than five Aβ monomers, as none are observed by TEM. It is notable that a gradient of 1.0 in Figure 3.04b (R=0.998) implies a K_d very close to 5 μM. Albumin binding to the monomeric Aβ effectively reduces the concentration of free Aβ available to form fibres. The lag-phase in fibril growth is strongly affected by the Aβ concentration, which would explain the reduction in lag-times observed. It seems unlikely that the fibre growth inhibition is due to HSA interacting with

Aβ fibres as the fibre elongation growth rates are not reduced once a nucleating seed has formed. This suggests that HSA has a role in preventing the formation of nucleating seeds but once they are formed, it has less effect in monomer addition to the ends of growing fibres.

There have been a number of protein binding partners of Aβ indicated, in particular, the cellular prion protein (Laurén *et al.* 2009) but also serum amyloid P (SAP) (Likó *et al.* 2007), islet amyloid polypeptide (IAPP) (Andreetto *et al.* 2010) and transthyretin (Buxbaum *et al.* 2008). The composition of plaques from the brain supports the idea that HSA interacts with a non-fibrillar / monomeric form of Aβ as HSA is not found within plaques, in contrast to SAP (Coria *et al.* 1988).

HSA is known for its ability to bind many hydrophobic molecules, in particular a number of pharmaceuticals, including warfarin and diazepam, as well as endogenous fatty acids (Carter *et al.* 1994). A crystal structure of HSA with fatty acids bound has indicated the location of hydrophobic pockets formed within HSA (Curry *et al.* 1998), which may be where part of the hydrophobic C-terminal residues of Aβ could bind to HSA. It has been suggested that there are pharmaceutical and endogenous hydrophobic molecules that could compete with Aβ binding to HSA (Bohrmann *et al.* 1999). Albumin is also responsible for the transport of the labile pool of Cu^{2+} ions in blood plasma (Patel *et al.* 1993). Of note, the Aβ-Cu^{2+} interaction and its role in AD have received significant interest (Sarell *et al.* 2010, Viles 2012, You *et al.* 2012) and Cu^{2+} may be transferred from Aβ to HSA (Perrone *et al.* 2010), meaning albumin could have two mechanisms by which it inhibits fibre formation.

The concentration of HSA that will delay the fibrillisation of Aβ is of interest, in particular, the level where HSA has a significant effect on Aβ fibre formation *in vitro* as it is strikingly similar to the extracellular albumin levels found *in vivo*. HSA is found at a concentration of ~ 3 μM in the cerebrospinal fluid and brain interstitium (Licastro *et al.* 1993). Although HSA is at substantially lower levels than in blood plasma, 3 μM still represents a major constituent of the CSF and the brain interstitium. With a 1 nM concentration of Aβ in the CSF and a 5 μM K_d for albumin, it can be assumed that 37 % of Aβ will be bound to albumin in the CSF. Considerable variation in CSF levels of albumin (1-5 μM) have been reported (Christenson *et al.* 1983). A reduction to 1 μM levels of albumin will lead to 83 % of the Aβ remaining free in solution. Thus a decrease in the concentration of HSA could cause an increase in the amount of amyloid fibrils produced and as such lead to the build-up of amyloid plaques. It may therefore be possible that a small change in HSA in the CSF and interstitium may represent a significant risk factor in AD. However, both elevated and reduced levels of albumin have been reported in AD patients (Elovaara *et al.* 1986, Elovaara *et al.* 1987). It has been noted that Aβ plaques are only ever observed in the brain and not the peripheral tissue, probably because HSA concentrations are of a much higher magnitude (640 μM) in the blood plasma (Licastro *et al.* 1993). Interestingly serum albumin levels, *in vivo*, decrease with age, which is also a known risk factor in AD (Klonoff-Cohen *et al.* 1992). Furthermore levels of albumin are often reduced in association with inflammation also linked with AD.

In conclusion, although the affinity of Aβ for HSA is not thought to be remarkable (K_d = 5 μM), it follows that with levels of albumin in the CSF and brain interstitium of 3 μM, 40 % of Aβ in the CSF will be bound to albumin. I show that this Aβ bound to albumin is trapped in a non-fibrillar form thus reducing the amount of Aβ available to form fibres.

Furthermore, based on my fibre growth studies small variations in albumin in CSF are therefore likely to regulate the amount of extracellular fibril formation in the CSF and brain interstitium. Currently HSA is showing promise in phase II clinical trial, using an albumin plasma exchange schedule to reduce levels of Aβ in blood plasma (Boada *et al.* 2009). A reduction of the Aβ pool in plasma will, in turn, reduce Aβ levels in the CSF as Aβ is in a dynamic equilibrium and is able to cross the blood-brain barrier (Mackic *et al.* 1998).

CHAPTER FOUR:

UNDERSTANDING THE ALBUMIN-Aβ INTERACTION, AND THE COMPETITIVE EFFECTS OF CHOLESTEROL AND FATTY ACIDS

4.1 ABSTRACT

In Chapter 3, I have shown that albumin is capable of inhibiting Aβ fibrillisation from monomeric Aβ at physiological concentrations. However, albumin's effect on mature fibres has yet to be elucidated. Here I show, in contrast to its effect on Aβ monomers, that albumin will not disassemble mature Aβ fibres over a month timescale. This work in combination with size exclusion chromatography and mass spectrometry indicates albumin binds monomeric or a small oligomer of Aβ to inhibit fibre formation. Albumin binds a variety of endogenous hydrophobic molecules *in vivo,* including cholesterol and fatty acids. High fat diet and cholesterol levels have both been linked with an increased risk of AD. Here I show Aβ competes with both of these hydrophobic molecules for HSA binding, negating the inhibitory effect of HSA on Aβ fibrillisation kinetics. My observations suggest a role for HSA in the associated risk of high cholesterol and fat for AD development. My work indicates the use of albumin plasma exchange could be a powerful tool to treat AD through clearance of Aβ-HSA complexes, but also replacement of HSA bound to cholesterol and fatty acids with HSA free to bind Aβ may be beneficial.

4.2 INTRODUCTION

The kinetics of Aβ fibril growth in the presence of HSA show that micromolar levels of albumin inhibits Aβ fibre formation during nucleation (Chapter 3 and (Stanyon *et al.* 2012)) but the effect of HSA on the later stages of fibrillisation and fibril disassembly are yet to be elucidated. The effect of albumin on these stages is important for understanding the mechanism through which albumin exchange as a treatment for AD, which is showing promise in phase II clinical trial, is effective (Boada *et al.* 2009). If albumin only has an effect on Aβ fibrillisation in the early stages, the treatment would only be effective in reducing Aβ burden in the early stages of AD development prior to Aβ plaque deposition.

Despite HSA being known to bind Aβ *in vivo* (Biere *et al.* 1996), it is not yet confirmed where Aβ binds or the stoichiometry of the complex formed. There is disagreement as to whether HSA binds oligomers (Milojevic *et al.* 2014, Milojevic *et al.* 2007, Milojevic *et al.* 2011, Milojevic *et al.* 2009, Reyes Barcelo *et al.* 2009) or monomers (Kuo *et al.* 2000, Rózga *et al.* 2007). It is important to determine the size and stoichiometry of the HSA-Aβ complex to understand the role of HSA in the progression of AD. Current perspectives on Aβ neurotoxicity implicate diffusible soluble pre-fibrillar oligomers as the major cause rather than mature Aβ fibres (Brouillette *et al.* 2012, Cleary *et al.* 2004, Dahlgren *et al.* 2002, Kim *et al.* 2003, Walsh *et al.* 2002). Therefore, if HSA arrests Aβ fibrillisation as highly toxic soluble oligomers, elevated albumin levels would increase the rate of neurodegeneration. However, if HSA binds Aβ monomers, increased albumin would decrease Aβ neurotoxicity.

Albumin is the most abundant protein in the blood plasma at approximately 640 μM (Carter *et al.* 1994) and is capable of transporting many different hydrophobic molecules,

including cholesterol (Peng *et al.* 2008, Teir *et al.* 2012) and fatty acids (Ashbrook *et al.* 1975, Bhattacharya *et al.* 2000, Saifer *et al.* 1961, Spector 1975). Interestingly, cholesterol and a high fat diet are known to increase the risk of developing AD when at elevated concentrations in the blood plasma (Kalmijn *et al.* 1997, Kivipelto *et al.* 2002, Laitinen *et al.* 2006, Morris *et al.* 2003, Solomon *et al.* 2007, Whitmer *et al.* 2005). These endogenous hydrophobic molecules are likely to influence Aβ-HSA interactions *in vivo*. Through using these as competing ligands during fibril growth, it is possible to gain insight into whether disruption of the Aβ-HSA interaction could be a mechanism for the associated increased risk of developing AD and provide information on the locus of Aβ binding. A more detailed background of albumin structure and function can be found in Chapter 1.

4.2.1 The Link Between Cholesterol and AD.

High total serum cholesterol at midlife is a risk factor for the development of dementia and AD (Kivipelto *et al.* 2002, Solomon *et al.* 2007, Whitmer *et al.* 2005). Furthermore, GWAS point to cholesterol metabolism as a key risk factor (Jones *et al.* 2010, Wollmer 2010). High total serum cholesterol is classed as a concentration higher or equal to 6.5 mM, or 240 mg/ dL (Kivipelto *et al.* 2001, Notkola *et al.* 1998). The total serum cholesterol is found in two forms; esterified and non-esterified. The majority (~75 %) is transported in the esterified form, particularly as low density lipoproteins (LDLs) bound to apolipoproteins such as ApoE (Demeester *et al.* 2000). The non-esterified, or free, cholesterol therefore comprises ~ 25 % of the total cholesterol. In the cerebrospinal fluid this shifts such that the percentage of free cholesterol increases to 30 % (Demeester *et al.* 2000). The central nervous system (CNS) contains 25 % of the total body cholesterol content despite the CNS being only 2 % of the body weight (Dietschy *et al.* 2004) thus this 5 % shift between esterified and free-cholesterol represents a significant amount of

cholesterol. CNS cholesterol levels are normally unaffected by serum levels of cholesterol as the blood brain barrier (BBB) is not permeable to cholesterol (Chobanian *et al.* 1962). However, an increased flux of cholesterol across the CNS can be observed in aging and early AD (Lütjohann *et al.* 1996). Cholesterol accumulation is observed in association with plaques in AD (Mori *et al.* 2001). Studies in rabbits and mice have shown that higher brain accumulation of Aβ plaques occurs when cholesterol levels are elevated and increase AD pathology (Hooijmans *et al.* 2009, Refolo *et al.* 2000, Sparks *et al.* 1994, Zatta *et al.* 2002).

There are many different proposed mechanisms by which cholesterol increases AD risk. One hypothesis is that cholesterol influences the composition of the membrane in neurons, perturbing membrane fluidity and signal transduction thus promoting neuronal degeneration (Mattson 2004). Another popular hypothesis is that the cholesterol concentration increases in lipid rafts, promoting APP cleavage into Aβ, as both APP and γ-secretase are associated with lipid rafts (Cordy *et al.* 2006, Ehehalt *et al.* 2003, Hicks *et al.* 2012, Vetrivel *et al.* 2010). However, these hypotheses do not account for why high serum cholesterol at mid-life increases the risk of developing AD as there is no equilibrium between serum cholesterol and brain cholesterol.

Cholesterol can bind to albumin, the most abundant protein in blood plasma and cerebrospinal fluid, in "Sudlow site I". Cholesterol has a relatively weak affinity for HSA (25 μM) (Peng *et al.* 2008) but this is still tight enough for binding to occur *in vivo* due to the high concentrations of albumin and cholesterol available in the plasma. Indeed, it has been shown that 24 % of all non-esterified cholesterol is bound to albumin in the rat serum (Deliconstantinos *et al.* 1986). It is therefore likely that a significant proportion of cholesterol is bound to albumin in human blood plasma also.

4.2.2 The Role of Fatty Acids in AD

High intake of fat, particularly saturated fats has been associated with an increased risk of dementia (Kalmijn *et al.* 1997, Laitinen *et al.* 2006, Morris *et al.* 2003). Indeed, a study in APP transgenic mice has shown a high fat diet increases cognitive impairment and that diet control is capable of ameliorating the memory deficits and Aβ deposition induced by the high fat diet (Maesako *et al.* 2012a, Maesako *et al.* 2012b). Palmitic acid (PA) and oleic acid are the predominant forms of non-esterified fatty acids in human plasma, comprising nearly 50 % in fasting humans (Dole 1956). Palmitic acid is therefore one of the most physiologically important saturated fatty acids. No direct link has been established between increased PA levels and AD. However, traumatic brain injury, which is also an independent risk factor for developing AD, is characterised by increased levels of saturated fatty acids in the brain; palmitic acid levels increase three-fold to ~ 180 μM (Lipton 1999).

Fatty acids have been shown to bind HSA *in vivo*. Under normal physiological conditions, HSA carries 0.1-2 moles of fatty acids per mole of albumin (Fredrickson *et al.* 1958). A crystal structure of HSA with PA bound shows that there are 7 distinct hydrophobic pockets that PA will bind (Figure 4.01) (Bhattacharya *et al.* 2000). It is possible that these hydrophobic pockets could also act as biding sites for Aβ and that PA may therefore compete with Aβ for binding to HSA thus prevent inhibition of Aβ fibril growth.

4.3 AIMS

I aim to investigate the effect of HSA on pre-formed mature Aβ fibres and characterise the stoichiometry of the Aβ-HSA complex. Finally, I will ascertain whether cholesterol and palmitic acid loaded HSA negates the inhibitory effect of albumin on Aβ fibrillisation kinetics.

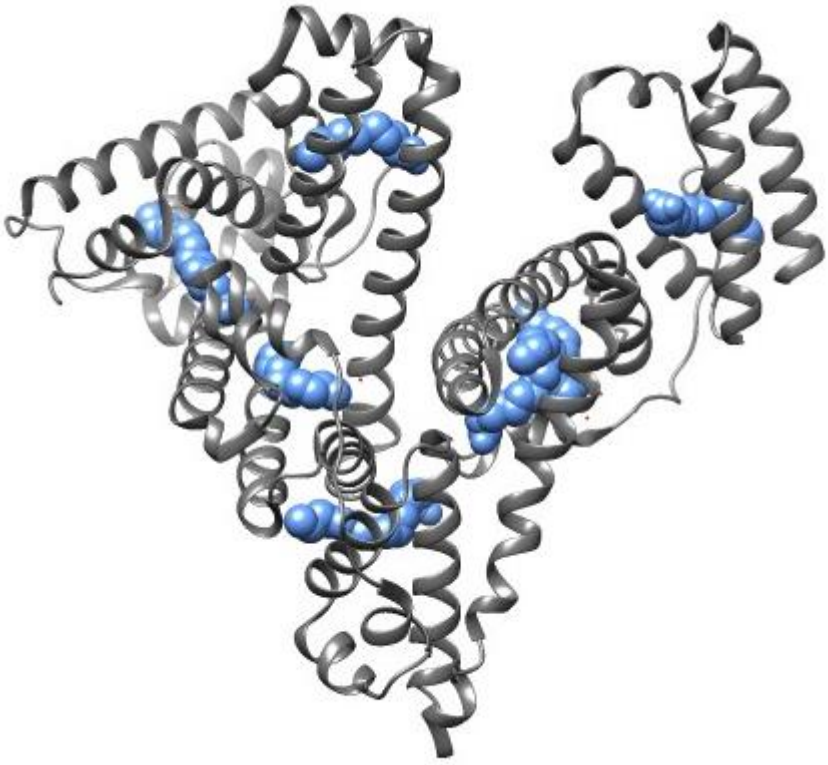

Figure 4.01. The Crystal Structure of HSA Complexed with Palmitic Acid.

The structure of HSA is represented as ribbons in grey. The 7 bound palmitic acid molecules are shown in a space-filling representation in blue. The structure was created from PDB code 1E7H (Bhattacharya *et al*, 2000) using UCSF Chimera.

4.4 EXPERIMENTAL

4.4.1 Albumin Preparation

Cholesterol-Loaded Albumin

Cholesterol was solubilised in dimethyl sulfoxide (DMSO) such that when diluted in aqueous buffer to the desired cholesterol concentration, the final DMSO concentration would be 2 % (v/v). Each HSA monomer binds one cholesterol molecule (Peng *et al.* 2008), thus an equimolar concentration of cholesterol and HSA was used throughout. The cholesterol and HSA, which had been solubilised as described in Chapter 2, was incubated together at room temperature to allow complex formation for a minimum of 30 minutes prior to use.

Palmitic Acid-Loaded Albumin

Palmitic acid was solubilised in DMSO. HSA can bind up to 7 palmitic acid molecules (Bhattacharya *et al.* 2000) thus essentially fatty acid free HSA was loaded with 7 mole equivalents of palmitic acid. Stocks of palmitic acid mixed with HSA, which had been diluted with water to contain 6 % DMSO, were incubated for 2.5 hours at room temperature to allow binding to occur. Excess palmitic acid was removed through 5 concentration/dilution cycles, using a 10,000 Da molecular weight cut-off centrifugal concentrator (Vivaspin, Sartorius) and diluting the complex with 6 % DMSO. Final concentrations of palmitic acid-loaded HSA used were diluted such that the samples contained 2 % DMSO.

4.4.2 Aβ Fibre Growth and Disassembly

Multi-Well Fluorescence, ThT Binding and Fibre Formation Kinetics

Fibre growth was monitored using ThT fluorescence as described in Chapter 2.

Single-Cell Fluorescence

Fibre growth and disassembly was followed using ThT Fluorescence. 10 μM Aβ(1-40) was incubated with 20 μM ThT in 160 mM NaCl and 30 mM HEPES, at pH 7.4. Samples contained 0.002 % (w/v) sodium azide to prevent microbial growth. The ThT measurements were conducted on a temperature-controlled Hitachi F-2500 fluorescence spectrophotometer at 30 ^{o}C. An excitation wavelength of 440 nm was used and data were collected between 460 nm and 650 nm. Samples were placed in a 1 cm quartz cuvette (Hellma) and three readings were averaged at each time point. Readings were taken every day for up to 50 days with samples being subjected to constant shaking at 30 ^{o}C between readings. The samples were kept in the dark to reduce possible degradation of the fluorophore and microbial growth.

4.4.3 Size-Exclusion Chromatography

The Tricorn Superdex 200 10/300 analytical gel-filtration chromatography column (GE Healthcare) was used on an automated AKTA FPLC system (GE Healthcare), at a flow rate of 0.5 ml/min at 4 ^{o}C. The column was equilibrated with 1.5 column volumes of buffer (160 mM NaCl and 30 mM HEPES, at pH 7.4). A 0.5 ml injection volume was used to load the protein sample onto the column. The approximate molecular weights of species observed was estimated using the standards bovine serum albumin, lysozyme, dextran blue and acetone. The column is capable of separating proteins below 600 kDa. Equation 4.01 is used to determine the proportion of pores available to the molecules.

$$K_{av} = \frac{V_e - V_0}{V_t - V_0} \qquad \text{(eq 4.01)}$$

Where, V_e is the elution volume, V_0 is the void volume, and V_t is the total volume of the column. The K_{av} of the standards can be plotted against the log of their molecular weights

to obtain a linear relationship between the two that can be used to approximate the molecular weights of the samples.

4.4.4 Mass-Spectrometry (MS)

Samples

Samples were either diluted into 30% acetonitrile/0.1% (v/v) formic acid or 10 mM ammonium bicarbonate at pH 7.3 for denaturing or native-like conditions, respectively. Prior to use, albumin was subjected to a minimum of four desalting steps into 10 mM ammonium bicarbonate pH 7.3 using a BioMax Ultrafree-0.5 PBCC Centrifugal Filter Unit with a 10 kDa molecular weight cut-off. Native-like samples were incubated for 20 hours at 30 ^{o}C, shaking at 250 rpm.

Instrumental Details:

MS experiments were performed on a Synapt HDMS System (Waters Corporation, Milford, MA, USA). Samples were introduced into the source region of the instrument by direct, static infusion nano-ESI by means of gold-coated fused silica nanospray needles (Waters Corporation, Milford, MA, USA). The instrument was operated in ESI positive mode with a capillary voltage of typically 1.2 kV, cone voltage of 100 V, extraction voltage of 3 V, trap and transfer collision energy of 12 V, trap DC bias of 4V and a source temperature of 80 °C for all experiments. The time of flight mass analyser was tuned in V-mode to give an operating resolution of 7,000 (Full Width Half Maximum) and was calibrated using 1 mg/mL sodium iodide in 50% aqueous propan-2-ol. A mass acquisition range of 500-7500 *m/z* was used. Optimised native-like conditions were achieved at an indicated pressure of 0.3 mbar backing pressure in the source region.

Tandem MS (MS/MS) data were collected from precursor *m/z* 4718 (15+ charge state plus Aβ) using the maximum precursor window, approximately 250 atomic mass units (amu). Collision energy was increased until fragment ions were apparent in the *m/z* region 500-1600 then held at a constant 45 V.

Data Processing:

MassLynx™ (v4.1) software (Waters Corporation, Milford, MA, USA) was used to acquire data and perform subsequent processing. Mass spectra were recorded at an acquisition rate of one spectrum per 2.4 sec with an interscan delay of 100 ms. Spectra obtained were deconvoluted onto a true mass scale with MaxEnt, a maximum entropy modelling program available within MassLynx™ (v4.1) software. ESI-MS data were smoothed, subtracted and centred.

4.5 RESULTS

4.5.1 Albumin Perturbs the Kinetics and Thermodynamic Equilibrium of Aβ Fibre Formation

It is clear from the data in Chapter 3 that HSA slows the formation of Aβ fibres and reduces the total number of fibres generated. However, as some assays showed a suggestion of a slight increase of fluorescence over the plateau phase once fibres had formed, I wanted to establish whether Aβ will continue forming fibres in the presence of albumin, just at a very much slower rate, until the total number of fibres generated equals that of Aβ in the absence of HSA. To investigate this further, I have followed Aβ(1–40) fibre growth over an extended period of time in both the presence and absence of one mole equivalent (10 μM) of HSA. It is clear from Figure 4.02 that HSA will almost completely inhibit Aβ fibre formation even over a fifty day period. In the absence of albumin, Aβ forms fibres in less than 24 hours, whereas fibre formation reaches a

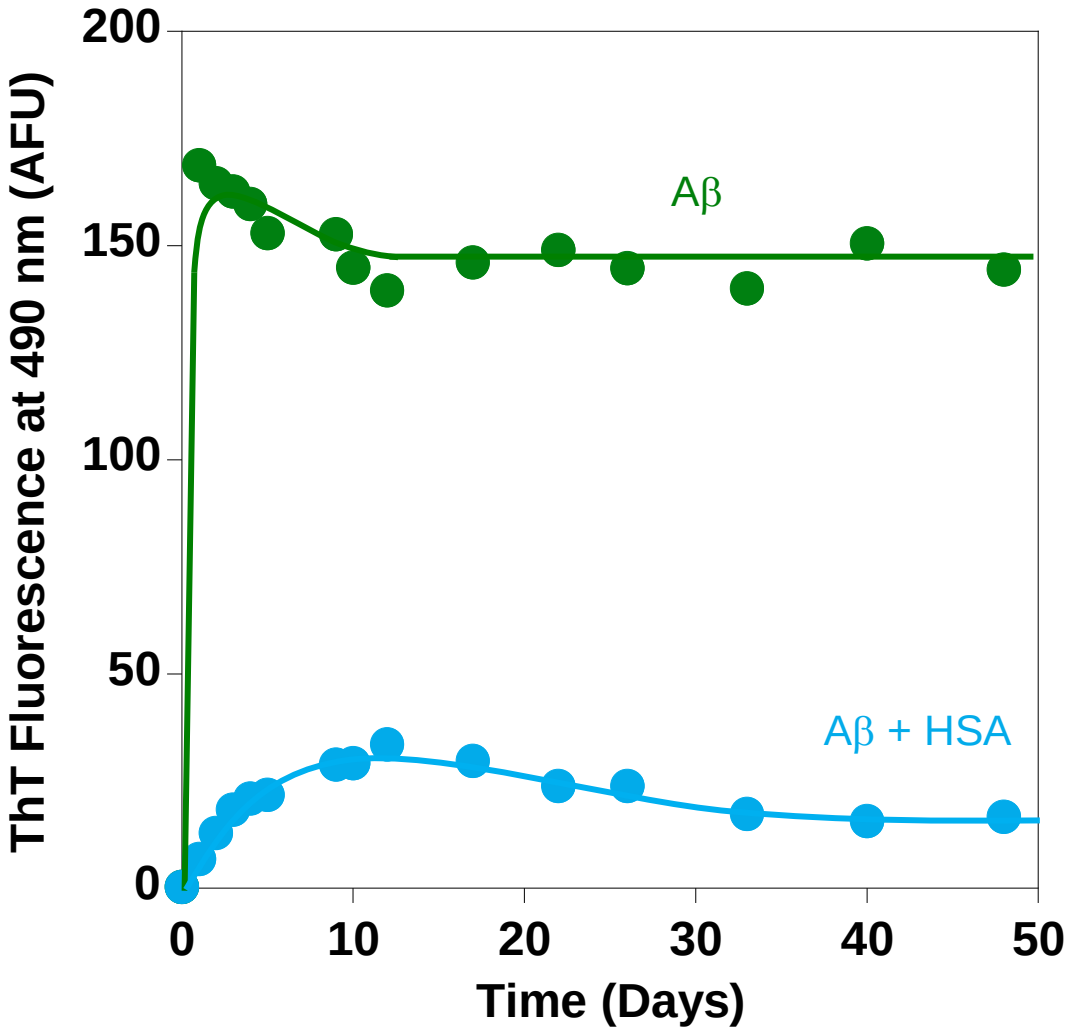

Figure 4.02. HSA Almost Completely Inhibits Aβ Fibre Formation Over Fifty Days.

10 μM Aβ(1-40) fibril growth in the absence and presence of 10 μM HSA measured over an extended period, detected using ThT fluorescence. Aβ(1-40) was incubated in 160 mM NaCl, 0.002 % sodium azide (w/v) and 30 mM HEPES at pH 7.4 at 30 ^{o}C with constant agitation.

maximum after 10 days in the presence of HSA. The total number of fibres generated in the presence of albumin, as indicated by the maximum ThT fluorescence, only reaches ~ 10 % of that of Aβ alone, even after 50 days. It is clear from Figure 4.02 that there is no evidence of a gradual increase in fibre content even after 50 days of incubation.

4.5.2 Albumin Does Not Perturb Preformed Mature Aβ Fibres

Next, I performed the reverse experiment, here HSA was added to preformed mature fibres. The addition of HSA to preformed Aβ(1–40) fibres also has no effect on the ThT signal consistent with the fibre formation not being reversed (Figure 4.03), even over a period of one month.

There is a slight drop in ThT fluorescence over this time period (~15 %), which is not significant and is likely to be due to degradation of the fluorophore rather than the fibres. This variation in fluorophore intensity is often observed, for example, in Figure 4.02 for Aβ in the absence of albumin.

4.5.3 The Stoichiometry of the Aβ-HSA Complex

In order to gain more insight into the mechanism by which albumin is able to inhibit Aβ fibrillisation, I have probed the stoichiometry of the complex formed using a variety of techniques. My fibrillisation studies and TEM (Chapter 3) are suggestive of one Aβ monomer binding an albumin monomer but there is much conjecture in the literature over whether monomers or oligomers bind albumin.

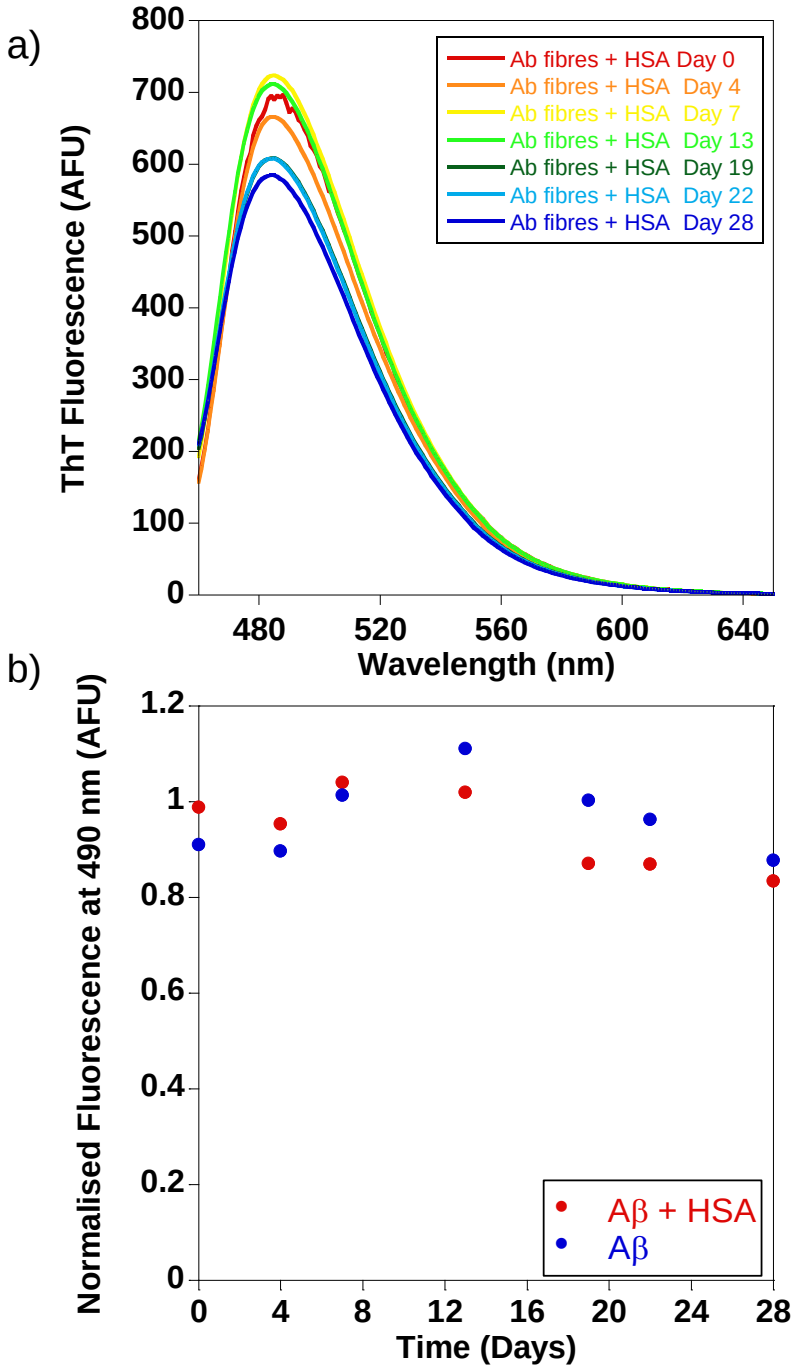

Figure 4.03. HSA Does Not Cause Disassembly of Mature Aβ Fibres Over 28 Days.

The state of 10 μM Aβ fibres in 30 mM HEPES and 160 mM NaCl at pH 7.4 in the presence of 20 μM HSA was monitored using ThT fluorescence over 4 weeks. a) The ThT fluorescence spectra of Aβ fibres in the presence of HSA. b) The ThT fluorescence signal obtained at 490 nm over 4 weeks for Aβ fibres in the absence and presence of HSA.

Size-Exclusion Chromatography

Size exclusion chromatography (SEC) can be used to estimate the molecular weight of the albumin-Aβ complex. The size-exclusion chromatograph of albumin, Aβ, and albumin and Aβ incubated together is shown in Figure 4.04. Monomeric Aβ(1-40) has a molecular weight of ~4 kDa but elutes at a volume which corresponds to ~26 kDa. This is because the masses are calculated assuming the molecules have a small axial ratio (i.e. globular rather than rod-like or unstructured in shape). Natively unstructured Aβ therefore always elutes at a volume like that of a larger molecule, approximately five times larger than the real mass (Talmard *et al.* 2007). Converting the elution peaks of albumin alone gives a molecular weight of ~69 kDa for the monomer and ~113 kDa for the dimer, as expected. The molecular weight of the dimer is not exactly double that of the monomer, highlighting the imprecision of SEC as a method for determining molecular weight. In comparison to HSA alone, the shift observed in the elution peaks of albumin and Aβ incubated together is slight but is indicative of a larger complex, with molecular weights of ~82 kDa and ~137 kDa, respectively. There are no extra elution peaks for larger complexes, thus HSA binding a large oligomer can be ruled out. This suggests an Aβ monomer or small oligomer (≤ 5 monomers) binds to one HSA monomer, when albumin is in both monomeric and dimeric form. However, there is much overlap of the retention volume and the decrease in elution time for the HSA-Aβ mixture may not be significant. It is clear a large Aβ-HSA complex with multiple Aβ monomers bound does not elute from the column.

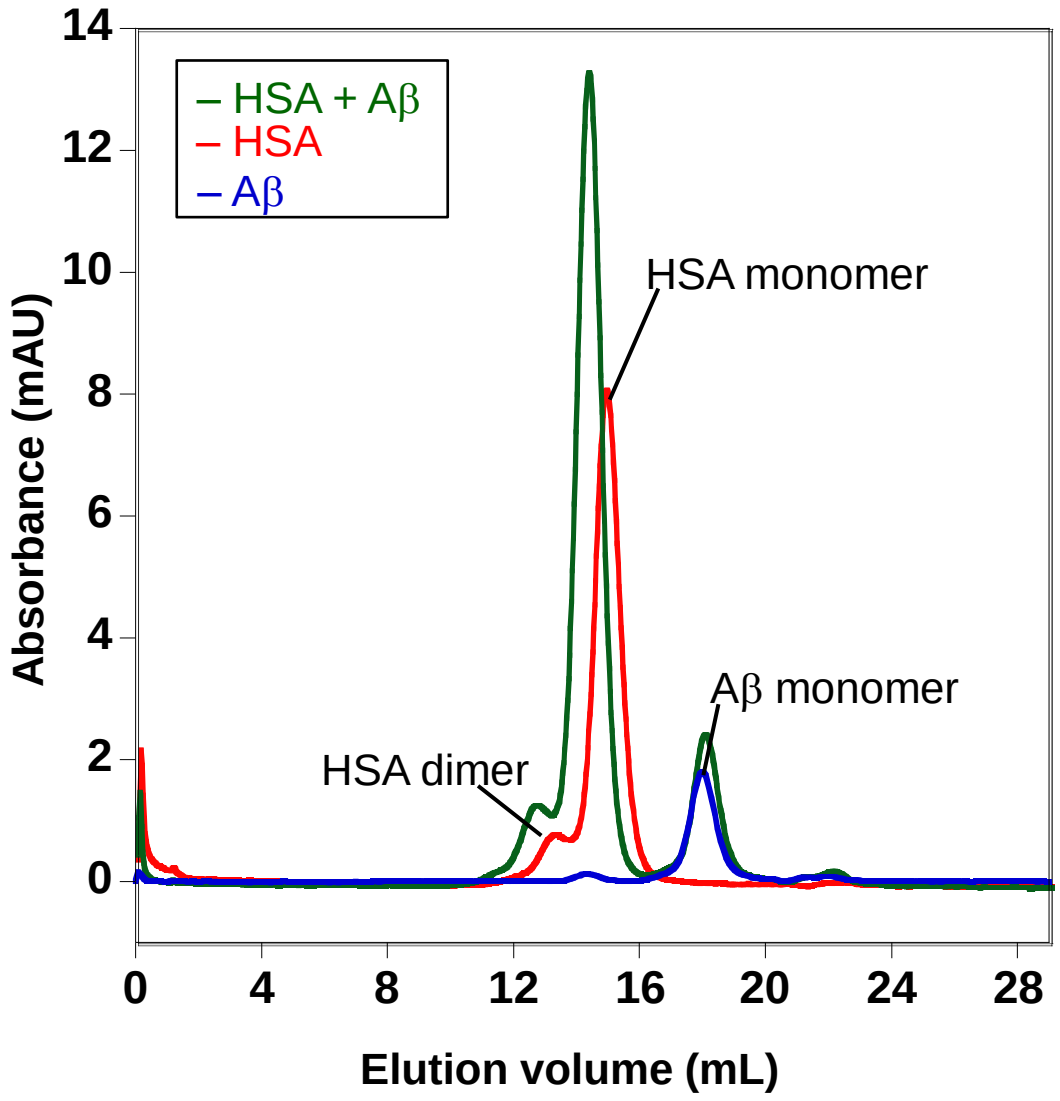

Figure 4.04. Size Exclusion Chromatography of Aβ(1-40) and HSA.

Size exclusion chromatography was performed on 500 μL samples of 3 μM HSA, producing peaks at ~113 and ~69 kDa (red); fresh 10 μM Aβ(1-40), producing peaks at ~26 kDa (blue); and 3 μM HSA and 10 μM Aβ(1-40) incubated together, producing peaks at ~137, ~82 and 27 kDa (green). Samples were in 30 mM HEPES and 160 mM NaCl at pH 7.4 and run through a Superdex-200 column at a flow rate of 0.5 mL/minute.

Mass Spectrometry (MS)

Next I wanted to probe the Aβ-HSA complex via mass spectrometry (MS). Monomeric Aβ when run under denaturing and native-like conditions on a mass spectrometer gives identical spectra (Figure 4.05) due to Aβ having no secondary structure. Three distinct *m/z* peaks are visible that are the +3, +4 and +5 charge states. These give Aβ a mass of 4330, as would be expected from the sequence, with an additional proton for each sequential charge state.

Human serum albumin is a globular protein so the denaturing conditions can give a much more accurate *m/z* spectrum than native conditions, which can be deconvoluted to obtain a mass of albumin (Figure 4.06). Even under denaturing conditions, a range of masses is evident as the sample is heterogeneous and contains albumin with Na^+ bound as well as the cysteinylated form (at Cys^{34}) in addition to the unmodified form. The native-like albumin has very broad peaks so it is not possible to deconvolute the data using MaxEnt (Figure 4.07). There are five distinct peaks for the +14 to +18 charge states. The calculated average mass is slightly higher when run in the native state at approximately 66,780 Da. This value is calculated from the centre of the Gaussian peak for each charge state as shown in Figure 4.07b. This method does not account for the relative abundance of multiple naturally occurring isotopes, ^{13}C in particular. The molecular mass based on the sequence alone, accounting for the relative isotope abundance should be 66,438 Da, as identified by MaxEnt from Figure 4.06.

When Aβ(1–40) and albumin are incubated together over-night, the native spectrum is very similar to that of albumin alone except for appearance of unbound Aβ charge states in the lower *m/z* range and the broadening of the peaks denoting the HSA +14-+18 charge

a)

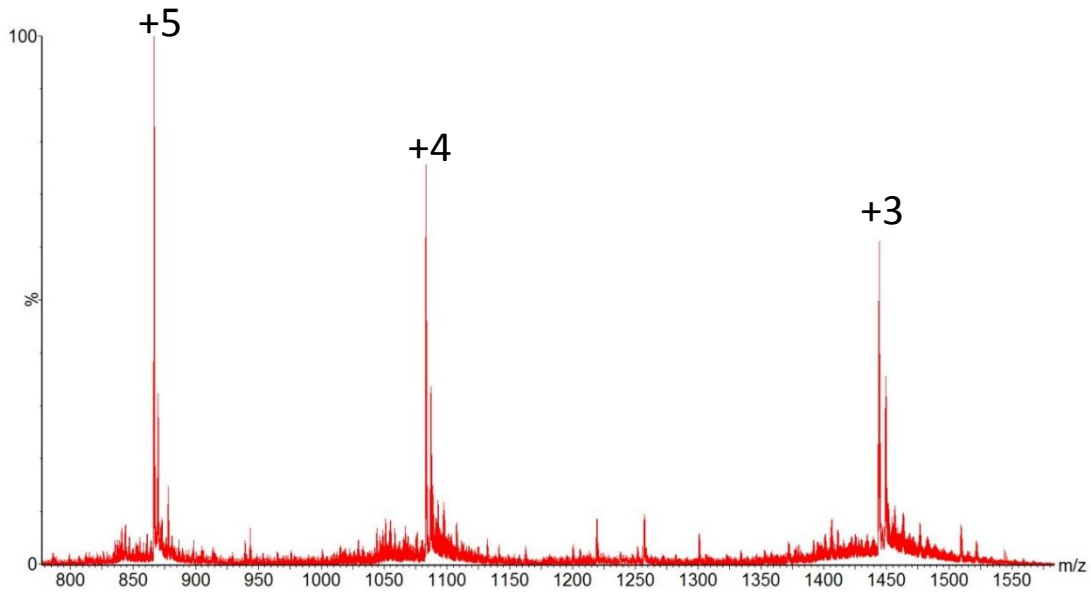

b)

m/z	**z**	**Mass (Da)**
12996	+3	4332
17332	+4	4333
21670	+5	4334

Figure 4.05. Mass Spectrum of Aβ(1-40) Under Denaturing Conditions.

a) Mass spectrum of 20 μM Aβ in 30 % acetonitrile (v/v) and 1 % formic acid (v/v). The dominant peaks represent the +3-+5 charge states, which correspond to the masses shown in b).

a)

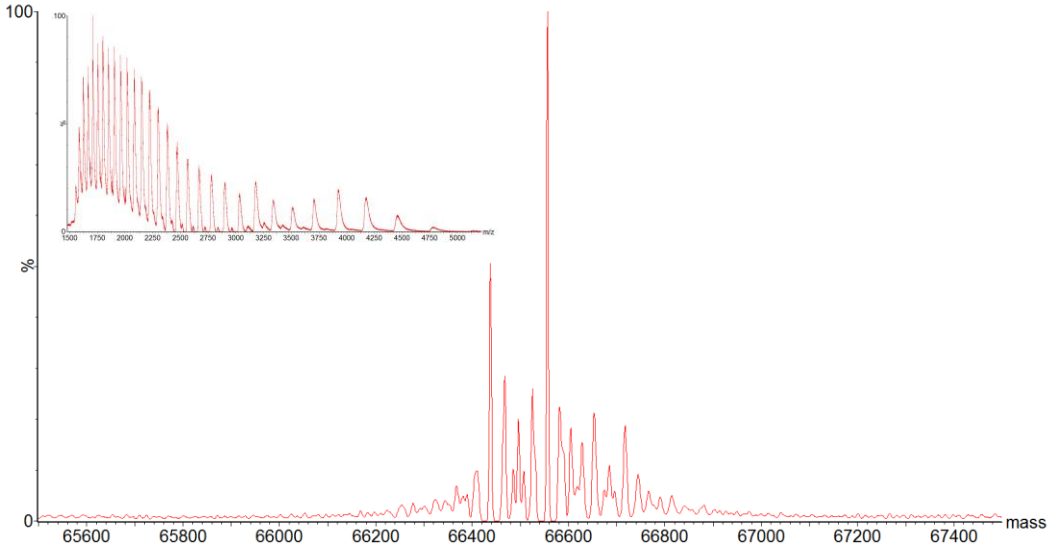

b)

Mass (Da)	Change from 66438	HSA species
66438	0	Unmodified
66465	27	Unmodified + Na
66490	52	Unmodified + 2 Na
66509	71	Unmodified + 3 Na
66529	91	Unmodified + 4 Na
66556	118	Cysteinylated
66580	142	Cysteinylated + Na
66603	165	Unmodified + 1 Glucose

Figure 4.06. Mass Spectrum of HSA Under Denaturing Conditions.

a) Deconvolution of the mass spectrum of 10 μM HSA in 30 % acetonitrile (v/v) and 1 % formic acid (v/v) to obtain the most abundant species. Insert shows the mass spectrum that has been deconvoluted. b) Table showing the breakdown of the species to which the masses from a) correspond.

a)

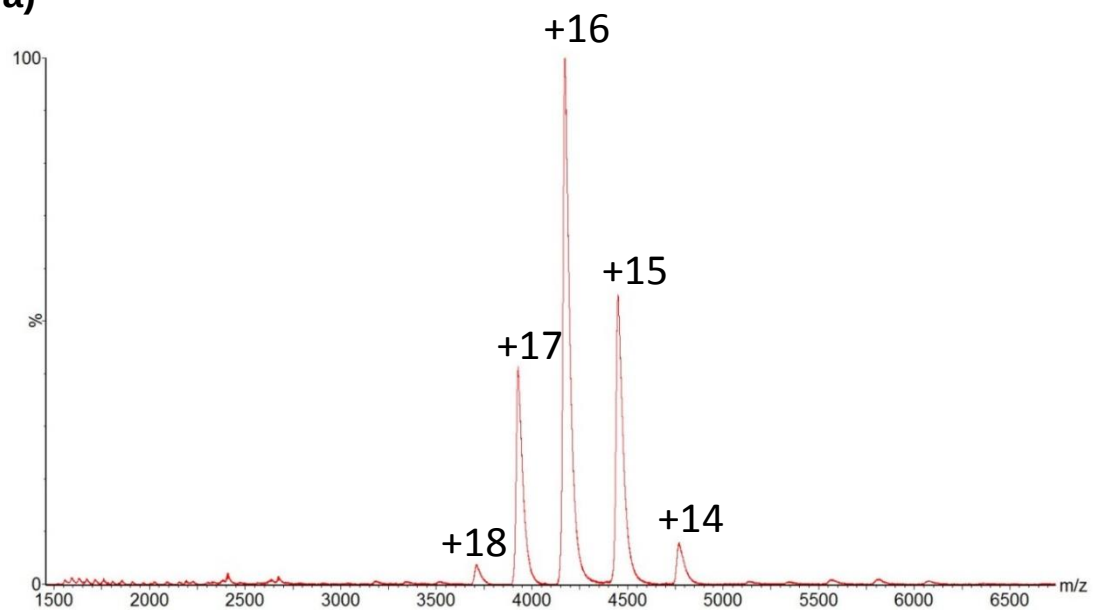

b)

Charge	Mass (Da)
+14	66794
+15	66765
+16	66768
+17	66793
+18	66780

Figure 4.07. Mass Spectrum of HSA Under Native Conditions.

a) Mass spectrum of 5 μM HSA in 10 mM Ammonium bicarbonate at pH 7.3. The dominant peaks represent the +14 to +18 charge states that correspond to the masses shown in b).

states (Figure 4.08). This shift from the expected Gaussian distribution could represent the overlap of two peaks derived from albumin alone at one charge state and one Aβ(1–40) monomer bound to a single HSA monomer at a sequentially higher charge state. In order to test this, tandem MS was performed. Tandem MS can be used to select ions with a particular *m/z* value. It is then subjected to mild fragmentation and the resulting mass spectrum recorded. Here tandem MS selecting for 4718 *m/z* was employed, as this is the *m/z* value expected for one Aβ monomer bound to one HSA at the 15+ charge state, with a window of 250 amu. The fragmented mass spectrum of this selected ion is shown in Figure 4.09. The spectrum suggests no evidence of the Aβ monomer present at 4718 *m/z*.

I hypothesised the broadening of the MS spectra observed for HSA incubated with Aβ was due to the high salt content, I therefore looked at the effect of salt. Figure 4.10a shows the effect of not desalting albumin on the mass spectrum. The peaks become much broader, similar to the peak broadening observed with incubation with Aβ. It was not possible to desalt the Aβ prior to incubating with HSA; therefore it is feasible that HSA MS peaks are broadened by the high concentrations of salt acquired from Aβ. Figure 4.10b compares the spectrum of HSA incubated with 2 mole equivalents of Aβ(1-40) with and without desalting after incubation. It is evident that the peak width shrinks after desalting.

It is clear that even under the mild ionising conditions used here; the Aβ-HSA complex has disassociated upon ionisation and is not detected.

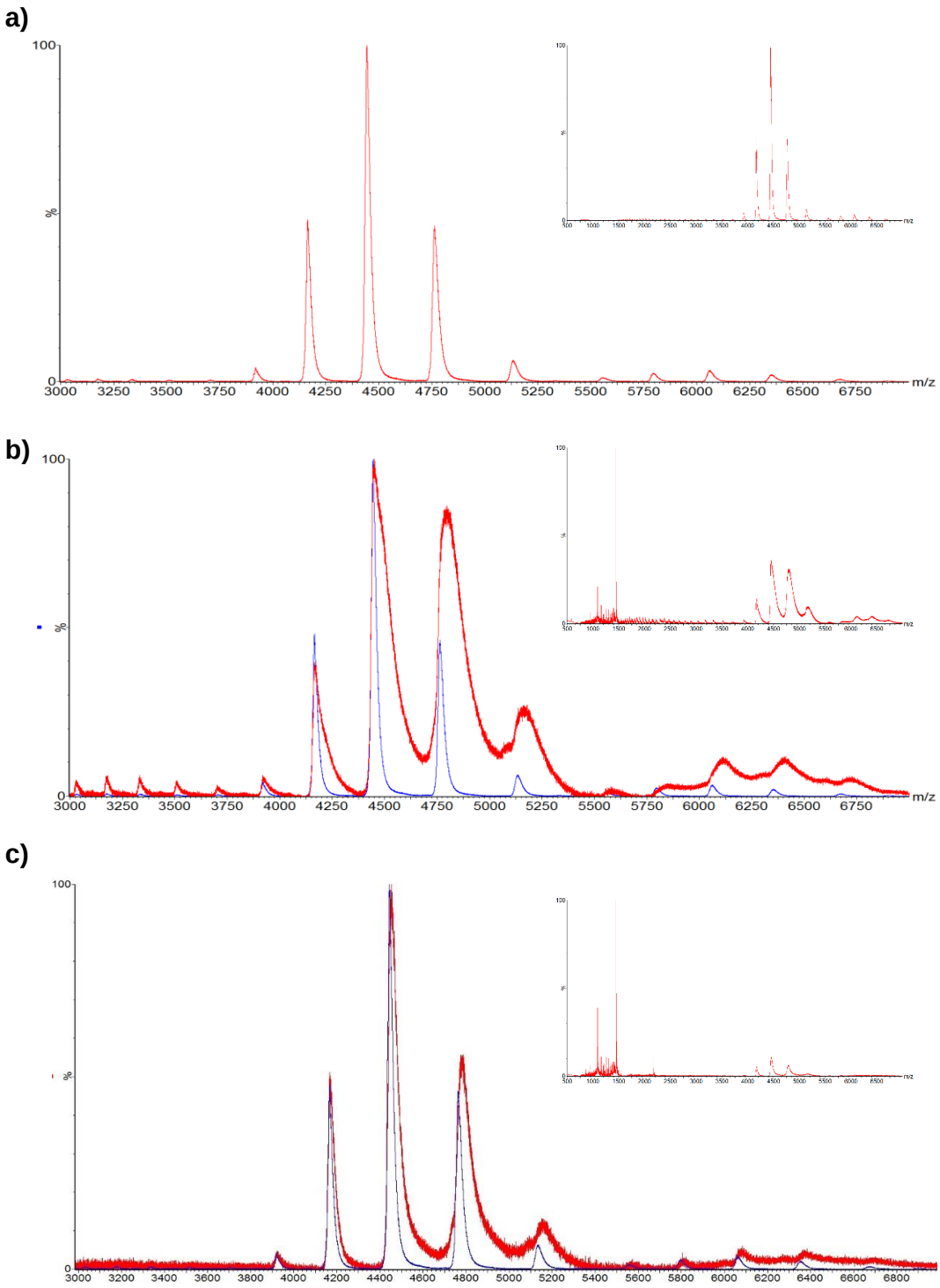

Figure 4.08 Mass Spectrum of HSA Incubated with Aβ(1-40) Under Native Conditions.

a) Mass spectrum of 10 μM HSA alone, b) with one mole equivalent, and c) with 2 mole equivalents of Aβ(1-40) in 10 mM Ammonium bicarbonate at pH 7.3 after overnight incubation. Blue spectra in b) and c) are the spectrum of HSA alone shown in a) for comparison. Insets show full spectrum between 500 and 7000 *m/z*, showing the unbound Aβ charge states to smaller *m/z* values.

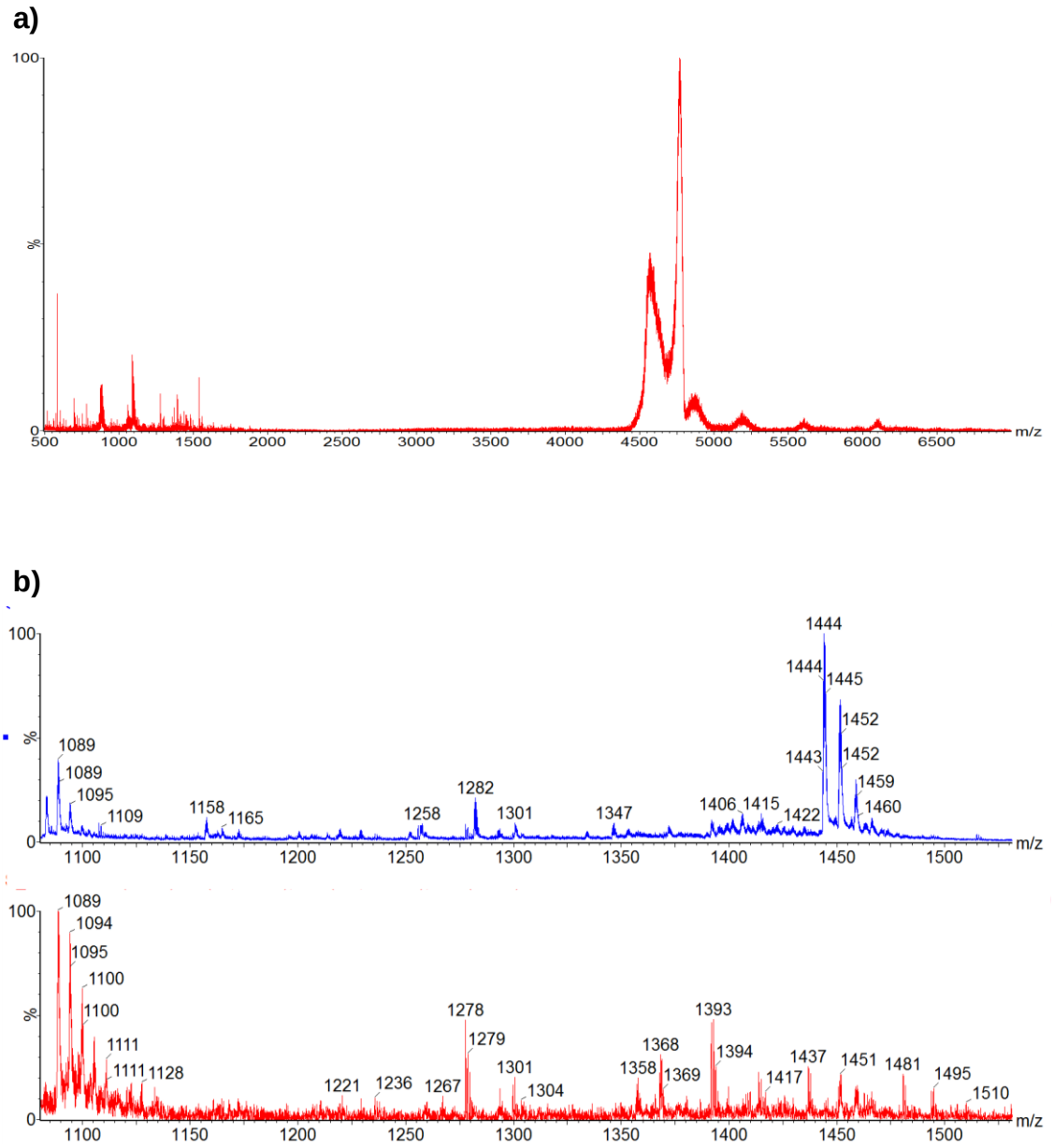

Figure 4.09. Tandem MS of HSA and Aβ(1-40)

a) Tandem MS of 10 μM HSA + 10 μM Aβ(1-40) in 10 mM Ammonium bicarbonate at pH 7.3 after overnight incubation selected for m/z 4718 with a window of ~ 250 amu. b) The results from MS of HSA and Aβ incubated together (as shown in Figure 4.08b) in the range Aβ charge states are normally observed (above) compared with the results of the tandem MS in a) (below).

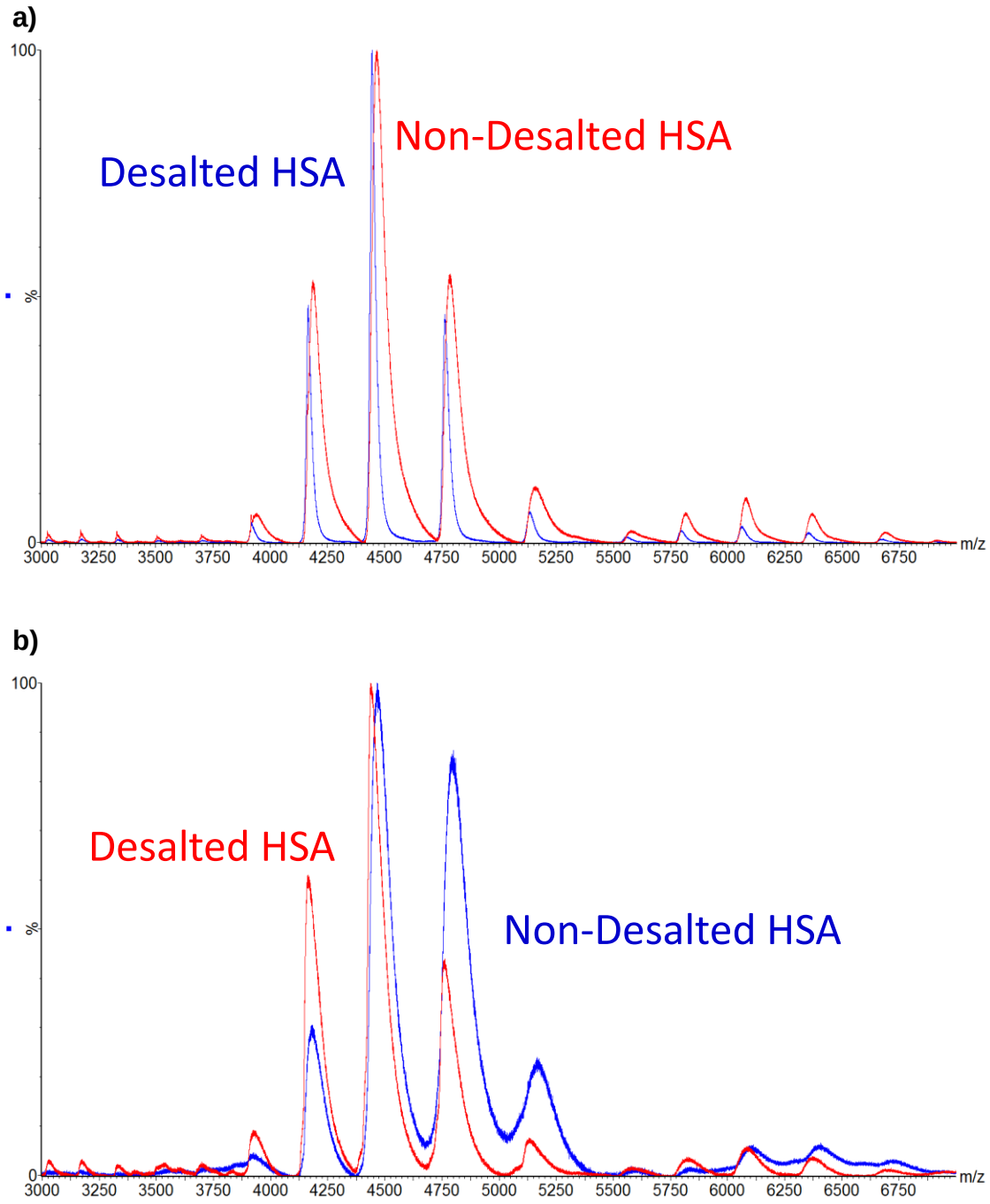

Figure 4.10. The Presence of Salt Broadens the Albumin Peaks in Mass Spectrometry

a) Mass spectrum of 10 μM HSA in 10 mM Ammonium bicarbonate at pH 7.3 with and without desalting. b) Mass spectrum of 1:1 HSA:Aβ before and after desalting.

4.5.4 Cholesterol-Loaded HSA Negates Albumin's Inhibition Of Aβ Fibrillisation

Cholesterol is a known risk factor for developing AD and also binds HSA. Therefore, I have studied the effect of cholesterol-loaded HSA on Aβ fibrillisation kinetics to determine if cholesterol may influence the risk of developing AD by blocking albumin from inhibiting Aβ fibre formation. Figure 4.11 shows the ThT binding curves obtained for Aβ in the presence of HSA, cholesterol-loaded HSA and cholesterol alone. It is evident that 20 μM albumin will completely inhibit fibrillisation of Aβ(1-40). However, albumin loaded with an equimolar concentration of cholesterol does not fully inhibit fibre growth. Fibrillisation is partially recovered such that the t_{lag} is six times longer and the total number of fibres generated is dropped by one third. It is likely that some albumin may not have any cholesterol bound, and would therefore be able to bind Aβ, which would account for the percentage drop in Aβ that forms fibres compared to Aβ alone. The control of cholesterol alone has no effect on the total number of Aβ fibres generated but has slowed the lag time of fibre growth a little. This means that the recovery of fibre growth cannot be due to cholesterol increasing the rate of fibrillisation alone and must therefore be due to cholesterol being bound to albumin, preventing Aβ from binding to albumin. Cholesterol is not soluble in water and was therefore solubilised in DMSO prior to loading in into albumin. To ensure that any effect observed on fibrillisation in the presence of cholesterol was due to the cholesterol rather than the low levels of DMSO, Aβ fibril growth in the presence of 2 % DMSO was also studied as a control. Figure 4.11e demonstrates that the lag time, rate of fibrillisation and total number of fibres generated is unaffected by 2 % (v/v) DMSO.

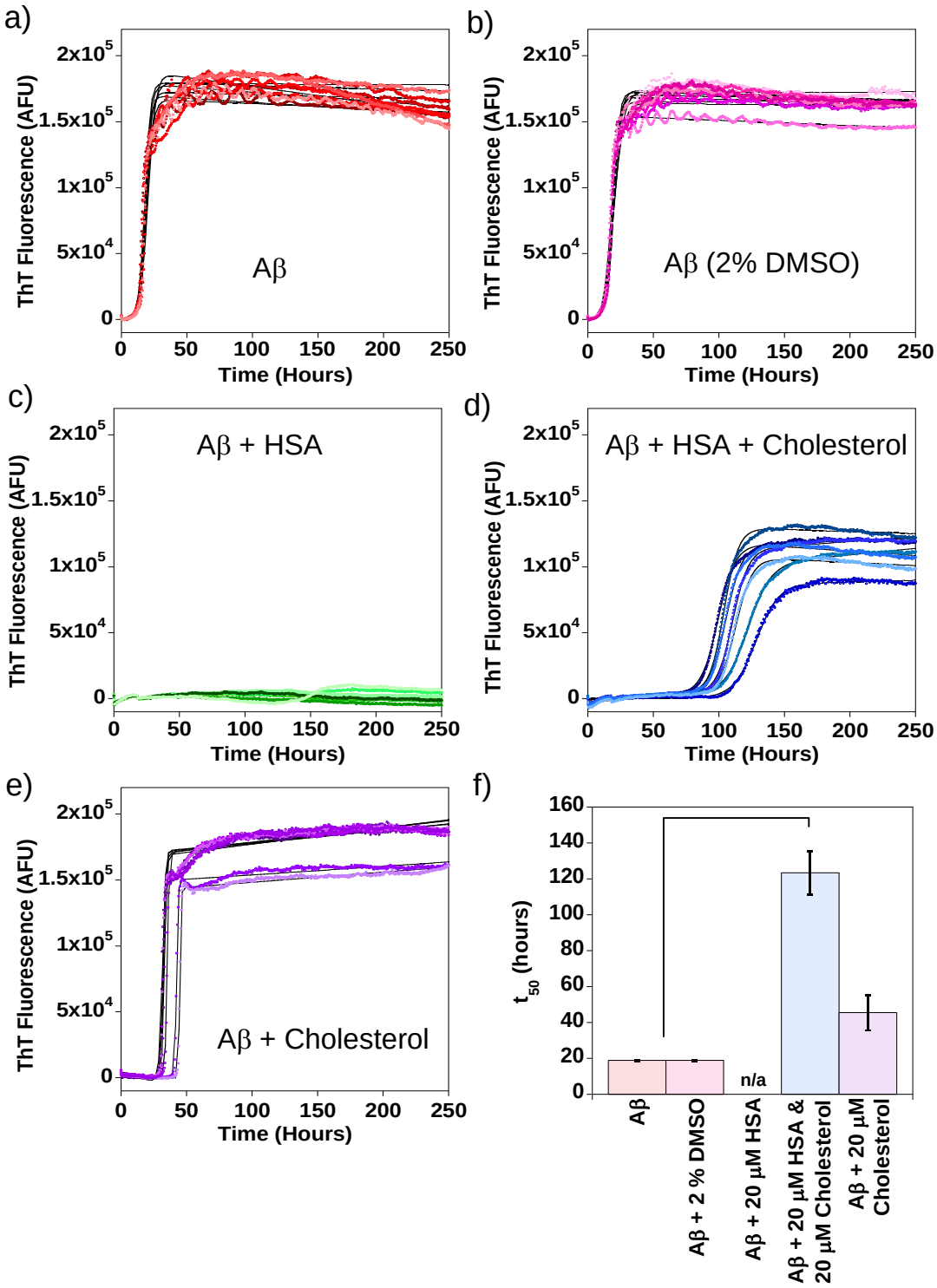

Figure 4.11. Aβ(1-40) Fibril Growth in the Presence of HSA and Cholesterol

Fibrillisation of 10 μM Aβ(1-40) monitored using ThT fluorescence. Here individual traces of a) Aβ alone, and Aβ in the presence of b) 2 % DMSO, c) 20 μM HSA, d) 20 μM HSA and 20 μM cholesterol, and e) 20 μM cholesterol are shown. f) The mean t_{50} values obtained are shown with standard error. Significant differences from Aβ alone are shown by connecting lines at $\alpha = 0.05$.

The average kinetic parameters of fibril growth were obtained for the growth curves shown in Figure 4.11 as well as further fibre growth experiments in the presence of 10 μM cholesterol-loaded and cholesterol-free HSA. At 10 μM albumin, the same pattern is evident as with 20 μM HSA shown by the average kinetic parameters in Figure 4.12. There is inhibition of Aβ fibril growth by HSA but to a lesser extent when the albumin is loaded with cholesterol. Cholesterol has little effect on Aβ fibrillisation by itself.

The concentration of HSA in the CSF is 3 μM so I next studied the effect of this physiological concentration on Aβ(1–40) fibrillisation (Figure 4.13). This lower concentration of HSA will not completely inhibit fibril formation but the increase in the nucleation time (t_{lag}) and decrease in the rate of elongation (k_{app}) is still significantly different compared to Aβ fibre growth on its own. The cholesterol-loaded HSA also significantly inhibits fibre growth in terms of nucleation rate and elongation rate compared to Aβ fibrillisation but the rate of elongation is increased in comparison to Aβ fibre growth in the presence of cholesterol-free HSA. This indicates that cholesterol bound to HSA can negate its inhibitory action on Aβ(1–40) fibre formation at concentrations found in the CSF. It is clear, based on experiments with 3, 10 and 20 μM albumin that cholesterol bound to albumin will compete with the Aβ-albumin interaction.

4.5.5 Albumin Will Not Inhibit Aβ Fibrillisation when Complexed with Palmitic Acid

The effect albumin has on Aβ(1–40) fibrillisation when loaded with 7 mole equivalents of palmitic acid (PA) is shown in Figure 4.14. Albumin will completely inhibit fibre formation at 10 μM when it is essentially fatty acid free but when the HSA is loaded with

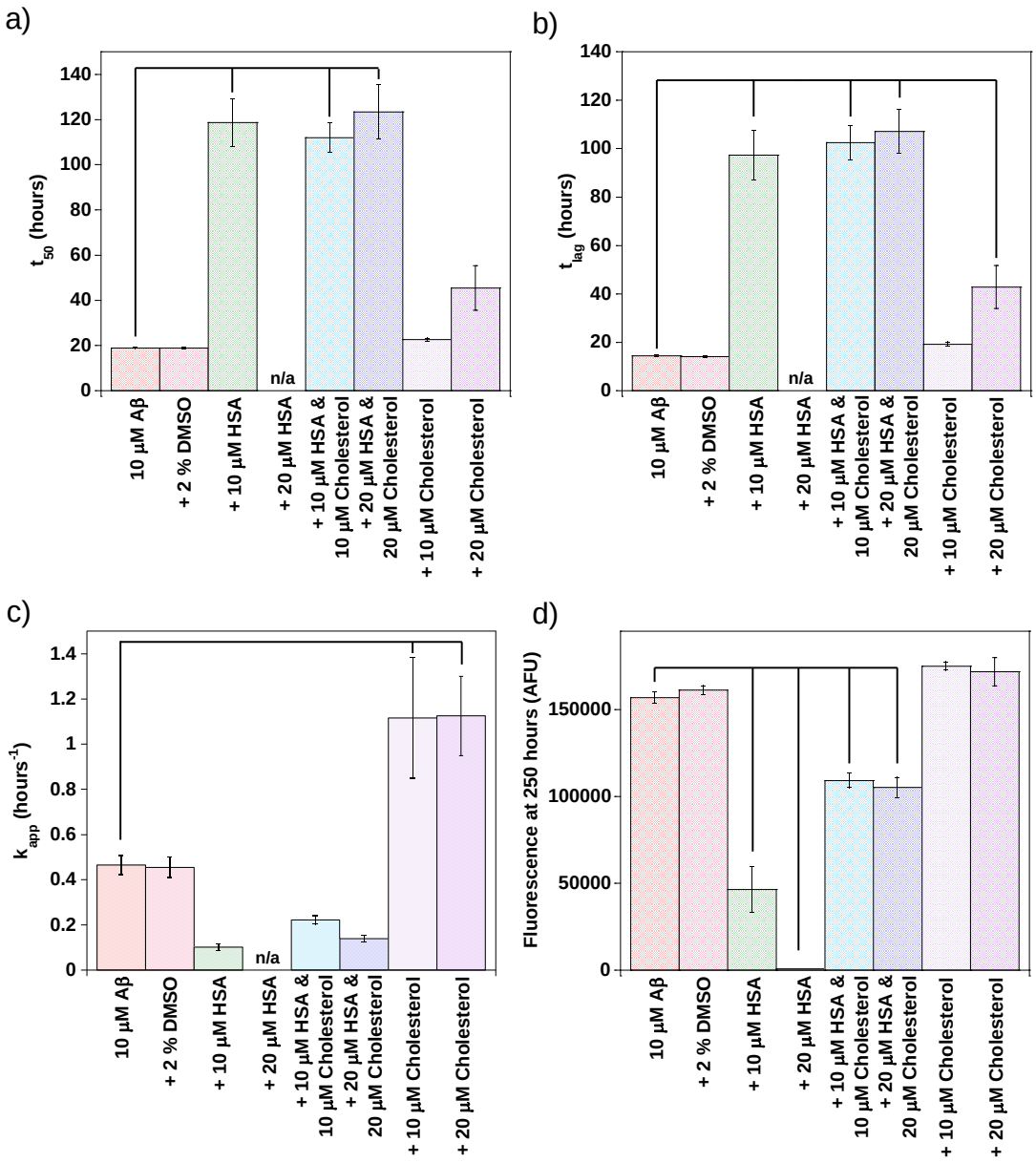

Figure 4.12. Kinetics of Aβ(1-40) Fibril Growth in the Presence of HSA and Cholesterol

Fibrillisation of 10 µM Aβ(1-40) monitored using ThT fluorescence. Here the mean a) t_{50}, b) t_{lag}, c) k_{app}, and d) maximum fluorescence values obtained are shown with standard error. Significant differences from Aβ alone are shown by connecting lines at $\alpha = 0.05$.

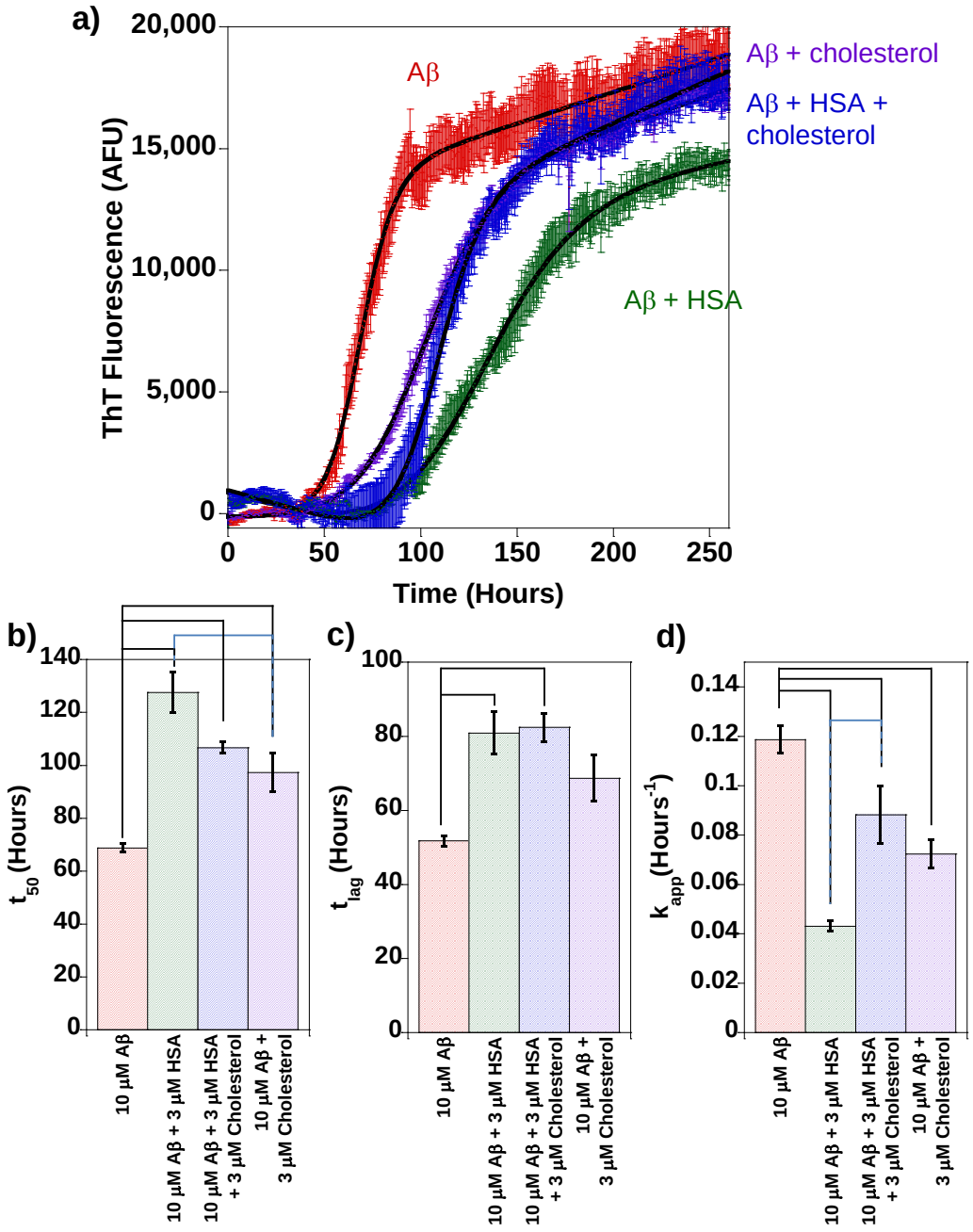

Figure 4.13. Aβ(1-40) Fibril Growth in the Presence of Physiological Concentrations of HSA and Cholesterol

a) Average traces of 10 μM Aβ(1-40) fibrillisation in the presence of 3 μM, cholesterol, cholesterol-loaded and cholesterol-free HSA monitored using ThT fluorescence. b-d) The mean kinetic parameters obtained from the fibril growth in a) under each condition: b) t_{50}, c) t_{lag}, and d) k_{app}. Significant differences are shown by connecting lines at $\alpha = 0.05$.

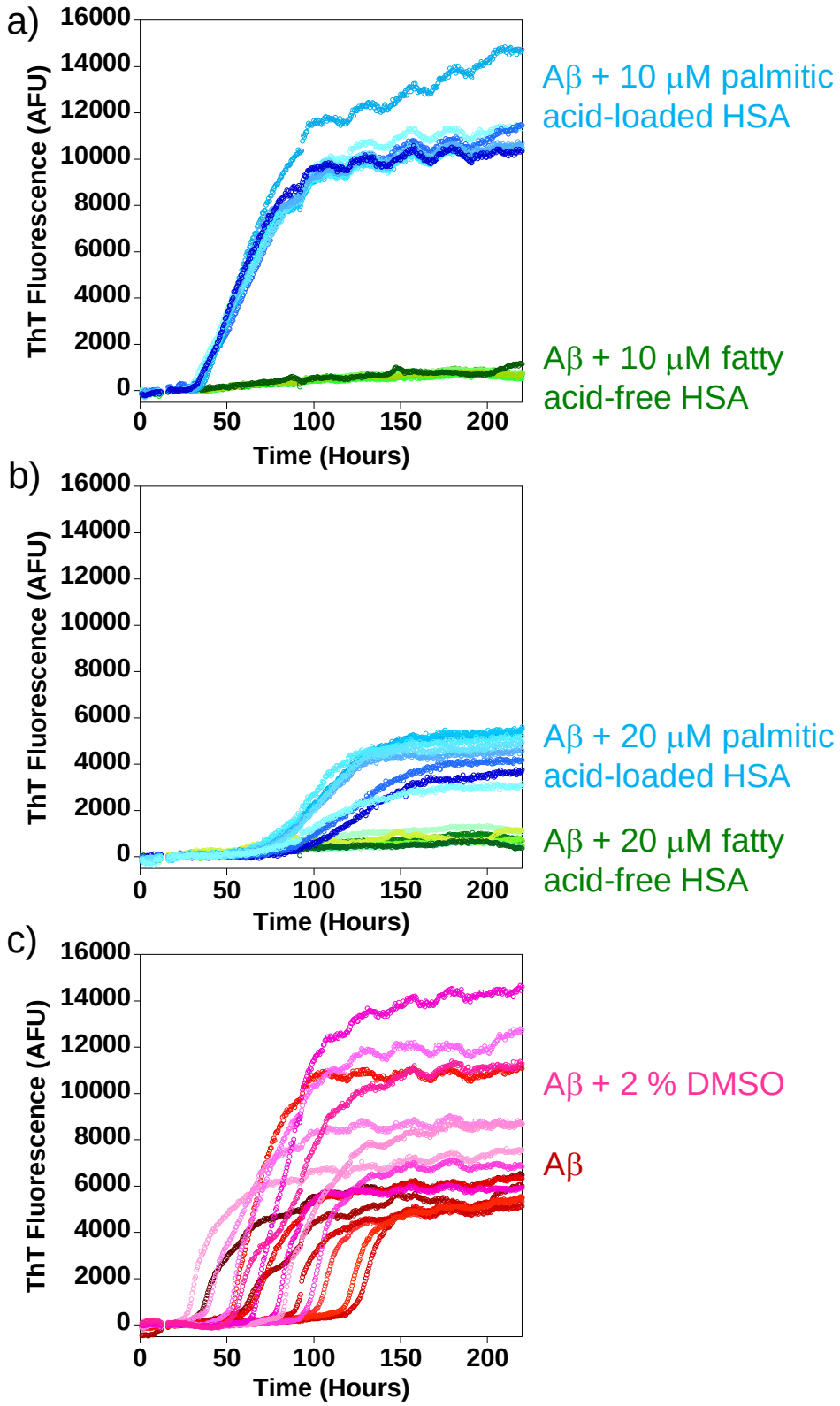

Figure 4.14. Aβ(1-40) Fibril Growth in the Presence of Palmitic Acid Loaded-HSA

Fibrillisation of 10 μM Aβ(1-40) monitored using ThT fluorescence. Here individual traces of Aβ growth in the presence of a) 10 μM palmitic acid-loaded and fatty acid-free HSA, b) 20 μM palmitic acid-loaded and fatty acid-free HSA, and c) in the presence of 2 % DMSO and alone are shown.

PA, the Aβ fibre growth has the same rate as fibrillisation in the absence of albumin. This can also be seen for fibre growth in the presence of 20 μM HSA. The PA is insoluble in water so PA was solubilised with DMSO in order to load it into the albumin and diluted such that only 2 % DMSO remained. It is evident in Figure 4.14c that DMSO has no effect on the fibrillisation of Aβ.

A repeat of this experiment gave similar results, Figure 4.15. The Aβ(1-40) fibre formation is completely inhibited by 20 μM fatty acid-free albumin but the PA-loaded albumin completely ameliorates this inhibition such that the rate of fibrillisation returns to that of Aβ(1-40) in the absence of HSA. In addition to the rate of fibril growth being similar, the total number of fibres generated is also equal for the Aβ(1-40) grown in the presence of PA-loaded HSA and Aβ(1-40) grown without albumin. The extent of inhibition for 10 μM fatty acid-free HSA is not complete but the total number of fibres generated is reduced by approximately 50 % as well as the t_{lag} being significantly increased. However, this is not true for PA-loaded HSA at 10 μM; as observed for 20 μM HSA, the rate and extent of Aβ(1-40) fibrillisation is strikingly similar to that of Aβ fibre growth alone. Like cholesterol, PA binds to HSA and disrupts the interaction of Aβ with albumin.

4.6 DISCUSSION

4.6.1 Albumin May Not Reverse Fibre Formation

As I show in Chapter 3, albumin will bind Aβ, preventing Aβ self-association into fibres. It is likely in the presence of Aβ monomer, the Aβ-HSA complex forms relatively fast. The formation of Aβ fibres and the Aβ-HSA complex can therefore be thought of as the following equilibrium:

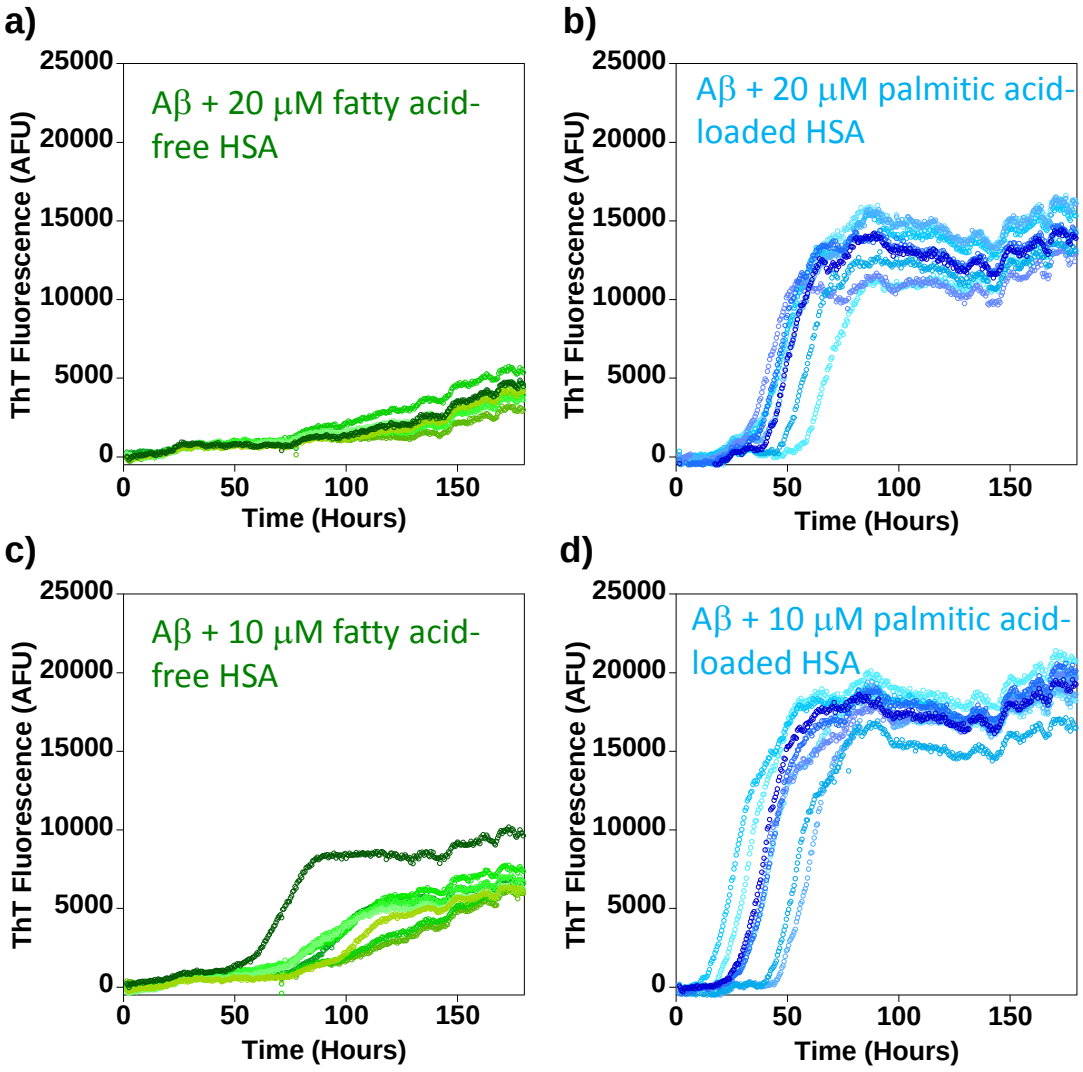

Figure 4.15. Aβ(1-40) fibril growth in the presence of palmitic acid loaded-HSA (Repeat)

Fibrillisation of 10 μM Aβ(1-40) monitored using ThT fluorescence. Here individual traces of Aβ growth in the presence of a) 20 μM fatty acid-free HSA, b) 20 μM palmitic acid-loaded HSA, c) 10 μM fatty acid-free HSA, and d) 10 μM palmitic acid-loaded HSA are shown.

Aβ-HSA $\rightleftharpoons$ Aβ monomer $\rightleftharpoons$ Aβ fibres
(on/off fast) (on/off slow)

Aβ binding to HSA will also dissociate and if Aβ has a weaker affinity for albumin than Aβ self-association in fibres, it could be expected that the extent of fibre formation would eventually equal that of fibre growth in the absence of HSA as the Aβ dissociates from HSA and self-associates with the existing Aβ fibres. However, as shown in Figure 4.02, Aβ(1-40) fibre growth is almost completely inhibited by one mole equivalent of HSA even after a 50 day duration, with no sign of the total number of fibres generated increasing over time.

The affinity of Aβ monomer for Aβ fibres has previously been calculated to be in the 1 μM range (O'Nuallain *et al.* 2005). This is only marginally tighter than the reported affinity of Aβ for HSA (5 μM) (Rózga *et al.* 2007) thus the concentration of albumin and fibres available for Aβ monomer binding becomes extremely important. Fibres only form through Aβ monomer self-association therefore the number of fibres cannot equal the number of Aβ monomers in the system. In this experiment, an equimolar concentration of HSA and Aβ(1-40) monomer was used thus the number of albumin molecules was greater than the number of fibres. Despite the tighter affinity for Aβ fibres, the Aβ monomer is therefore more likely to bind albumin due to the number of molecules available to bind compared to fibres making Aβ fibre elongation kinetically unfavourable.

Aβ fibres are in dynamic equilibrium with Aβ monomers and oligomers so it could be expected that the presence of albumin complexed with Aβ would push the equilibrium such that over time fibres disassemble if Aβ bound to HSA does indeed represent the

more thermodynamically favourable state and thus returning the equilibrium to its preferred state. However, when HSA is added to preformed fibres, there is no evidence of fibril disassembly observed (Figure 4.03), even of a period of 28 days.

It is clear that there are conflicting observations in Figures 4.02 and 4.03 suggesting that at least one of the reactions must not have reached true thermodynamic equilibrium, even after more than four weeks at room temperature. It is clear that one of the reactions is kinetically trapped. It could be albumin that traps Aβ as a monomer or that Aβ becomes trapped as a fibre once formed. Fibre formation could be kinetically trapped because the rate of association is slow, which is evident by the time taken for fibre growth to occur; it takes days for fibres to form. Alternatively once fibres are formed, dissociation is kinetically slow. It remains a possibility that at true equilibrium fibres may be favoured over the Aβ-HSA complex, but albumin is able to trap Aβ as a monomer. Crucially, the kinetics of fibre formation are what determines whether AD develops so it is clear that albumin has a profound influence on fibre formation.

Overall, albumin has little effect on Aβ fibrillisation beyond the nucleation and elongation stage and is therefore likely to bind Aβ only when Aβ is in its monomeric state or is a small oligomer. The use of albumin exchange as a treatment for Alzheimer's disease, is showing promise in phase II clinical trial (Boada *et al.* 2009). My studies suggest it is therefore likely to be effective at reducing Aβ burden through removal of fresh Aβ monomer and would be less effective at reversing plaque formation. Thus this treatment may only be effective in mild to moderate AD to prevent further progression of the disease.

4.6.2 The Stoichiometry of the Aβ-HSA Complex

There is debate over the stoichiometry of Aβ binding HSA. The calculated K_d of 5 μM, which corresponds well with the extent of inhibition of Aβ fibrillisation by HSA observed in Chapter 3, is based upon a one to one stoichiometry (Rózga *et al.* 2007). This is also supported by Kuo et al (Kuo *et al.* 2000). Milojevic *et al* have performed a series of experiments that are consistent with HSA binding Aβ oligomers but not monomers or fibres (Milojevic *et al.* 2014, Milojevic *et al.* 2007, Milojevic *et al.* 2011, Milojevic *et al.* 2009). Albumin has also been shown to trap Aβ as soluble oligomers (Reyes Barcelo *et al.* 2009).

There are a number of hydrophobic pockets in HSA that are sufficiently large for a hydrophobic side-chain to insert and these could be sites for Aβ binding to HSA. Melacini and colleagues have used saturation transfer NMR and the effect of individual domains of HSA on Aβ fibrillisation in an attempt to characterise the albumin binding site (Algamal *et al.* 2013, Milojevic *et al.* 2011). They show that each of albumin's three domains are able to inhibit Aβ fibrillisation (Milojevic *et al.* 2011). Further investigation of Aβ fibre growth in the presence of domain 3 of HSA shows that each separate subdomain is also capable of inhibiting fibrillisation (Algamal *et al.* 2013). A 22 residue fragment of HSA from domain 3B, HSA(494-515), was tested for its ability to inhibit Aβ fibrillisation as it has a high of degree of sequence similarity to the central hydrophobic core of Aβ. This fragment is also capable of inhibiting Aβ fibre formation, demonstrating hydrophobic interactions between Aβ and HSA are key to inhibiting Aβ fibrillogenesis (Algamal *et al.* 2013).

Studying the stoichiometry using SEC indicated no complex larger than HSA bound to ~ 5 Aβ monomers forms (Figure 4.04) thus HSA binding a large Aβ oligomer can be ruled out. However, the resolution is not sufficient to determine whether HSA binds 1 Aβ monomer, a small oligomer, or indeed several monomers at different sites.

There was no evidence of Aβ binding HSA using native-like MS. Of course, this does not mean an Aβ-HSA complex should be ruled out. Native-like MS utilises a weaker vacuum than traditional MS but it is still much stronger than atmospheric pressure thus the non-covalent Aβ-HSA interaction may not be strong enough to survive the vacuum it is subjected to when running the sample on MS. Another possibility is that the Aβ-HSA interaction may require the presence of salt, thus it cannot be observed with native-like MS.

Overall, the evidence from SEC in combination with the effect of HSA on Aβ fibrillisation shown in Chapter 3 and Figures 4.02 and 4.03, is suggestive of HSA binding monomeric Aβ, however, a small oligomer of less than 5 Aβ monomers cannot be ruled out. This supports the use of albumin exchange for reducing Aβ burden in AD such as that showing promise in phase II clinical trial (Boada *et al.* 2009). A reduction of the Aβ pool in plasma through albumin exchange can reduce Aβ levels in the CSF only because soluble Aβ is in a dynamic equilibrium between the two and is able to cross the blood-brain barrier. Thus albumin must bind monomeric Aβ or a small oligomer for this to happen.

4.6.3 Ligands that Complex with Albumin Negate its Inhibitory Action on Aβ Fibrillisation

Both cholesterol and palmitic acid are hydrophobic ligands that bind in hydrophobic pockets on albumin. When albumin is complexed with either of these ligands, the extent of inhibition on Aβ fibrillisation is reduced. From this I can determine that residues involved in binding cholesterol and palmitic acid must also affect Aβ binding. Aβ binding could be inhibited directly, through cholesterol and palmitic acid binding the same residues in albumin, or indirectly, through conformational changes that occur upon cholesterol and palmitic acid binding. It has been shown that the α-helical content of albumin reduces upon cholesterol binding, increasing the β-sheet content (Teir *et al.* 2012). Algamal *et al.* have demonstrated that myristic acid (MA), another fatty acid that has been shown to bind albumin, also reduces the inhibitory effect of albumin on Aβ fibre formation. Mutants of albumin subdomains that disrupt myristic acid binding still inhibit Aβ fibrillisation, indicating that Aβ binding is normally restricted through conformational changes in albumin rather than direct competition with MA (Algamal *et al.* 2013). It may also be the case for PA as the HSA-PA complex has been shown to be very similar to the HSA-MA complex.

Irrespective of the mechanism by which Aβ competes with cholesterol and palmitic acid for binding HSA, it can be assumed that an increase in levels of albumin complexed with either of these ligands would result in a decrease in the levels of Aβ-albumin. Indeed, a decrease in serum levels of Aβ-albumin complexes is observed in AD (Yamamoto *et al.* 2013).

Biological Significance of the HSA-Cholesterol and HSA-PA Interaction

High serum cholesterol at mid-life has been identified as an independent risk factor for developing AD (Kivipelto *et al.* 2002, Kivipelto *et al.* 2001, Notkola *et al.* 1998, Whitmer *et al.* 2005) yet there is much debate over the mechanism by which it increases risk. Cholesterol levels in the brain are unaffected by serum levels as brain cholesterol is synthesised in the brain and does not cross the blood-brain barrier (Chobanian *et al.* 1962). It is therefore surprising that elevated serum levels of cholesterol is associated with a higher risk of AD. The observation that cholesterol will impede binding of Aβ to albumin could account for this. Indeed, as total cholesterol increases, the proportion of free-cholesterol also increases (Leonard *et al.* 1965), meaning there is more cholesterol available for binding HSA.

Palmitic acid is one of the most physiologically important fatty acids, comprising nearly 25 % of non-esterified fatty acids in human plasma. In addition it also accounts for nearly one quarter of all fatty acids found bound to albumin *in vivo* (Saifer *et al.* 1961). Therefore, the observation that palmitic acid bound to albumin will negate the inhibition of Aβ fibrillisation that is caused by fatty acid-free albumin becomes physiologically relevant. The ability to bind albumin is not exclusive to palmitic acid; the binding sites of several other fatty acids have also been identified through crystallisation, all of which share common binding modes (Bhattacharya *et al.* 2000). It could be assumed that other fatty acids could therefore also negate the effect of HSA on Aβ fibrillisation, indeed myristic acid has been shown to have this effect too (Algamal *et al.* 2013). A high dietary intake of fats, particularly saturated fats has previously been identified to increase the risk of developing AD (Kalmijn *et al.* 1997, Laitinen *et al.* 2006, Morris *et al.* 2003). This study provides a possible mechanism through which fats could influence AD development.

A number of hydrophobic pharmaceuticals have been shown to bind to HSA (Ghuman *et al.* 2005). This raises the possibility that sustained use of, for example the anti-coagulant warfarin, might influence Aβ-HSA binding.

4.7 CONCLUSIONS

Overall, this study shows that albumin is effective at inhibiting Aβ fibre growth when it is not restricted by the presence of hydrophobic molecules such as cholesterol and fatty acids. The clearance of Aβ from the CSF might therefore be enhanced by reduction of plasma levels of cholesterol and fatty acids, for example, through regulation of diet and exercise. Indeed both exercise and regulation of diet have been shown to be effective at ameliorating memory deficits and Aβ deposition caused by a high fat diet in APP transgenic mice (Maesako *et al.* 2012b). The use of therapeutic albumin in mild to moderate cases of AD (Boada *et al.* 2009) could therefore also be effective through clearance of both HSA that already has Aβ bound and HSA that is blocked by cholesterol and fatty acids.

With albumin's profound effect on Aβ fibre formation, it is perhaps surprising that as yet a clear correlation between albumin levels and AD pathology has not been identified. AD is a multi-factorial disease and thus a reduction of HSA in the CSF may be masked by other effects. If albumin levels in the CSF do not link to the extent of fibre formation, this may suggest that the majority load of fibres are in vesicle granules trafficked along the axon before they are released at the synapse.

CHAPTER FIVE:

COMPARISON OF Cu^{2+} AFFINITY FOR Aβ FIBRES, OLIGOMERS AND MONOMERS

5.1. ABSTRACT

Cu^{2+} bound to Aβ is concentrated in plaques of Alzheimer's disease (AD) patients. Furthermore, for a number of animal models of AD, disruption of Cu^{2+} homeostasis heightens the disease/phenotypes. However, a role for Cu^{2+} in AD remains controversial, a concern expressed is the affinity of Cu^{2+} for Aβ with K_ds reported ranging from micromolar to attomolar. In this chapter, I determine the affinity of Cu^{2+} for Aβ in monomeric, fibrillar, and in the case of Aβ(1-42) in an oligomeric form. Using two detection methods and competitive ligands, I show all alloforms have similar K_ds in the 10-20 pM range. This K_d is close to the affinity of albumin (1 pM), the most abundant protein in the blood plasma and CSF, which acts as a Cu^{2+} transport protein. I show that despite this close affinity, Aβ cannot sequester Cu^{2+} ions from albumin in a one to one solution. However, at the synapse, where there are fluxes of Cu^{2+}, Aβ is likely to bind to Cu^{2+} ions.

5.2. INTRODUCTION

The role of copper on Alzheimer's disease has received increased interest recently. The levels of copper ions in the brain of AD patients are significantly elevated compared to control and have been found to be particularly concentrated within the plaques of AD patients (Dong *et al.* 2003, Lovell *et al.* 1998, Miller *et al.* 2006). Studies in both cell lines and animal models have shown that Cu^{2+} increases the cytotoxicity of Aβ (Sanokawa-Akakura *et al.* 2010, Sarell *et al.* 2010, Sparks *et al.* 2003). Specifically, an AD model in *Drosophila melanogaster* has been exacerbated by impaired copper homeostasis (Sanokawa-Akakura *et al.* 2010), while rabbits fed copper in combination with a high cholesterol diet develop learning deficits and amyloid plaques (Sparks *et al.* 2003). The study of cytotoxicity of Aβ in cell lines demonstrates that the stoichiometry of Cu^{2+} ions to Aβ is important as sub-stoichiometric levels of Cu^{2+} enhance toxicity while supra-stoichiometric levels become protective (Sarell *et al.* 2010).

Interestingly, Cu^{2+} can bind to Aβ and influence the fibrillisation pathway. Supra-stoichiometric levels of Cu^{2+} have been shown to induce amorphous aggregation of both Aβ(1-40) and Aβ(1-42). Recent work within the group has shown that, surprisingly, at sub-stoichiometric concentrations the effect of Cu^{2+} on Aβ(1-40) and Aβ(1-42) fibrillisation is markedly different (Matheou *et al.* 2014). Aβ(1-40) fibrillisation is accelerated significantly, indeed Sarell *et al* show Cu^{2+} consistently halves the time taken for Aβ(1-40) fibres to form (Sarell *et al.* 2010). The morphology of the Aβ(1-40) fibres formed in the presence of Cu^{2+} is consistent with fibres formed in the absence of Cu^{2+} (Sarell *et al.* 2010). However, in the presence of sub-stoichiometric concentrations of Cu^{2+}, the kinetics of Aβ(1-42) fibrillisation are inhibited; the lag-time and t_{50} are increased while the k_{app} is reduced (Matheou *et al.* 2014). In addition, the total number of

fibres generated is also reduced. TEM reveals that fibre formation is inhibited in preference for the formation of oligomeric species (Figure 5.01) (Matheou *et al.* 2014).

The stoichiometry of Cu^{2+} binding to both Aβ monomer and fibres is one to one. Aβ-Cu^{2+} forms a tetragonal complex which involves the imidazole rings of His^{6}, His^{13} and His^{14} as well as the N-terminal amino group and carboxylate side chains (Antzutkin 2004, Damante *et al.* 2008, Dorlet *et al.* 2009, Drew *et al.* 2009, Hou *et al.* 2006, Karr *et al.* 2008, Minicozzi *et al.* 2008, Sarell *et al.* 2009, Shin *et al.* 2008, Streltsov *et al.* 2008, Syme *et al.* 2004). The exact positioning of the coordinating nitrogen and oxygen ligands between the equatorial and axial planes is dynamic, with pH particularly affecting the distribution of complexes formed (Dorlet *et al.* 2009, Drew *et al.* 2009, Sarell *et al.* 2009, Shin *et al.* 2008). The coordination geometry of the complex is shown in Figure 5.02.

The coordination geometry of Cu^{2+} bound to some Aβ fibrillisation states may be different to that found in monomer. The Cu^{2+} coordinating ligands fall just on the edge of the β-pleated core region of Aβ fibres, which occurs between residues 14 to 40. It has been indicated that the fibrillar structure can accommodate Cu^{2+} coordination in Aβ(1-40) from solid-state NMR and pulsed EPR of the Cu^{2+} complex (Gunderson *et al.* 2012, Parthasarathy *et al.* 2011). However it may be that in oligomers or some fibre morphologies the Cu(II) coordination geometry may be different from that found in the monomer, conceivably a cross-linked inter-molecular coordination may occur (Hane *et al.* 2013).

In addition to the coordination geometry of the Cu^{2+}-Aβ complex, there have been many studies on the affinity of Cu^{2+} for Aβ. The affinity of Aβ for Cu^{2+} is an important factor in understanding the role of Cu^{2+} in AD *in vivo* and has often been disputed due to some

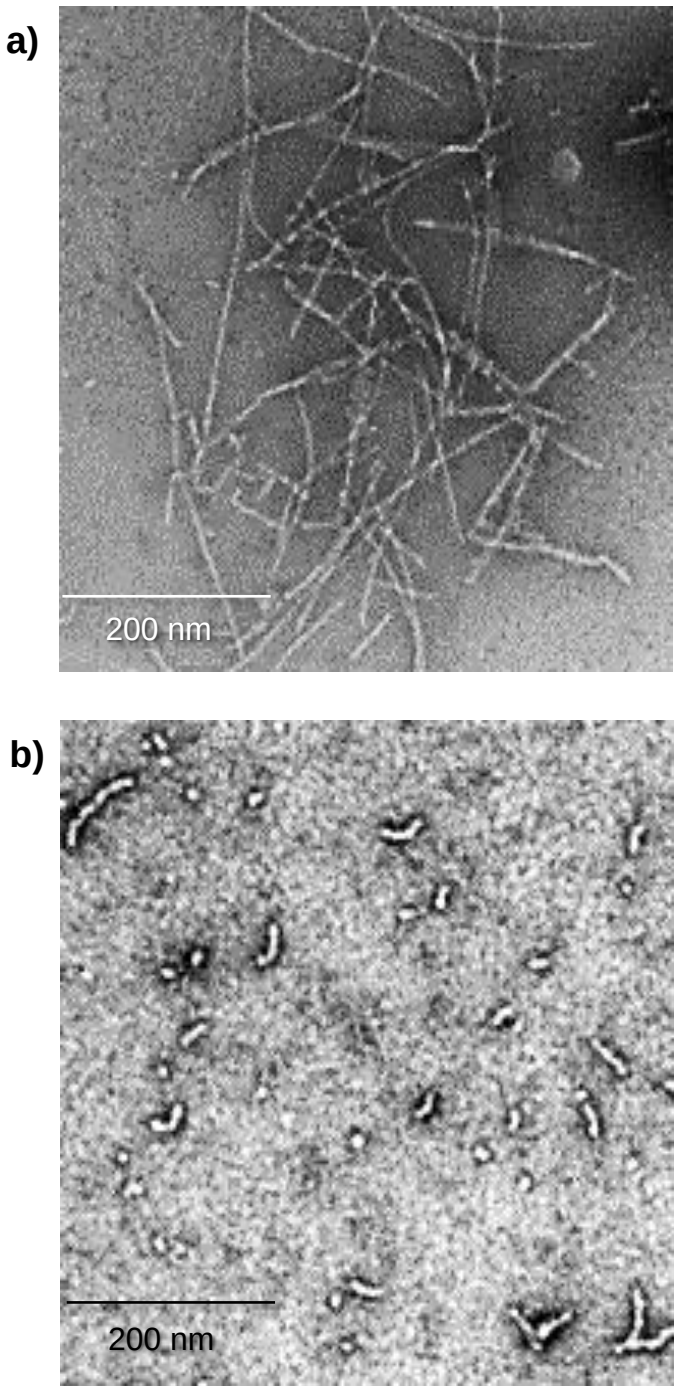

Figure 5.01. Aβ(1-42) Self-Association With and Without Cu^{2+}.

a) TEM image of Aβ(1-42) fibres formed in the absence of Cu^{2+}. b) TEM images of Aβ(1-42) oligomers and protofibrils formed with 0.4 molar equivalents of Cu^{2+}. Scale bar, 200 nm. Adapted from (Matheou *et al.* 2014). In the presence of substoichiometric Cu^{2+}, Aβ(1-42) almost exclusively forms oligomers/protofibrils but not fibres.

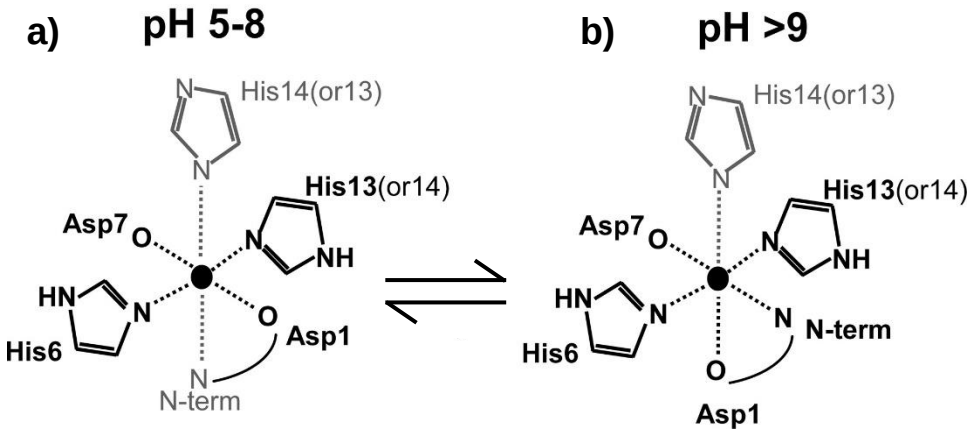

Figure 5.02. The Coordination Geometry of the Aβ-Cu^{2+} Complex.

The coordination geometry of Cu^{2+} binding Aβ at a) pH 5-8 and b) above pH 9. There is a switch between the equatorial and axial planes for the N-terminal nitrogen and side-chain oxygen of Asp[1] with pH. This figure has been adapted from (Sarell *et al.* 2009).

affinities reported being too weak to be physiologically relevant. Previously published affinities (summarised in Table 5.01) vary considerably, with K_ds reported in the micromolar, nanomolar, picomolar and attomolar ranges (Atwood *et al.* 2000, Danielsson *et al.* 2007, Garzon-Rodriguez *et al.* 1999, Guilloreau *et al.* 2006, Hatcher *et al.* 2008, Hong *et al.* 2008, Hong *et al.* 2010, Hou *et al.* 2006, Jiang *et al.* 2012, Karr *et al.* 2005, Ma *et al.* 2006, Maiti *et al.* 2008, Raman *et al.* 2005, Rózga *et al.* 2009, Sarell *et al.* 2009, Syme *et al.* 2004, Tõugu *et al.* 2008). The disparity between these values could be attributed to the very different conditions from which the K_ds have been obtained. However, metal affinity measurements are also often plagued by common pitfalls in measurements and calculations, as reviewed by Xiao *et al* (Xiao *et al.* 2010). For example, the effect of pH dependence, the solubility of the metal ion and competing ligand, competing buffers, or multiple binding modes of competing ligands are sometimes not considered or incorrectly understood. For a more complete review of Aβ-Cu^{2+} affinities specifically and discussion of the effect of competing buffers and multiple ligand binding modes, see Faller 2009 (Faller *et al.* 2009).

Something approaching a consensus for the affinity of Aβ for Cu^{2+} is emerging, with recent affinities reported to be closer to 50-500 pM (Hatcher *et al.* 2008, Hong *et al.* 2010, Sarell *et al.* 2009). These are focused primarily on monomeric Aβ and shorter fragments. There are few studies that compare the affinity of Aβ of different morphologies, particularly fibrillar and oligomeric assemblies.

A recent study by Jiang *et al.* used Aβ(1-16) (Y10W) as a competitive ligand for Cu^{2+} binding Aβ(1-42) monomers and aggregates. They suggested that both Aβ(1-42) aggregates formed in the presence of one mole equivalent of Cu^{2+} and Aβ(1-42) fibres

formed in the absence of Cu^{2+} have an elevated affinity for copper compared to Aβ(1-42) monomers. This elevated binding strength is sufficient to sequester copper ions from human serum albumin when the Aβ aggregates are 5-fold more concentrated than the albumin (Jiang *et al.* 2012).

5.3. AIMS

A recent study suggests that the affinity for Aβ(1-42) in an aggregated state is tighter than monomeric Aβ(1-42) (Jiang *et al.* 2012). This was surprising as previous studies have indicated no significant differences in affinity between fibre and monomer (Sarell *et al.* 2009). Recent unpublished studies in the Viles lab indicate that Cu^{2+} causes Aβ(1-42) to form oligomers almost exclusively at substoichiometric concentrations but only fibres with Aβ(1-40) (Matheou *et al.* 2014). We hypothesised this might be the reason for the difference in affinities reported in the two papers. In this chapter I aim to compare the affinities of different Aβ peptides, Aβ(1-16), Aβ(1-40) and Aβ(1-42), and aggregation states, monomers, oligomers, and fibres, for Cu^{2+} ions. I also aim to determine whether the Cu^{2+} affinity for Aβ is tight enough to compete with albumin, a major Cu^{2+} transport protein.

Table 5.01. A Summary of Previously Published Affinities for Cu^{2+} Binding Aβ Peptides.

Peptide	K_d	pH	Buffer	Method	Reference
Aβ(1-16)	1 μM	7.4	10 mM PBS	Direct Tyr fl.	Maiti *et al.* 2008
Aβ(1-16)	0.4 μM	7.4	10 mM PBS	Competitive Tyr fl.	Maiti *et al.* 2008
Aβ(1-16)	0.3 nM	7.4	20 mM PIPES	ITC	Hong *et al.* 2010
Aβ(1-16)	0.1 μM	7.8	Water	Competitive Tyr fl.	Ma *et al.* 2006
Aβ(1-16)	0.7 nM	7.2	20 mM HEPES	ITC	Hong *et al.* 2008
Aβ(1-16)	47 μM	7.4	100 mM Tris	Direct Tyr fl.	Karr *et al.* 2005
Aβ(1-16)	0.3 nM	7.4	20 mM HEPES	ITC	Hatcher *et al.* 2008
Aβ(1-16)	0.3 nM	7.4	20 mM PIPES	ITC	Hatcher *et al.* 2008
Aβ(1-16)	0.1 μM	7.4	50 mM HEPES	ITC/Direct and Competitive Tyr fl.	Guilloreau *et al.* 2006
Aβ(1-28)	23 μM	7.4	20 mM ACES	ITC	Sacco *et al.* 2012
Aβ(1-28)	70 nM	7.4	50 mM HEPES	ITC	Guilloreau *et al.* 2006
Aβ(1-28)	50-100 pM	7.8	Water	CD and Competitive Tyr fl.	Syme *et al.* 2004
Aβ(1-28)	40 pM	7.4	Water	CD	Sarell *et al.* 2009
Aβ(1-28)	28 μM	7.5	100 mM Tris	Direct Tyr fl.	Karr *et al.* 2005
Aβ(1-28)	2.5 μM	7.2	10 mM HEPES	Competitive Tyr fl.	Danielsson *et al.* 2007
Aβ(1-40)	0.9 μM	7.4	50 mM HEPES	Direct Tyr fl.	Tougu *et al.* 2008
Aβ(1-40)	0.5 μM	7.4	50 mM HEPES	Competitive Tyr fl.	Tougu *et al.* 2008
Aβ(1-40)	1.6 μM	7.4	10 mM Tris	Direct Tyr fl.	Garzon-Rodriguez *et al.* 1999
Aβ(1-40)	~0.5 nM	7.4	20 mM PIPES	ITC	Hong *et al.* 2010
Aβ(1-40)	11 μM	7.5	100 mM Tris	Direct Tyr fl.	Karr *et al.* 2005
Aβ(1-40)	1.6 μM	7.3	5 mM Phospate buffer	NMR	Hou *et al.* 2006
Aβ(1-40)	8 μM	7.4	50 mM PBS	Direct Tyr fl.	Raman *et al.* 2005
Aβ(1-40)	0.4 nM	7.4	20 mM HEPES	ITC	Hatcher *et al.* 2008
Aβ(1-40)	1.1 nM	7.2	20 mM PIPES	ITC	Hatcher *et al.* 2008
Aβ(1-40)	50 pM	7.4	20 mM Tris	CMCA	Atwood *et al.* 2000
Aβ(1-40)	57 nM	7.4	50 mM HEPES	Tyr fl.	Rozga *et al.* 2010
Aβ(1-42)	0.7 μM	7.4	10 mM PBS	Direct Tyr fl.	Maiti et *al.* 2008
Aβ(1-42)	2 μM	7.4	10 mM Tris	Direct Tyr fl.	Garzon-Rodriguez *et al.* 1999
Aβ(1-42)	7 aM	7.4	20 mM Tris	CMCA	Atwood *et al.* 2000
Aβ(1-42)	0.76 μM	7.4	20 mM HEPES	Direct Tyr fl.	Tougu *et al.* 2008
Aβ(1-42)	36-62 pM	7.4	Water	Competitive Tyr fl.	Sarell *et al.* 2009
Aβ(1-42) fibres	50-69 pM	7.4	Water	Competitive Tyr fl.	Sarell *et al.* 2009
Aβ(1-42) fibres	~4 pM	7.4	10 mM HEPES	Competitive Tyr fl.	Jiang *et al.* 2012
Aβ(1-42) aggregates	~1 pM	7.4	10 mM HEPES	Competitive Tyr fl.	Jiang *et al.* 2012

5.4. EXPERIMENTAL

5.4.1. Sample Preparation

Aβ Monomers

Aβ(1-40) and Aβ(1-42) was solubilised as described in Chapter 2. Aβ(1-16) was solubilised directly into UHQ water. All preparations were centrifuged for 10 minutes at 14000 x *g* to remove any particulates that could act as seeds to ensure the sample remained monomeric.

Aβ Fibres

Aβ(1-40) and Aβ(1-42) fibres were grown as described in Chapter 2 in multi-well plates, followed by ThT fluorescence. Fibre samples used in this chapter are ThT-free but grew alongside fibres generated in the presence of ThT in otherwise identical conditions. Unless otherwise specified, the fibres were grown in 30 mM HEPES at pH 7.4 and 160 mM NaCl at 30 ^{o}C with shaking for 30 seconds every 30 minutes.

Aβ Oligomers

Aβ(1-42) oligomers were produced in the same manner as the Aβ(1-42) fibres, however, they were grown in the presence of substoichiometric concentrations of Cu^{2+} ions, added in the form of $CuCl_2$. Unless otherwise specified, fibres were grown in the presence of 0.4 mole equivalents of Cu^{2+}. Once again, oligomeric Aβ samples were grown in the absence of ThT alongside oligomers generated in the presence of ThT in otherwise identical conditions.

DAH and Albumin

Albumin was solubilised and the concentration determined as described in Chapter 2. DAH peptide, the first 3 residues of human serum albumin, was purchased from Imperial College as a lyophilised powder. It was synthesised using Fmoc chemistry with a free N-terminal amino group and an amidated C-terminus to mimic the continuation of the albumin sequence. It was solubilised in UHQ water. The concentration cannot be calculated using absorbance at 280 nm as it does not contain any aromatic residues. The lyophilised peptide had approximately 20 % water content but the exact concentration was determined from saturation of Cu^{2+} binding, as it is known to bind with 1:1 stoichiometry (Sadler *et al.* 1994), followed using visible CD.

5.4.2. Fluorescence

The intrinsic tyrosine fluorescence of Aβ was studied. Data were collected between 300 and 450 nm on a Hitachi F-2500 fluorescence spectrophotometer using an excitation wavelength of 280 nm at 25 ^{O}C. Samples were placed in a 1 cm quartz cuvette (Hellma).

5.4.3. Affinity Measurements

The competing ligand NTA was used to determine the affinity of Aβ for Cu^{2+}. There is a linear relationship between the extent of the tyrosine fluorescence that is quenched and the amount of Cu^{2+} bound to Aβ (Sarell *et al.* 2009). Therefore the return of fluorescence upon NTA binding the Cu^{2+} can be used to calculate the affinity. At half maximal fluorescence, the K_d is equal to the free Cu^{2+} concentration, the concentration of Cu^{2+} not bound to either NTA or Aβ. The K_d can therefore be calculated using equations 2.15 and 2.16, described in Chapter 2.

5.4.4. EPR

Samples were run in 50 mM TIP buffer at pH 7.5 at 10 K using a Bruker Elexsys E580 spectrometer, as described in Chapter 2.

5.4.5. Visible CD

Samples were run on a Chirascan CD spectrophotometer, as described in Chapter 2, between 350 and 700 nm. Samples were run in 160 mM NaCl and 30 mM HEPES at pH 7.4 at 25 ^{o}C in a 1 cm pathlength quartz cuvette (Hellma).

5.5. RESULTS

5.5.1. Cu^{2+} Affinity Measurements for Aβ(1-42) Monomers and Oligomers

Affinities of Cu^{2+} for different alloforms of Aβ were determined from reversal of tyrosine (Tyr10) fluorescence quenching caused upon Cu^{2+} binding, using NTA as a competing ligand, which has a 20 pM affinity for Cu^{2+} at pH 7.4. Figure 5.03 shows the binding curves for the NTA competition of the Cu^{2+} complex for monomeric and oligomeric Aβ(1-42). Oligomers were prepared under the same conditions as Matheou *et al.*, who have shown that the addition of substoichiometric Cu^{2+} to Aβ(1-42) almost exclusively generates oligomers and protofibrils but not fibres, see Figure 5.01 (Matheou *et al.* 2014). The binding curves are essentially identical with the half maximal fluorescence being reached at 1.5 mole equivalents of NTA relative to Cu^{2+}. The corresponding conditional K_ds at pH 7.4 are therefore also essentially the same at 10 pM, when calculated from both equations (equation 2.15 and equation 2.16), as can be seen in Table 5.02. The K_ds have been calculated using a substoichiometric concentration of Cu^{2+} as Aβ(1-42) oligomers are generated at these substoichiometric molar ratios. It was also necessary to calculate

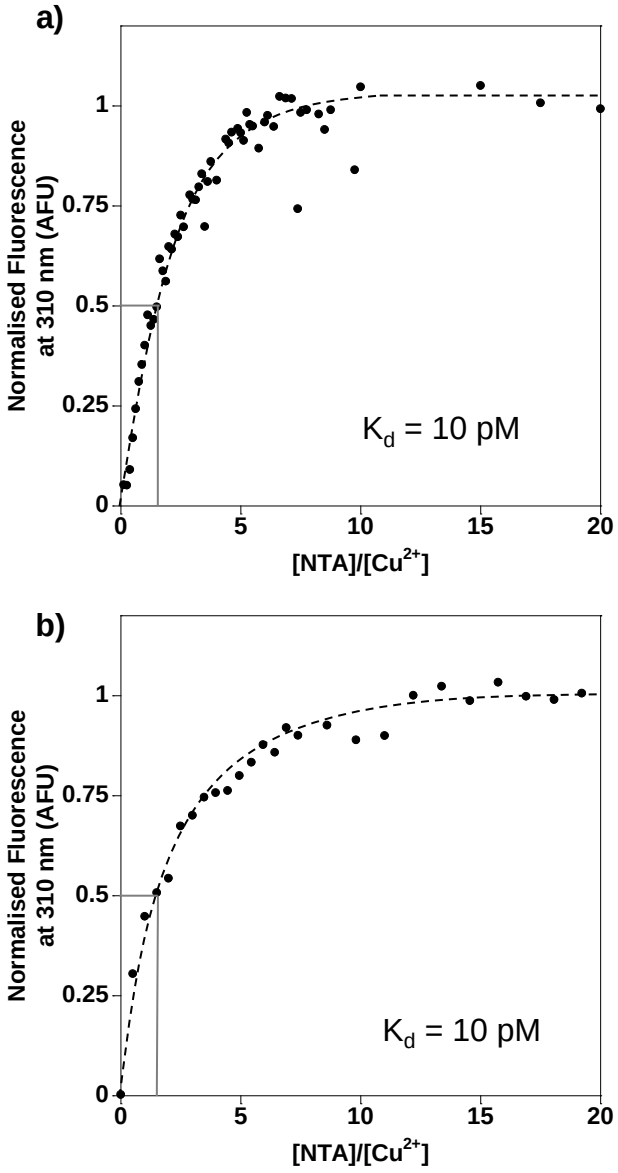

Figure 5.03. The Affinity of Different Aβ(1-42) Oligomerisation States for Cu^{2+}.

Tyrosine fluorescence binding curves of different Aβ(1-42) oligomerisation states with 0.4 mole equivalents of Cu^{2+} using NTA as a competing ligand. a) 10 μM Aβ(1-42) monomers and b) 10 μM Aβ(1-42) oligomers. Titrations were carried out in the presence of 160 mM NaCl and 30 mM HEPES at pH 7.4 at 25 ^{o}C.

the K_d in the presence of 30 mM HEPES, and 160 mM NaCl as these were the conditions in which the oligomers were formed and characterised.

Table 5.02 The Affinity of Different Aβ(1-42) Oligomerisation States for Cu^{2+}.

Sample	Aβ(1-42) Monomers	Aβ(1-42) Oligomers
$[Cu^{2+}_{total}]$ (μM)	4	4
$[Cu^{2+}_{bound}]$ (μM)	2	2
$[NTA_{total}]$ (μM)	6	6
$[NTA_{free}]$ (μM)	4	4
K_d (from eq 2.15) (pM)	10	10
K_d (from eq 2.16) (pM)	10	10

Values obtained from the binding curves in Figure 5.03 to calculate the K_d at pH 7.4. Titrations were carried out in the presence of 160 mM NaCl and 30 mM HEPES at pH 7.4 at 25 ^oC.

5.5.2. Cu^{2+} Affinity Measurements for Aβ(1-16) at Different Stoichiometries, and With/Without Buffer

I wanted to confirm that using substoichiometric (0.4 mole equivalents) and stoichiometric (1 mole equivalent) amounts of Cu^{2+} did not directly influence affinity values determined. Furthermore, I want to confirm that competition studies using NTA give the same K_d with or without the presence of buffer (30 mM HEPES at pH 7.4 and 160 mM NaCl). Buffer can compete for metal ions and thus complicate affinity

measurements, but for this type of competition experiment this may not be a concern. The effect of different Cu^{2+} mole equivalents and presence of buffer on the affinity values obtained was studied using the non-native Aβ fragment Aβ(1-16) as this peptide is not prone to aggregation or self-assembly but contains the Cu^{2+} binding ligands. Figure 5.04 shows the binding curves obtained for 10 μM Aβ(1-16) with one mole equivalent of Cu^{2+} (Figure 5.04a), and 0.4 mole equivalents of Cu^{2+} in the presence and absence of 30 mM HEPES and 160 mM NaCl (Figure 5.04b and Figure 5.04c, respectively). The binding curves are very similar with half maximal fluorescence being reached at approximately one mole equivalent of NTA. Calculating the K_d from each of these binding curves reveals Aβ(1-16) has a picomolar affinity, which is summarised in Table 5.03. The variation in the values obtained between the three conditions (17-20 pM) is very small (standard error = 1 pM) and within the typical experimental variation from fitting the binding curve, slight variation in pH or errors in concentration measurements. The Cu^{2+} affinities obtained for the physiologically relevant Aβ(1-42) alloforms, using buffer and substoichiometric concentrations of Cu^{2+} are therefore validated.

The NTA competition experiments suggest that the conditional affinity of Cu^{2+} for Aβ at pH 7.4 is the same, within the associated errors for these experiments, for Aβ(1-16) and Aβ(1-42) irrespective of monomeric or oligomeric form for Aβ(1-42).

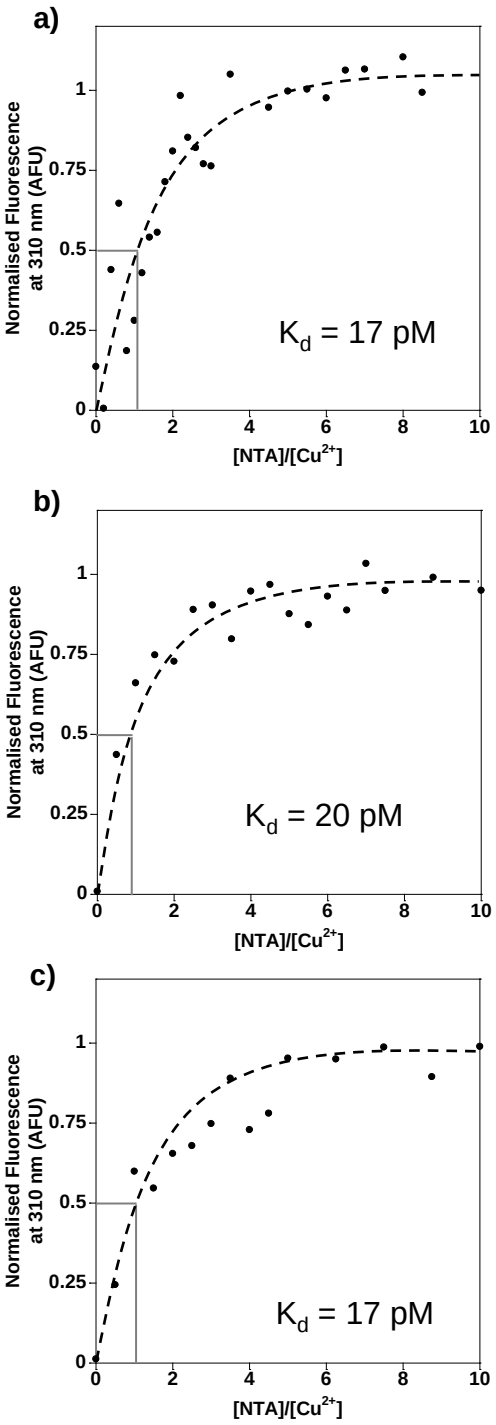

Figure 5.04. The Influence of Buffer and Stoichiometry on the Affinity of Aβ(1-16) for Cu^{2+}.

Tyrosine fluorescence binding curves of 10 μM Aβ(1-16) with Cu^{2+} using NTA as a competing ligand. a) Aβ with one mole equivalent Cu^{2+} in the presence of 160 mM NaCl and 30 mM HEPES at pH 7.4. b) Aβ fluorescence in the presence of 0.4 mole equivalents Cu^{2+} in the presence of 160 mM NaCl and 30 mM HEPES at pH 7.4. c) Aβ with 0.4 mole equivalents Cu^{2+} in the absence of buffer and salt, at pH 7.4.

Table 5.03. The affinity of Aβ(1-16) for Cu^{2+}.

Sample	**Aβ(1-16) 1.0 m.e Cu^{2+} Buffer**	**Aβ(1-16) 0.4 m.e Cu^{2+} Buffer**	**Aβ(1-16) 0.4 m.e. Cu^{2+} No Buffer**
$[Cu^{2+}_{total}]$ (μM)	10	4	4
$[Cu^{2+}_{bound}]$ (μM)	5	2	2
$[NTA_{total}]$ (μM)	11	4	4.4
$[NTA_{free}]$ (μM)	6	2	2.4
K_d (from eq 2.15) (pM)	17	20	17
K_d (from eq 2.16) (pM)	17	20	17

Values obtained from the binding curves in Figure 5.04 to calculate the K_d at pH 7.4

5.5.3. The N-terminal Cu^{2+}-Binding site of Albumin Sequesters Cu^{2+} from Aβ(1-16)

Jiang *et al.* use albumin as a competitor to measure the affinity of Cu^{2+} for Aβ using EPR (Jiang *et al.* 2012). A similar experiment was therefore performed. The N-terminal residues, NH_2-Asp-Ala-His-$CONH_2$ (DAH) have previously been identified as a tight Cu^{2+} binding site in albumin (Patel *et al.* 1993). The N-terminal residues were chosen rather than full-length albumin to avoid the direct interaction between Aβ and albumin, as described in Chapter 3 (Stanyon *et al.* 2012). EPR is a useful technique for following the competition as the coordination geometries of Aβ-Cu^{2+} and DAH-Cu^{2+} are very different, producing markedly different spectra. The albumin complex is a 4N square-planar complex while the Aβ complex is 2N2O. The g_{II} and A_{II} values for the two

complexes are therefore clearly resolved (Peisach *et al.* 1974). The EPR spectra of Cu^{2+} complexes of other competing ligands investigated, such as NTA and glycine, have substantial overlap with the Cu^{2+}-Aβ spectrum and were not appropriate. Figure 5.05 shows the titration of DAH into Cu^{2+}-Aβ(1-16) at a 0.8:1 ratio to ensure there are no free Cu^{2+} ions. It is apparent that the Aβ-Cu^{2+} spectrum has hyperfine peaks at 2.49 *g* and 2.34 *g* (black dashed lines) that diminish as DAH is titrated in. These hyperfines are replaced by those at 2.42 *g* and 2.26 *g*, which are a signature of Cu^{2+} binding to DAH tripeptide. The ratio of the intensity between these two sets of hyperfines can be used to create a binding curve (Figure 5.05b). The binding of Cu^{2+} to the DAH tripeptide is tighter than Aβ as the EPR spectra give signal for Cu^{2+}-DAH only after just one mole equivalent of DAH relative to Cu^{2+} has been added.

This observation is supported by return of Aβ tyrosine fluorescence as DAH sequesters Cu^{2+} from Aβ(1-16). Maximal fluorescence is achieved at one mole equivalent of DAH to Cu^{2+} (Figure 5.06), indicating Cu^{2+} binding Aβ(1-16) is weaker than binding DAH.

5.5.4. The Competitive Effects of DAH on Cu^{2+} Binding to Different Aβ(1-40) and Aβ(1-42) Alloforms

Next the competitive effects of the DAH tripeptide on Cu^{2+}-Aβ(1-42) were investigated. Figure 5.07 shows the results of DAH competition with Aβ(1-42) monomers for Cu^{2+}. It is evident that the Cu^{2+}-DAH signal rapidly removes all the Cu^{2+} from Aβ after one mole equivalent and that Aβ(1-42) monomers therefore have a weaker affinity for Cu^{2+} than DAH. This is supported by a similar experiment with Aβ intrinsic tyrosine fluorescence (Figure 5.08).

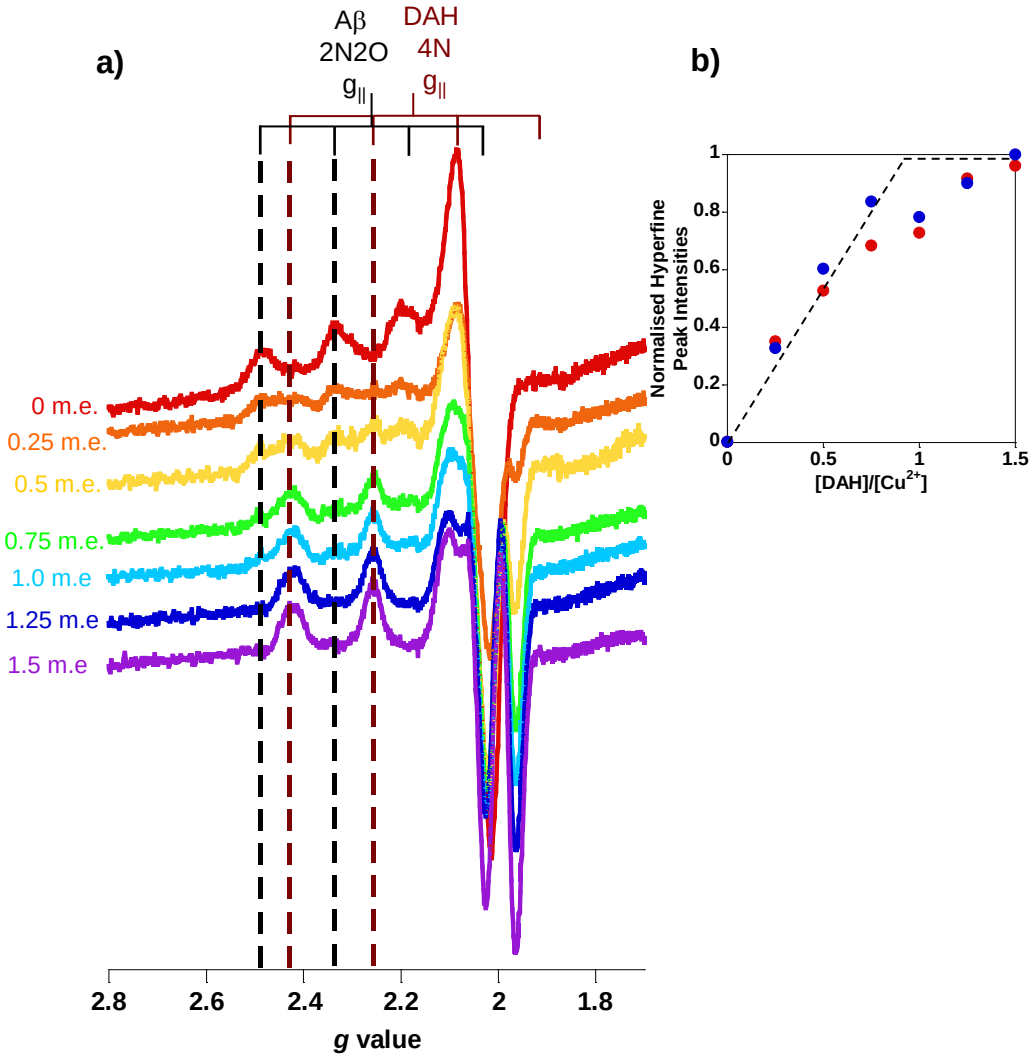

Figure 5.05. EPR Shows Aβ(1-16) has a Weaker Affinity for Cu^{2+} than DAH.

a) EPR spectra of 62.5 μM Aβ(1-16) with 50 μM Cu^{2+} with 0-1.5 mole equivalents of DAH tripeptide in relation to Cu^{2+} in 50 mM TIP buffer at pH 7.5. The black dashed lines represent the hyperfines associated with the Aβ-Cu^{2+} complex and the burgundy dashed lines the hyperfines associated with the DAH-Cu^{2+} complex. b) The binding curve obtained from the normalised ratio between the DAH-Cu^{2+} and Aβ-Cu^{2+} hyperfines from a) against DAH mole equivalents.

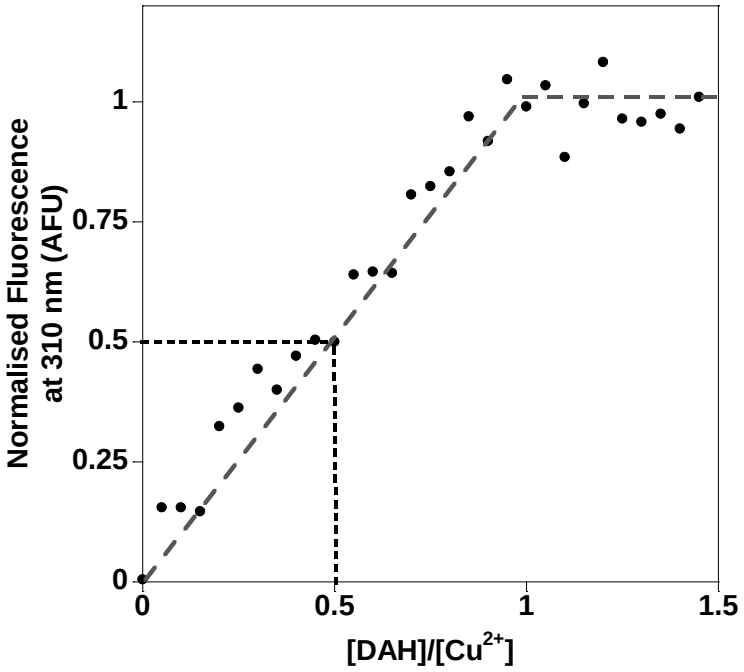

Figure 5.06. Intrinsic Tyr Fluorescence Shows Aβ(1-16) has a Weaker Affinity for Cu^{2+} than DAH.

Normalised tyrosine fluorescence at 310 nm from 100 μM Aβ(1-16) with 80 μM Cu^{2+} with 0-1.5 mole equivalents of DAH tripeptide in relation to Cu^{2+} in 50 mM TIP buffer at pH 7.5 at 25 ^{o}C.

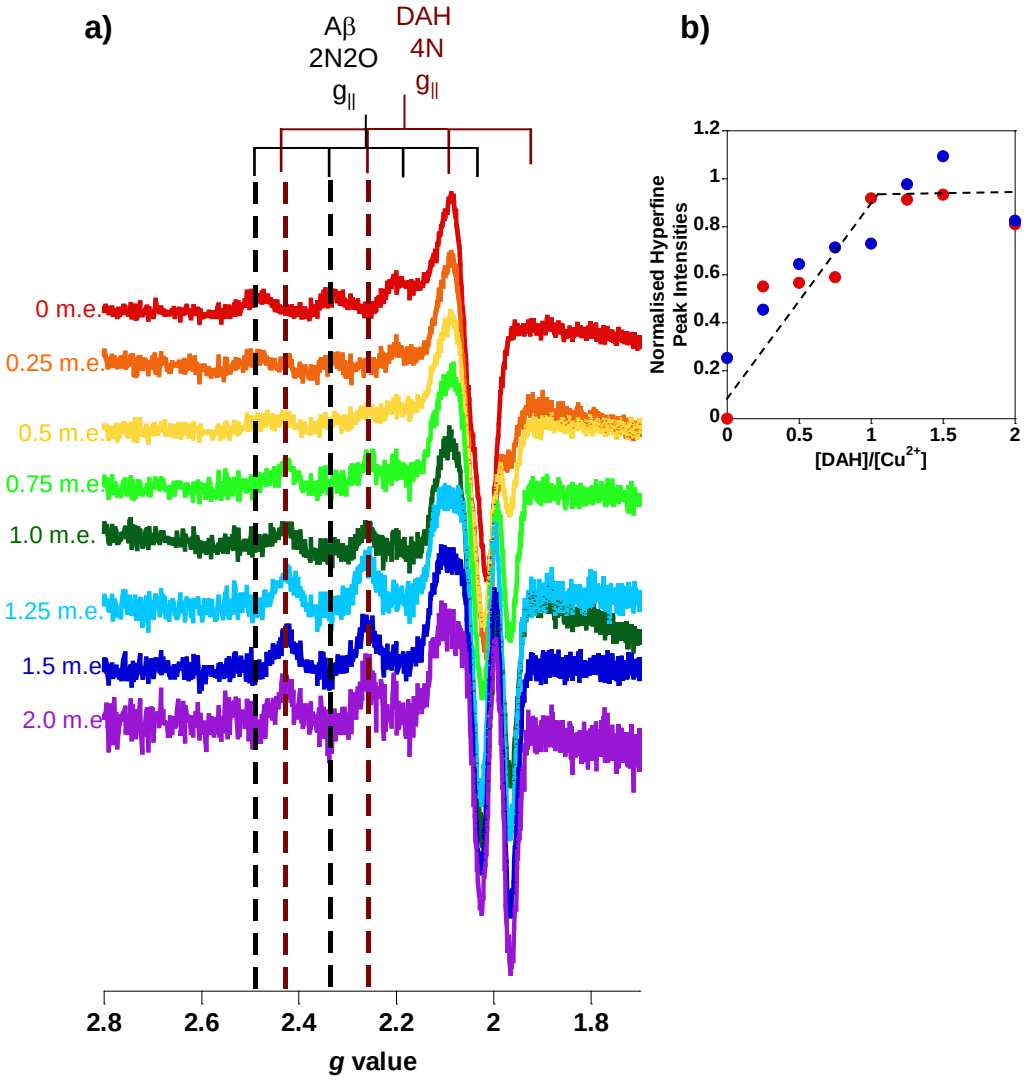

Figure 5.07. EPR Shows Aβ(1-42) Monomers have a Weaker Affinity for Cu^{2+} than DAH.

a) EPR spectra of 62.5 μM Aβ(1-42) monomers with 50 μM Cu^{2+} with 0-2 mole equivalents of DAH tripeptide in relation to Cu^{2+} in 50 mM TIP buffer at pH 7.5. The black dashed lines represent the hyperfines associated with the Aβ-Cu^{2+} complex and the burgundy dashed lines the hyperfines associated with the DAH-Cu^{2+} complex. b) The binding curve obtained from the normalised ratio between the DAH-Cu^{2+} and Aβ-Cu^{2+} hyperfines from a) against DAH mole equivalents in relation to the Cu^{2+} concentration.

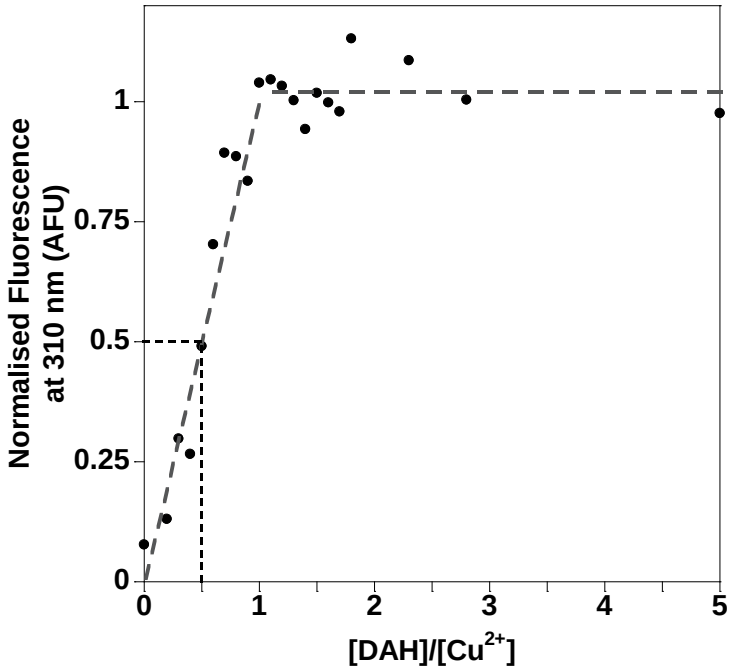

Figure 5.08. Intrinsic Tyr Fluorescence Shows Aβ(1-42) Monomers have a Weaker Affinity for Cu^{2+} than DAH.

Normalised tyrosine fluorescence at 310 nm from 20 μM Aβ(1-42) monomers with 18 μM Cu^{2+} with 0-5 mole equivalents of DAH tripeptide in relation to Cu^{2+} in 50 mM TIP buffer at pH 7.5 at 25 ^{o}C.

The study by Jiang *et al.* suggests Aβ(1-42) oligomers might produce a different, tighter Cu^{2+} complex to that of Aβ(1-42) monomer. However, here Aβ(1-42) oligomers produced the same results as Aβ(1-42) monomers, with DAH sequestering all Cu^{2+} from the Aβ after the addition of only one mole equivalent of DAH (Figure 5.09). This demonstrates that DAH also has a tighter affinity for Cu^{2+} than Aβ(1-42) oligomers.

The relative affinity of Aβ(1-40) monomers and fibres for Cu^{2+} compared to DAH was also tested. Figure 5.10 shows the EPR spectra obtained following the titration of DAH into Aβ(1-40) monomers. It is evident that Aβ(1-40) monomers also have all the Cu^{2+} stripped from them by DAH after just one mole equivalent has been added. Aβ(1-40) monomers, therefore, have a K_d weaker than 1 pM for Cu^{2+} ions. The EPR spectrum of Aβ(1-40) fibres bound to Cu^{2+} is readily replaced by the spectrum of Cu^{2+} bound to DAH as DAH is titrated in (Figure 5.11), reaching complete transfer at one mole equivalent. The K_d of DAH for Cu^{2+} is therefore stronger than the K_d of Aβ(1-40) fibres for Cu^{2+} ions.

The ability of albumin to sequester Cu^{2+} ions from Aβ(1-40) monomers and fibres was also tested using visible CD (Vis-CD), using a 1:1:1 stoichiometric ratio of Aβ:Cu^{2+}:albumin. Vis-CD does not detect the d-d transitions of the Aβ-Cu^{2+} complex as the Cu^{2+} ions are not in a chiral environment (Syme *et al.* 2004), therefore the appearance of a signal relates to albumin sequestering and binding the Cu^{2+} ions. Figure 5.12 shows that the Vis-CD spectrum of Cu^{2+} bound to albumin is the same as albumin added to the Aβ-Cu^{2+} complexes, even in intensity. All Cu^{2+} has been sequestered from both Aβ(1-40) monomers and fibres and therefore must have a weaker affinity for Cu^{2+} than albumin.

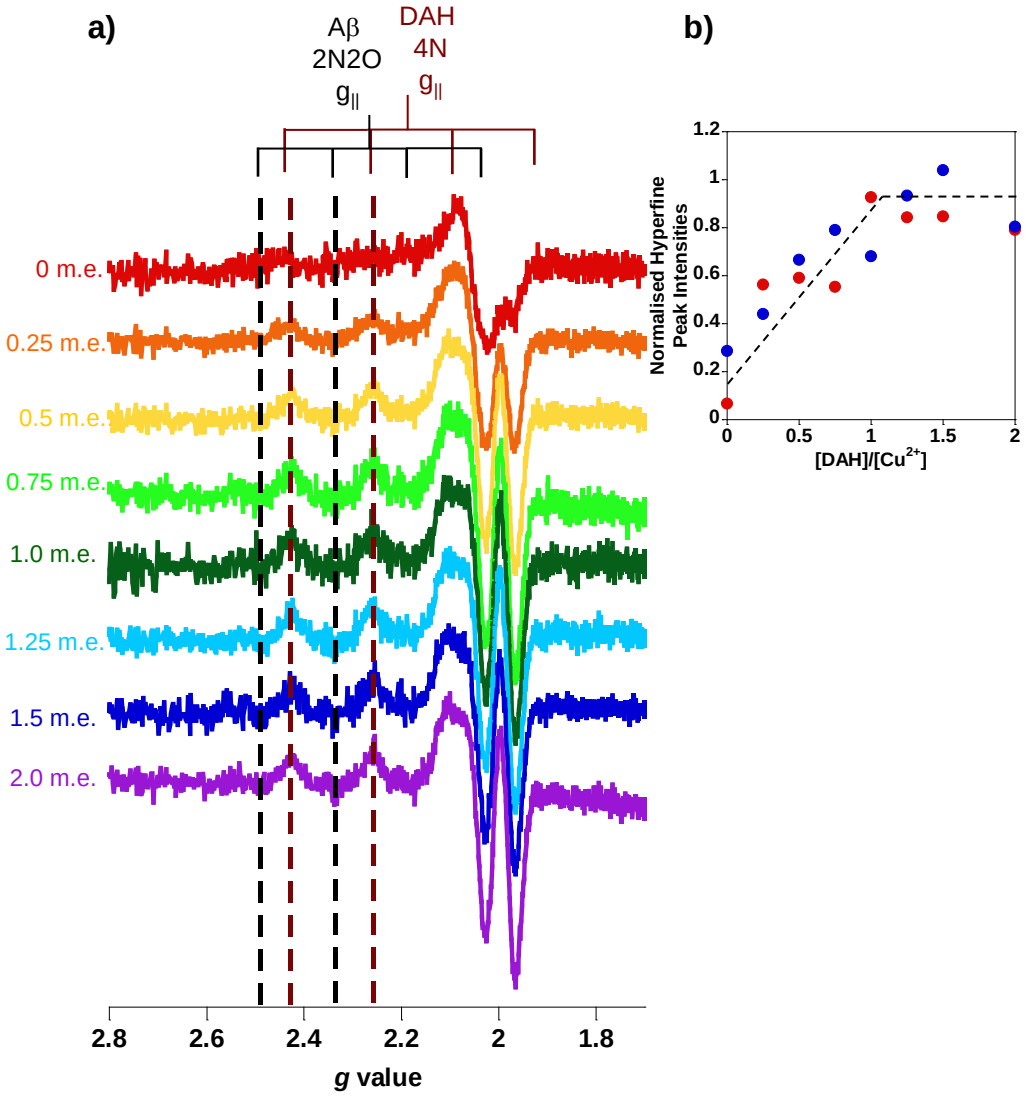

Figure 5.09. EPR Shows Aβ(1-42) Oligomers have a Weaker Affinity for Cu^{2+} than DAH.

a) EPR spectra of 62.5 μM Aβ(1-42) oligomers with 50 μM Cu^{2+} with 0-2 mole equivalents of DAH tripeptide in relation to Cu^{2+} in 50 mM TIP buffer at pH 7.5. The black dashed lines represent the hyperfines associated with the Aβ-Cu^{2+} complex and the burgundy dashed lines the hyperfines associated with the DAH-Cu^{2+} complex. b) The binding curve obtained from the normalised ratio between the DAH-Cu^{2+} and Aβ-Cu^{2+} hyperfines from a) against DAH mole equivalents relative to Cu^{2+} concentration.

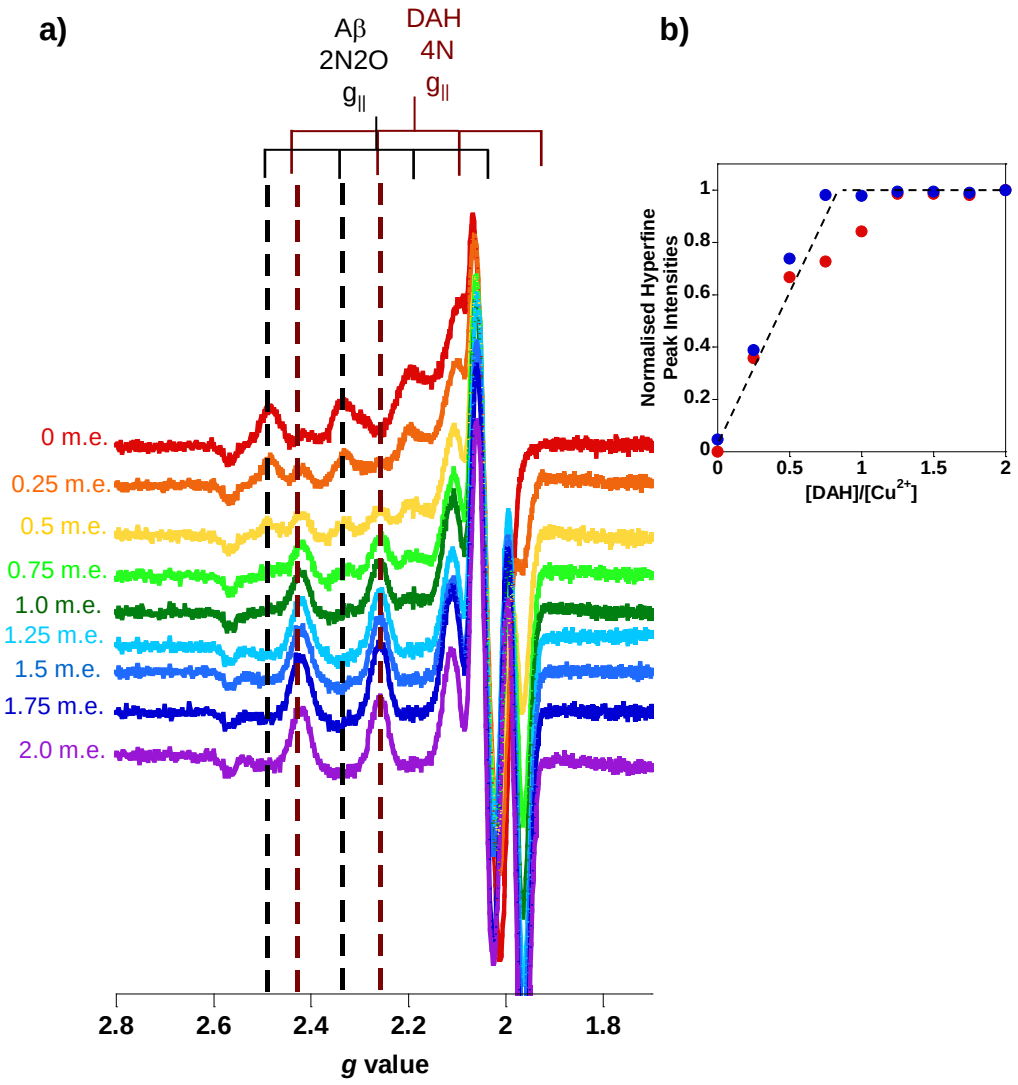

Figure 5.10. EPR Shows Aβ(1-40) Monomers have a Weaker Affinity for Cu^{2+} than DAH.

a) EPR spectra of 100 μM Aβ(1-40) monomers with 80 μM Cu^{2+} with 0-2 mole equivalents of DAH tripeptide in relation to Cu^{2+} in 50 mM TIP buffer at pH 7.5. The black dashed lines represent the hyperfines associated with the Aβ-Cu^{2+} complex and the burgundy dashed lines the hyperfines associated with the DAH-Cu^{2+} complex. b) The binding curve obtained from the normalised ratio between the DAH-Cu^{2+} and Aβ-Cu^{2+} hyperfines from a) against DAH mole equivalents relative to Cu^{2+} concentration.

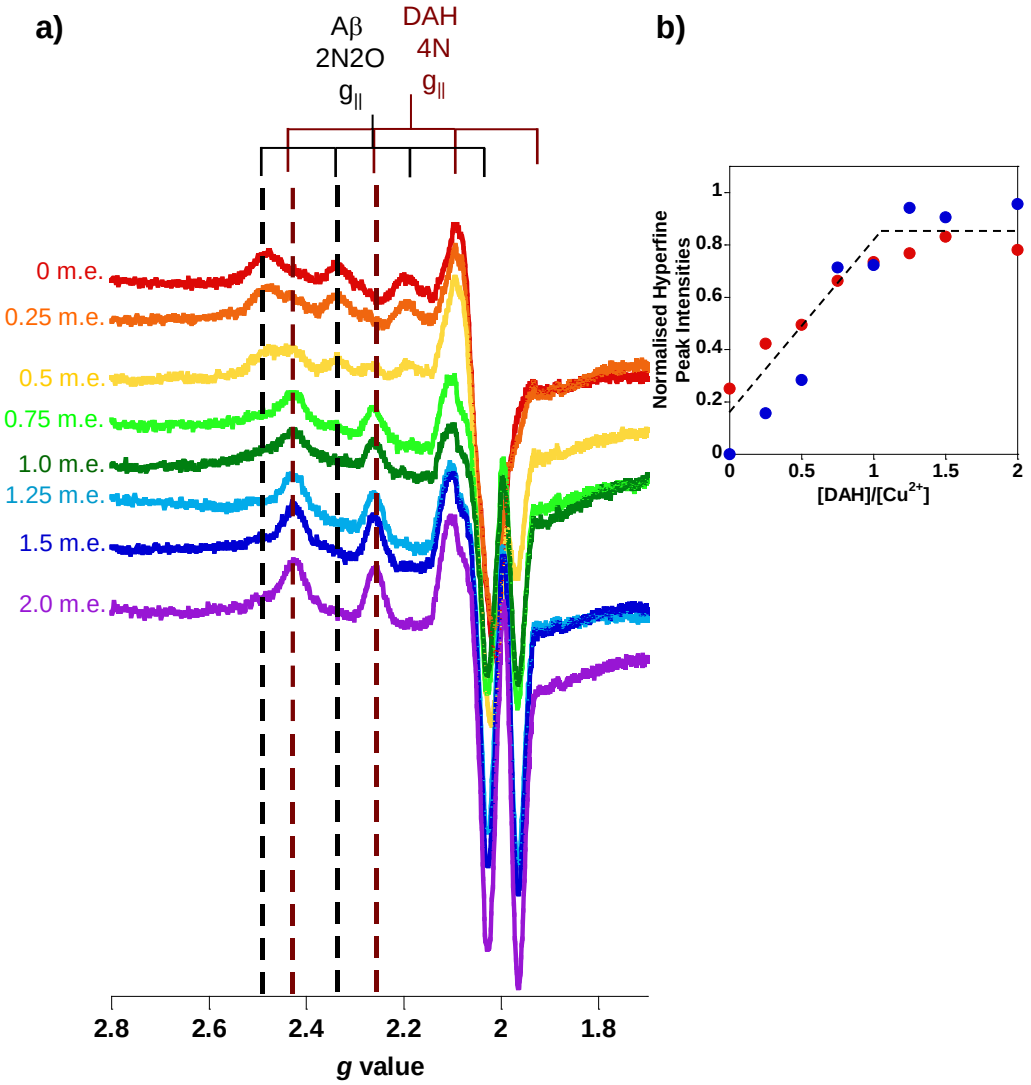

Figure 5.11. EPR Shows Aβ(1-40) Fibres have a Weaker Affinity for Cu^{2+} than DAH.

a) EPR spectra of 62.5 μM Aβ(1-40) fibres with 50 μM Cu^{2+} with 0-2 mole equivalents of DAH tripeptide in relation to Cu^{2+} in 50 mM TIP buffer at pH 7.5. The black dashed lines represent the hyperfines associated with the Aβ-Cu^{2+} complex and the burgundy dashed lines the hyperfines associated with the DAH-Cu^{2+} complex. b) The binding curve obtained from the normalised ratio between the DAH-Cu^{2+} and Aβ-Cu^{2+} hyperfines from a) against DAH mole equivalents relative to Cu^{2+} concentration.

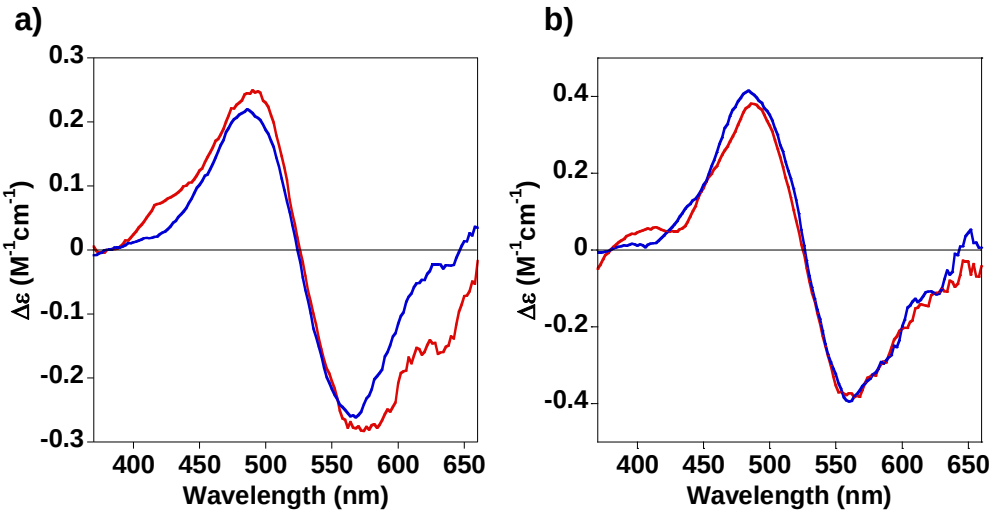

Figure 5.12 Visible-CD Shows Albumin Sequesters Cu^{2+} Ions from Monomeric and Fibrillar Aβ(1-40).

Visible CD of 50 μM Aβ(1-40) a) monomers and b) fibres pre-complexed with 50 μM Cu^{2+} plus one mole equivalent of albumin (red). The Vis-CD spectrum of 50 μM HSA with 50 μM Cu^{2+} is shown in blue in each panel for comparison. Samples were run at 25 ^{o}C in 160 mM NaCl and 30 mM HEPES at pH 7.4.

All alloforms of Aβ studied have demonstrated a weaker affinity for Cu^{2+} ions than the DAH tripeptide, which has an affinity of 1 pM (Rózga *et al.* 2007).

5.5.5. Aβ Does Not Sequester Cu^{2+} Ions from HSA

The effect of the reverse titration, adding different Aβ alloforms as a competitor into Cu^{2+}-DAH and Cu^{2+}-albumin complexes was also investigated. Figure 5.13a shows that at a 1:1 stoichiometry of Aβ to Cu^{2+} ions, the DAH-Cu^{2+} complex EPR spectrum is still observed for each alloform of Aβ used; Aβ(1-40) monomers, Aβ(1-40) fibres, Aβ(1-42) monomers and Aβ(1-42) fibres. The Aβ(1-42) oligomers were not tested as these are only stable in the presence of Cu^{2+}. However, it could have been expected that as Aβ(1-42) fibres rapidly become oligomers upon binding Cu^{2+} (Matheou *et al.* 2014), that the Aβ(1-42) fibres would sequester Cu^{2+} from DAH as oligomers would. This indicates that the affinity reported here for Aβ of 10-20 pM is not tight enough to sequester Cu^{2+} ions from DAH, when a 1:1 stoichiometric ratio is used.

Similarly, the ability of Aβ to sequester Cu^{2+} ions from human serum albumin (as well as DAH) was also investigated (Figure 5.13b). The EPR spectrum for Cu^{2+} bound to albumin is the same as the Cu^{2+}-DAH spectrum as would be expected because the Cu^{2+} only coordinates with the main chain amides of the first three residues of albumin (Patel *et al.* 1993). The spectra obtained at a 1:1 stoichiometry of Aβ to Cu^{2+} titrated into albumin-Cu^{2+} for all four alloforms of Aβ are the same as Cu^{2+}-albumin alone. This demonstrates that the affinity of albumin for Cu^{2+} is considerably tighter, at least an order of magnitude, than the affinity of all forms of Aβ studied; monomers, fibres, or oligomers.

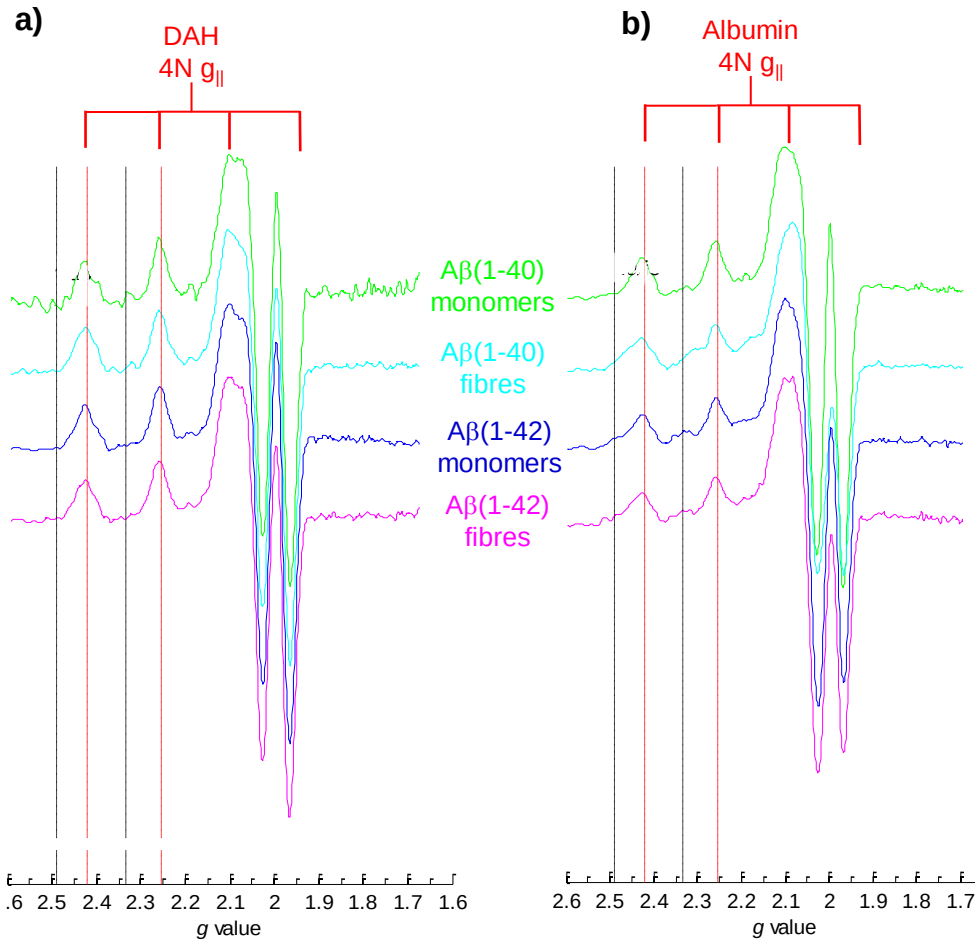

Figure 5.13. Aβ Can Not Sequester Cu^{2+} Ions from DAH nor Full-Length Albumin.

EPR spectra of 62.5 μM DAH (a) and 62.5 μM albumin (b) with 50 μM Cu^{2+} following addition of 62.5 μM of different Aβ alloforms; monomeric Aβ(1-40) (green), fibrillar Aβ(1-40) (cyan), monomeric Aβ(1-42) (dark blue), and fibrillar Aβ(1-42) (magenta). Black dashed lines represent the centre of the hyperfine peaks observed for the Aβ-Cu^{2+} complex and the red lines those observed for the Cu^{2+}-DAH/albumin complex. All samples were in 50 mM TIP buffer at pH 7.5.

5.6. DISCUSSION

5.6.1. Aβ has a Picomolar Affinity for Cu^{2+} Ions Irrespective of Aβ Alloform

Determining the affinity of Cu^{2+} for Aβ is, of course, an important parameter. It will indicate the likelihood of Cu^{2+} being bound to Aβ at physiological concentrations. The fluorescence quenching studies using NTA as a competitive ligand for Cu^{2+} binding have revealed that regardless of Aβ alloform or fibrillisation state that the K_d of Cu^{2+} binding to Aβ is in the 10-20 pM range. The affinities are marginally tighter than those reported by Sarell *et al.* but are otherwise in agreement that the Aβ fibrillisation state does not alter the binding constant of Cu^{2+} for Aβ. The elevated affinity reported is closer to that described by Jiang *et al.* for Aβ(1-42) aggregates (~1 pM), however, no difference was observed between Aβ(1-42) monomers or Aβ(1-42) oligomers, or for that matter between Aβ(1-16), Aβ(1-40) or Aβ(1-42).

5.6.2. The Source of Discrepancy Between Previously Reported Affinities

There is a small but significant difference between the K_d determined by Sarell *et al.* in the Viles lab (54 ± 5 pM) (Sarell *et al.* 2009) and this present work (10-20 pM). It is not clear where the systematic errors occur. I wondered if the differences were due to how the concentration of Aβ was measured as previously the scatter observed in the UV-Vis absorption spectrum was accounted for in a different manner. This might have led up to a 20 % over-estimation of concentration compared to that obtained from equation 2.06 in Chapter 2. Where Sarell *et al.* obtained a K_d of 50 pM, recalculation of this accounting for a 20 % decrease in Aβ concentration gives a K_d of 27 pM. This value is closer to the 10-20 pM obtained in this work. It highlights the accuracy in measuring affinity and thus differences by as much as an order of magnitude can be simply due to small errors in measuring concentrations.

This triggered the question of the effect of systematic discrepancies in the concentrations of all solutions used. Table 5.04 shows the different K_d values Aβ(1-42) monomers have for Cu^{2+}, Figure 5.02a, when accounting for concentration discrepancies. The individual effects of a discrepancy in concentration are not significant but an over-estimation of competing ligand (NTA) concentration has the most dramatic effect, with a 20 % over-estimation increasing the K_d from 10 pM to 14 pM.

The discrepancies between the reported affinities, particularly between those reported by Jiang *et al.*, may be attributed to the different conditions in which the complexes were formed and the competing ligands used. Rather than using competing ligands with well documented affinities for Cu^{2+}, Jiang *et al.* used an Aβ analogue, Aβ(1-16)(Y10W). The affinity of this analogue was calculated to be 135 nM, using direct fluorescence quenching in a high concentration of HEPES buffer (500 mM). The buffer effect was then corrected to give a K_d of 320 pM. The use of direct fluorescence quenching for determining Cu^{2+}-peptide affinity is inherently difficult as the concentration of peptide used must be extremely low (<320 pM) to avoid tight binding and will therefore be on the limit of accurate fluorescence detection. Using a buffer to compete with the probe for Cu^{2+} means the concentration of Aβ(1-16)(Y10W) used can be higher, however, HEPES is not an optimal buffer for this because Aβ concentration must still be in the range of the apparent K_d, which is in the nM range in HEPES (Faller *et al.* 2009). An error in determining the affinity of the competing ligand would therefore transfer in calculating the affinity of Aβ(1-42) for Cu^{2+}. The difference in affinity between Aβ(1-16)(Y10W) and Aβ(1-42) is surprising. The bulky Trp residue close to the Cu^{2+} binding site His^{6}-$His^{13,14}$ may reduce its affinity for Cu^{2+} compared to wild type Aβ(1-16) and Aβ(1-42).

Table 5.04. The Affinity of Aβ(1-42) Monomer for Cu^{2+} Accounting for Possible Concentration Discrepancies.

Sample	Original Values	Original [NTA] Over-estimation		Original [NTA] Under-estimation		Original [Cu^{2+}] Over-estimation		Original [Cu^{2+}] Under-estimation	
		10 %	20 %	10 %	20 %	10 %	20 %	10 %	20 %
[Cu^{2+}_{total}] (μM)	4	4	4	4	4	3.6	3.2	4.4	4.8
[Cu^{2+}_{bound}] (μM)	2	2	2	2	2	1.8	1.6	2.2	2.4
[NTA_{total}] (μM)	6	5.4	4.8	6.6	7.2	6	6	6	6
[NTA_{free}] (μM)	4	3.4	2.8	4.6	5.2	4	4	4	4
K_d (from eq 2.15) (pM)	**10**	**12**	**14**	**9**	**8**	**9**	**8**	**11**	**12**

The original values are those tabulated in Table 5.01 column a. An over-estimation of the original concentration would mean the concentration would actually be weaker and an under-estimation would mean the concentration would be stronger.

The affinities Jiang *et al.* calculated using EPR and albumin as a competitor rely on no ternary complex being formed between Cu^{2+}, Aβ and albumin. This ternary complex formation has previously been proposed by Rozga *et al.* to be a mechanism for mediating Cu^{2+}-related Aβ toxicity (Rozga *et al.* 2010). This could result in monomeric Aβ, the Aβ species thought to bind HSA, being removed from the pool of Aβ free to sequester Cu^{2+}. Therefore the concentration of Aβ(1-42) monomer required to sequester Cu^{2+} from albumin would be elevated compared to Aβ(1-42) aggregates that are unable to bind HSA. Furthermore, the affinities were calculated from a single EPR spectrum rather than a titration of Aβ into the HSA-Cu^{2+} complex, adding to potential inaccuracies. However, the ratio between the hyperfines of the HSA-Cu^{2+} and Aβ-Cu^{2+} complexes in the EPR spectrum obtained from Aβ(1-42) incubated for 6 hours does appear to be 0.5:0.5, when a 5 times excess of Aβ compared to HSA is used. The estimated K_d from this spectrum is 6 pM (Jiang *et al.* 2012), which is only slightly tighter than the affinities calculated in this work, 10-20 pM.

Finally, the Aβ(1-42) aggregates studied by Jiang *et al* were formed in the presence of one mole equivalent of Cu^{2+}, so are likely to be amorphous aggregates rather than the oligomers and protofibrils that are preferentially formed in the presence of substoichiometric levels of Cu^{2+}. Amorphous aggregates are not neurotoxic whereas oligomers are thought to be the most toxic species of Aβ. The fact that the oligomers have the same affinity for Cu^{2+} as monomeric Aβ(1-42), and indeed Aβ(1-16), demonstrates that the increased neurotoxicity of oligomers is not due to a heightened ability to bind Cu^{2+}.

5.6.3. Biological Significance

Aβ levels are estimated to be greater than 0.5 nM at the synapse (Seubert *et al.* 1992), thus Aβ would be expected to be able to compete with other metal chelators for the binding of Cu^{2+} ions with an affinity of 10-20 pM, especially during depolarisation, when Cu^{2+} can reach concentrations as high as 250 μM within the synaptic cleft (Hartter *et al.* 1988, Kardos *et al.* 1989).

To conclude, the difference between the affinities of Aβ(1-16), Aβ(1-40) and Aβ(1-42) in monomeric, fibrillar or oligomeric state for Cu^{2+} are small and not significant. Variations in calculated affinities (see Table 5.04) may actually be down to discrepancies in measuring Aβ or competing ligand concentration. Perhaps K_d values between 10 and 100 pM might be a reasonable conditional dissociation constant for all forms of Aβ at pH 7.4.

CHAPTER SIX:

DEVELOPING VISIBLE CD FOR STUDYING COPPER BINDING TO N-TERMINAL PEPTIDES. APPLICATIONS FOR THE PRION PROTEIN AND α-SYNUCLEIN; AFFINITY MEASUREMENTS AND COORDINATION GEOMETRY

ABSTRACT

Circular Dichroism (CD) spectroscopy in the visible region (Vis-CD) is a powerful technique to study metal-protein interactions. In this chapter I develop insight into the relationship between the Vis-CD spectrum of Cu^{2+}-peptide complexes and coordination geometry and apply this to Cu^{2+} binding to the prion protein (PrP^C) of transmissible spongiform encephalopathies and alpha-synuclein (αSyn) of Parkinson's disease. The chapter has been subdivided into 3 distinct parts:

Part A: Developing Predictive Rules for Coordination Geometry from Visible Circular Dichroism of Copper(II) and Nickel(II) Ions in Histidine and Amide Main-Chain Complexes.

Part B: Copper(II) Sequentially Loads on to the N-terminal Amino Group of the Prion Protein (PrP^C) Before the Individual Octa-Repeats.

Part C: Comparisons of Cu^{2+} Binding to N-terminal Model Peptides of Alpha-Synuclein, using Visible Circular Dichroism Spectroscopy: Affinity, Coordination Geometry, pH Dependence and Stoichiometry.

In Part A, I compare experimental and computed Vis-CD spectra of Cu^{2+}-loaded model peptides in square-planar complexes. I find that the spectra can readily discriminate the coordination pattern of Cu^{2+} bound exclusively to main-chain amides from that also involving a side chain (i.e. histidine side chain). Based on the results, I develop a set of empirical rules that relates the appearance of particular Vis-CD spectral features to the conformation of the complex. These rules can be used to gain insight into coordination geometries of other Cu^{2+} or Ni^{2+}-protein complexes, such as those associated with Prion Disease (Part B) and Parkinson's disease (Part C).

The cellular prion protein (PrP^C) binds to Cu^{2+} ions *in vivo* and a misfolded form of PrP^C is responsible for a range of transmissible spongiform encephalopathies. Recently, disruption of Cu^{2+} homeostasis in mice has been shown to impart resistance to scrapie infection. Using full-length PrP^C and model peptide fragments I monitor the sequential loading of Cu^{2+} ions on to PrP^C using Vis-CD. I show the N-terminal amino group of PrP^C is not the principal binding site for Cu^{2+}; however surprisingly, it has a tighter affinity for Cu^{2+} than the individual octa-repeat binding sites present within PrP^C. I re-evaluate what is understood of the sequential Cu^{2+} loading onto the full-length protein and show for the first time that Cu^{2+} loads on to the N-terminal amino group before the single octa-repeat binding sites.

Copper dyshomeostasis has been reported in Parkinson's disease (PD) and Cu^{2+} binding to alpha-synuclein (αSyn) can accelerate amyloid fibre formation. However, there is still some controversy over the coordination geometry and affinity of Cu^{2+} for αSyn. Here I show Vis-CD spectra of Cu^{2+} loaded model peptides of the N-terminus of αSyn. Using Gly as a competitor I determine the affinity of the complexes. It is clear that the Aspartate coordination of Cu^{2+} in αSyn has a stabilising influence on the Cu^{2+} complex. Affinities (at pH 7.4) are much tighter for the αSyn N-terminus tripeptide, MDV, compared to MAV with K_ds of 0.3 nM and 36 nM. The incorporation of a putative histidine side-chain in the N-terminal αSyn complex results in a significant increase in the affinity for Cu^{2+} to 30 pM at pH 7.4. These model peptides are related to studies of Cu^{2+} binding to full-length αSyn.

The work presented in Part A and Part B of this chapter forms the basis of work published in FEBS Journal 2014 and Biochemistry 2014, respectively (Stanyon *et al.* 2014a, Stanyon *et al.* 2014b).

CHAPTER 6: PART A

DEVELOPING PREDICTIVE RULES FOR COORDINATION GEOMETRY FROM VISIBLE CIRCULAR DICHROISM OF COPPER(II) AND NICKEL(II) IONS IN HISTIDINE AND AMIDE MAIN-CHAIN COMPLEXES

6A.1. INTRODUCTION

Circular Dichroism (CD) spectroscopy is a technique that is most commonly utilised in the far UV region to study protein secondary structure; however, it can also be used in the visible region (Vis-CD) to study transition metal ions in a chiral environment, such as metal-protein complexes. Transition metal ions produce Vis-CD spectra that are due to a combination of absorption bands arising from d-d electronic transitions. The signal that metal ion complexes generate in the visible range of CD can be attributed to three effects: the vicinal effect, the conformational effect, and the configurational effect (Martin 1974). For Cu^{2+} or Ni^{2+} square-planar complexes that typically involve amide main-chain coordination within proteins, the vicinal effect dominates, and is modulated by the placement of the chiral amino acid side chain above or below the quasi plane of the complex (Martin 1974, Tsangaris *et al.* 1970).

Cu^{2+} visible absorption bands are derived from three overlapping d-d transitions (Martin 1974). As CD records the difference in absorption between left and right circularly polarised light, individual transitions can produce bands of opposite sign. Thus the contribution of each band can be better resolved than with direct absorption spectra. As a consequence, CD bands are not always centred on the same wavelength as their counterpart band in absorption spectra. The CD spectra produced are unique to the coordination geometry of the metal complexed to the protein, although predictive rules that correlate Vis-CD spectra with the coordination geometry are not fully developed. Comparisons of Vis-CD spectra simulated with quantum chemical methods to experimental data can be used to deduce precise coordination geometry of the chiral complex (Autschbach 2009, Mori *et al.* 2011, Pescitelli *et al.* 2009, Stephens *et al.* 2010).

Natively unstructured proteins, such as those associated with protein misfolding diseases, have the ability to coordinate Cu^{2+} (and Ni^{2+}) ions via main-chain amide nitrogen lone-pairs (Martin 1974). Cu^{2+} complexes that involve amide main-chains are typically stabilised by favourable side-chain coordination, often a nitrogen in the imidazole ring of histidine, and/or the N-terminal amino group. Examples of these types of complexes include Cu^{2+} coordination to prion protein (Klewpatinond *et al.* 2008, Viles *et al.* 1999), α-synuclein (Binolfi *et al.* 2012, Rasia *et al.* 2005), and the N-terminal residues of serum albumin (Martin 1974, Milojevic *et al.* 2014).

6A.2. AIMS

With an aim to develop a set of empirical rules that correlates the appearance of Vis-CD spectra with the coordination geometries of Cu^{2+} and Ni^{2+} square-planar complexes, here I compare the appearance of the Vis-CD spectra of three sets of Cu^{2+}-loaded model peptides and of two sets of Ni^{2+}-loaded complexes. In particular, I study Cu^{2+}-loaded peptides including: N-terminally acetylated peptides (Ac-XXH) that have a combination of chiral and non-chiral ligands preceding the His residue (where X= Ala or Gly), as well as two related sets of peptides that have a free N-terminal amino group with and without His residue; NH_2-XXH and NH_2-XXX respectively. I compare experimental spectra with computed spectra based on density functional theory (DFT) (Hasnip *et al.* 2014) and geometry-optimized structures and time-dependent (TD)-DFT calculations (Bauernschmitt *et al.* 1996). I aim to provide a rationale for the observed spectral signatures of the complexes as well as the signatures of the linear combinations of experimentally derived Vis-CD spectra.

6A.3. EXPERIMENTAL

6A.3.1. Peptides

Fmoc chemistry was used to synthesise the various peptides used. All peptides were C-terminally amidated in order to mimic the continuation of the peptide sequence in the larger protein. The peptides were removed from the resin and de-protected before purification by reverse-phase HPLC. The samples were characterised using mass spectrometry and ^{1}H NMR spectroscopy.

The following tripeptides studied included:

Free N-terminus	Free N-terminus	Acetylated N-terminus
NH_2-AGG	NH_2-GGH	Ac-GGH
NH_2-GAG	NH_2-GAH	Ac-GAH
NH_2-GGA	NH_2-AGH	Ac-AGH
NH_2-AAA	NH_2-AAH	Ac-AAH

Purchased from Generon Ltd (Maidenhead, UK), A.B.C., Imperial College London and China Peptides (Shanghai).

The lyophilised weight of each peptide was used to estimate the concentration, assuming 20 % moisture content. However, it was the known concentration of metal ions at substoichiometric levels to the peptide that was used for the conversion to molar ellipticity in CD spectra. The concentration of albumin was determined from UV-visible electronic absorption spectra at 280 nm obtained, ε_{280} = 30,770 M^{-1} cm^{-1}.

6A.3.2. Circular Dichroism

CD spectra were obtained as described in Chapter 2.

6A.3.3.Simulations

All simulations were carried out by my collaborators; Xiaojing Cong, Giulia Rossetti, Jens Dreyer, George Papamokos, and Paolo Carloni. Tripeptide models of GGH and AGH in complex with Cu^{2+} were constructed using Accelrys® Discovery Studio Visualizer 3.5 according to the presumed coordination (Klewpatinond *et al.* 2007a) The tripeptides were C-terminally amidated and either N-terminally acetylated (Ac-XGH) in order to mimic the His^{96} and His^{111} region in PrP or had a free N-terminal amino group (NH_2-XGH). The geometries of these complexes were optimized in implicit aqueous solution using DFT with the Heyd-Scuseria-Ernzerhof (HSE) functional (Heyd *et al.* 2006) and the 6-311++G** basis set (Strati *et al.* 2002). The solvent was treated by employing the conductor polarised continuum solvent model (CPCM) (Cossi *et al.* 2003). Frequency calculations on the optimized geometries confirmed that these were true minima since no imaginary frequency was found. Free energies were obtained at 298.15 K and 1 atm. To simulate the electronic CD spectra, TD-DFT calculations were carried out on the optimized ground state geometries to explore their electronically excited states. This was performed using the same functional, basis set and solvent model as those used for geometry optimization. The first 15 states were requested to produce the electronic CD spectrum. All calculations were carried out using Gaussian 09 (Frisch *et al.* 2009). The obtained electronic CD data were analysed and the CD spectra were plotted using GaussSum 2.2 (O'Boyle *et al.* 2008). The calculation of the CD spectrum at a given wavelength (or energy, E) is done by convoluting the stick spectra with Gaussian band shapes for all transitions, using the relation:

$$\Delta\varepsilon(E) = \left(2\Delta E/2.296 \times 10^{-39}\sqrt{\pi}\sigma\right) \times R\exp\{-[2(E-\Delta E)/\sigma]^2\},$$

where ΔE is transition energy, and σ is the bandwidth at $1/e$ peak height (σ = 0.6 eV is used empirically here) (Stephens *et al.* 2010).

6A.4. RESULTS AND DISCUSSION

6A.4.1. His-Cu^{2+} Complexes Preceded by Amide Coordination Only

I have directly compared Cu^{2+}-loaded Vis-CD spectra of four possible combinations of tripeptides with His at the 3rd position (GAH, GGH, AGH and AAH) for those containing a free N-terminal amino group against those with an acetylated N-terminus to mimic Cu^{2+} coordination via residues in the middle of a protein sequence and those centred at the N-terminal amino group (Figure 1). I chose Ala and Gly for the model peptides as alanine is the simplest chiral residue and glycine is non-chiral thus will not directly contribute to Vis-CD spectra. In this way the contribution from individual side-chains at different coordination positions can be determined.

Comparisons of Vis-CD spectra for the four NH_2-XXH model peptides (Figure 6A.01, first column) have very similar appearance with positive signal to shorter wavelengths and negative signal to longer wavelengths. There is some variation in the relative intensities of the spectra, for example, the NH_2-AAH spectrum has a greater negative signal than the NH_2-GGH spectrum. The four peptides are compared to the Vis-CD spectra for the related tripeptides with an acetylated N-terminal amino group (Figure 6A.01, second column). When non-chiral glycine is in the first position, a positive d-d transition band to shorter wavelengths and a negative band to longer wavelengths is observed in the Vis-CD spectra, which is very similar to the non-acetylated N-terminal peptide. In contrast, with alanine in the first position the Vis-CD spectra invert so that the signal becomes positive at longer wavelengths and negative to shorter wavelengths.

The same behaviour is observed for peptide fragments from the binding sites within full length prion protein, PrP(23-231), centred at His^{96} and His^{111}. Depending on the presence of the chiral or non-chiral (glycine) side chain two residues preceding the His imidazole

coordination, the appearance of the Vis-CD is dramatically altered (Berti *et al.* 2007, Di Natale *et al.* 2009, Gralka *et al.* 2008, Jackson *et al.* 2001, Jones *et al.* 2005, Klewpatinond *et al.* 2007a, Klewpatinond *et al.* 2007b, Ősz *et al.* 2007). The spectra of PrP(92-96) and PrP(107-111) are shown in Figure 6A.02. This inversion of the spectrum has been observed for a number of peptides influenced by the presence or absence of a side chain two residues preceding the His side-chain. For example a whole series of penta-peptides, eight in all, related to PrP(92-96) and PrP(107-111) (Klewpatinond *et al.* 2007a). Furthermore, the Cu^{2+} Ac-GGGH and Ac-GGHG visible CD spectra (Orfei *et al.* 2003) have the striking appearance of Ac-GGH, while Cu^{2+} and Ni^{2+} square-planar, four nitrogen complexes of Ac-ELAKHA (Karavelas *et al.* 2005) and Ac-TESHAK peptides (Mylonas *et al.* 2002a, Mylonas *et al.* 2002b), models of the C-terminal tail of histone H2A, have the inverted appearance of Ac-AAH, as predicted.

6A.4.2. Simulation Data of Ac-GGH and Ac-AGH Cu^{2+} Complexes

Simulations were performed in order to elucidate the reasons for the mirror image relation between Vis-CD spectra of Cu^{2+} loaded Ac-AGH and Ac-GGH. The former contains a non-chiral Gly residue in the first position, whereas the latter has a side-chain and is chiral at this position. Three possible stereoisomers for Cu(Ac-GGH) were identified. These also resemble the three possible stereoisomer conformations for Cu(Ac-AGH) (Figure 6A.03). Their corresponding simulated Vis-CD spectra are also shown in Figure 6A.03, calculated using TD-DFT. The isomers are denoted 1, 2 and 3 for both the Cu(Ac-GGH) and Cu(Ac-AGH) complexes. Isomer 1 generates almost the mirror image spectrum of isomer 2 and 3. It can be concluded that Cu(Ac-GGH)_1 is the major isomer of Cu(Ac-GGH) in solution, as its spectrum is the only one resembling the experimental one. This agrees well with the free energy of the structures (see Figure 6A.03). Consistently, the free energy of Cu(Ac-GGH)_1 is significantly lower than that of the other two isomers

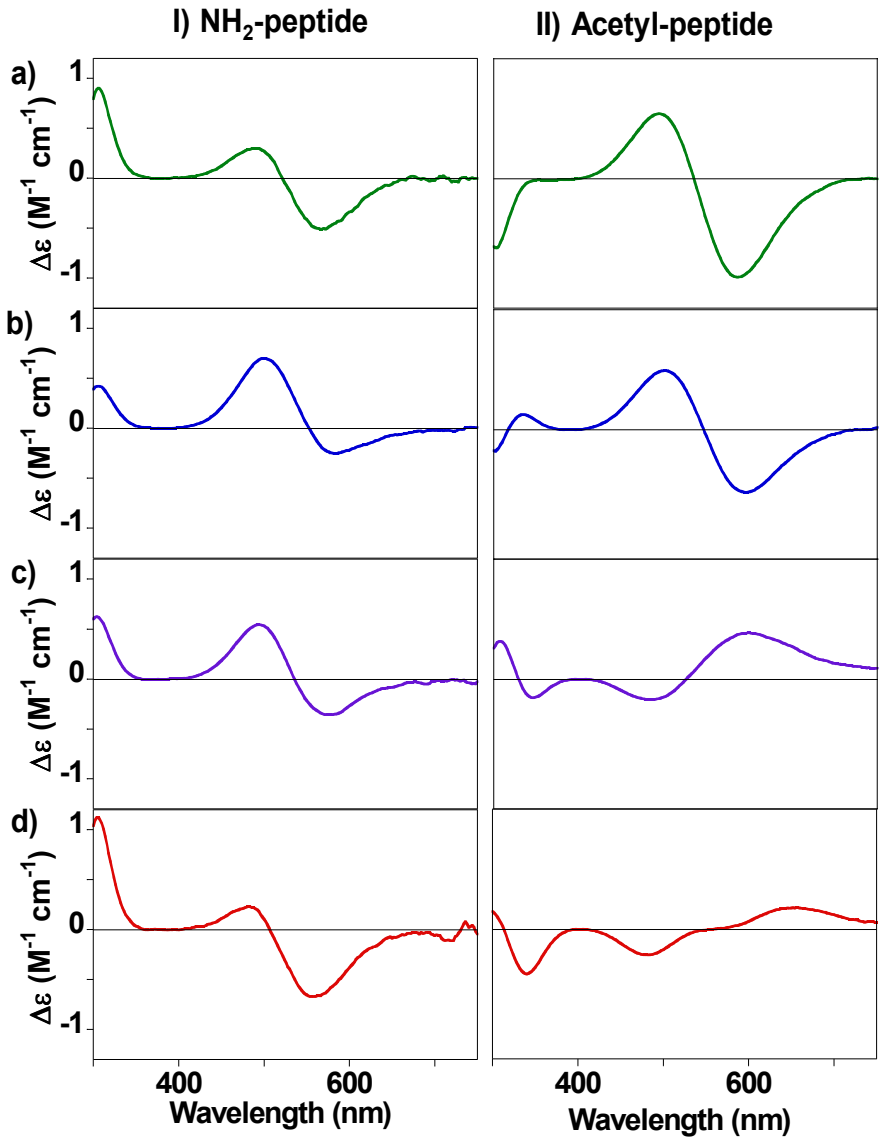

Figure 6A.01. Comparison of Vis-CD Spectra of Cu^{2+} Bound to Free and Acetylated Model Tripeptides.

Column I): Cu^{2+} binding to free N-terminal peptides at pH 7.4, column II): Cu^{2+} binding to acetylated N-terminal peptides at pH 9.5. Row a) = GAH, b) = GGH, c) = AGH, d) = AAH. The presence of a chiral residue for the acetylated peptides causes an inversion of the CD bands but has little effect for peptides with a free N-terminal amino group.

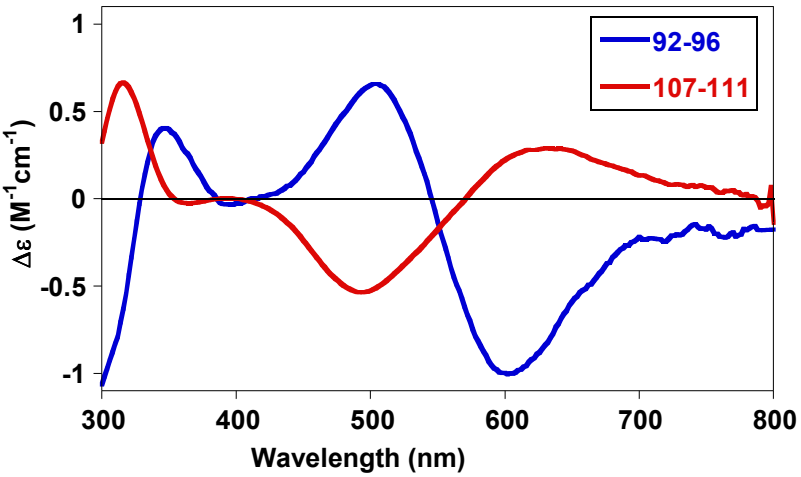

Figure 6A.02. Inverted Vis-CD spectra Within the Prion Protein.

Vis-CD of one mole equivalent of Cu^{2+} bound to 100 μM PrP(92–96) and PrP(107–111) at pH 7.8. Data originally published in (Klewpatinond *et al.* 2007b).

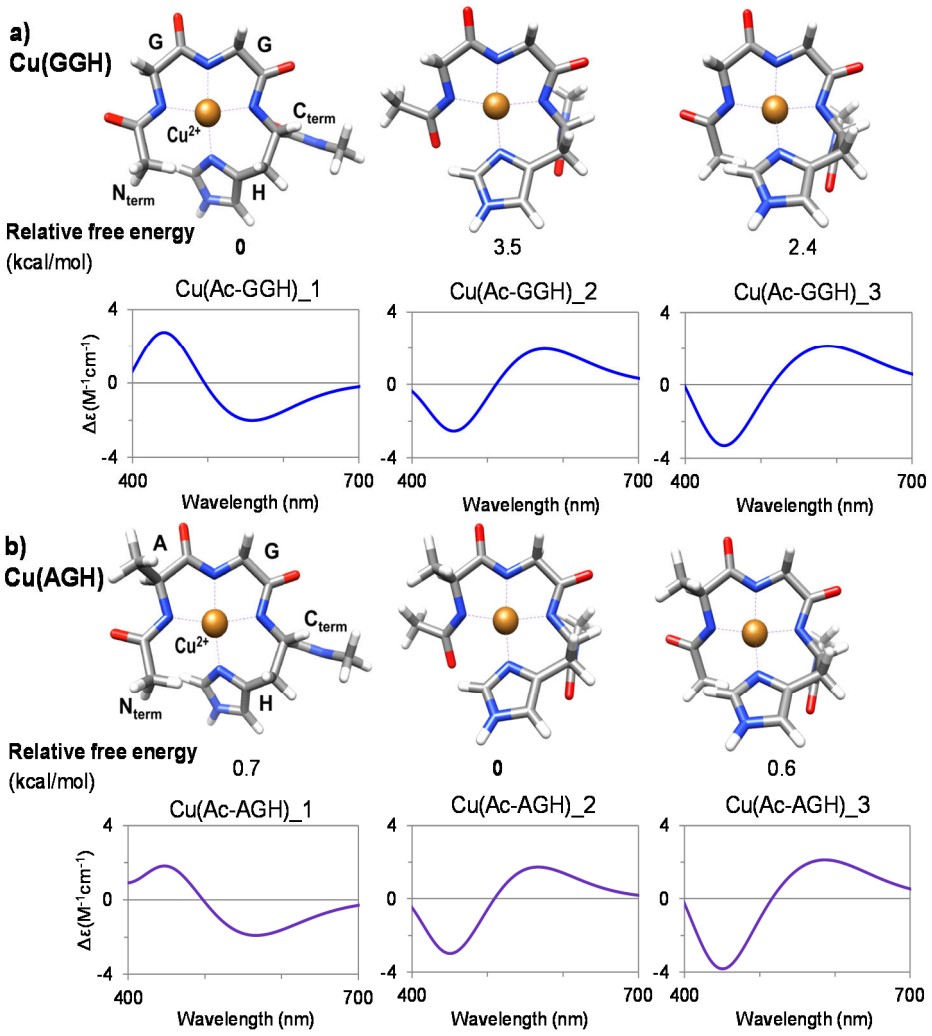

Figure 6A.03. Calculated Vis-CD Spectra of the Three Possible Stereoisomers of a) Cu(Ac-GGH) and of b) Cu(Ac-AGH).

The isomers 1 and 2 (of each complex) are cis/trans isomers referring to the acetyl O and Cu^{2+} atoms, whilst 1 differs from 2 and 3 in the histidine imidazole that is either below or above the plane of the peptide backbone. The calculated free energy of each isomer with respect to the lowest-energy one (set as 0 kcal/mol) is also given. Coloured by elements: C, gray; N, blue; O, red; H, white and Cu, orange.

This figure was kindly supplied by my collaborators; Xiaojing Cong, Giulia Rossetti, Jens Dreyer, George Papamokos, and Paolo Carloni from the German Research School for Simulation Sciences.

(about -4 and -1 kcal/mol for Cu(Ac-GGH)_2 and Cu(Ac-GGH)_3, respectively). In contrast, Cu(Ac-AGH)_2 and Cu(Ac-AGH)_3 are the major isomers of Cu(Ac-AGH) in solution, as their spectra are the only ones resembling the experimental one. In this case, however, there are only minor differences (within 1 kcal/mol) in free energy among the isomers. These results raise the question why stereoisomer 1 is favourable for Cu(Ac-GGH), but not Cu(Ac-AGH). A possible explanation is that in Cu(Ac-AGH)_2 the Alanine side chain forms hydrophobic interactions with the acetyl group, which may compensate the penalty of forming this conformation. Indeed, the energetic contribution of such hydrophobic interactions is expected to be a few kcal/mol, corresponding to the energy difference between Cu(Ac-GGH)_1 and Cu(Ac-GGH)_2(Pace *et al.* 2011). The same effect is observed *in vitro* for penta-peptides PrP(92-96) and PrP(105-111) (Klewpatinond *et al.* 2007a) and the same binding in full-length PrP^C (Klewpatinond *et al.* 2008).

These results suggest that the absence or presence of a Gly in the first position causes a change of the spectrum to its mirror image *indirectly*. Indeed, the Gly favours the position of the His side chain imidazole ring "below" the quasi-plane defined by the Cu^{2+} and the backbone N atoms in these isomers (see the scheme in Figure 6A.04a). On the other hand, when Ala is the first residue, it favours instead the "above" position (Figure 6A.04b). These positions correlate with the generation of a spectrum or its mirror image: isomer 1 of each complex differs from the isomers 2 and 3 in the position of the imidazole ring with respect to the plane of the backbone N atoms (Figure 6A.03). Hence, the nature of the first residue affects the His conformation, which affects the chirality of the complexes. This in turn determines the Vis-CD spectral pattern observed experimentally both in the peptide models and, for example, in the His^{96} and His^{111} sites of PrP (Klewpatinond *et al.*

2007a) and other histidine-containing peptides (Karavelas *et al.* 2005, Mylonas *et al.* 2002a, Mylonas *et al.* 2002b)

6A.4.3. Simulated NH_2-XXH Spectra

The *in vitro* Vis-CD spectra of Cu^{2+} loaded XXH tripeptides with free N-terminal amino group ($Cu(NH_2$-XXH)) have been compared to those of the N-terminal acetylated tripeptides (Cu(Ac-XXH)) (Figure 6A.01). The presence or absence of a side chain (Ala) at the first position does not appear to modulate the spectra greatly as the signatures for all four peptides AAH, GGH, AGH, GAH are quite similar. Again DFT and TD-DFT calculations have been used on two of the complexes, $Cu(NH_2$-GGH) and $Cu(NH_2$-AGH), to understand this effect. Geometry optimisation shows that without the N-terminal acetylation group there is only one stereoisomer for each complex (Figure 6A.05). The stereoisomer resembles Cu(Ac-GGH)_1 in which the His imidazole ring is "below" the quasi-plane of Cu^{2+} and the peptide backbone. Correspondingly, the Vis-CD spectra of $Cu(NH_2$-GGH) and of $Cu(NH_2$-AGH) (Figure 6A.05) also resemble that of Cu(Ac-GGH)_1 (Figure 6A.03), consistent with the *in vitro* spectra (Figure 6A.01). This is not unexpected because Cu(Ac-GGH)_1 is the energetically most favoured stereoisomer of Cu(Ac-GGH). In the case of Cu(Ac-AGH), stereoisomer 2 is favoured likely due to the presence of acetyl (as discussed above), which is absent in $Cu(NH_2$-AGH) complex.

6A.4.4. Vis-CD Spectra of Ni^{2+} Complexes are Similar to Cu^{2+} Complexes

The ability of metal ions to deprotonate amides and coordinate is unusual but not exclusive to Cu^{2+} ions; Ni^{2+} ions (Jones *et al.* 2005) and Pd^{2+} ions (Garnett *et al.* 2006) also have this property (Martin 1974). Ni^{2+} binds to albumin with a similar coordination

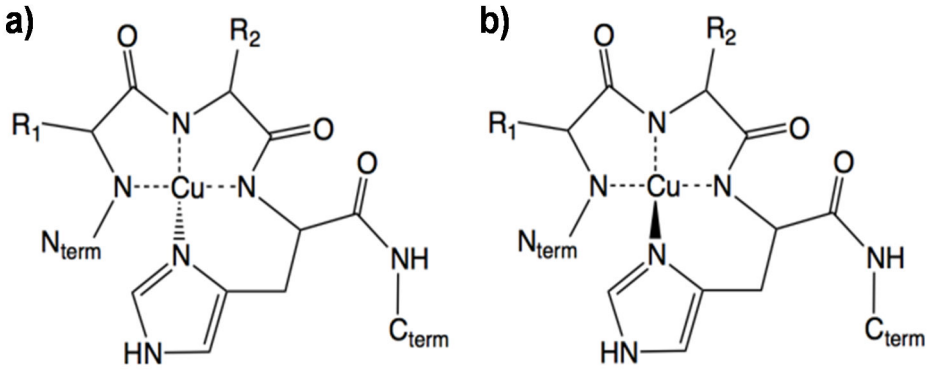

Figure 6A.04. Schematic Representation of Cu-XXH Stereoisomers.

Possible stereoisomers of Cu^{2+} bound to XXH tripeptides, where X is any residue, with the histidine imidazole ring a) "below" and b) "above" the quasi plane, defined by the backbone N atoms and the Cu^{2+} ion.

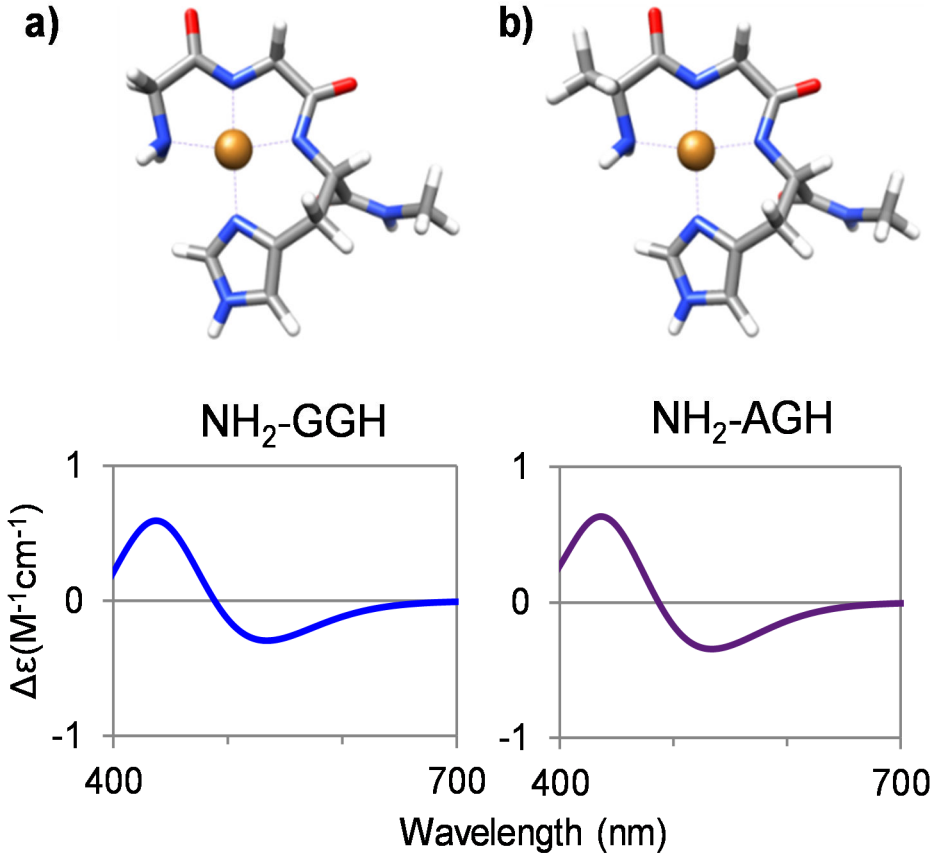

Figure 6A.05. The Calculated Configuration and Vis-CD spectra for Cu^{2+} Binding to Free N-Terminal Peptides.

a) NH_2-GGH, b) NH_2-AGH.

This figure was kindly supplied by my collaborators; Xiaojing Cong, Giulia Rossetti, Jens Dreyer, George Papamokos, and Paolo Carloni from the German Research School for Simulation Sciences.

to Cu^{2+} ions (Sadler *et al.* 1994). To determine whether the Vis-CD spectra follow the same behaviour as Cu^{2+}, I studied the same set of peptides bound to Ni^{2+} ions. Figure 6A.06 shows that Ni^{2+} bound to the histidine-containing tripeptides produces Vis-CD spectra similar to those produced by Cu^{2+} ions. In particular, the CD bands are negative to longer wavelengths for NH_2-XXH tripeptides with a free N-terminal amino group. Similarly, the Ni^{2+} complexes of Ac-XXH tripeptides, with an acetylated N-terminus, exhibit the same behaviour as Cu^{2+}, where with Gly at the first position a positive CD band is observed at shorter wavelengths, while with an amino acid with a side-chain (Ala) and the associated steric effect, the appearance of the d-d CD bands is inverted.

The CD bands observed for the Ni^{2+}-peptide complexes have all shifted to a shorter wavelength in comparison to the corresponding Cu^{2+}-peptide complexes. Cu^{2+} d-d absorption bands for four nitrogen ligands are typically centred at 540 nm, while similar Ni^{2+} complexes absorb at 440 nm.

6A.4.5. Contributions of Residues Around the Chelate Plane are Additive to CD Spectra

Figure 6A.07a shows the series of four Cu^{2+} loaded NH_2-XXH peptides overlaid. The variation in the relative intensity of the positive and negative CD bands is quite apparent. The GGH spectrum has the most intense positive signal, while AAH has the most intense negative signal. Replacement of each glycine with an alanine creates a more negative signal, which is particularly apparent when the GGH spectrum is subtracted from the individual spectra of AGH, GAH and AAH, Figure 6A07b. These difference spectra (Figure 6A.07b) have a very similar appearance to the spectra of Cu^{2+} loaded NH_2-AGG NH_2-GAG and NH_2-AAG, shown in Figure 6A.08a.

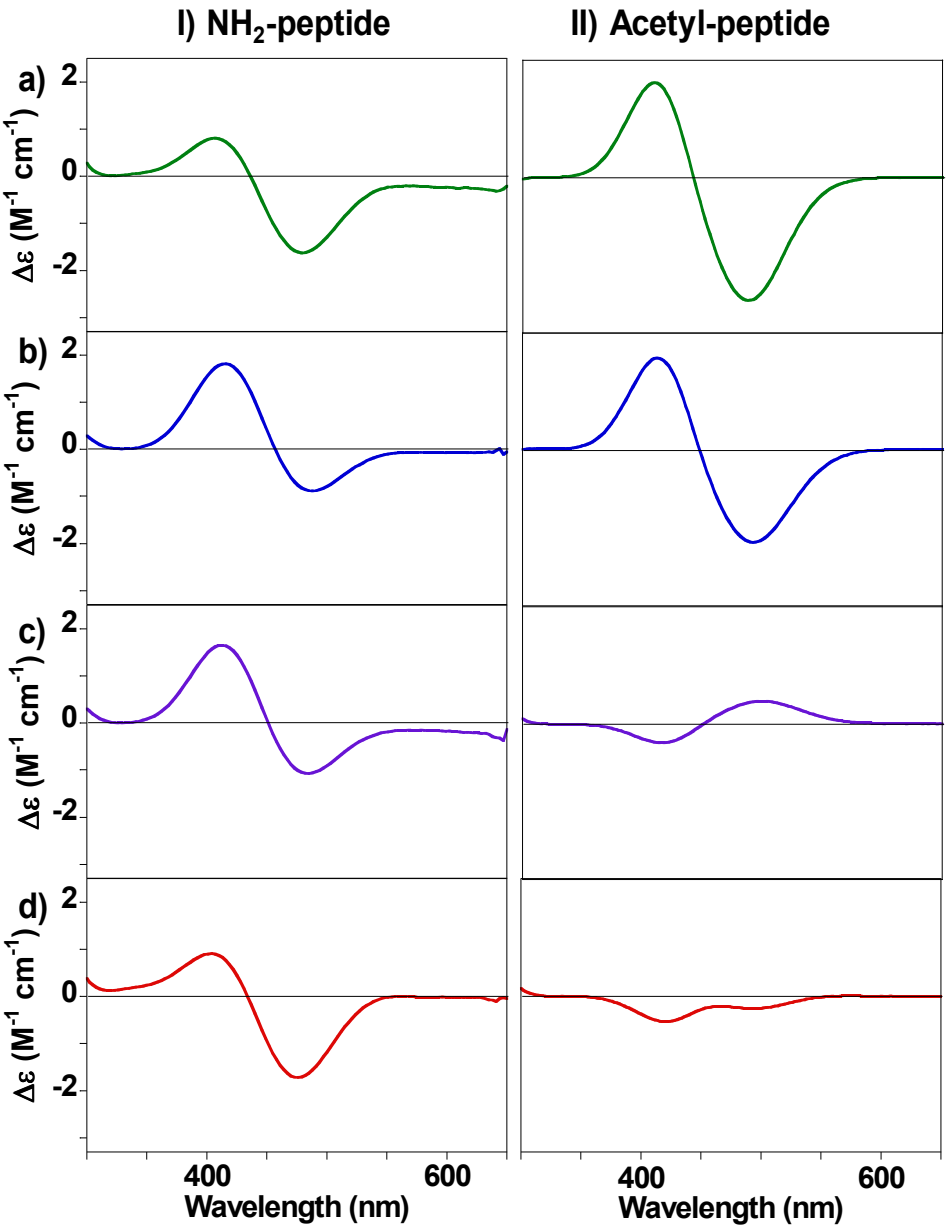

Figure 6A.06. Comparison of Free and Acetylated Model Tripeptides Shows the Side Chain of Residue 1 Affects Ni^{2+} Vis-CD spectra.

Column I) free N-terminal Ni^{2+} binding at pH 7.4, column II) acetylated N-terminal Ni^{2+} binding at pH 9.5. Row a) = GAH, b) = GGH, c) = AGH, d) = AAH.

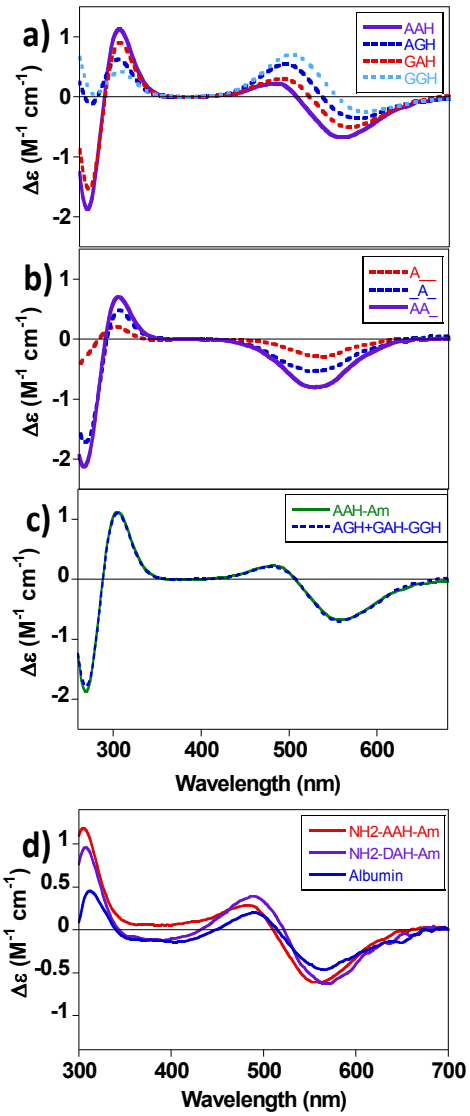

Figure 6A.07. Vis-CD spectra of N-terminal Cu^{2+} coordination involving Histidine

a) The spectra of AAH, AGH, GAH and GGH bound to Cu^{2+} at pH 7.4. b) The difference spectra from a) with the spectrum of GGH subtracted from each. c) The sum of the visible CD spectra to get AAH (AGH+GAH-GGH) overlaid with AAH coordinated to Cu^{2+}. d) The spectra of full-length human serum albumin, N-terminal model of human serum albumin (DAH), and AAH bound to one mole equivalent of Cu^{2+}. All spectra were obtained using 100 μM peptide and 100 μM Cu^{2+} at pH 7.4.

Figure 6A.07c shows the comparison of the Cu^{2+} loaded Vis-CD spectrum for AAH with a convoluted spectrum generated by the combination of three Cu^{2+}-loaded spectra; AGH plus GAH minus GGH. The generated spectrum is strikingly close to that of AAH. It is clear that by replacing the alanines with glycines, the individual contributions of each residue can be obtained and summed together to simulate the spectrum of AAH, as previously shown for AAA tripeptides by Tsangaris and Martin (Tsangaris *et al.* 1970). This approach is therefore also applicable for coordination that involves side chain coordination of this type as well as amide main-chain coordination.

Cu^{2+} complexed with proteins often involves both N-terminal amino group and His imidazole coordination. These complexes have a particularly high affinity for Cu^{2+} in the picomolar range, such as the N-terminal binding domain of serum albumin (Kumar *et al.* 2011, Teir *et al.* 2012). Cu^{2+} binding to the N-terminus of serum albumin is well characterised and is thought to be responsible for transport of exchangeable Cu^{2+} in blood plasma (Patel *et al.* 1993). Serum albumin is an example of a protein that binds Cu^{2+} to produce a visible CD spectrum that has both negative and positive CD bands with side-chain coordination as well as main-chain amide coordination, Figure 6A.07d. The Vis-CD spectrum produced for albumin has the same appearance as the tripeptide DAH, the first three N-terminal residues of human serum albumin. Furthermore, the DAH spectrum is almost identical to the spectrum of AAH, Figure 6A.07d.

6A.4.6. Cu^{2+} Square-Planar Complexes in the Absence of Side-Chain Coordination

More than 40 years ago Tsangaris and Martin indicated that Cu^{2+} binding to the N-terminal of peptides via the amide backbone, forming a 4N square-planar complex will always generate negative CD bands for the copper d-d electronic transitions (Tsangaris *et al.* 1970). I have confirmed this for peptides containing glycine and alanine residues

(Figure 6A.08a). Cu^{2+} binding to the N-terminal amino group of PrP^C shows this type of spectrum (Stanyon *et al.* 2014b), while Cu^{2+} binding to the N-terminal amino group of α-synuclein does not because of the additional coordination of an Asp side-chain (Binolfi *et al.* 2012).

Tsangaris and Martin also suggested that contributions from individual residues to the Vis-CD spectrum are additive, meaning the individual spectra of three different tripeptides containing one chiral residue in each position can be added together to closely simulate the spectrum of the tripeptide containing all of those chiral residues (Tsangaris *et al.* 1970). In particular, the Cu^{2+} bound spectra of the three tripeptides with Alanine at each position of the tripeptides (AGG, GAG and GGA) added together has the appearance of Cu^{2+} bound to AAA (tri-alanine). Indeed, the Vis-CD signal for Cu^{2+} bound tri-glycine (GGG) is not detected (Figure 6A.09) because of the lack of main-chain chirality, thus there is no vicinal effect (Martin 1974). Figure 6A.08b highlights how closely individual residue combinations can predict the appearance of other spectra, with a striking similarity between the combined spectrum derived from the addition of three different tripeptides and the spectrum of tri-alanine.

6A.5. CONCLUSION

Vis-CD is a powerful probe (Bal *et al.* 1997, Binolfi *et al.* 2008, Karavelas *et al.* 2005, Laitinen *et al.* 2006, Martin 1974, Milojevic *et al.* 2014, Mylonas *et al.* 2002a, Mylonas *et al.* 2002b, Stanyon *et al.* 2014b, Tsangaris *et al.* 1970) for determining pH dependence of binding (Viles *et al.* 1999), stoichiometry (Klewpatinond *et al.* 2008) and affinity of transition metal ions (Nadal *et al.* 2009, Stanyon *et al.* 2014b). Here I have presented a broad set of observations correlating the Vis-CD spectra of Cu^{2+} or Ni^{2+} square-planar complexes with the coordination geometry:

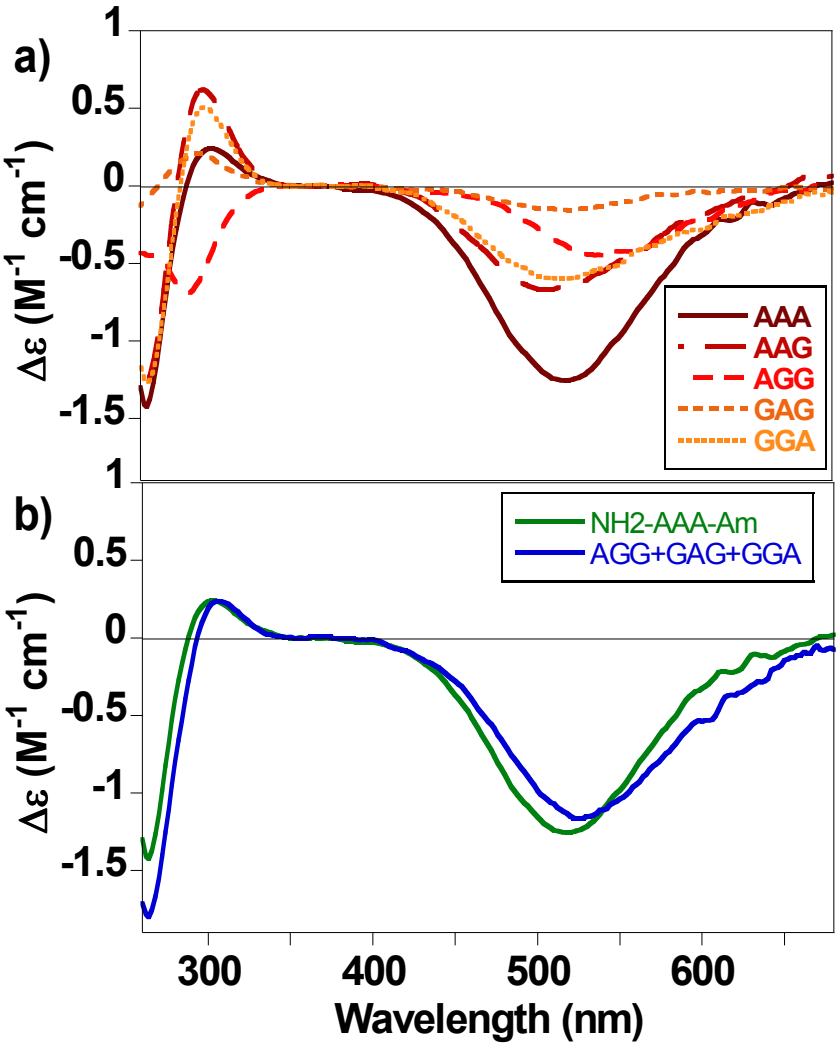

Figure 6A.08. Vis-CD Spectra of Square-Planar Cu^{2+} Coordination at the N-Terminal of Peptides, Which Lacks Side-Chain Coordination, Always has a Negative d-d Band in the CD spectrum

a) The visible CD spectra of one mole equivalent of Cu^{2+} bound to 100 μM of the model N-terminal tripeptides: AAA, AAG, AGG, GAG, and GGA, at pH 9.5. b) Comparison of the summed spectra of (AGG+GAG+GGA) with spectra of AAA bound to Cu^{2+} at pH 9.5.

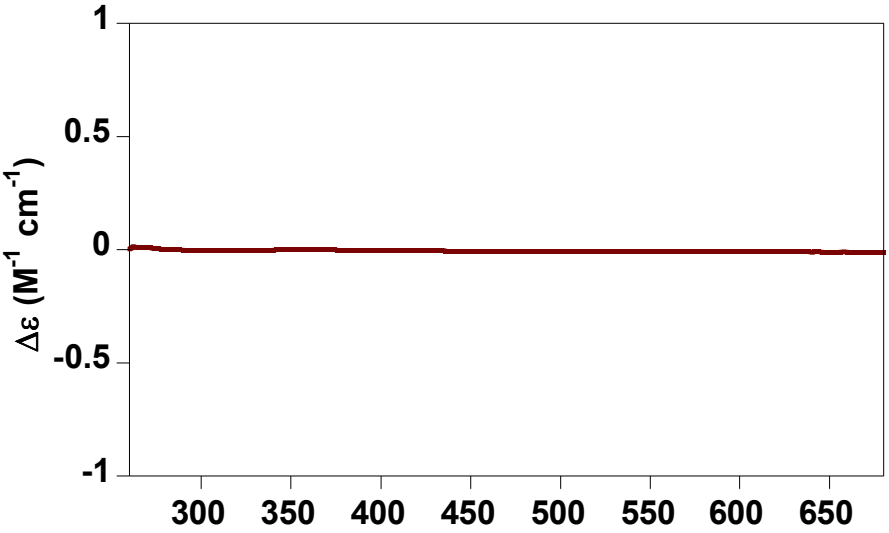

Figure 6A.09. Tri-Glycine Bound to Cu^{2+} Does Not Produce a Vis-CD signal.

1 mM tri-glycine bound to one mole equivalent of Cu^{2+} at pH 9.5.

i) Entirely negative d-d bands suggest N-terminus and main-chain amide coordination but no side-chain coordination.

ii) N-terminal coordination with His at the second position (such as that found for albumin) contains both positive and negative d-d CD bands with the band at longer wavelengths being negative.

iii) Coordination of His residue and preceding amide distant from the N-terminal amino group (often observed at higher pH) is modulated by the presence of a side-chain and its steric effect at the third position before the His residue. If a side-chain is present here the positive and negative bands are inverted compared to coordination involving histidine and a free N-terminal amino group, three residues apart, with negative signal to shorter wavelengths.

iv) Spectra can be additive with each chiral residue around the Cu^{2+} having its own individual contribution thus aiding the predictive power of Vis-CD spectra in indicating coordination geometry.

In conclusion, I have been able to provide a set of rules, which gives insights into the coordination geometry of Cu^{2+} and Ni^{2+} binding to proteins and corresponds to the appearance of Vis-CD spectra for these biologically relevant transition metal ions.

CHAPTER 6: PART B

COPPER(II) SEQUENTIALLY LOADS ON TO THE N-TERMINAL AMINO GROUP OF THE PRION PROTEIN (PRP^C) BEFORE THE INDIVIDUAL OCTA-REPEATS

6B.1. INTRODUCTION

There is intense interest in Cu^{2+} and other metal ions binding to amyloidogenic proteins, in particular amyloid-beta peptide (Aβ) in Alzheimer's Disease, alpha-synuclein (αSyn) in Parkinson's Disease, and the prion protein (PrP) in transmissible spongiform encephalopathies (TSEs) (Gaggelli *et al.* 2006, Viles 2012). Cu^{2+} ions bind to PrP^C *in vivo* (Brown *et al.* 1997) and induces PrP^C endocytosis (Perera *et al.* 2001), while PrP^C mediates Zn^{2+} ion uptake (Watt *et al.* 2012). Recently it has been shown that transgenic mice with a Menkes disease (Atp7a) mutation are resistant to scrapie infection, making a strong link between copper homoeostasis and prion disease (Siggs *et al.* 2012). Furthermore, prion related scrapie isolates have been found to contain Cu^{2+} ions (Wadsworth *et al.* 1999). Moreover, copper chelation has been shown to delay the onset of prion disease in mice (Refolo *et al.* 2001). Interestingly Cu^{2+} binding to PrP^C has also been linked to Aβ toxicity in Alzheimer's Disease (You *et al.* 2012). It is for these reasons, much effort has been directed at characterizing the coordination and affinity of Cu^{2+} binding to PrP^C; for reviews see (Millhauser 2004, Viles 2012, Viles *et al.* 2008). As many as six Cu^{2+} ions have been shown to coordinate to the natively unstructured N-terminal domain of PrP^C (Klewpatinond *et al.* 2008), with two binding sites in the amyloidogenic region anchored at His^{111} and His^{96}, and up to four binding sites anchored at the four His residues within the octa-repeat region (Figure 6B.01). Vis-CD has proven to be quite a powerful approach to study Cu^{2+} coordination with broadly four different types of Cu^{2+} coordination described, which generate very different Vis-CD spectra (Klewpatinond *et al.* 2008, Morris *et al.* 2003, Nadal *et al.* 2009, Ősz *et al.* 2007, Viles *et al.* 1999, Viles *et al.* 2008, Wells *et al.* 2006).

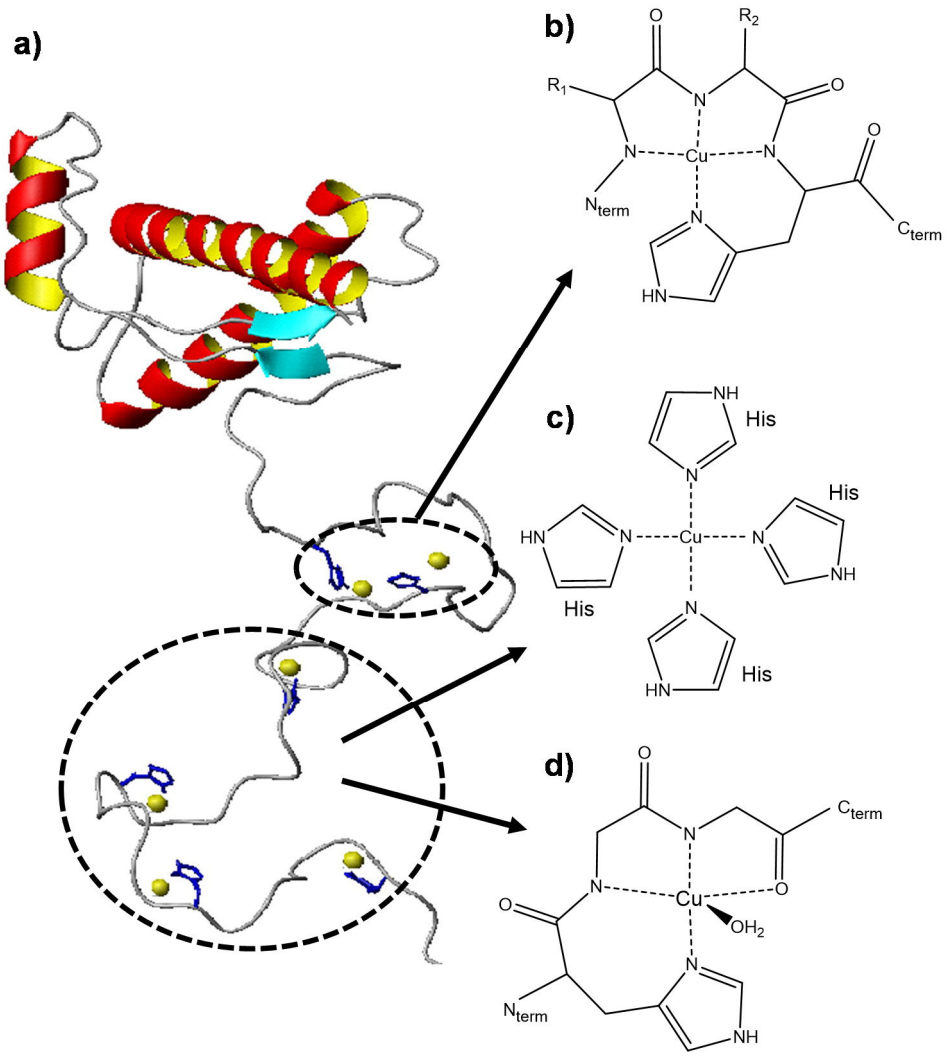

Figure 6B.01. Cu^{2+} Coordination to the Prion Protein.

a) The structure of the prion protein with the histidine residues involved in copper coordination highlighted. b) The coordination geometry of Cu^{2+} binding centred around His^{96} and His^{111}. R_1 and R_2 represent the different amino acid residue side-chains preceding each His residue. c) The coordination geometry of Cu^{2+} bound to all four imidazole side-chains of the His residues in the octa-repeats region, and d) the coordination geometry of Cu^{2+} binding to a single octa-repeat.

The locus of binding of Cu^{2+} to both αSyn and Aβ has been shown to directly involve coordination at the N-terminal amino group (Binolfi *et al.* 2012, Sarell *et al.* 2009). In contrast, Cu^{2+} binding via the N-terminal amino group of PrP^C has not previously been highlighted (Klewpatinond *et al.* 2008, Millhauser 2004).

6B.2. AIMS

Probe Cu^{2+} coordination and determine the affinity of Cu^{2+} binding directly at the N-terminal amino group of PrP^C. Here I use Vis-CD to directly monitor Cu^{2+} binding affinity using glycine as a competitive ligand, and compare Cu^{2+} binding to model peptides of the N-terminus to Cu^{2+} binding to full-length PrP^C.

6B.3. EXPERIMENTAL

6B.3.1. Peptides

Fmoc chemistry was used to synthesise the various peptides used. All peptides were C-terminally amidated in order to mimic the continuation of the peptide sequence in the larger protein. Peptides with amidated C-termini and free N-terminal amino groups studied included KKR, MKK and AAA. The single octa-repeats peptide and PrP(58-91) were acetylated at the N-terminus in addition to amidation at the C-terminus (sequences GQPHGGGWGQP and GQPHGGGWGQPHGGGWGQPHGGGWGQPHGGGWGQP, respectively). Purchased from Generon Ltd (Maidenhead, UK).

The extinction coefficient at 280 nm was used to determine the concentration of PrP^C fragments, calculated from the total sum of the extinction coefficients for the number of aromatic residues and disulphide bridges in the peptide. Precise concentrations of peptides that did not contain aromatic residues were obtained via Cu^{2+} titrations with saturation at 1:1. Typically, lyophilized peptide contained 20 % moisture content.

6B.3.2. Circular Dichroism (CD)

CD spectra were recorded as described in Chapter 2.

6B.3.3. Electron Paramagnetic Resonance (EPR)

EPR spectra were recorded as described in Chapter 2. Samples were run in 50 mM temperature-independent pH buffer composed of 60 % HEPES and 40 % phosphate buffer (Sieracki *et al.* 2008), at either pH 7.5 or pH 10.

6B.3.4. Affinity Measurements

Affinity measurements were carried out as described in Chapter 2. Glycine was the competing Cu^{2+} chelator used in calculating the affinity of the Cu^{2+}-peptide complexes. The values used to calculate the affinities are shown in Table 6B.01.

There is a small discrepancy between the data given in Table 6B.01 and the values previously reported (Nadal *et al.* 2009) due to the total glycine concentration previously being used in calculations rather than the [Gly_{free}].

The accuracy in the conditional dissociation constants at pH 7.4 reported in Table 6B.01 is indicated by the number of significant figures the values are reported to (two significant figures). An indication of the errors in the K_d values determined can be gained from comparison of values for: PrP(23-231); PrP(23-231 Δocta); mPrP(90-114); and hPrP(91-115 H96A). K_ds are: 34 nM; 26 nM, 32 nM and 45 nM respectively. These values are for the same binding site with a mean of 34 +/- 8 nM (sd), the standard deviation indicates the significant figures given for K_d values are appropriate. Furthermore, determination of the concentration of the competitor glycine at the mid-point of the titration (50% loaded) is influenced by the fit of the binding curve, particularly the Δε value before a competitor

is added and also the baseline signal once all the Cu^{2+} is bound to the CD silent competitor. Determining the mid-point of the titration from more than one CD band indicates the precision associated with the fit of the binding curve.

Table 6B.01. Values Used for Calculating the Affinities of Cu^{2+} for Different Binding Sites Within PrP^C at pH 7.4.

PrP Fragment	$[PrP_{total}]$ (μM)	$[Cu^{2+}_{total}]$ (μM)	$[Cu^{2+}_{bound}]$ (μM)	$[Gly_{total}]$ (μM)	$[Gly_{free}]$ (μM)	K_d (nM)
KKR	200	200	100	267 262	81 77	**240[a]** **260[b]**
MKK	200	200	100	278 308	91 118	**190[a]** **120[b]**
mPrP(57-67) (Single octa)[#]	100 50	100 50	50 25	111 86	27 42	**800** **200[c]**
mPrP(23-231)[#]	105	105	52.5	262.5	162	**34**
mPrP(23-231Δocta)[#]	50	50	25	175	127	**26**
hPrP(91-115 H96A)[#]	100	100	50	231	136	**45**
mPrP(90-114)[#]	100	100	50	258	162	**32**
mPrP(57-90) (Multiple octa)[#]	50	50	25	172	124	**27[c]**

[a]Determined from Vis-CD signal at 540 nm. [b]Determined from Vis-CD signal at 310 nm. [c]Determined using tryptophan fluorescence instead of Vis-CD. [#]Data obtained from (Nadal *et al.* 2009).

6B.4. RESULTS AND DISCUSSION

Firstly I used Vis-CD to probe Cu^{2+} binding to a simple tripeptide from the N-terminus of human/mouse PrP^C, KKR (residues 23-25). The tripeptide MKK was also studied because methionine is present in recombinant constructs of full-length PrP^C, previously used by ourselves and others. In the presence of Cu^{2+} ions at pH 7.4, the Vis-CD spectra of these two different N-terminal sequences are essentially the same with a negative ellipticity at 540 nm, associated with the d-d electronic absorption band, and a positive band at 318 nm. Cu^{2+} binds to these N-terminal tripeptides with a 1:1 stoichiometry, see Figure 6B.02. EPR spectra of the paramagnetic Cu^{2+} complex of MKK and KKR indicate a square-planar (type II) coordination geometry with A_{II} and g_{II} typical of four nitrogen (4N) ligands at pH 10. This suggests the Cu^{2+} coordination involves the N-terminal amino group and the following amide main-chain nitrogens, Figure 6B.03. At physiological pH the axial, square-planar, EPR spectrum is retained but there is a clear shift in the $A_{||}$ and $g_{||}$ values to those more typical of nitrogen and oxygen ligands; a 3N1O or 2N2O complex, as highlighted in a Peisach and Blumberg plot (Peisach *et al.* 1974) in Figure 6B.04. The pH dependence of the N-terminal complex is further probed by Vis-CD, shown in Figure 6B.05. The position of this negative CD band is pH dependent, with higher pH values shifting the band to shorter wavelengths. This shift with pH is due to the change in coordination geometry, such that a complex consistent with a 4N square-planar geometry is favoured at pHs above 8.5 (Bryce *et al.* 1966). It is notable that the transition between a probable 4N to a 3N1O complex and a low pH complex with no amide coordination (CD silent) is quite similar for both tripeptides with a pK_a of ~6.5 for the transition between an optically active complex and one that gives no CD signal. Although, these pK_as are only approximate due to spectra overlap.

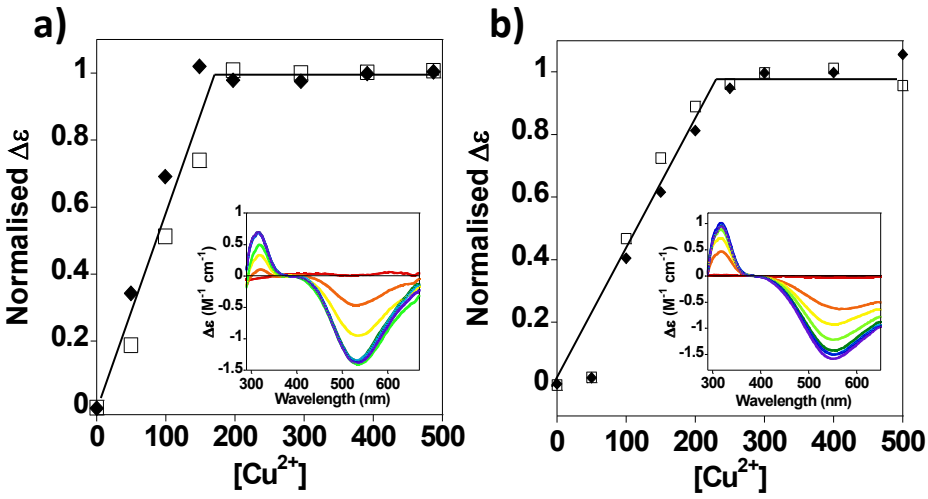

Figure 6B.02. Vis-CD Spectra of Cu^{2+} Binding the N-Terminal Tripeptide of PrP

Cu^{2+} binding at pH 7.4 to a) 200 μM KKR at 318 nm (squares) and 534 nm (diamonds) with full spectra inset, and b) 200 μM MKK at 318 nm (squares) and 549 nm (diamonds) with full spectra inset. The binding curves indicate a 1:1 stoichiometry for both tripeptides.

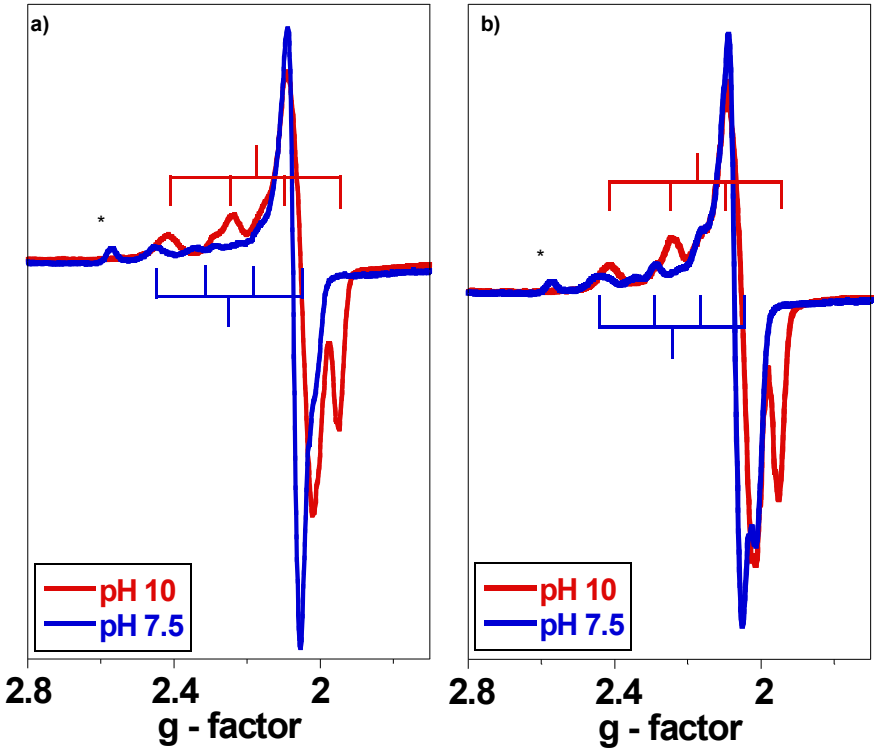

Figure 6B.03. EPR Spectra of Cu^{2+} Complexed to the N-Terminal Amino Group of PrP^C

a) 200 μM KKR bound to 150 μM Cu^{2+} at pH 7.5 and pH 10, and b) 200 μM MKK bound to 150 μM Cu^{2+} at pH 7.5 and pH 10. EPR spectra of the paramagnetic Cu^{2+} complex indicate a square-planar (type II) coordination geometry with $A_{\|}$ and $g_{\|}$ typical of 4N ligands at pH 10. There is a clear shift in the $A_{\|}$ and $g_{\|}$ values at physiological pH more typical of a 3N1O or 2N2O complex at pH 7.5. * represents a contaminant.

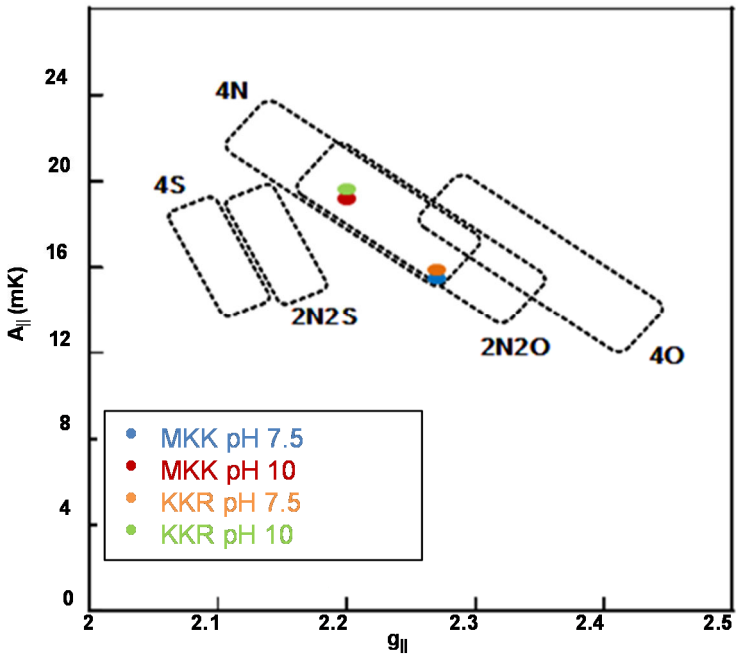

Figure 6B.04. Peisach-Blumberg Plot Showing the Relationship Between A_{II} and g_{II} for the Tripeptides at pH 7.5 and 10

(Peisach *et al.* 1974)

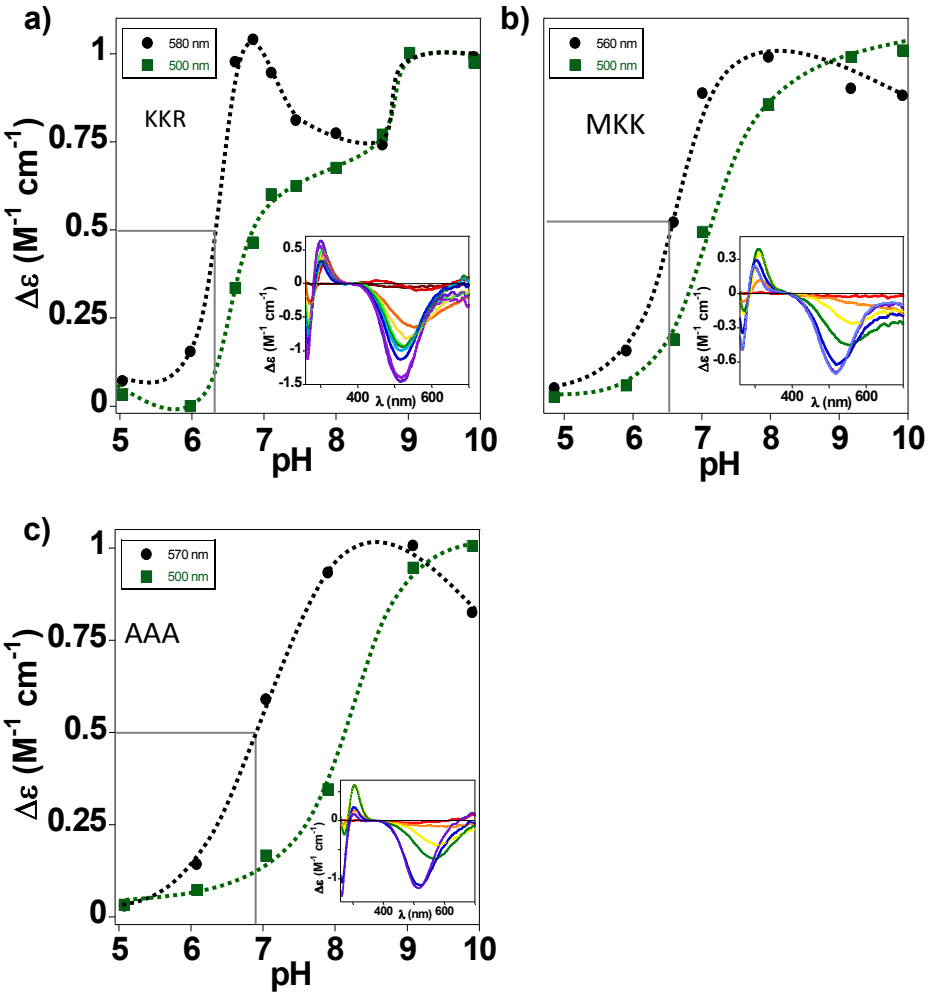

Figure 6B.05. Comparing the pH Dependence of Cu^{2+} Binding to the N-Terminal of PrP^{C}.

The normalised peak intensities of bands at 500 and ~570 nm corresponding to Visible CD spectra (inset) for 100 μM Cu^{2+} binding to 100 μM a) KKR, b) MKK, and c) AAA at increasing pH. Wavelengths have been chosen to emphasise the approximate pH dependence of the 4N complex (~570 nm) and the 3N1O complex (500 nm), although there is considerable overlap in peak intensities.

The affinity of the N-terminal tripeptides complex at pH 7.4 was determined using glycine as a competing ligand, as shown in Figure 6B.06. Non-chiral glycine has a known micromolar affinity for Cu^{2+} (Dawson *et al.* 1986) and the resulting $Cu(Gly)_2$ complex is CD silent. Increasing additions of free glycine to the Cu-peptides causes a reduction in the CD bands at 540 nm and 318 nm. The concentration of glycine to cause a 50 % reduction in the CD band intensity can be used to determine the apparent dissociation constant, K_d, at pH 7.4, (see Chapter 2 and experimental for details). It is clear from the binding curves that the affinity for the tripeptides is 250 nM for KKR and similarly 170 nM for MKK, compared to full-length PrP^C that has an affinity of ~30 nM for the first mole equivalent of Cu^{2+} binding to PrP^C (Nadal *et al.* 2009).

Table 6B.02 compares the affinities of Cu^{2+} binding to recombinant full-length PrP^C, and smaller recombinant and synthetic peptide fragments of PrP^C (previously determined (Nadal *et al.* 2009)) to those of the model N-terminal tripeptides studied here. Previously as many as six mole equivalents of Cu^{2+} have been shown to bind PrP^C. The tight binding mode is thought to involve all four histidine residues from the octa-repeat region (K_d of 30 nM or tighter (Walter *et al.* 2006, Wells *et al.* 2006)), along with two Cu^{2+} binding sites centered at His^{110} and His^{95} (K_d of ~30 nM) with weaker affinity (K_d of ~500 nM) for individual octa-repeat binding sites.

It was surprising that copper binding to the individual octa-repeats was weaker than that of Cu^{2+} binding to the N-terminal amino group (K_d of 150-250 nM) as binding of Cu^{2+} to the N-terminal amino group has not previously been identified (Millhauser 2004, Viles *et al.* 2008). To support this observation, I performed a simple competition experiment between a single-octa repeat and an N-terminal tripeptide. Figure 6B.07 shows the Vis-

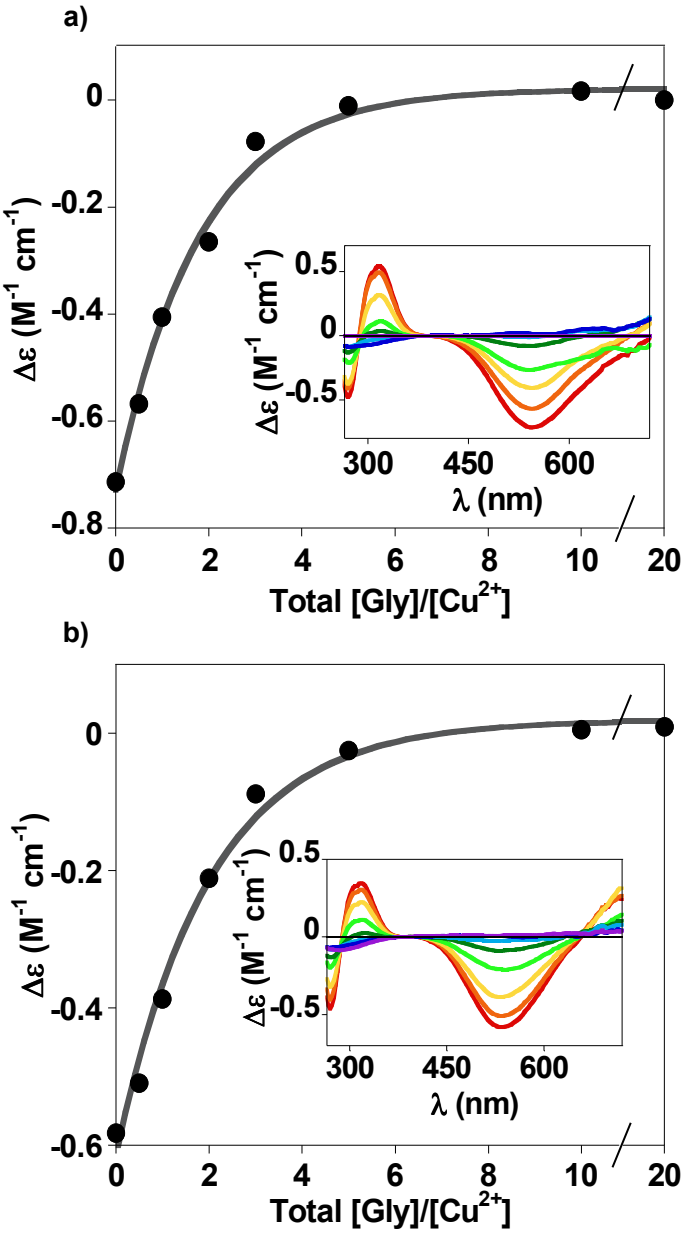

Figure 6B.06. Visible CD and Affinity of Cu^{2+} Binding to the N-Terminus of PrP^C

The glycine competition binding curve taken at 540 nm for 200 μM Cu^{2+} bound to a) 200 μM KKR, and b) 200 μM MKK at pH 7.4. Full spectra are inset for 0-20 mole equivalents glycine; red trace is no glycine and the purple trace is 20 mole equivalents. K_d calculated as 240 and 190 nM, respectively.

Table 6B.02. Comparison of Cu^{2+} Binding Affinities for Different Sites on PrP^C at pH 7.4.

PrP Fragment	K_d (nM)	PrP Fragment	K_d (nM)
NH_3(KKR)[a]	240, 260	PrP(23-231 Δocta)[b]	26
NH_3(MKK)[a]	190, 120	hPrP(91-115 H96A)[b]	45
mPrP(23-231)[b]	34	mPrP(90-114)[b]	32
mPrP(57-67)[b] (single-octa)	800, 200[c]	mPrP(57-90)[b] (multiple octas)	27[c]

[a]Determined from Vis-CD bands at 540 nm and 318 nm, respectively. [b]Adapted from (Nadal *et al.* 2009). [c]Determined using tryptophan fluorescence instead of Vis-CD.

CD spectrum of an equimolar mixture of MKK and a single octa-repeat (PrP(58-68)) with increasing amounts of Cu^{2+}. It is clear that the Cu^{2+} ions load sequentially on to the MKK tripeptides first as indicated by the initial appearance of a negative Vis-CD band at 540 nm. At one mole equivalent of Cu^{2+} ions a new set of Vis-CD bands appear, typical for the very different Vis-CD signals observed for Cu^{2+} binding to a single octa-repeat. This sequential loading is highlighted by difference spectra shown in Figure 6B.07c and 6B.07d. This data strongly supports the affinity measurements (Figure 6B.06 and Table 6B.02) indicating that for these model peptide fragments, Cu^{2+} preferentially binds to the N-terminal amino group before the single octa-repeats.

Next I performed a similar competition experiment with the intact four octa-repeats peptide, PrP(58-91), shown in Figure 6B.08. The spectra are dominated by the more intense CD bands for the individual octa-repeats (Figure 6B.08a). However, it is clear from the plot of the normalized intensity of the CD signal, Figure 6B.08b, that the Cu^{2+}

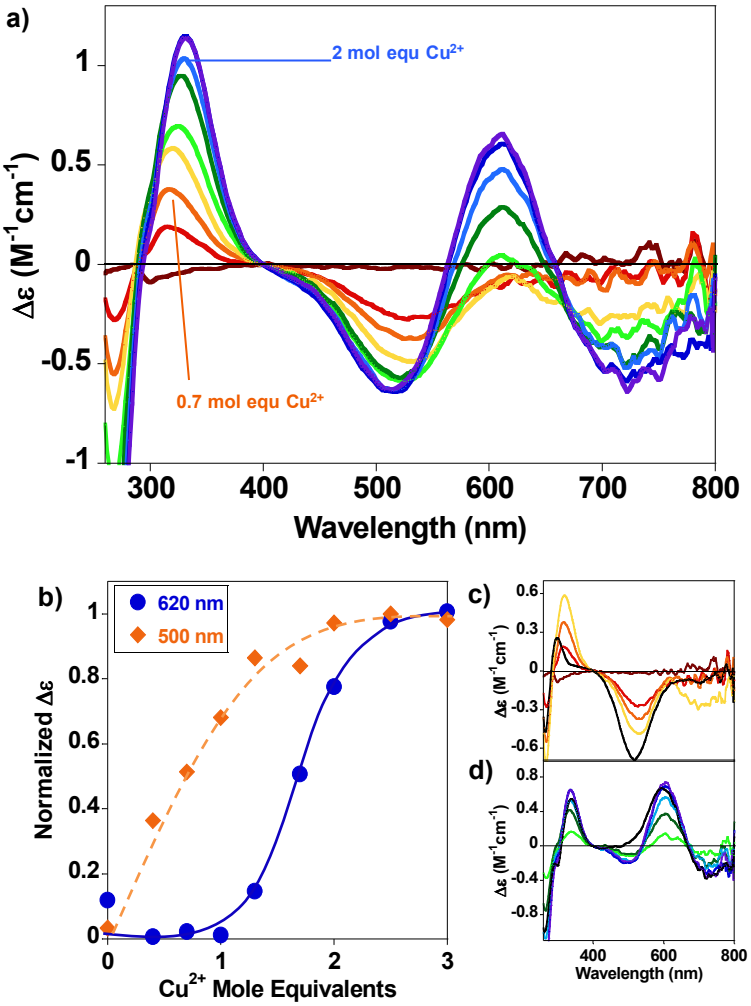

Figure 6B.07. Visible CD Competition of Cu^{2+} for MKK and an Individual Octa-Repeat

a) 100 μM MKK and 100 μM single octa-repeat plus Cu^{2+} in 30 μM steps at pH 7.4 (red through to purple). b) Normalised intensity of the bands at 620 nm and 500 nm with increasing Cu^{2+}. c) The data presented in a) for 0-1 mole equivalent of Cu^{2+} (red through to yellow) and 1 mole equivalent of Cu^{2+} bound to MKK (black). d) The data presented in a) for the following two equivalents with the spectrum from the first equivalent subtracted (light green through to purple) and 1 mole equivalent of Cu^{2+} bound to a single octa-repeat (black). Cu^{2+} preferentially binds to MKK over the single octa-repeats.

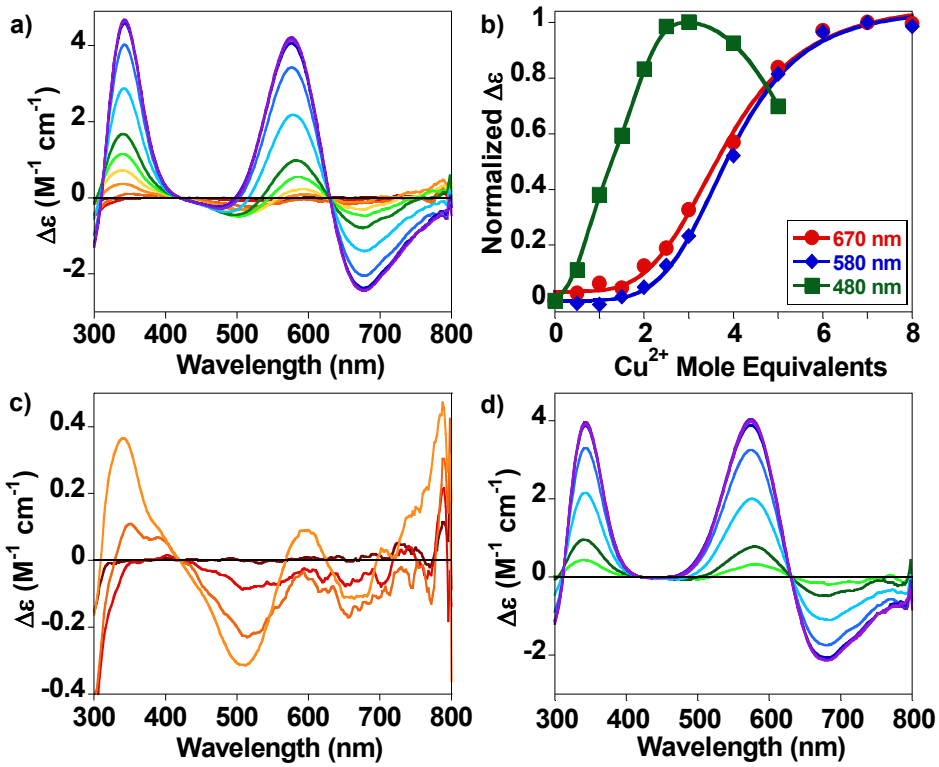

Figure 6B.08. Visible CD Competition of Cu^{2+} for MKK and PrP(58-91)

a) 100 μM MKK and 100 μM PrP(58-91) plus Cu^{2+} in 50 μM steps at pH 7.4 (red through to purple). b) Normalised intensity of the bands at 480, 580 and 670 nm with increasing Cu^{2+}. c) The data presented in a) for 0-1.5 mole equivalents of Cu^{2+} (red to orange), highlighting the MKK contribution. d) Difference spectra of the data presented in a) for 2.5-8 mole equivalents of Cu^{2+} (light green to purple), with the spectrum from the second equivalent subtracted from the subsequent spectra. The signal from MKK is not observed in the difference spectra.

loads onto MKK (480 nm signal) before the individual octa-repeats (CD bands at 580 and 670 nm). The MKK band saturates at ~ 2 mole equivalents due to Cu^{2+} ions also forming the tighter affinity tetra-histidine complex, which is Vis-CD silent. The bands at 580 nm and 670 nm, typical of Cu^{2+} ions binding to a single octa-repeat, saturate at ~5 mole equivalents as one Cu^{2+} ion binds each of the four octa-repeats.

The wavelength of the Vis-CD signal for the N-terminal amino group binding in these competition experiments does not precisely match the CD spectra for the MKK tri-peptide alone with a negative peak centred at 540 nm. This is because the single octa-repeats have positive CD signal at wavelengths above 540 nm, which has the effect of cancelling out the negative N-terminal CD signal to the longer wavelengths and so shifts the negative CD band to shorter wavelengths (~480 nm). This effect is apparent in Figures 6B.07a, 6B.08a and 6B.09b, and also the simulated data in Figure 6B.09d.

Finally, I wanted to determine if there was evidence for Cu^{2+} binding to the N-terminal amino group preferentially over the individual octa-repeats within full-length PrP^{C}(23-231). Figure 6B.09 shows Vis-CD spectra of Cu^{2+} binding full-length mouse PrP^{C}(23-231) adapted from data previously published (Klewpatinond *et al.* 2008). The general appearance of the series of spectra is rather complicated due to the multiple binding modes of Cu^{2+}, as shown in Figure 6B.10. However, when the spectrum of the first two equivalents of Cu^{2+} addition (Figure 6B.09a) are subtracted from subsequent spectra (Figure 6B.09b) a clearer picture of Cu^{2+} binding sites sequentially loading on to PrP^{C} is apparent. In previous studies the significance of the relatively weak negative CD band centered at ~470 nm was overlooked. Re-visiting this data, it is clear that this Vis-CD band is due to Cu^{2+} binding at the N-terminal amino group**.** Figures 6B.09c and 6B.09d show how binding of Cu^{2+} to individual sites using small peptide fragments contributes

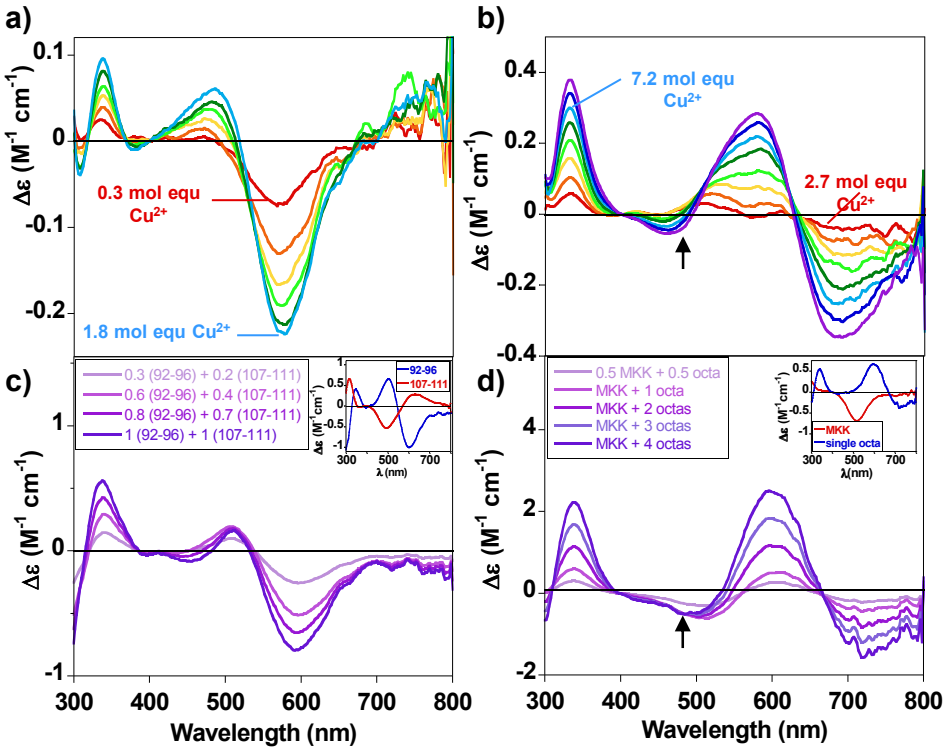

Figure 6B.09. Visible CD of Cu^{2+} Bound to Full-Length PrP^{C}(23-231)

a) Cu^{2+} titration into PrP(23-231) in 0.3 mole equivalents up to two mole equivalents. b) 2-9 mole equivalents of Cu^{2+} bound to PrP(23-231) with the first 2 mole equivalents subtracted. c) Simulated Vis-CD spectra of the titration of the first two mole equivalents of Cu^{2+} into PrP(23-231) from individual spectra of PrP(107-111) and PrP(92-96) (inset). d) Simulated Vis-CD spectra of the subsequent titration of Cu^{2+} into PrP(23-231) after the first two mole equivalents from individual spectra of MKK plus four single octa-repeats (inset). The arrow indicates the signal assigned to binding at the N-terminal amino group; there is a shift from 540 nm for MKK signal to 480 nm due to overlap with the octa-repeat signal. Panel a) and b) are taken from data previously published (Klewpatinond *et al.* 2008).

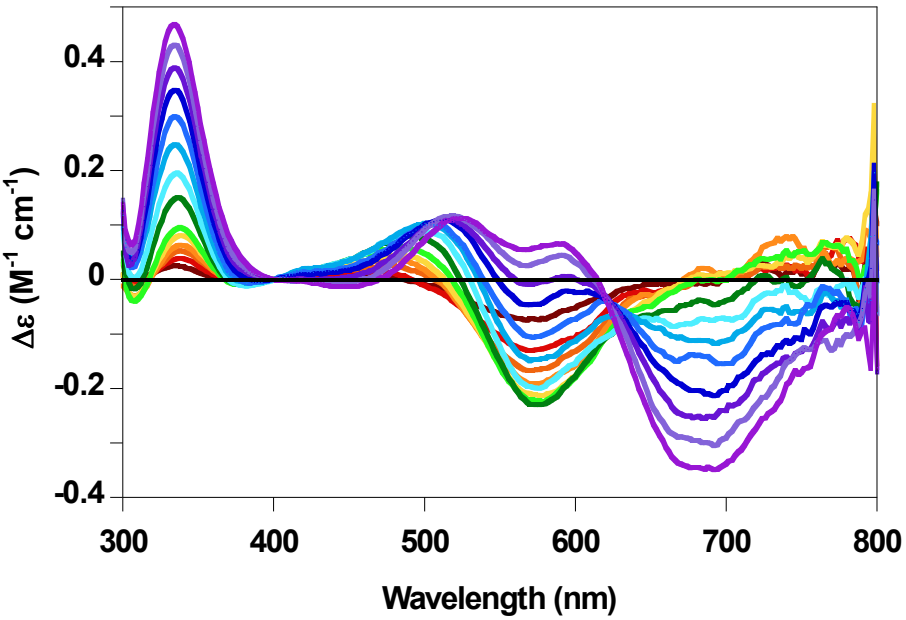

Figure 6B.10. Visible CD of Cu^{2+} Titration of PrP(23-231)

Addition of 0 -9 mole equivalents of Cu^{2+} to 100 μM mouse PrP^{C}(23-231). This data is shown in Figure 6B.08b with the spectrum of the first two equivalents of Cu^{2+} subtracted from subsequent spectra.

almost precisely to the appearance of the Vis-CD for the full-length protein. With Cu^{2+} binding centered at His^{95} and His^{110} (Figure 6B.09a,c) followed by binding at the N-terminal amino group and individual octa- repeats (Figure 6B.09b,d). Note that the tighter binding for the multiple octa-repeats (K_d of 27 nM) is not observed in Vis-CD as it does not give a signal because there is no coordination to the chiral main-chain. The sequential loading agrees with the affinities calculated, shown in Table 6B.02. In full-length PrP^C(23-231) it is clear that binding at the N- terminal amino group has a similar or tighter affinity to binding at the individual octa-repeats.

6B.5. BIOLOGICAL SIGNIFICANCE

PrP^C is responsible for generating a range of TSEs in humans, cattle and sheep and is linked with Cu^{2+} ion imbalance (Siggs *et al.* 2012). The presence of Cu^{2+} is associated with scrapie prion isolates and strains of prion disease (Wadsworth *et al.* 1999) and Cu^{2+} destabilizes the native fold of PrP^C (Younan *et al.* 2011). Furthermore, Cu^{2+} binds to PrP^C *in vivo* at the synapse (Brown *et al.* 1997) and can trigger PrP^C endocytosis (Perera *et al.* 2001). The concentration of Cu^{2+} can reach as high as 15-250 μM at the synapse after neuronal depolarization (Brown *et al.* 1997, Kardos *et al.* 1989); consequently nanomolar affinity is tight enough for binding to occur *in vivo*. The binding modes of Cu^{2+} to PrP^C via multiple histidines, rather than individual histidines within the octa-repeats (Walter *et al.* 2006, Wells *et al.* 2006), or within the amyloidogenic region (His^{95} and His^{110}) have a considerably tighter affinity than the N-terminal amino group. The binding of Cu^{2+} at the N-terminal amino group of PrP^C is not a novel coordination mode as most proteins could bind Cu^{2+} in this way with similar ~ 200 nM affinities. The principle Cu^{2+} binding site of Aβ and αSyn involve the N-terminal amino group but with a thousand times tighter affinity, with a K_d of 50 pM (Sarell *et al.* 2009) and 200 pM (Hong *et al.* 2009), respectively. These tighter affinities are due to the additional involvement of side-chain

coordination. This raises the question, whether *in vivo,* loading of Cu^{2+} to the relatively weak individual octa-repeat binding sites is physiologically significant. However, PrP^{C} is marked by its well conserved natively unstructured domain of ~100 residues that is capable of binding multiple Cu^{2+} ions. Transient high occupancy of these binding sites should not be ruled out during fluxes of Cu^{2+} ions in the micro-environment of the synaptic cleft.

CHAPTER 6: PART C

COMPARISONS OF Cu^{2+} BINDING TO N-TERMINAL MODEL PEPTIDES OF ALPHA-SYNUCLEIN, USING VISIBLE CIRCULAR DICHROISM SPECTROSCOPY: AFFINITY, COORDINATION GEOMETRY, pH DEPENDENCE AND STOICHIOMETRY

6C.1. INTRODUCTION

Parkinson's disease (PD) is a neurodegenerative disease marked by the presence of Lewy bodies in the substantia nigra. These Lewy bodies are comprised of amyloid fibres of the protein alpha-synuclein (αSyn). In solution, monomeric αSyn is natively unstructured but it has the propensity to form alpha helices when bound to lipids, the crystal structure of which is shown in Figure 6C.01 (Ulmer *et al.* 2005). The sequence of αSyn can be split into three sections; the N-terminal domain, the central non-amyloid β component (NAC) domain, and the C-terminal domain. The NAC domain is a hydrophobic region spanning residues 61 to 95 that is involved in amyloid formation.

In PD increased Cu^{2+} concentrations in the cerebrospinal fluid are reported (Pall *et al.* 1987) and those with chronic exposure to copper in industry have an increased rate of PD (Gorell *et al.* 1998). Metals have been proposed as triggers for misfolding and assembly of αSyn in Parkinson's disease (PD). More than a decade ago the acceleration of the kinetics of fibrillisation of αSyn by metal ions was described (Paik *et al.* 1999, Uversky *et al.* 2001, Yamin *et al.* 2003). However, these early studies used concentrations of metal ions higher than those normally found physiologically. Significantly, subsequent studies using much lower concentrations of Cu^{2+} ions also accelerated fibre formation (Rasia *et al.* 2005). They showed that a 1:1 binding of Cu^{2+} with 100 μM of αSyn will significantly reduce the lag-time of fibrillisation. Cu^{2+} has also been shown to exacerbate toxicity of αSyn in cell cultures (Wright *et al.* 2009). αSyn is largely found intracellularly at presynaptic terminals in the reducing environment of the cytosol where copper ions are predominantly Cu^{+}. There have been some studies of Cu^{+} coordination to αSyn (Binolfi *et al.* 2010a). However, a proportion of αSyn is secreted by neuronal cells extracellularly (Borghi *et al.* 2000, Lee 2008) and so Cu^{2+} binding is also relevant. It is for these reasons

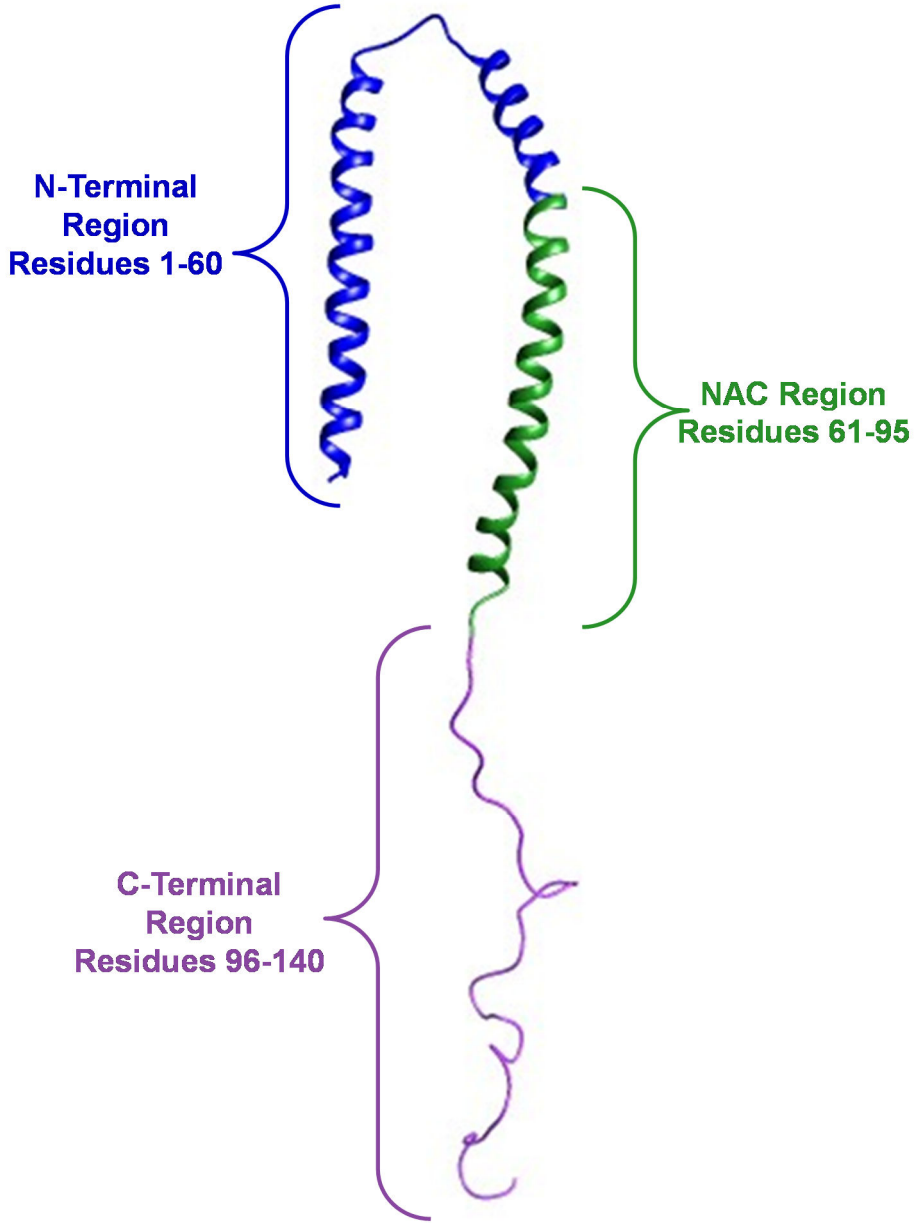

Figure 6C.01. The Crystal Structure of Alpha-Synuclein.

The structure of micelle-bound αSyn highlighting the 3 separate domains of the sequence; the N-terminal region, the non-amyloid β component (NAC) region, and the C-terminal region. The structure was created from PDB code 1XQ8 (Ulmer *et al.* 2005) using UCSF Chimera.

that much effort has been directed at characterising the coordination and affinity of Cu^{2+} binding to αSyn. For reviews see (Binolfi *et al.* 2012, Hasegawa *et al.* 2002, Viles 2012).

The coordination of Cu^{2+} and other metal ions can affect the misfolding protein in a number of possible ways. The change in charge may affect the self-association, or the morphologies (strain) of the amyloids concerned (Uversky *et al.* 2001, Wright *et al.* 2009). Furthermore, the redox activity of Cu^{2+} can lead to hydroxyl radical and other reactive oxygen species production, a hallmark of protein misfolding diseases (Davies *et al.* 2010, Meloni *et al.* 2011, Wang *et al.* 2010). The coordination geometry and affinity of the complex is therefore clearly important in understanding these processes.

The locus of binding of Cu^{2+} to αSyn has been shown to involve the N-terminal amino group (Binolfi *et al.* 2012, Drew *et al.* 2008, Kowalik-Jankowska *et al.* 2005, Rasia *et al.* 2005). Various values have been suggested for the affinity of Cu^{2+} for αSyn (Binolfi *et al.* 2010b, Davies *et al.* 2010, Dudzik *et al.* 2011, Hong *et al.* 2009) and for assorted model peptides (Binolfi *et al.* 2010b, Jackson *et al.* 2009), with K_ds ranging between ~200 nM (Jackson *et al.* 2009) and 100 pM (Dudzik *et al.* 2011). Here I use Vis-CD to directly monitor Cu^{2+} binding affinity using glycine as a competitive ligand, and compare Cu^{2+} binding to model peptides of the N-terminus to the full-length αSyn.

It has been suggested that αSyn binds Cu^{2+} ions through two different modes; solely at the N-terminal residues MDV (Figure 6C.02a) (Binolfi *et al.* 2008, Binolfi *et al.* 2010b, Kowalik-Jankowska *et al.* 2005) or alternatively, via the N-terminal residues together with imidazole of histidine at position 50 (Figure 6C.02b) (Bortolus *et al.* 2010, Drew *et al.* 2008, Dudzik *et al.* 2011, Kowalik-Jankowska *et al.* 2005). To investigate the

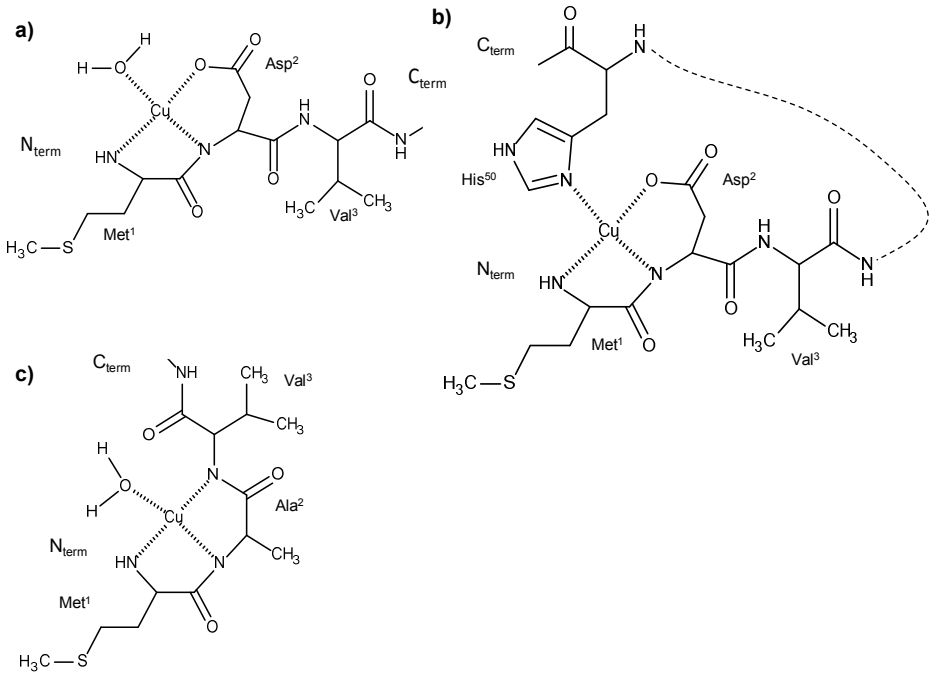

Figure 6C.02. The Square-Planar Cu^{2+} Coordination Geometries of a Variety of Peptides

The coordination geometries of a) mode 1 of Cu^{2+} binding to αSyn via MDV, b) mode 2 of Cu^{2+} binding to αSyn via MDV…H^{50}, and c) Cu^{2+} bound to MAV.

influence of His^{50} on Cu^{2+} coordination, I have designed a peptide that has the sequence of residues 1-7 and 46-52 of αSyn (MDVFMKGEGVVHGV). These complexes are compared with Cu^{2+} complexes found in other misfolding proteins.

6C.2. AIMS

Cu^{2+} binding to αSyn has been studied a good deal with Vis-CD (Binolfi *et al.* 2008, Binolfi *et al.* 2010b, Kowalik-Jankowska *et al.* 2005, Rasia *et al.* 2005) and I aim to build upon these studies. I aim to understand the influence side-chain coordination of Cu^{2+} by Asp^2 and His^{50} have on the affinity, pH dependence and appearance of the Vis-CD spectra for the N-terminal αSyn Cu^{2+} complex and resolve some of the conflicting observations regarding coordination geometry and affinity made surrounding Cu^{2+} binding to αSyn.

6C.3. EXPERIMENTAL

6C.3.1. Peptides

Fmoc chemistry was used to synthesise the various peptides used. All peptides were C-terminally amidated in order to mimic the continuation of the peptide sequence in the larger protein. The peptides were removed from the resin and de-protected before purification by reverse-phase HPLC. The samples were characterised using mass spectrometry.

Peptides with amidated C-termini and free N-terminal amino groups studied included MDV, MAV, AAA and MDVFMKGEGVVHGV, a designed sequence based on alpha synuclein residues 1-7 and 46-52, all purchased from Generon Ltd (Maidenhead, UK).The peptides did not contain aromatic residues thus concentrations were obtained via Cu^{2+} titrations with saturation at 1:1. Typically, lyophilised peptide contained 20 % moisture content.

6C.3.2. Circular Dichroism (CD)

CD spectra were recorded as described in Chapter 2.

6C.3.3. Absorbance

Visible absorption spectra were obtained with a Hitachi U-3010 double beam spectrophotometer between 400 and 800 nm, sampling points every 2 nm, using a 1 cm pathlength quartz cuvette. Typically 3 scans were recorded and the baseline spectrum subtracted from each scan.

Small aliquots of fresh aqueous solutions were used to add metal ions (Cu^{2+} as $CuCl_2.2H_2O$). Titrations were carried out in the presence of 20 mM ethylmorpholine buffer at pH 7.4. The pH was measured before and after acquiring each spectrum.

6C.3.4. Affinity Measurements

Affinity measurements were carried out as described in Chapter 2. Glycine was the competing Cu^{2+} chelator used in calculating the affinity of the Cu^{2+}-peptide complexes.

6C.4. RESULTS AND DISCUSSION

6C.4.1. Cu^{2+} Affinity of αSyn

To investigate the influence of side chain-coordination upon Cu^{2+} binding at the N-terminal amino group of αSyn, three peptides have been generated; MDV, MAV and αSyn(1-7,46-52) (MDVFMKGEGVVHGV), which include side chains thought to be involved in Cu^{2+} coordination in αSyn (Asp^2 and His^{50}). The Cu^{2+} affinity of these three αSyn-related peptides at pH 7.4 have been calculated using glycine competition experiments (Figure 6C.03, Table 6C.01). The difference in affinity for the 3 peptides is quite marked. In particular, only 1.2 mole equivalents of glycine are required to remove

half of the Cu^{2+} from MAV, whereas considerably more glycine, 8.5 mole equivalents, is required to remove Cu^{2+} from MDV, while as much as 34 mole equivalents are required to compete off half of the Cu^{2+} from the αSyn model tetradecamer peptide containing a histidine. This equates to a conditional dissociation constant (K_d), at pH 7.4 of 270 nM, 320 pM and, and 30 pM respectively. The Cu^{2+} complex that involves a histidine is tighter than the N-terminal tripeptide complex in the absence of histidine side-chain coordination. The aspartate in MDV makes binding more than two orders of magnitude tighter than MAV. MAV has an affinity more similar to that of the N-terminus of PrP at pH 7.4 (Stanyon *et al.* 2014b), see Table 6C.02. The affinity of Cu^{2+} for MDV calculated here is very similar to that reported for full-length αSyn, described by a number of groups using a range of techniques, these studies give similar results with K_ds in the 10^{-7} M range at pH 7.4 (Table 6C.01) (Davies *et al.* 2010, Dudzik *et al.* 2011, Hong *et al.* 2009). Others have reported affinities weaker than the 100 pM (Binolfi *et al.* 2010b, Jackson *et al.* 2009) but none have suggested an affinity as tight as our designed peptide containing a His residue twelve residues from the N-terminus.

Table 6C.01. Comparison of Cu^{2+} Binding Affinities for αSyn

Protein/peptide	**K_d**	**pH**	**Author**	**Method**
MDV	0.32 nM	7.4	This work	Vis-CD
MAV	270 nM	7.4	This work	Vis-CD
αSyn(1-7,46-52)	28 pM	7.4	This work	Vis-CD
αSyn	0.2 nM	7.4	(Hong *et al.* 2009)	ITC
αSyn	0.1 nM	7.4	(Dudzik *et al.* 2011)	EPR
αSyn	0.4 nM	7.0	(Davies *et al.* 2010)	ITC

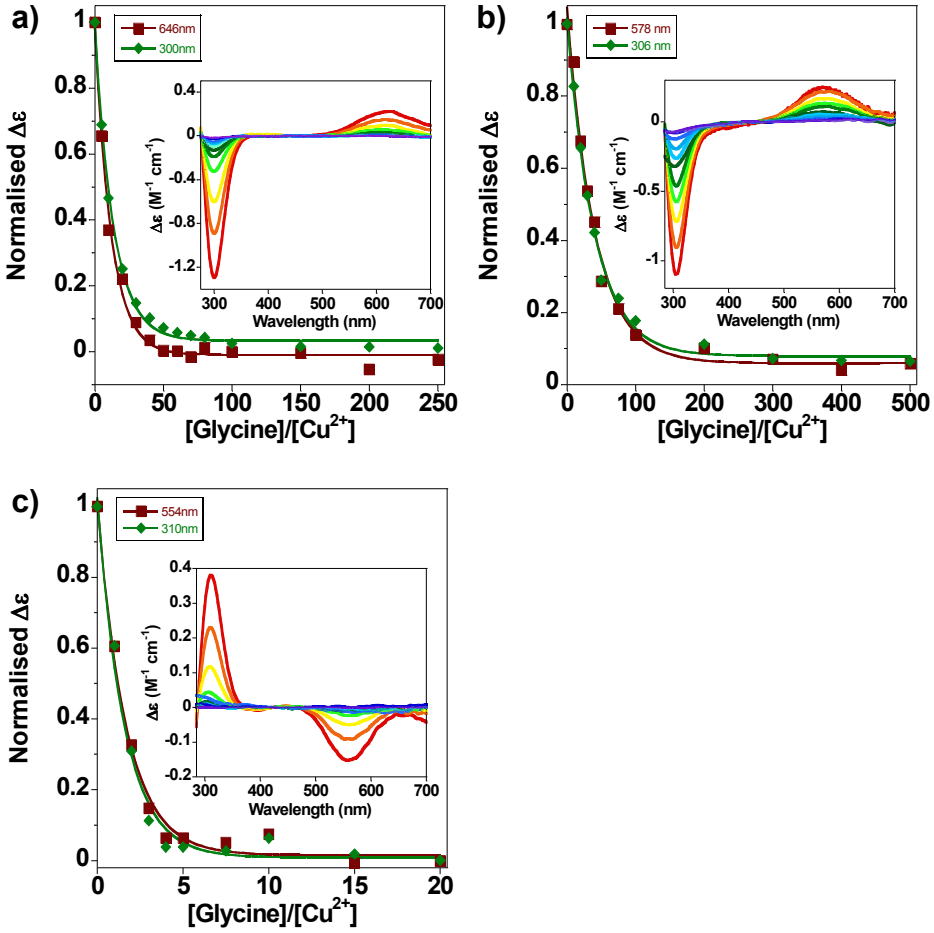

Figure 6C.03. The Affinity of Cu^{2+} Binding to Alpha-Synuclein

The glycine competition binding curves for one mole equivalent of Cu^{2+} bound to a) 500 μM MDV, b) 300 μM αSyn(1-7.46-52), and c) 500 μM MAV at pH 7.4. Full spectra are inset for 0-20 mole equivalents glycine; red trace is no glycine and the purple trace is 20 mole equivalents.

6C.4.2.Vis-CD of Cu^{2+} Coordination at the N-Terminal Residues of αSyn

It is well established that Cu^{2+} can bind to the N-terminal amino group of proteins with additional main-chain amide nitrogen coordination (Martin 1974, Stanyon *et al.* 2014a, Stanyon *et al.* 2014b)(Parts A and B of this chapter). These Cu^{2+} complexes with no side-chain coordination produce Vis-CD spectra with only negative signal for the d-d absorption bands. Comparison of these spectra with the Vis-CD spectrum of the tripeptide MDV, known to be the Cu^{2+} binding site for αSyn at the N-terminus (Drew *et al.* 2008, Dudzik *et al.* 2011, Rasia *et al.* 2005), shows a very different spectrum, producing a positive band for the d-d-transition bands (Figure 6C.04a). However, strikingly, replacing the aspartate with alanine (to give MAV) produces a very different spectrum, which is much closer in appearance to the AAA tripeptides (Figure 6C.04a). The switch in the appearance of the MDV spectrum is due to the aspartate side chain being involved in coordination (Binolfi *et al.* 2010b, Drew *et al.* 2008, Dudzik *et al.* 2011). It is clear that for complexes that involve side-chain coordination, in addition to amide main-chain coordination, very different Vis-CD spectra can be observed.

The spectrum of αSyn(1-7,46-52) is shown in Figure 6C.04b. The Vis-CD spectrum has similarities to MDV but the positive d-d transition band is shifted to a shorter wavelength, with a Vis-CD maximum at 570 nm for αSyn(1-7,46-52) while MDV has a Vis-CD maximum at 610 nm. This is thought to be due to a shift from a 2N2O coordination complex (two nitrogen and two oxygen square-planar coordination geometry) (Figure 6C.02a) to a 3N1O complex as a nitrogen from the histidine replaces a coordinating oxygen from water (Figure 6C.02b). This shift to a shorter wavelength for αSyn(1-7,46-52) is also evident in the visible absorption spectra (Figure 6C.04c), with a maximum at 630 nm for MDV and 605 nm for the tetradecamer containing histidine. The wavelength maximum shifts to a shorter wavelength with each increase in the number of peptide

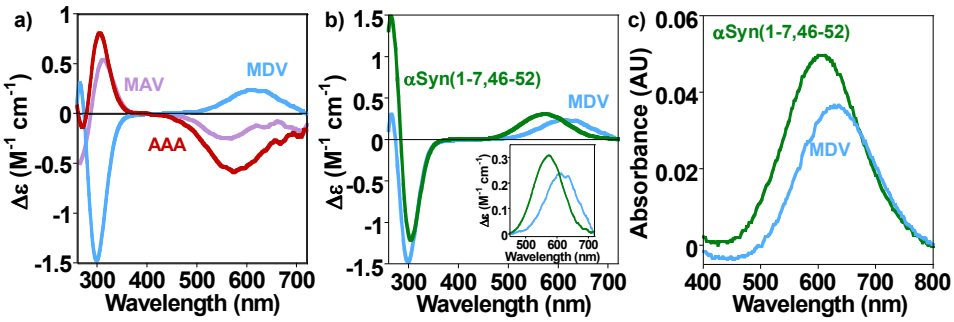

Figure 6C.04. Model Peptides of αSyn Give Very Different Spectra Due to Aspartate Side-Chain Coordination

Visible CD spectra of Cu^{2+} bound at pH 7.4 to a) MDV (light blue), MAV (light purple) and AAA (dark red), and b) αSyn(1-7,46-52) (dark blue) and MDV (light blue). Inset highlights the shift in the d-d transition band from 610 nm to 570 nm. c) The visible absorption spectra of 600 μM MDV and αSyn(1-7,46-52) binding one mole equivalent of Cu^{2+}.

nitrogens involved in forming the complex. Generally, 4N complexes have an absorbance band centred at 540 nm, 3N1O are at 625 nm, and 1N3O are at 765 nm (Bryce *et al.* 1966).

6C.4.3. Stoichiometry of Cu^{2+} Coordination

Titration of Cu^{2+} on to MDV and MAV shows a clear 1:1 stoichiometry with fixed CD bands at 612 and 555 nm, respectively, that increase in intensity until saturation at 1 mole equivalent (Figure 6C.05). In contrast, the stoichiometry of αSyn(1-7,46-52) is different with a CD band at 580 nm that increases in intensity up to one mole equivalent and then reduces to be replaced by a band at 540 nm (Figure 6C.05c**).** This is indicative of a second binding mode, the spectrum of which has been obtained by subtracting the MDV at one mole equivalent spectrum from the αSyn(1-7,46-52) spectrum at two mole equivalents (Figure 6C.06). This spectrum is similar to that of Cu^{2+} coordinated to the peptide acetyl-GAH-amide, suggesting the second binding site is centred around the His residue (Chapter 6A) (Klewpatinond *et al.* 2007a).

6C.4.4. Comparison with Full-Length αSyn

It is notable that studies for full-length αSyn report Vis-CD spectra much closer to our MDV spectrum than the spectrum of αSyn(1-7,46-52) (Binolfi *et al.* 2008, Binolfi *et al.* 2010b, Rasia *et al.* 2005). Both Vis-CD and EPR data strongly support the dominant Cu^{2+} complex as not containing His^{50} in αSyn (Binolfi *et al.* 2010b). The considerable reduction in the number of residues between the N-terminus and the His in the model peptide used here of αSyn(1-7,46-52) (twelve residues) promotes His coordination in the N-terminal complex. In the case of full-length αSyn, it remains to be established if His^{50} can participate in coordination under certain conditions, for example fibre or oligomer

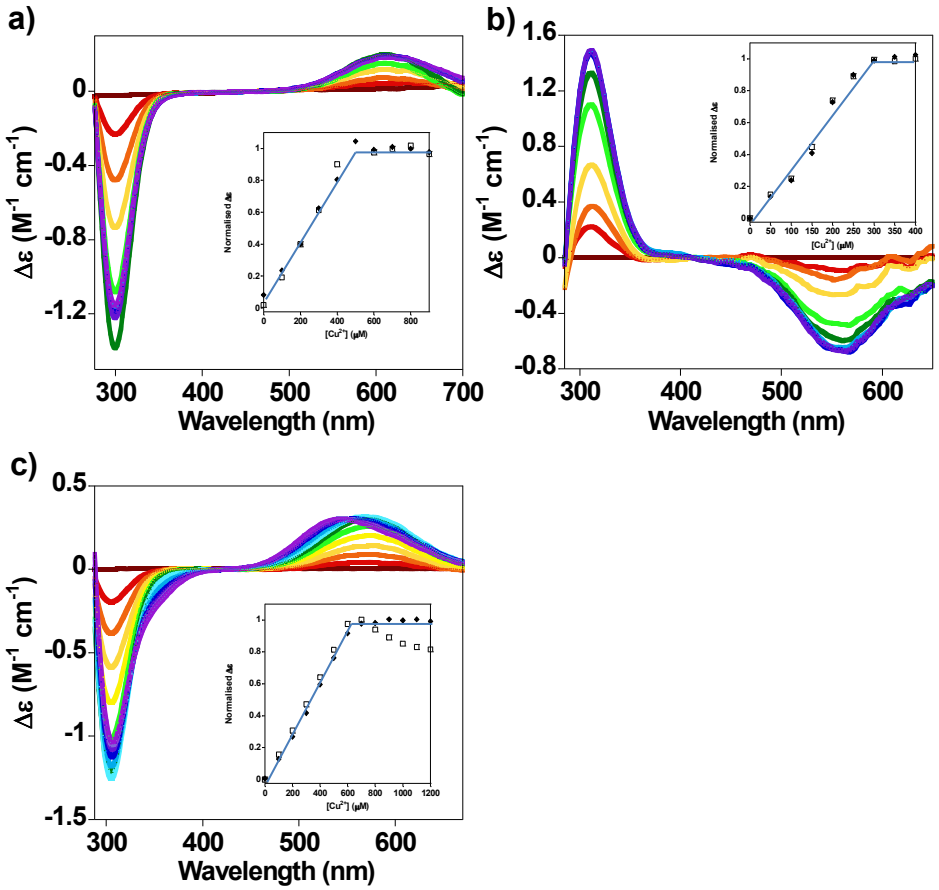

Figure 6C.05. The N-Terminal of αSyn Binds Cu^{2+} with a 1:1 Stoichiometry

Stoichiometry of copper binding at pH 7.4 to a) 500 μM MDV – inset normalised Δε from bands at 300 nm (squares) and 612 nm (diamonds) , b) 300 μM MAV – inset normalised Δε from bands at 312 nm (squares) and 555 nm (diamonds), and c) 600 μM αSyn(1-7,46-52) – inset normalised Δε from bands at 304 nm (squares) and 550 nm (diamonds).

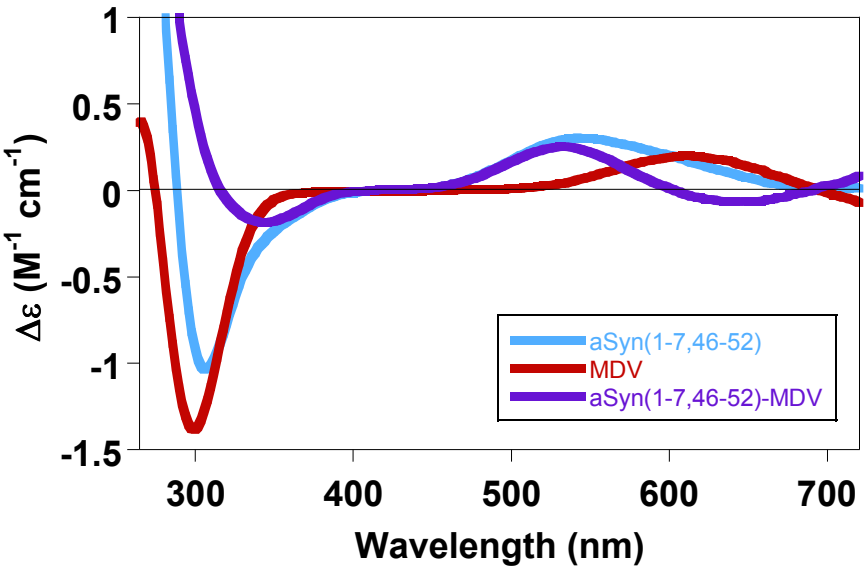

Figure 6C.06. Difference Spectrum of αSyn(1-7,46-52) and MDV

The spectrum of MDV (red) subtracted from αSyn(1-7,46-52) (blue) gives the contribution of Histidine side-chain coordination in the αSyn(1-7,46-52) complex.

formation at lower pH or in the presence of cryoprotectants, such as glycerol, used in low temperature EPR measurements. It is notable that Bortolus *et al.* described His^{50} involvement at pH 6.5 (Bortolus *et al.* 2010). While Drew points to a mixture of both coordination geometries, their relative proportions are likely to be pH sensitive (Drew *et al.* 2008).

6C.4.5. pH Dependence of Cu^{2+} Binding

The pH dependence of Cu^{2+} binding to the 3 different αSyn model peptides (Figure 6C.07a-c) shows that αSyn(1-7,46-52) coordination with a 3N1O geometry remains dominant from basic conditions to as low as pH 5 (Figure 6C.07a). Similarly, the 2N2O complex of MDV remains very stable over a range of pHs, with no indication of a shift to other coordination geometries with an increase in pH (Figure 6C.07b). The mid-point of Cu^{2+} complex formation occurs at a relatively low pH of 4.6 for MDV (Fig 6C.07b). The pH dependence of the MDV complex agrees closely with studies by Binolfi *et al.* on the first six residues of αSyn (MDVFMK) that also showed a pK_a of 4.6 (Binolfi *et al.* 2010b). It is clear that the Asp has a significantly stabilising influence in the complex even at a relatively low pH. In contrast, for MAV, the Vis-CD suggests complete loss of amide Cu^{2+} coordination complex below pH 7, with a mid-point at pH 7.5, compared to pH 4.6 for MDV (Figure 6C.07c). This type of pH dependence for MAV is similar to the tripeptide AAA, shown in Figure 6C.07d.

6C.5. COMPARISONS OF Cu^{2+} BINDING α–SYNUCLEIN WITH OTHER AMYLOIDOGENIC PROTEINS

A common feature of the amyloid forming proteins Aβ, αSyn and PrP^C is that they are natively unfolded, either partially or in their entirety. This facilitates Cu^{2+} coordination via the main-chain. The ability of αSyn, Aβ (Sarell *et al.* 2009) and to a lesser extent PrP^C

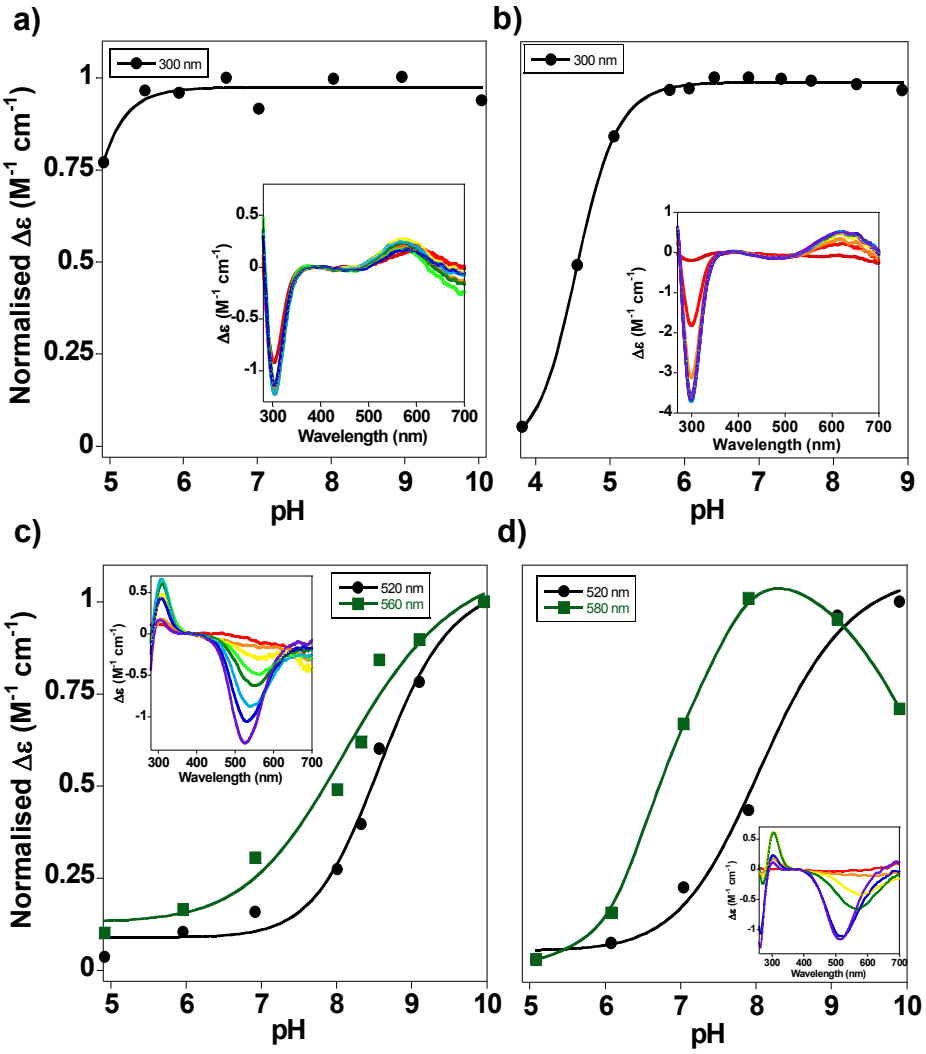

Figure 6C.07. Comparison of the pH Dependence of Cu^{2+} Binding αSyn(1-7,46-52), MDV, MAV, and AAA

The normalised peak intensities of bands corresponding to Visible CD spectra (inset) for one mole equivalent of Cu^{2+} binding to 100 μM a) αSyn(1-7,46-52), b) MDV, c) MAV, and d) AAA at increasing pH.

(Stanyon *et al.* 2014b) to bind Cu^{2+} at the N-terminus is a common feature among the three amyloidogenic proteins. However, the affinity of Cu^{2+} for these proteins is quite different (Sarell *et al.* 2009, Stanyon *et al.* 2014b). The N-terminal of PrP^C has an affinity much weaker than αSyn and Aβ (See Table 6C.02) yet is comparable to the affinity of Cu^{2+} for MAV. The coordination of Cu^{2+} binding to these sites occurs solely through main-chain amides. αSyn and Aβ have appreciably greater affinities for Cu^{2+} binding directly at the N-terminus, at neutral pH, due to the involvement of additional side-chain coordination; Asp^2 in the case of αSyn (Binolfi *et al.* 2012) and $His^{6,13,14}$ as well as carboxylates in the case of Aβ (Drew *et al.* 2009, Sarell *et al.* 2009). The affinity of Cu^{2+} for αSyn is approximately an order of magnitude weaker compared to Aβ yet as the concentration of Cu^{2+} can reach as high as 15-250 μM at the synapse after neuronal depolarisation, this affinity is still strong enough for binding to occur *in vivo* (Brown *et al.* 1997, Kardos *et al.* 1989). The tight affinity of Cu^{2+} for the designed peptide is very similar to that of Cu^{2+} binding to Aβ, which also coordinates via Asp and His and the N-terminus. The question remains as to whether under certain conditions, such as fibrillisation, oligomerisation or low pH, a larger macro-chelate is favoured in αSyn similar to that described here using the designed peptide.

Table 6C.02. Comparison of Cu^{2+} Binding Affinities of Amyloid Proteins that Involve the N-Terminal Amino Group

αSyn Model Peptide	**K_d at pH 7.4 (This Work)**	**Protein**	**K_d at pH 7.4**	**Author**
αSyn(1-7,46-52)	28 pM	Aβ	50 pM	(Sarell *et al.* 2009)
MDV	0.32 nM	αSyn	0.2 nM	(Hong *et al.* 2009)
MAV	270 nM	PrP^C	250 nM	Chapter 6B

CHAPTER SEVEN:

CONCLUSION

Amyloid beta (Aβ) is the main constituent of extracellular plaques in the brain of Alzheimer's disease (AD) patients. The fibrillisation of Aβ is central to the development of AD. It is known that the majority of Aβ found in blood plasma is bound to human serum albumin (Biere *et al.* 1996, Kuo *et al.* 2000). The high levels of albumin found in blood plasma are thought to be the explanation for why amyloid plaques do not occur in the peripheral tissue despite Aβ levels in blood being similar to the levels in the brain interstitium. The main risk factor for developing AD is age and it is also known that albumin concentrations decrease with age (Klonoff-Cohen *et al.* 1992). The key aim of this thesis was to understand the role albumin plays in Aβ fibrillisation at physiological concentrations and in the presence of other extracellular components.

I have shown in this thesis that HSA can inhibit Aβ fibrillisation at concentrations as low as those found in the cerebrospinal fluid (3 μM). The extent of inhibition closely correlates with the percentage of Aβ monomer that can bind to albumin based on the published modest K_d of 5 μM (Rózga *et al.* 2007a). This work raises the possibility that albumin may be protective against the development of AD and *in vivo* studies to test this in the future are important. Albumin is less able to inhibit Aβ fibrillisation in the presence of other molecules that bind the hydrophobic pockets of albumin. In this thesis, I have demonstrated this for cholesterol and palmitic acid. Interestingly, both elevated levels of serum cholesterol and a high fat diet increase the risk of developing AD (Kalmijn *et al.* 1997, Kivipelto *et al.* 2002, Kivipelto *et al.* 2001, Laitinen *et al.* 2006, Morris *et al.* 2003, Whitmer *et al.* 2005). This raises the possibility that this elevated risk may therefore be due to the interaction with albumin, preventing Aβ from binding to albumin and inhibiting fibrillisation. The fact that albumin replacement is showing promise as a treatment for

AD (Boada *et al.* 2009) may be through clearance of fatty acid or cholesterol loaded albumin in addition to clearance of the Aβ-albumin complex.

Albumin levels are known to decrease with age but there has been no connection reported between albumin levels and the susceptibility of developing AD. With the current development of big data science, the association may become apparent in the near future as vast patient databases can be analysed. It may also be possible to establish whether the use of certain pharmaceuticals in the treatment of other disease also increase the risk of developing AD, such as prolonged use of the anti-coagulant warfarin, a drug that binds a hydrophobic pocket of albumin.

Albumin is not just a transport protein for hydrophobic molecules but also binds Cu^{2+} ions at its N-terminus with a one picomolar affinity (Rózga *et al.* 2007b). Disruption of Cu^{2+} homeostasis has been linked to the development of AD in several animal models (Sanokawa-Akakura *et al.* 2010, Sparks *et al.* 2003). Cu^{2+} binding to Aβ *in vitro* has been shown to influence the fibrillisation of Aβ (Matheou *et al.* 2014, Sarell *et al.* 2010). The determination of the affinity of Cu^{2+} for Aβ is therefore important in ascertaining whether this interaction is physiologically relevant and whether albumin can sequester Cu^{2+} from Aβ.

In this thesis, I have shown that the affinity of Aβ for Cu^{2+} is in the 10-20 pM range. The affinity is not influenced by peptide length nor fibrillisation state; oligomeric Aβ(1-42) has an affinity in the same range as monomeric Aβ(1-42) and Aβ(1-40). This is a very tight affinity, making an interaction between Aβ and Cu^{2+} *in vivo* extremely likely. This is especially true when considering at the synapse, the major release site of Aβ, the

concentration of Cu^{2+} can reach 15-250 μM after depolarisation (Hartter *et al.* 1988, Kardos *et al.* 1989). However, the affinity of the Aβ-Cu^{2+} complex is weaker than the affinity of Cu^{2+} for albumin and I have demonstrated that albumin can sequester Cu^{2+} from all Aβ alloforms and fibrillisation states. This ability gives albumin a second potential protective mechanism against Aβ toxicity.

Cu^{2+} dyshomeostasis is linked to several other neurodegenerative diseases in addition to AD, including Parkinson's disease and prion diseases, such as Creutzfeld-Jacob disease (Gorell *et al.* 1998, Siggs *et al.* 2012). In this thesis I have determined the affinity of Cu^{2+} for the amyloids associated with these diseases, alpha-synuclein (αSyn) and the cellular prion protein (PrP^C), respectively. The affinities are weaker than the Aβ-Cu^{2+} complex but are still physiologically relevant. αSyn binds a single Cu^{2+} ion at its N-terminal with a K_d in the 10^{-10} M range whereas PrP^C can bind up to seven Cu^{2+} ions with affinities in the nanomolar range. This raises the possibility that albumin could be protective against other neurodegenerative diseases as well by sequestering Cu^{2+} from all amyloid proteins involved.

This thesis highlights the importance of overlapping interactions with endogenous proteins and molecules in the development of neurodegenerative disease. I focus on the interaction of Aβ with common, abundant extracellular components, specifically albumin and Cu^{2+} ions. Future *in vitro* studies of neurodegenerative disease must take into account the complex nature of interactions that occur *in vivo* to be physiologically relevant. The synapse has a multitude of molecules that can interact as visualised in Figure 6.01. Not only can Aβ interact with albumin and Cu^{2+} but also PrP^C. Indeed the toxicity of Aβ is dependent on interactions with Cu^{2+}, PrP^C and N-methyl-D aspartate receptors, demonstrating a link between neurodegenerative diseases.

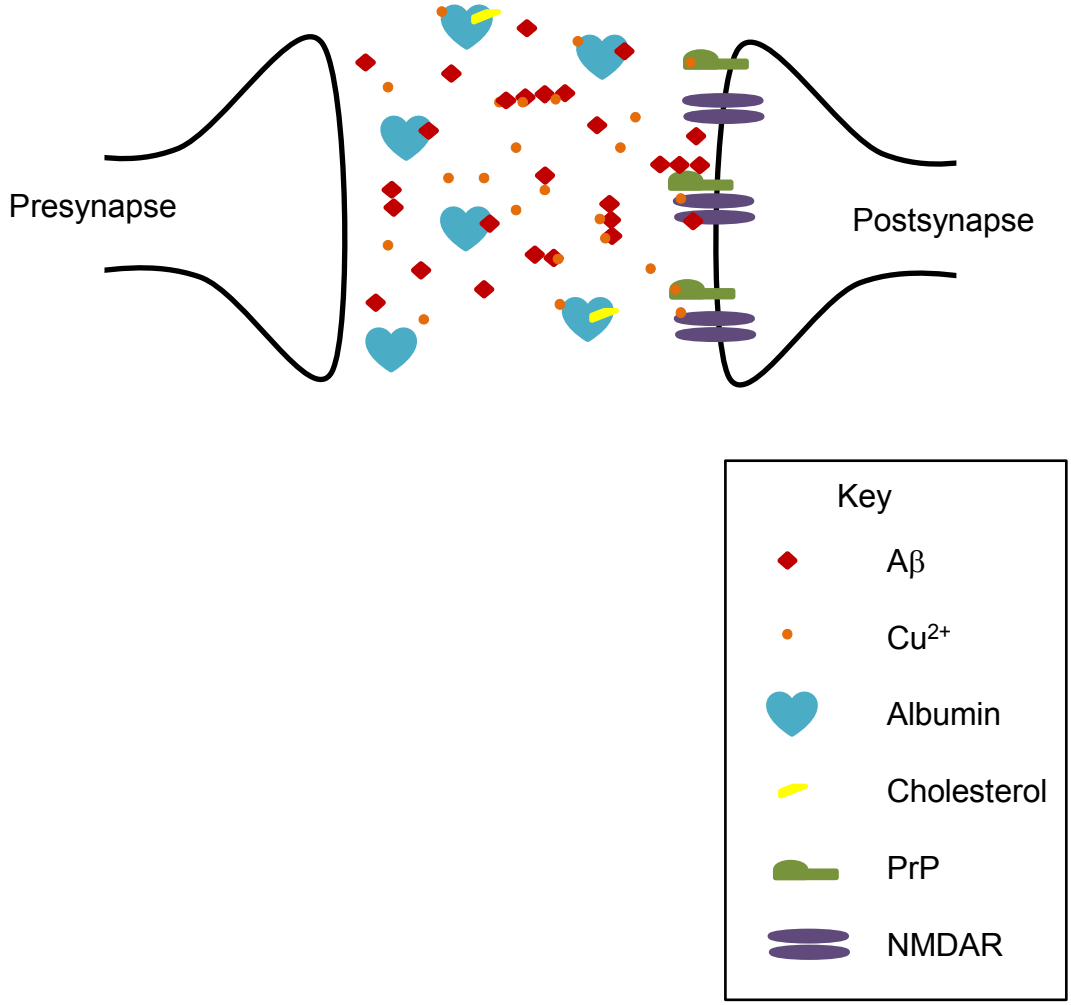

Figure 7.01. Interactions at the Synapse Between Components That Can Influence AD Development

REFERENCES

Alberdi, E., Sánchez-Gómez, M. V., Cavaliere, F., Pérez-Samartín, A., Zugaza, J. L., Trullas, R., ... Matute, C. (2010). "Amyloid β Oligomers Induce Ca^{2+} Dysregulation and Neuronal Death through Activation of Ionotropic Glutamate Receptors." *Cell Calcium* **47**(3): 264-272.

Algamal, M., Milojevic, J., Jafari, N., Zhang, W. and Melacini, G. (2013). "Mapping the Interactions between the Alzheimer's Aβ-Peptide and Human Serum Albumin Beyond Domain Resolution." *Biophysical Journal* **105**(7): 1700-1709.

Alzheimer's Disease International (2009). "World Alzheimer Report 2009: The Global Prevalence of Dementia."

Alzheimer's Society (2014). Dementia UK: Second Edition.

Alzheimer, A. (1907). "Ueber Eine Eigenartige Erkrankung Der Hirnrinde." *Allgemeine Zeitschrift für Psychiatrie und Psychisch-Gerichtliche Medizin* **64**: 146-148.

Andrea, T. A., Cavalieri, R. R., Goldfine, I. D. and Jorgensen, E. C. (1980). "Binding of Thyroid Hormones and Analogs to the Human Plasma Protein Prealbumin." *Biochemistry* **19**(1): 55-63.

Andreetto, E., Yan, L.-M., Tatarek-Nossol, M., Velkova, A., Frank, R. and Kapurniotu, A. (2010). "Identification of Hot Regions of the Aβ–IAPP Interaction Interface as High-Affinity Binding Sites in Both Cross- and Self-Association." *Angewandte Chemie International Edition* **49**(17): 3081-3085.

Antzutkin, O. N. (2004). "Amyloidosis of Alzheimer's Aβ Peptides: Solid-State Nuclear Magnetic Resonance, Electron Paramagnetic Resonance, Transmission Electron Microscopy, Scanning Transmission Electron Microscopy and Atomic Force Microscopy Studies." *Magnetic Resonance in Chemistry* **42**(2): 231-246.

Antzutkin, O. N., Leapman, R. D., Balbach, J. J. and Tycko, R. (2002). "Supramolecular Structural Constraints on Alzheimer's β-Amyloid Fibrils from Electron Microscopy and Solid-State Nuclear Magnetic Resonance." *Biochemistry* **41**(51): 15436-15450.

Arispe, N., Diaz, J. C. and Simakova, O. (2007). "Abeta Ion Channels. Prospects for Treating Alzheimer's Disease with Abeta Channel Blockers." *Biochimica et Biophysica Acta* **1768**(8): 1952-1965.

Arispe, N., Pollard, H. B. and Rojas, E. (1993). "Giant Multilevel Cation Channels Formed by Alzheimer Disease Amyloid Beta-Protein [AβP-(1-40)] in Bilayer Membranes." *Proceedings of the National Academy of Sciences* **90**(22): 10573-10577.

Ashbrook, J. D., Spector, A. A., Santos, E. C. and Fletcher, J. (1975). "Long Chain Fatty Acid Binding to Human Plasma Albumin." *Journal of Biological Chemistry* **250**(6): 2333-2338.

Atwood, C. S., Scarpa, R. C., Huang, X., Moir, R. D., Jones, W. D., Fairlie, D. P., ... Bush, A. I. (2000). "Characterization of Copper Interactions with Alzheimer Amyloid β Peptides." *Journal of Neurochemistry* **75**(3): 1219-1233.

Autschbach, J. (2009). "Computing Chiroptical Properties with First-Principles Theoretical Methods: Background and Illustrative Examples." *Chirality* **21**(1E): E116-E152.

Bal, W., Jeżowska-Bojczuk, M. and Kasprzak, K. S. (1997). "Binding of Nickel(II) and Copper(II) to the N-Terminal Sequence of Human Protamine HP2." *Chemical Research in Toxicology* **10**(8): 906-914.

Balbach, J. J., Petkova, A. T., Oyler, N. A., Antzutkin, O. N., Gordon, D. J., Meredith, S. C. and Tycko, R. (2002). "Supramolecular Structure in Full-Length Alzheimer's β-Amyloid Fibrils: Evidence for a Parallel β-Sheet Organization from Solid-State Nuclear Magnetic Resonance." *Biophysical Journal* **83**(2): 1205-1216.

Balducci, C., Beeg, M., Stravalaci, M., Bastone, A., Sclip, A., Biasini, E., ... Forloni, G. (2010). "Synthetic Amyloid-Beta Oligomers Impair Long-Term Memory Independently of Cellular Prion Protein." *Proceedings of the National Academy of Sciences* **107**(5): 2295-2300.

Barrow, C. J., Yasuda, A., Kenny, P. T. and Zagorski, M. G. (1992). "Solution Conformations and Aggregational Properties of Synthetic Amyloid Beta-Peptides of Alzheimer's Disease. Analysis of Circular Dichroism Spectra." *Journal of Molecular Biology* **225**(4): 1075-1093.

Bauernschmitt, R. and Ahlrichs, R. (1996). "Treatment of Electronic Excitations within the Adiabatic Approximation of Time Dependent Density Functional Theory." *Chemical Physics Letters* **256**(4-5): 454-464.

Benilova, I., Karran, E. and De Strooper, B. (2012). "The Toxic Aβ Oligomer and Alzheimer's Disease: An Emperor in Need of Clothes." *Nature Neuroscience* **15**(3): 349-357.

Benzinger, T. L., Gregory, D. M., Burkoth, T. S., Miller-Auer, H., Lynn, D. G., Botto, R. E. and Meredith, S. C. (1998). "Propagating Structure of Alzheimer's β-Amyloid (10–35) Is Parallel β-Sheet with Residues in Exact Register." *Proceedings of the National Academy of Sciences* **95**(23): 13407-13412.

Berti, F., Gaggelli, E., Guerrini, R., Janicka, A., Kozlowski, H., Legowska, A., ... Valensin, G. (2007). "Structural and Dynamic Characterization of Copper(II) Binding of the Human Prion Protein Outside the Octarepeat Region." *Chemistry – A European Journal* **13**(7): 1991-2001.

Bhattacharya, A. A., Grüne, T. and Curry, S. (2000). "Crystallographic Analysis Reveals Common Modes of Binding of Medium and Long-Chain Fatty Acids to Human Serum Albumin." *Journal of Molecular Biology* **303**(5): 721-732.

Biere, A. L., Ostaszewski, B., Stimson, E. R., Hyman, B. T., Maggio, J. E. and Selkoe, D. J. (1996). "Amyloid β-Peptide Is Transported on Lipoproteins and Albumin in Human Plasma." *Journal of Biological Chemistry* **271**(51): 32916-32922.

Biessels, G. J., Staekenborg, S., Brunner, E., Brayne, C. and Scheltens, P. (2006). "Risk of Dementia in Diabetes Mellitus: A Systematic Review." *The Lancet Neurology* **5**(1): 64-74.

Binolfi, A., Quintanar, L., Bertoncini, C. W., Griesinger, C. and Fernández, C. O. (2012). "Bioinorganic Chemistry of Copper Coordination to Alpha-Synuclein: Relevance to Parkinson's Disease." *Coordination Chemistry Reviews* **256**(19–20): 2188-2201.

Binolfi, A., Valiente-Gabioud, A. A., Duran, R., Zweckstetter, M., Griesinger, C. and Fernandez, C. O. (2010a). "Exploring the Structural Details of Cu(I) Binding to Alpha-Synuclein by NMR Spectroscopy." *Journal of the American Chemical Society* **133**(2): 194-196.

Binolfi, A. S., Lamberto, G. R., Duran, R., Quintanar, L., Bertoncini, C. W., Souza, J. M., ... Fernández, C. O. (2008). "Site-Specific Interactions of Cu(II) with α and β-Synuclein: Bridging the Molecular Gap between Metal Binding and Aggregation." *Journal of the American Chemical Society* **130**(35): 11801-11812.

Binolfi, A. S., Rodriguez, E. E., Valensin, D., D'amelio, N., Ippoliti, E., Obal, G., ... Fernández, C. O. (2010b). "Bioinorganic Chemistry of Parkinson's Disease: Structural Determinants for the Copper-Mediated Amyloid Formation of Alpha-Synuclein." *Inorganic Chemistry* **49**(22): 10668-10679.

Boada, M., Ortiz, P., Anaya, F., Hernandez, I., Muñoz, J., Núñez, L., ... Tarraga, L. (2009). "Amyloid-Targeted Therapeutics in Alzheimer's Disease: Use of Human Albumin in Plasma Exchange as a Novel Approach for Aβ Mobilization." *Drug News & Perspectives* **22**(6): 325-339.

Bobek, L. A. and Levine, M. J. (1992). "Cystatins—Inhibitors of Cysteine Proteinases." *Critical Reviews in Oral Biology & Medicine* **3**(4): 307-332.

Bohrmann, B., Tjernberg, L., Kuner, P., Poli, S., Levet-Trafit, B., Näslund, J., ... Nordstedt, C. (1999). "Endogenous Proteins Controlling Amyloid β-Peptide Polymerization. Possible Implcations for β-Amyloid Foramtion in the Central Nervous System and in Peripheral Tissues." *Journal of Biological Chemistry* **274**(23): 15990-15995.

Borghi, R., Marchese, R., Negro, A., Marinelli, L., Forloni, G., Zaccheo, D., ... Tabaton, M. (2000). "Full Length Alpha-Synuclein Is Present in Cerebrospinal Fluid from Parkinson's Disease and Normal Subjects." *Neuroscience Letters* **287**(1): 65-67.

Bortolus, M., Bisaglia, M., Zoleo, A., Fittipaldi, M., Benfatto, M., Bubacco, L. and Maniero, A. L. (2010). "Structural Characterization of a High Affinity Mononuclear Site in the Copper(II)-α-Synuclein Complex." *Journal of the American Chemical Society* **132**(51): 18057-18066.

Brito-Moreira, J., Paula-Lima, A. C., Bomfim, T. R., Oliveira, F. B., Sepulveda, F. J., De Mello, F. G., ... Ferreira, S. T. (2011). "Abeta Oligomers Induce Glutamate Release from Hippocampal Neurons." *Current Alzheimer Research* **8**(5): 552-562.

Brouillette, J., Caillierez, R., Zommer, N., Alves-Pires, C., Benilova, I., Blum, D., ... Buée, L. (2012). "Neurotoxicity and Memory Deficits Induced by Soluble Low-Molecular-Weight Amyloid-β1–42 Oligomers Are Revealed In Vivo by Using a Novel Animal Model." *The Journal of Neuroscience* **32**(23): 7852-7861.

Brown, D. R., Qin, K., Herms, J. W., Madlung, A., Manson, J., Strome, R., ... Kretzschmar, H. (1997). "The Cellular Prion Protein Binds Copper In Vivo." *Nature* **390**(6661): 684-687.

Bryce, G. F. and Gurd, F. R. N. (1966). "Visible Spectra and Optical Rotatory Properties of Cupric Ion Complexes of L-Histidine-Containing Peptides." *Journal of Biological Chemistry* **241**(1): 122-129.

Buckner, R. L., Snyder, A. Z., Shannon, B. J., Larossa, G., Sachs, R., Fotenos, A. F., ... Mintun, M. A. (2005). "Molecular, Structural, and Functional Characterization of Alzheimer's Disease: Evidence for a Relationship between Default Activity, Amyloid, and Memory." *The Journal of Neuroscience* **25**(34): 7709-7717.

Buxbaum, J. N., Ye, Z., Reixach, N., Friske, L., Levy, C., Das, P., ... Bartfai, T. (2008). "Transthyretin Protects Alzheimer's Mice from the Behavioral and Biochemical Effects of Aβ Toxicity." *Proceedings of the National Academy of Sciences* **105**(7): 2681-2686.

Calella, A. M., Farinelli, M., Nuvolone, M., Mirante, O., Moos, R., Falsig, J., ... Aguzzi, A. (2010). "Prion Protein and Abeta-Related Synaptic Toxicity Impairment." *EMBO Molecular Medicine* **2**(8): 306-314.

Carter, D. and Ho, J. (1994). "Structure of Serum Albumin." *Advances in Protein Chemistry* **45**: 153-203.

Chen, Q.-S., Wei, W.-Z., Shimahara, T. and Xie, C.-W. (2002). "Alzheimer Amyloid β-Peptide Inhibits the Late Phase of Long-Term Potentiation through Calcineurin-Dependent Mechanisms in the Hippocampal Dentate Gyrus." *Neurobiology of Learning and Memory* **77**(3): 354-371.

Chen, S. and Wetzel, R. (2001). "Solubilization and Disaggregation of Polyglutamine Peptides." *Protein Science* **10**(4): 887-891.

Chen, S., Yadav, S. P. and Surewicz, W. K. (2010). "Interaction between Human Prion Protein and Amyloid-Beta (Abeta) Oligomers: Role of N-Terminal Residues." *J Biological Chemistry* **285**(34): 26377-26383.

Chen, W.-T., Liao, Y.-H., Yu, H.-M., Cheng, I. H. and Chen, Y.-R. (2011). "Distinct Effects of Zn^{2+}, Cu^{2+}, Fe^{3+}, and Al^{3+} on Amyloid-β Stability, Oligomerization, and Aggregation: Amyloid-β Destabilization Promotes Annular Protofibril Formation." *Journal of Biological Chemistry* **286**(11): 9646-9656.

Cho, P. Y., Joshi, G., Johnson, J. A. and Murphy, R. M. (2014). "Transthyretin-Derived Peptides as β-Amyloid Inhibitors." *ACS Chemical Neuroscience* **5**(7): 542-551.

Chobanian, A. V. and Hollander, W. (1962). "Body Cholesterol Metabolism in Man. I. The Equilibration of Serum and Tissue Cholesterol." *Journal of Clinical Investigation* **41**(9): 1732.

Christenson, R. H., Behlmer, P., Howard, J. F., Winfield, J. B. and Silverman, L. M. (1983). "Interpretation of Cerebrospinal Fluid Protein Assays in Various Neurologic Diseases." *Clinical Chemistry* **29**(6): 1028-1030.

Cleary, J. P., Walsh, D. M., Hofmeister, J. J., Shankar, G. M., Kuskowski, M. A., Selkoe, D. J. and Ashe, K. H. (2004). "Natural Oligomers of the Amyloid-β Protein Specifically Disrupt Cognitive Function." *Nature Neuroscience* **8**(1): 79-84.

Corder, E., Saunders, A., Strittmatter, W., Schmechel, D., Gaskell, P., Small, G., ... Pericak-Vance, M. (1993). "Gene Dose of Apolipoprotein E Type 4 Allele and the Risk of Alzheimer's Disease in Late Onset Families." *Science* **261**(5123): 921-923.

Cordy, J. M., Hooper, N. M. and Turner, A. J. (2006). "The Involvement of Lipid Rafts in Alzheimer's Disease." *Mol Membr Biol* **23**(1): 111-122.

Cordy, J. M., Hussain, I., Dingwall, C., Hooper, N. M. and Turner, A. J. (2003). "Exclusively Targeting β-Secretase to Lipid Rafts by GPI-Anchor Addition Up-Regulates β-Site Processing of the Amyloid Precursor Protein." *Proceedings of the National Academy of Sciences* **100**(20): 11735-11740.

Coria, F., Castano, E., Prelli, F., Larrondo-Lillo, M., Van Duinen, S., Shelanski, M. and Frangione, B. (1988). "Isolation and Characterization of Amyloid P Component from Alzheimer's Disease and Other Types of Cerebral Amyloidosis." *Laboratory Investigation; a Journal of Technical Methods and Pathology* **58**(4): 454-458.

Cossi, M., Rega, N., Scalmani, G. and Barone, V. (2003). "Energies, Structures, and Electronic Properties of Molecules in Solution with the C-PCM Solvation Model." *Journal of Computational Chemistry* **24**(6): 669-681.

Costa, R., Goncalves, A., Saraiva, M. and Cardoso, I. (2008). "Transthyretin Binding to A-Beta Peptide–Impact on A-Beta Fibrillogenesis and Toxicity." *FEBS Letters* **582**(6): 936-942.

Cullen, W. K., Wu, J., Anwyl, R. and Rowan, M. J. (1996). "β-Amyloid Produces a Delayed Nmda Receptor- Dependent Reduction in Synaptic Transmission in Rat Hippocampus." *NeuroReport* **8**(1): 87-92.

Curry, S., Mandelkow, H., Brick, P. and Franks, N. (1998). "Crystal Structure of Human Serum Albumin Complexed with Fatty Acid Reveals an Assymetric Distribution of Binding Sites." *Nature Structural Biology* **5**: 827-835.

Dahlgren, K. N., Manelli, A. M., Stine, W. B., Baker, L. K., Krafft, G. A. and Ladu, M. J. (2002). "Oligomeric and Fibrillar Species of Amyloid-β Peptides Differentially Affect Neuronal Viability." *Journal of Biological Chemistry* **277**(35): 32046-32053.

Damante, C. A., Ösz, K., Nagy, Z., Pappalardo, G., Grasso, G., Impellizzeri, G., ... Sóvágó, I. (2008). "The Metal Loading Ability of β-Amyloid N-Terminus: A Combined

Potentiometric and Spectroscopic Study of Copper(II) Complexes with β-Amyloid(1−16), Its Short or Mutated Peptide Fragments, and Its Polyethylene Glycol (PEG)-ylated Analogue." *Inorganic Chemistry* **47**(20): 9669-9683.

Danielsson, J., Pierattelli, R., Banci, L. and Gräslund, A. (2007). "High-Resolution Nmr Studies of the Zinc-Binding Site of the Alzheimer's Amyloid β-Peptide." *FEBS Journal* **274**(1): 46-59.

Davies, P., Wang, X., Sarell, C. J., Drewett, A., Marken, F., Viles, J. H. and Brown, D. R. (2010). "The Synucleins Are a Family of Redox-Active Copper Binding Proteins." *Biochemistry* **50**(1): 37-47.

Dawson, R. M. C., Elliot, D.C., Elliot, W.H., Jones, K.M (1986). *Data for Biochemical Research*. Oxford UK, Claredon Press.

Decker, H., Jürgensen, S., Adrover, M. F., Brito-Moreira, J., Bomfim, T. R., Klein, W. L., ... Ferreira, S. T. (2010). "N-Methyl-D-Aspartate Receptors Are Required for Synaptic Targeting of Alzheimer's Toxic Amyloid-β Peptide Oligomers." *Journal of Neurochemistry* **115**(6): 1520-1529.

Deliconstantinos, G., Tsopanakis, C., Karayiannakos, P. and Skalkeas, G. (1986). "Evidence for the Existence of Non-Esterified Cholesterol Carried by Albumin in Rat Serum." *Atherosclerosis* **61**(1): 67-75.

Demeester, N., Castro, G., Desrumaux, C., De Geitere, C., Fruchart, J., Santens, P., ... Vandekerckhove, J. (2000). "Characterization and Functional Studies of Lipoproteins, Lipid Transfer Proteins, and Lecithin: Cholesterol Acyltransferase in CSF of Normal Individuals and Patients with Alzheimer's Disease." *Journal of Lipid Research* **41**(6): 963-974.

Di Natale, G., ÖSz, K., Nagy, Z. N., Sanna, D., Micera, G., Pappalardo, G., ... Rizzarell, E. (2009). "Interaction of Copper(II) with the Prion Peptide Fragment HuPrP(76−114) Encompassing Four Histidyl Residues within and Outside the Octarepeat Domain." *Inorganic Chemistry* **48**(9): 4239-4250.

Dietschy, J. M. and Turley, S. D. (2004). "Thematic Review Series: Brain Lipids. Cholesterol Metabolism in the Central Nervous System During Early Development and in the Mature Animal." *Journal of Lipid Research* **45**(8): 1375-1397.

Do, T. D., Economou, N. J., Chamas, A., Buratto, S. K., Shea, J.-E. and Bowers, M. T. (2014). "Interactions between Amyloid-β and Tau Fragments Promote Aberrant Aggregates: Implications for Amyloid Toxicity." *The Journal of Physical Chemistry B*.

Dole, V. P. (1956). *Fractionation of Plasma Non-Esterified Fatty Acids*. Proceedings of the Society for Experimental Biology and Medicine. Society for Experimental Biology and Medicine (New York, NY), Royal Society of Medicine.

Domingues, A., Almeida, S., Da Cruz E Silva, E. F., Oliveira, C. R. and Rego, A. C. (2007). "Toxicity of β-Amyloid in HEK293 Cells Expressing NR1/NR2A or NR1/NR2B N-Methyl-D-Aspartate Receptor Subunits." *Neurochemistry International* **50**(6): 872-880.

Dong, J., Atwood, C. S., Anderson, V. E., Siedlak, S. L., Smith, M. A., Perry, G. and Carey, P. R. (2003). "Metal Binding and Oxidation of Amyloid-Beta within Isolated Senile Plaque Cores: Raman Microscopic Evidence." *Biochemistry* **42**(10): 2768-2773.

Dorlet, P., Gambarelli, S., Faller, P. and Hureau, C. (2009). "Pulse EPR Spectroscopy Reveals the Coordination Sphere of Copper(II) Ions in the 1–16 Amyloid-β Peptide: A Key Role of the First Two N-Terminus Residues." *Angewandte Chemie International Edition* **48**(49): 9273-9276.

Drake, A. F. (1994a). Chapter 12: Optical Spectroscopy. Principles and Instrumentation. *Microscopy, Optical Spectroscopy, and Macroscopic Techniques*. C. Jones, B. Mulloy and A. H. Thomas. Totowa, NJ, Humana Press Inc. **22:** 151-172.

Drake, A. F. (1994b). Chapter 13: The Measurement of Electronic Absorption Spectra in Th Ultraviolet and Visible. *Microscopy, Optical Spectroscopy, and Macroscopic Techniques*. C. Jones, B. Mulloy and A. H. Thomas. Totowa, NJ, Humana Press Inc. **22:** 173-182.

Drake, A. F. (1994c). Chapter 16: Circular Dichroism. *Microscopy, Optical Spectroscopy, and Macroscopic Techniques*. C. Jones, B. Mulloy and A. H. Thomas. Totowa, NJ, Humana Press Inc. **22:** 219-244.

Drew, S. C., Ling Leong, S., Pham, C. L. L., Tew, D. J., Masters, C. L., Miles, L. A., ... Barnham, K. J. (2008). "Cu^{2+} Binding Modes of Recombinant A-Synuclein − Insights from EPR Spectroscopy." *Journal of the American Chemical Society* **130**(24): 7766-7773.

Drew, S. C., Noble, C. J., Masters, C. L., Hanson, G. R. and Barnham, K. J. (2009). "Pleomorphic Copper Coordination by Alzheimer's Disease Amyloid-β Peptide." *Journal of the American Chemical Society* **131**(3): 1195-1207.

Dries, D. R. and Yu, G. (2008). "Assembly, Maturation, and Trafficking of the γ-Secretase Complex in Alzheimer's Disease." *Current Alzheimer Research* **5**(2): 132.

Du, J. and Murphy, R. M. (2010). "Characterization of the Interaction of β-Amyloid with Transthyretin Monomers and Tetramers." *Biochemistry* **49**(38): 8276-8289.

Dudzik, C. G., Walter, E. D. and Millhauser, G. L. (2011). "Coordination Features and Affinity of the Cu^{2+} Site in the α-Synuclein Protein of Parkinson's Disease." *Biochemistry* **50**(11): 1771-1777.

Ehehalt, R., Keller, P., Haass, C., Thiele, C. and Simons, K. (2003). "Amyloidogenic Processing of the Alzheimer β-Amyloid Precursor Protein Depends on Lipid Rafts." *The Journal of Cell Biology* **160**(1): 113-123.

Elovaara, I., Maury, C. P. J. and Palo, J. (1986). "Serum Amyloid A Protein, Albumin and Prealbumin in Alzheimer's Disease and in Demented Patients with Down's Syndrome." *Acta Neurologica Scandinavica* **74**(3): 245-250.

Elovaara, I., Palo, J., Erkinjuntti, T. and Sulkava, R. (1987). "Serum and Cerebrospinal Fluid Proteins and the Blood-Brain Barrier in Alzheimer's Disease and Multi-Infarct Dementia." *European Neurology* **26**(4): 229-234.

Emsley, J., White, H. E., O'hara, B. P., Oliva, G., Srinivasan, N., Tickle, I. J., ... Wood, S. P. (1994). "Structure of Pentameric Human Serum Amyloid P Component." *Nature* **367**(6461): 338-345.

Faller, P. and Hureau, C. (2009). "Bioinorganic Chemistry of Copper and Zinc Ions Coordinated to Amyloid-β Peptide." *Dalton Transactions*(7): 1080-1094.

Ferreira, I. L., Bajouco, L. M., Mota, S. I., Auberson, Y. P., Oliveira, C. R. and Rego, A. C. (2012). "Amyloid Beta Peptide 1–42 Disturbs Intracellular Calcium Homeostasis through Activation of Glun2B-Containing N-Methyl-D-Aspartate Receptors in Cortical Cultures." *Cell Calcium* **51**(2): 95-106.

Fezoui, Y., Hartley, D. M., Harper, J. D., Khurana, R., Walsh, D. M., Condron, M. M., ... Teplow, D. B. (2000). "An Improved Method of Preparing the Amyloid Beta-Protein for Fibrillogenesis and Neurotoxicity Experiments." *Amyloid* **7**(3): 166-178.

Finckh, U., Von Der Kammer, H., Velden, J., Michel, T., Andresen, B., Deng, A., ... Menzer, G. (2000). "Genetic Association of a Cystatin C Gene Polymorphism with Late-Onset Alzheimer Disease." *Archives of Neurology* **57**(11): 1579-1583.

Fowler, D. M., Koulov, A. V., Balch, W. E. and Kelly, J. W. (2007). "Functional Amyloid – from Bacteria to Humans." *Trends in Biochemical Sciences* **32**(5): 217-224.

Fredrickson, D. S. and Gordon, R. S., Jr. (1958). "The Metabolism of Albumin Bound C14-Labeled Unesterified Fatty Acids in Normal Human Subjects." *The Journal of Clinical Investigation* **37**(11): 1504-1515.

Frid, P., Anisimov, S. V. and Popovic, N. (2007). "Congo Red and Protein Aggregation in Neurodegenerative Diseases." *Brain Res Brain Res Rev* **53**(1): 135-160.

Frisch, M. J., Trucks, G. W., Schlegel, H. B., Scuseria, G. E., Robb, M. A., Cheeseman, J. R., ... Fox, D. J. (2009). *Gaussian 09, Revision A.02*. Wallingford CT.

Gaggelli, E., Kozlowski, H., Valensin, D. and Valensin, G. (2006). "Copper Homeostasis and Neurodegenerative Disorders (Alzheimer's, Prion, and Parkinson's Diseases and Amyotrophic Lateral Sclerosis)." *Chemical Reviews* **106**(6): 1995-2044.

Gamblin, T. C., Chen, F., Zambrano, A., Abraha, A., Lagalwar, S., Guillozet, A. L., ... Cryns, V. L. (2003). "Caspase Cleavage of Tau: Linking Amyloid and Neurofibrillary Tangles in Alzheimer's Disease." *Proceedings of the National Academy of Sciences* **100**(17): 10032-10037.

Garnett, A. P., Jones, C. E. and Viles, J. H. (2006). "A Survey of Diamagnetic Probes for Copper^{2+} Binding to the Prion Protein. 1H NMR Solution Structure of the Palladium^{2+} Bound Single Octarepeat." *Dalton Transactions*(3): 509-518.

Garzon-Rodriguez, W., Yatsimirsky, A. K. and Glabe, C. G. (1999). "Binding of Zn(II), Cu(II), and Fe(II) Ions to Alzheimer's Aβ Peptide Studied by Fluorescence." *Bioorganic & Medicinal Chemistry Letters* **9**(15): 2243-2248.

Ghidoni, R., Benussi, L., Paterlini, A., Missale, C., Usardi, A., Rossi, R., ... Binetti, G. (2007). "Presenilin 2 Mutations Alter Cystatin C Trafficking in Mouse Primary Neurons." *Neurobiology of Aging* **28**(3): 371-376.

Ghiso, J., Matsubara, E., Koudinov, A., Choi-Miura, N. H., Tomita, M., Wisniewski, T. and Frangione, B. (1993). "The Cerebrospinal-Fluid Soluble Form of Alzheimer's Amyloid Beta Is Complexed to SP-40, 40 (Apolipoprotein J), an Inhibitor of the Complement Membrane-Attack Complex." *Biochemical Journal* **293**: 27-30.

Ghuman, J., Zunszain, P. A., Petitpas, I., Bhattacharya, A. A., Otagiri, M. and Curry, S. (2005). "Structural Basis of the Drug-Binding Specificity of Human Serum Albumin." *Journal of Molecular Biology* **353**(1): 38-52.

Gill, S. C. and Von Hippel, P. H. (1989). "Calculation of Protein Extinction Coefficients from Amino Acid Sequence Data." *Analytical Biochemistry* **182**(2): 319-326.

Gimbel, D. A., Nygaard, H. B., Coffey, E. E., Gunther, E. C., Lauren, J., Gimbel, Z. A. and Strittmatter, S. M. (2010). "Memory Impairment in Transgenic Alzheimer Mice Requires Cellular Prion Protein." *Journal of Neuroscience* **30**(18): 6367-6374.

Giunta, S., Valli, M., Galeazzi, R., Fattoretti, P., Corder, E. and Galeazzi, L. (2005). "Transthyretin Inhibition of Amyloid Beta Aggregation and Toxicity." *Clinical Biochemistry* **38**(12): 1112-1119.

Gong, Y., Chang, L., Viola, K. L., Lacor, P. N., Lambert, M. P., Finch, C. E., ... Klein, W. L. (2003). "Alzheimer's Disease-Affected Brain: Presence of Oligomeric A Beta Ligands (ADDLs) Suggests a Molecular Basis for Reversible Memory Loss." *Proceedings of the National Academy of Sciences* **100**(18): 10417-10422.

Gorell, J., Johnson, C., Rybicki, B., Peterson, E., Kortsha, G., Brown, G. and Richardson, R. (1998). "Occupational Exposure to Manganese, Copper, Lead, Iron, Mercury and Zinc and the Risk of Parkinson's Disease." *Neurotoxicology* **20**(2-3): 239-247.

Gralka, E., Valensin, D., Porciatti, E., Gajda, C., Gaggelli, E., Valensin, G., ... Kozlowski, H. (2008). "CuII Binding Sites Located at His-96 and His-111 of the Human Prion Protein: Thermodynamic and Spectroscopic Studies on Model Peptides." *Dalton Transactions*(38): 5207-5219.

Grossi, C., Francese, S., Casini, A., Rosi, M. C., Luccarini, I., Fiorentini, A., ... Casamenti, F. (2009). "Clioquinol Decreases Amyloid-β Burden and Reduces Working Memory Impairment in a Transgenic Mouse Model of Alzheimer's Disease." *Journal of Alzheimer's Disease* **17**(2): 423-440.

Guilloreau, L., Damian, L., Coppel, Y., Mazarguil, H., Winterhalter, M. and Faller, P. (2006). "Structural and Thermodynamical Properties of CuII Amyloid-β16/28 Complexes

Associated with Alzheimer's Disease." *Journal of Biological Inorganic Chemistry* **11**(8): 1024-1038.

Gunderson, W. A., Hernandez-Guzman, J., Karr, J. W., Sun, L., Szalai, V. A. and Warncke, K. (2012). "Local Structure and Global Patterning of Cu^{2+} Binding in Fibrillar Amyloid-Beta [Abeta(1-40)] Protein." *Journal of the American Chemical Society* **134**(44): 18330-18337.

Gunther, E. C. and Strittmatter, S. M. (2010). "Beta-Amyloid Oligomers and Cellular Prion Protein in Alzheimer's Disease." *Journal of Molecular Medicine (Berl)* **88**(4): 331-338.

Guo, J.-P., Arai, T., Miklossy, J. and Mcgeer, P. L. (2006). "Aβ and Tau Form Soluble Complexes That May Promote Self Aggregation of Both into the Insoluble Forms Observed in Alzheimer's Disease." *Proceedings of the National Academy of Sciences* **103**(6): 1953-1958.

Gusnard, D. A. and Raichle, M. E. (2001). "Searching for a Baseline: Functional Imaging and the Resting Human Brain." *Nature Reviews Neuroscience* **2**(10): 685-694.

Haass, C. (2004). "Take Five—Bace and the γ-Secretase Quartet Conduct Alzheimer's Amyloid β-Peptide Generation." *The EMBO Journal* **23**(3): 483-488.

Haass, C., Kaether, C., Thinakaran, G. and Sisodia, S. (2012). "Trafficking and Proteolytic Processing of APP." *Cold Spring Harbor Perspectives in Medicine* **2**(5): a006270.

Haass, C., Koo, E. H., Mellon, A., Hung, A. Y. and Selkoe, D. J. (1992). "Targeting of Cell-Surface β-Amyloid Precursor Protein to Lysosomes: Alternative Processing into Amyloid-Bearing Fragments." *Nature* **357**(6378): 500-503.

Hamazaki, H. (1995a). "Amyloid P Component Promotes Aggregation of Alzheimer′s β-Amyloid Peptide." *Biochemical and Biophysical Research Communications* **211**(2): 349-353.

Hamazaki, H. (1995b). "Ca^{2+}-Dependent Binding of Human Serum Amyloid P Component to Alzheimers -Amyloid Peptide." *Journal of Biological Chemistry* **270**(18): 10392-10394.

Hammad, S. M., Ranganathan, S., Loukinova, E., Twal, W. O. and Argraves, W. S. (1997). "Interaction of Apolipoprotein J-Amyloid β-Peptide Complex with Low Density Lipoprotein Receptor-Related Protein-2/Megalin: A Mechanism to Prevent Pathological Accumulation of Amyloid β-Peptide." *Journal of Biological Chemistry* **272**(30): 18644-18649.

Hane, F., Tran, G., Attwood, S. J. and Leonenko, Z. (2013). "Cu^{2+} Affects Amyloid-Beta (1-42) Aggregation by Increasing Peptide-Peptide Binding Forces." *PLoS ONE* **8**(3): e59005.

Hansson, S. F., Andréasson, U., Wall, M., Skoog, I., Andreasen, N., Wallin, A., ... Blennow, K. (2009). "Reduced Levels of Amyloid-β-Binding Proteins in Cerebrospinal Fluid from Alzheimer's Disease Patients." *Journal of Alzheimer's Disease* **16**(2): 389-397.

Hardy, J. (1997). "Amyloid, the Presenilins and Alzheimer's Disease." *Trends in Neurosciences* **20**(4): 154-159.

Hardy, J. and Higgins, G. (1992). "Alzheimer's Disease: The Amyloid Cascade Hypothesis." *Science* **256**(5054): 184-185.

Hardy, J. and Selkoe, D. J. (2002). "Medicine - the Amyloid Hypothesis of Alzheimer's Disease: Progress and Problems on the Road to Therapeutics." *Science* **297**(5580): 353-356.

Hartley, D. M., Walsh, D. M., Ye, C. P., Diehl, T., Vasquez, S., Vassilev, P. M., ... Selkoe, D. J. (1999). "Protofibrillar Intermediates of Amyloid β-Protein Induce Acute Electrophysiological Changes and Progressive Neurotoxicity in Cortical Neurons." *The Journal of Neuroscience* **19**(20): 8876-8884.

Hartter, D. E. and Barnea, A. (1988). "Evidence for Release of Copper in the Brain: Depolarization-Induced Release of Newly Taken-up ^{67}Copper." *Synapse* **2**(4): 412-415.

Hasegawa, K., Ono, K., Yamada, M. and Naiki, H. (2002). "Kinetic Modeling and Determination of Reaction Constants of Alzheimer's β-Amyloid Fibril Extension and Dissociation Using Surface Plasmon Resonance." *Biochemistry* **41**(46): 13489-13498.

Hasnip, P. J., Refson, K., Probert, M. I., Yates, J. R., Clark, S. J. and Pickard, C. J. (2014). "Density Functional Theory in the Solid State." *Philosophical Transactions of the Royal Society A: Mathemtaical, Physical and Engineering Sciences* **372**(2011): 20130270.

Hatcher, L. Q., Hong, L., Bush, W. D., Carducci, T. and Simon, J. D. (2008). "Quantification of the Binding Constant of Copper(II) to the Amyloid-Beta Peptide." *The Journal of Physical Chemistry B* **112**(27): 8160-8164.

Hawkins, P. N., Rossor, M. N., Gallimore, J. R., Miller, B., Moore, E. G. and Pepys, M. B. (1994). "Concentration of Serum Amyloid P Component in the CSF as a Possible Marker of Cerebral Amyloid Deposits in Alzheimer′S Disease." *Biochemical and Biophysical Research Communications* **201**(2): 722-726.

He, Y., Cui, J., Lee, J. C.-M., Ding, S., Chalimoniuk, M., Simonyi, A., ... Sun, G. Y. (2011). "Prolonged Exposure of Cortical Neurons to Oligomeric Amyloid-β Impairs NMDA Receptor Function Via NADPH Oxidase-Mediated ROS Production: Protective Effect of Green Tea (-)-Epigallocatechin-3-Gallate." *ASN Neuro* **3**(1).

Heyd, J., Scuseria, G. E. and Ernzerhof, M. (2006). "Hybrid Functionals Based on a Screened Coulomb Potential (Vol 118, Pg 8207, 2003)." *Journal of Chemical Physics* **124**(21).

Hicks, D. A., Nalivaeva, N. N. and Turner, A. J. (2012). "Lipid Rafts and Alzheimer's Disease: Protein-Lipid Interactions and Perturbation of Signaling." *Frontiers in Physiology* **3**.

Hong, L., Bush, W. D., Hatcher, L. Q. and Simon, J. (2008). "Determining Thermodynamic Parameters from Isothermal Calorimetric Isotherms of the Binding of Macromolecules

to Metal Cations Originally Chelated by a Weak Ligand." *The Journal of Physical Chemistry B* **112**(2): 604-611.

Hong, L., Carducci, T. M., Bush, W. D., Dudzik, C. G., Millhauser, G. L. and Simon, J. D. (2010). "Quantification of the Binding Properties of Cu^{2+} to the Amyloid Beta Peptide: Coordination Spheres for Human and Rat Peptides and Implication on Cu^{2+}-Induced Aggregation." *The Journal of Physical Chemistry B* **114**(34): 11261-11271.

Hong, L. and Simon, J. D. (2009). "Binding of Cu(II) to Human α-Synucleins: Comparison of Wild Type and the Point Mutations Associated with the Familial Parkinson's Disease." *The Journal of Physical Chemistry B* **113**(28): 9551-9561.

Hooijmans, C. R., Van Der Zee, C. E. E. M., Dederen, P. J., Brouwer, K. M., Reijmer, Y. D., Van Groen, T., ... Kiliaan, A. J. (2009). "DHA and Cholesterol Containing Diets Influence Alzheimer-Like Pathology, Cognition and Cerebral Vasculature in APPswe/PS1dE9 Mice." *Neurobiology of Disease* **33**(3): 482-498.

Hortschansky, P., Schroeckh, V., Christopeit, T., Zandomeneghi, G. and Fändrich, M. (2005). "The Aggregation Kinetics of Alzheimer's β-Amyloid Peptide Is Controlled by Stochastic Nucleation." *Protein Science* **14**(7): 1753-1759.

Hoshi, M., Sato, M., Matsumoto, S., Noguchi, A., Yasutake, K., Yoshida, N. and Sato, K. (2003). "Spherical Aggregates of β-Amyloid (Amylospheroid) Show High Neurotoxicity and Activate Tau Protein Kinase I/Glycogen Synthase Kinase-3β." *Proceedings of the National Academy of Sciences* **100**(11): 6370-6375.

Hou, L. and Zagorski, M. G. (2006). "NMR Reveals Anomalous Copper(II) Binding to the Amyloid Aβ Peptide of Alzheimer's Disease." *Journal of the American Chemical Society* **128**(29): 9260-9261.

Hsieh, H., Boehm, J., Sato, C., Iwatsubo, T., Tomita, T., Sisodia, S. and Malinow, R. (2006). "AMPAR Removal Underlies Aβ-Induced Synaptic Depression and Dendritic Spine Loss." *Neuron* **52**(5): 831-843.

Huang, X., Atwood, C. S., Hartshorn, M. A., Multhaup, G., Goldstein, L. E., Scarpa, R. C., ... Bush, A. I. (1999). "The A Beta Peptide of Alzheimer's Disease Directly Produces Hydrogen Peroxide through Metal Ion Reduction." *Biochemistry* **38**(24): 7609-7616.

Humphreys, D. T., Carver, J. A., Easterbrook-Smith, S. B. and Wilson, M. R. (1999). "Clusterin Has Chaperone-Like Activity Similar to That of Small Heat Shock Proteins." *Journal of Biological Chemistry* **274**(11): 6875-6881.

Huse, J. T., Pijak, D. S., Leslie, G. J., Lee, V. M.-Y. and Doms, R. W. (2000). "Maturation and Endosomal Targeting of β-Site Amyloid Precursor Protein-Cleaving Enzyme: The Alzheimer's Disease β-Secretase." *Journal of Biological Chemistry* **275**(43): 33729-33737.

Hutchinson, W. L., Noble, G. E., Hawkins, P. N. and Pepys, M. B. (1994). "The Pentraxins, C-Reactive Protein and Serum Amyloid P Component, Are Cleared and Catabolized by Hepatocytes in Vivo." *Journal of Clinical Investigation* **94**(4): 1390.

Ittner, L. M. and Götz, J. (2011). "Amyloid-β and Tau — a Toxic Pas De Deux in Alzheimer's Disease." *Nature Reviews Neurosci* **12**(2): 67-72.

Ittner, L. M., Ke, Y. D., Delerue, F., Bi, M., Gladbach, A., Van Eersel, J., ... Napier, I. A. (2010). "Dendritic Function of Tau Mediates Amyloid-β Toxicity in Alzheimer's Disease Mouse Models." *Cell* **142**(3): 387-397.

Jackson, G. S., Murray, I., Hosszu, L. L. P., Gibbs, N., Waltho, J. P., Clarke, A. R. and Collinge, J. (2001). "Location and Properties of Metal-Binding Sites on the Human Prion Protein." *Proceedings of the National Academy of Sciences* **98**(15): 8531-8535.

Jackson, K., Barisone, G. A., Diaz, E., Jin, L.-W., Decarli, C. and Despa, F. (2013). "Amylin Deposition in the Brain: A Second Amyloid in Alzheimer Disease?" *Annals of Neurology* **74**(4): 517-526.

Jackson, M. S. and Lee, J. C. (2009). "Identification of the Minimal Copper(II)-Binding α-Synuclein Sequence." *Inorganic chemistry* **48**(19): 9303-9307.

Jang, H., Arce, F. T., Ramachandran, S., Capone, R., Azimova, R., Kagan, B. L., ... Lal, R. (2010). "Truncated β-Amyloid Peptide Channels Provide an Alternative Mechanism for Alzheimer's Disease and Down Syndrome." *Proceedings of the National Academy of Sciences* **107**(14): 6538-6543.

Janowski, R., Kozak, M., Jankowska, E., Grzonka, Z., Grubb, A., Abrahamson, M. and Jaskolski, M. (2001). "Human Cystatin C, an Amyloidogenic Protein, Dimerizes through Three-Dimensional Domain Swapping." *Nature Structural & Molecular Biology* **8**(4): 316-320.

Jiang, D., Zhang, L., Grant, P.G., Dudzik, C.G, Chen, S., Patel, S., Hao, Y., Millhauser, G.L. and Zhou, F. (2013). "The Elevated Copper Binding Strength of Amyloid-β Aggregates Allows the Sequestration of Copper from Albumin: A Pathway to Accumulation of Copper in Senile Plaques." *Biochemistry* **52**(3): 547-556.

Jones, C. E., Klewpatinond, M., Abdelraheim, S. R., Brown, D. R. and Viles, J. H. (2005). "Probing Copper^{2+} Binding to the Prion Protein Using Diamagnetic Nickel^{2+} and 1H NMR: The Unstructured N Terminus Facilitates the Coordination of Six Copper^{2+} Ions at Physiological Concentrations." *Journal of Molecular Biology* **346**(5): 1393-1407.

Jones, L., Holmans, P. A., Hamshere, M. L., Harold, D., Moskvina, V., Ivanov, D., ... Williams, J. (2010). "Genetic Evidence Implicates the Immune System and Cholesterol Metabolism in the Aetiology of Alzheimer's Disease." *PLoS ONE* **5**(11): e13950.

Juszczyk, P., Paraschiv, G., Szymanska, A., Kolodziejczyk, A. S., Rodziewicz-Motowidlo, S., Grzonka, Z. and Przybylski, M. (2009). "Binding Epitopes and Interaction Structure of the Neuroprotective Protease Inhibitor Cystatin C with β-Amyloid Revealed by Proteolytic Excision Mass Spectrometry and Molecular Docking Simulation." *Journal of Medicinal Chemistry* **52**(8): 2420-2428.

Kaeser, S. A., Herzig, M. C., Coomaraswamy, J., Kilger, E., Selenica, M.-L., Winkler, D. T., ... Jucker, M. (2007). "Cystatin C Modulates Cerebral β-Amyloidosis." *Nature Genetics* **39**(12): 1437-1439.

Kaether, C., Haass, C. and Steiner, H. (2006). "Assembly, Trafficking and Function of γ-Secretase." *Neurodegenerative Diseases* **3**(4-5): 275-283.

Kaether, C., Skehel, P. and Dotti, C. G. (2000). "Axonal Membrane Proteins Are Transported in Distinct Carriers: A Two-Color Video Microscopy Study in Cultured Hippocampal Neurons." *Molecular Biology of the Cell* **11**(4): 1213-1224.

Kalmijn, S., Launer, L. J., Ott, A., Witteman, J., Hofman, A. and Breteler, M. (1997). "Dietary Fat Intake and the Risk of Incident Dementia in the Rotterdam Study." *Annals of Neurology* **42**(5): 776-782.

Kamal, A., Almenar-Queralt, A., Leblanc, J. F., Roberts, E. A. and Goldstein, L. S. B. (2001). "Kinesin-Mediated Axonal Transport of a Membrane Compartment Containing β-Secretase and Presenilin-1 Requires APP." *Nature* **414**(6864): 643-648.

Kamenetz, F., Tomita, T., Hsieh, H., Seabrook, G., Borchelt, D., Iwatsubo, T., ... Malinow, R. (2003). "APP Processing and Synaptic Function." *Neuron* **37**(6): 925-937.

Kang, J., Lemaire, H.-G., Unterbeck, A., Salbaum, J. M., Masters, C. L., Grzeschik, K.-H., ... Müller-Hill, B. (1987). "The Precursor of Alzheimer's Disease Amyloid A4 Protein Resembles a Cell-Surface Receptor."

Karavelas, T., Mylonas, M., Malandrinos, G., Plakatouras, J. C., Hadjiliadis, N., Mlynarz, P. and Kozlowski, H. (2005). "Coordination Properties of Cu(II) and Ni(II) Ions Towards the C-Terminal Peptide Fragment –ELAKHA– of Histone H2B." *Journal of Inorganic Biochemistry* **99**(2): 606-615.

Kardos, J., Kovács, I., Hajós, F., Kálmán, M. and Simonyi, M. (1989). "Nerve Endings from Rat Brain Tissue Release Copper Upon Depolarization. A Possible Role in Regulating Neuronal Excitability." *Neuroscience Letters*: 103:139-144.

Karr, J. W., Akintoye, H., Kaupp, L. J. and Szalai, V. A. (2005). "N-Terminal Deletions Modify the Cu^{2+} Binding Site in Amyloid-β." *Biochemistry* **44**(14): 5478-5487.

Karr, J. W. and Szalai, V. A. (2008). "Cu(II) Binding to Monomeric, Oligomeric, and Fibrillar Forms of the Alzheimer's Disease Amyloid-β Peptide." *Biochemistry* **47**(17): 5006-5016.

Kayed, R., Pensalfini, A., Margol, L., Sokolov, Y., Sarsoza, F., Head, E., ... Glabe, C. (2009). "Annular Protofibrils Are a Structurally and Functionally Distinct Type of Amyloid Oligomer." *Journal of Biological Chemistry* **284**(7): 4230-4237.

Kessels, H. W., Nabavi, S. and Malinow, R. (2013). "Metabotropic NMDA Receptor Function Is Required for β-Amyloid–Induced Synaptic Depression." *Proceedings of the National Academy of Sciences* **110**(10): 4033-4038.

Kheterpal, I., Wetzel, R. and Cook, K. D. (2003). "Enhanced Correction Methods for Hydrogen Exchange-Mass Spectrometric Studies of Amyloid Fibrils." *Protein Science* **12**(3): 635-643.

Kim, H.-J., Chae, S.-C., Lee, D.-K., Chromy, B., Lee, S. C., Park, Y.-C., ... Hong, S.-T. (2003). "Selective Neuronal Degeneration Induced by Soluble Oligomeric Amyloid Beta Protein." *The FASEB Journal* **17**(1): 118-120.

Kins, S., Lauther, N., Szodorai, A. and Beyreuther, K. (2006). "Subcellular Trafficking of the Amyloid Precursor Protein Gene Family and its Pathogenic Role in Alzheimer's Disease." *Neurodegenerative Diseases* **3**(4-5): 218-226.

Kitaguchi, N., Takahashi, Y., Tokushima, Y., Shiojiri, S. and Ito, H. (1988). "Novel Precursor of Alzheimer's Disease Amyloid Protein Shows Protease Inhibitory Activity." *Nature* **331**(6156): 530-532.

Kivipelto, M., Helkala, E.-L., Laakso, M. P., HäNninen, T., Hallikainen, M., Alhainen, K., ... Nissinen, A. (2002). "Apolipoprotein E ε4 Allele, Elevated Midlife Total Cholesterol Level, and High Midlife Systolic Blood Pressure Are Independent Risk Factors for Late-Life Alzheimer Disease." *Annals of Internal Medicine* **137**(3): 149-155.

Kivipelto, M., Helkala, E.-L., Laakso, M. P., Hänninen, T., Hallikainen, M., Alhainen, K., ... Nissinen, A. (2001). "Midlife Vascular Risk Factors and Alzheimer's Disease in Later Life: Longitudinal, Population Based Study." *BMJ* **322**(7300): 1447-1451.

Klewpatinond, M., Davies, P., Bowen, S., Brown, D. R. and Viles, J. H. (2008). "Deconvoluting the Cu^{2+} Binding Modes of Full-Length Prion Protein." *Journal of Biological Chemistry* **283**(4): 1870-1881.

Klewpatinond, M. and Viles, J. H. (2007a). "Empirical Rules for Rationalising Visible Circular Dichroism of Cu^{2+} and Ni^{2+} Histidine Complexes: Applications to the Prion Protein." *FEBS Letters* **581**(7): 1430-1434.

Klewpatinond, M. and Viles, J. H. (2007b). "Fragment Length Influences Affinity for Cu^{2+} and Ni^{2+} Binding to His96 or His111 of the Prion Protein and Spectroscopic Evidence for a Multiple Histidine Binding Only at Low pH." *Biochemical Journal* **404**(3): 393-402.

Klonoff-Cohen, H., Barrett-Connor, E. L. and Edelstein, S. L. (1992). "Albumin Levels as a Predictor of Mortality in the Healthy Elderly." *Journal of Clinical Epidemiology* **45**(3): 207-212.

Koo, E. H., Sisodia, S. S., Archer, D. R., Martin, L. J., Weidemann, A., Beyreuther, K., ... Price, D. L. (1990). "Precursor of Amyloid Protein in Alzheimer Disease Undergoes Fast Anterograde Axonal Transport." *Proceedings of the National Academy of Sciences* **87**(4): 1561-1565.

Kowalik-Jankowska, T., Rajewska, A., Wiśniewska, K., Grzonka, Z. and Jezierska, J. (2005). "Coordination Abilities of N-Terminal Fragments of α-Synuclein Towards Copper(II) Ions: A Combined Potentiometric and Spectroscopic Study." *Journal of Inorganic Biochemistry* **99**(12): 2282-2291.

Kristofikova, Z., Ricny, J., Kolarova, M., Vyhnalek, M., Hort, J., Laczo, J., ... Ripova, D. (2014). "Interactions between Amyloid-β and Tau in Cerebrospinal Fluid of People with Mild Cognitive Impairment and Alzheimer's Disease." *Journal of Alzheimer's Disease* **42**(0): S91-S98.

Kumar, A., Bullard, R. L., Patel, P., Paslay, L. C., Singh, D., Bienkiewicz, E. A., ... Rangachari, V. (2011). "Non-Esterified Fatty Acids Generate Distinct Low-Molecular Weight Amyloid-β (Aβ42) Oligomers Along Pathway Different from Fibril Formation." *PLoS ONE* **6**(4): e18759.

Kuo, Y.-M., Kokjohn, T. A., Kalback, W. M., Luehrs, D., Galasko, D. R., Chevallier, N., ... Roher, A. E. (2000). "Amyloid-Beta Peptides Interact with Plasma Proteins and Erythrocytes: Implications for Their Quantitation in Plasma." *Biochemical and Biophysical Research Communications* **268**: 750-756.

Lai, A., Sisodia, S. S. and Trowbridge, I. S. (1995). "Characterization of Sorting Signals in the β-Amyloid Precursor Protein Cytoplasmic Domain." *Journal of Biological Chemistry* **270**(8): 3565-3573.

Laitinen, M., Ngandu, T., Rovio, S., Helkala, E.-L., Uusitalo, U., Viitanen, M., ... Kivipelto, M. (2006). "Fat Intake at Midlife and Risk of Dementia and Alzheimer's Disease: A Population-Based Study." *Dementia and geriatric cognitive disorders* **22**(1): 99-107.

Lakowicz, J. R. (1999). *Principles of Fluorescence Spectroscopy*, Springer.

Lambert, J.-C., Ibrahim-Verbaas, C. A., Harold, D., Naj, A. C., Sims, R., Bellenguez, C., ... Amouyel, P. (2013). "Meta-Analysis of 74,046 Individuals Identifies 11 New Susceptibility Loci for Alzheimer's Disease." *Nature Genetics* **45**(12): 1452-1458.

Lambert, M. P., Barlow, A. K., Chromy, B. A., Edwards, C., Freed, R., Liosatos, M., ... Klein, W. L. (1998). "Diffusible, Nonfibrillar Ligands Derived from Aβ1–42 Are Potent Central Nervous System Neurotoxins." *Proceedings of the National Academy of Sciences* **95**(11): 6448-6453.

Lame, M. E., Chambers, E. E. and Blatnik, M. (2011). "Quantitation of Amyloid Beta Peptides Aβ1–38, Aβ1–40, and Aβ1–42 in Human Cerebrospinal Fluid by Ultra-Performance Liquid Chromatography–Tandem Mass Spectrometry." *Analytical Biochemistry* **419**(2): 133-139.

Lasagna-Reeves, C. A., Glabe, C. G. and Kayed, R. (2011). "Amyloid-β Annular Protofibrils Evade Fibrillar Fate in Alzheimer Disease Brain." *Journal of Biological Chemistry* **286**(25): 22122-22130.

Lashuel, H. A., Hartley, D., Petre, B. M., Walz, T. and Lansbury, P. T. (2002). "Neurodegenerative Disease: Amyloid Pores from Pathogenic Mutations." *Nature* **418**(6895): 291-291.

Lashuel, H. A., Hartley, D. M., Petre, B. M., Wall, J. S., Simon, M. N., Walz, T. and Lansbury Jr, P. T. (2003). "Mixtures of Wild-Type and a Pathogenic (E22G) Form of Aβ40 in

Vitro Accumulate Protofibrils, Including Amyloid Pores." *Journal of Molecular Biology* **332**(4): 795-808.

Laurén, J., Gimbel, D. A., Nygaard, H. B., Gilbert, J. W. and Strittmatter, S. M. (2009). "Cellular Prion Protein Mediates Impairment of Synaptic Plasticity by Amyloid-β Oligomers." *Nature* **457**(7233): 1128-1132.

Lazarov, O., Lee, M., Peterson, D. A. and Sisodia, S. S. (2002). "Evidence That Synaptically Released β-Amyloid Accumulates as Extracellular Deposits in the Hippocampus of Transgenic Mice." *The Journal of Neuroscience* **22**(22): 9785-9793.

Lee, S. J. (2008). "Origins and Effects of Extracellular Alpha-Synuclein: Implications in Parkinson's Disease." *Journal of Molecular Neuroscience* **34**(1): 17-22.

Leonard, P., Shaper, A. and Jones, K. (1965). "Relationship between Free and Total Cholesterol Values in Human Serum." *The American Journal of Clinical Nutrition* **17**(6): 377-380.

Lesné, S., Ali, C., Gabriel, C., Croci, N., Mackenzie, E. T., Glabe, C. G., ... Buisson, A. (2005). "NMDA Receptor Activation Inhibits α-Secretase and Promotes Neuronal Amyloid-β Production." *The Journal of Neuroscience* **25**(41): 9367-9377.

Lesné, S., Koh, M. T., Kotilinek, L., Kayed, R., Glabe, C. G., Yang, A., ... Ashe, K. H. (2006). "A Specific Amyloid-β Protein Assembly in the Brain Impairs Memory." *Nature* **440**(7082): 352-357.

Levine, H., 3rd (1993). "Thioflavine T Interaction with Synthetic Alzheimer's Disease Beta-Amyloid Peptides: Detection of Amyloid Aggregation in Solution." *Protein Science* **2**(3): 404-410.

Levy, E., Jaskolski, M. and Grubb, A. (2006). "The Role of Cystatin C in Cerebral Amyloid Angiopathy and Stroke: Cell Biology and Animal Models." *Brain Pathology* **16**(1): 60-70.

Li, S., Hong, S., Shepardson, N. E., Walsh, D. M., Shankar, G. M. and Selkoe, D. (2009). "Soluble Oligomers of Amyloid β Protein Facilitate Hippocampal Long-Term Depression by Disrupting Neuronal Glutamate Uptake." *Neuron* **62**(6): 788-801.

Li, S., Jin, M., Koeglsperger, T., Shepardson, N. E., Shankar, G. M. and Selkoe, D. J. (2011a). "Soluble Aβ Oligomers Inhibit Long-Term Potentiation through a Mechanism Involving Excessive Activation of Extrasynaptic NR2B-Containing NMDA Receptors." *The Journal of Neuroscience* **31**(18): 6627-6638.

Li, X., Masliah, E., Reixach, N. and Buxbaum, J. N. (2011b). "Neuronal Production of Transthyretin in Human and Murine Alzheimer's Disease: Is It Protective?" *The Journal of Neuroscience* **31**(35): 12483-12490.

Licastro, F., Morini, M. C., Davis, L. J., Biagi, R., Prete, L. and Savorani, G. (1993). "Studies of Blood-Brain-Barrier Permeability and of Intrathecal IgG Synthesis in Patients with

Alzheimer's Disease and Multi-Infarct Dementia." *Advances in Biosciences* **87**: 283-284.

Likó, I., Mák, M., Klement, É., Hunyadi-Gulyás, É., Pázmány, T., Medzihradszky, K. F. and Urbányi, Z. (2007). "Evidence for an Extended Interacting Surface between β-Amyloid and Serum Amyloid P Component." *Neuroscience Letters* **412**(1): 51-55.

Lipton, P. (1999). "Ischemic Cell Death in Brain Neurons." *Physiological Reviews* **79**(4): 1431-1568.

Liu, B., Moloney, A., Meehan, S., Morris, K., Thomas, S. E., Serpell, L. C., ... Crowther, D. C. (2011). "Iron Promotes the Toxicity of Amyloid β Peptide by Impeding Its Ordered Aggregation." *Journal of Biological Chemistry* **286**(6): 4248-4256.

Liu, L. and Murphy, R. M. (2006). "Kinetics of Inhibition of β-Amyloid Aggregation by Transthyretin." *Biochemistry* **45**(51): 15702-15709.

Lovell, M. A., Robertson, J. D., Teesdale, W. J., Campbell, J. L. and Markesbery, W. R. (1998). "Copper, Iron and Zinc in Alzheimer's Disease Senile Plaques." *Journal of the Neurological Sciences* **158**(1): 47-52.

Lu, J.-X., Qiang, W., Yau, W.-M., Schwieters, C. D., Meredith, S. C. and Tycko, R. (2013). "Molecular Structure of β-Amyloid Fibrils in Alzheimer's Disease Brain Tissue." *Cell* **154**(6): 1257-1268.

Luo, J., Wärmländer, S. K. T. S., Gräslund, A. and Abrahams, J. P. (2014). "Non-Chaperone Proteins Can Inhibit Aggregation and Cytotoxicity of Alzheimer Amyloid β Peptide." *Journal of Biological Chemistry* **289**(40): 27766-27775.

Lütjohann, D., Breuer, O., Ahlborg, G., Nennesmo, I., Siden, A., Diczfalusy, U. and Björkhem, I. (1996). "Cholesterol Homeostasis in Human Brain: Evidence for an Age-Dependent Flux of 24S-Hydroxycholesterol from the Brain into the Circulation." *Proceedings of the National Academy of Sciences* **93**(18): 9799-9804.

Ma, Q.-F., Hu, J., Wu, W.-H., Liu, H.-D., Du, J.-T., Fu, Y., ... Li, Y.-M. (2006). "Characterization of Copper Binding to the Peptide Amyloid-β(1–16) Associated with Alzheimer's Disease." *Biopolymers* **83**(1): 20-31.

Mackic, J. B., Weiss, M. H., Miao, W., Kirkman, E., Ghiso, J., Calero, M., ... Zlokovic, B. V. (1998). "Cerebrovascular Accumulation and Increased Blood-Brain Barrier Permeability to Circulating Alzheimer's Amyloid β Peptide in Aged Squirrel Monkey with Cerebral Amyloid Angiopathy." *Journal of Neurochemistry* **70**(1): 210-215.

Maesako, M., Uemura, K., Kubota, M., Kuzuya, A., Sasaki, K., Asada, M., ... Kinoshita, A. (2012a). "Environmental Enrichment Ameliorated High-Fat Diet-Induced Aβ Deposition and Memory Deficit in APP Transgenic Mice." *Neurobiology of Aging* **33**(5): 1011.e1011-1011.e1023.

Maesako, M., Uemura, K., Kubota, M., Kuzuya, A., Sasaki, K., Hayashida, N., ... Kihara, T. (2012b). "Exercise Is More Effective Than Diet Control in Preventing High Fat Diet-

Induced β-Amyloid Deposition and Memory Deficit in Amyloid Precursor Protein Transgenic Mice." *Journal of Biological Chemistry* **287**(27): 23024-23033.

Mahdi, A. A., Tripathi, S., Neerja, J. and Hasan, M. (2010). "Aluminium Mediated Oxidative Stress: Possible Relationship to Cognitive Impairment of Alzheimer's Type." *Annals of Neurosciences* **13**(1): 18-24.

Maiti, N. C., Jiang, D., Wain, A. J., Patel, S., Dinh, K. L. and Zhou, F. (2008). "Mechanistic Studies of Cu (II) Binding to Amyloid-β Peptides and the Fluorescence and Redox Behaviors of the Resulting Complexes." *The Journal of Physical Chemistry B* **112**(28): 8406-8411.

Makin, O. S. and Serpell, L. C. (2005). "Structures for Amyloid Fibrils." *FEBS Journal* **272**(23): 5950-5961.

Manczak, M. and Reddy, P. H. (2013). "Abnormal Interaction of Oligomeric Amyloid-β with Phosphorylated Tau: Implications to Synaptic Dysfunction and Neuronal Damage." *Journal of Alzheimer's Disease* **36**(2): 285-295.

Marquez-Sterling, N. R., Lo, A. C., Sisodia, S. S. and Koo, E. H. (1997). "Trafficking of Cell-Surface β-Amyloid Precursor Protein: Evidence That a Sorting Intermediate Participates in Synaptic Vesicle Recycling." *The Journal of Neuroscience* **17**(1): 140-151.

Martin, R. B. (1974). "Optical Properties of Transition Metal Ion Complexes of Amino Acids and Peptides." *Metal Ions in Biological Systems* **1**: 129-156.

Martin, S. R. and Schilstra, M. J. (2008). Circular Dichroism and Its Application to the Study of Biomolecules. *Biophysical Tools for Biologists, Volume 1: In Vitro Techniques*. J. J. Correia and H. W. Detrich III. London, Academic Press. **84:** 263-293.

Maruyama, K., Ikeda, S.-I., Ishihara, T., Allsop, D. and Yanagisawa, N. (1990). "Immunohistochemical Characterization of Cerebrovascular Amyloid in 46 Autopsied Cases Using Antibodies to Beta Protein and Cystatin C." *Stroke* **21**(3): 397-403.

Masters, C. L., Simms, G., Weinman, N. A., Multhaup, G., Mcdonald, B. L. and Beyreuther, K. (1985). "Amyloid Plaque Core Protein in Alzheimer Disease and Down Syndrome." *Proceedings of the National Academy of Sciences* **82**(12): 4245-4249.

Matheou, C. J., Younan, N. D. and Viles, J. H. (2014). "Cu^{2+} Accentuates Distinct Misfolding for Aβ(1-40) and Aβ(1-42) Peptides, and Potentiates Membrane Disruption." *Biochemical Journal*.

Matsumura, S., Shinoda, K., Yamada, M., Yokojima, S., Inoue, M., Ohnishi, T., ... Hoshi, M. (2011). "Two Distinct Amyloid β-Protein (Aβ) Assembly Pathways Leading to Oligomers and Fibrils Identified by Combined Fluorescence Correlation Spectroscopy, Morphology, and Toxicity Analyses." *Journal of Biological Chemistry* **286**(13): 11555-11562.

Mattson, M. P. (2004). "Pathways Towards and Away from Alzheimer's Disease." *Nature* **430**(7000): 631-639.

Meinhardt, J., Sachse, C., Hortschansky, P., Grigorieff, N. and Fändrich, M. (2009). "Aβ(1-40) Fibril Polymorphism Implies Diverse Interaction Patterns in Amyloid Fibrils." *Journal of Molecular Biology* **386**(3): 869-877.

Meloni, G. and Vašák, M. (2011). "Redox Activity of α-Synuclein–Cu Is Silenced by Zn7-Metallothionein-3." *Free Radical Biology and Medicine* **50**(11): 1471-1479.

Meyer-Luehmann, M., Spires-Jones, T. L., Prada, C., Garcia-Alloza, M., De Calignon, A., Rozkalne, A., ... Hyman, B. T. (2008). "Rapid Appearance and Local Toxicity of Amyloid-Beta Plaques in a Mouse Model of Alzheimer's Disease." *Nature* **451**(7179): 720-724.

Mi, W., Pawlik, M., Sastre, M., Jung, S. S., Radvinsky, D. S., Klein, A. M., ... Mathews, P. M. (2007). "Cystatin C Inhibits Amyloid-β Deposition in Alzheimer's Disease Mouse Models." *Nature Genetics* **39**(12): 1440-1442.

Milanesi, L., Sheynis, T., Xue, W.-F., Orlova, E. V., Hellewell, A. L., Jelinek, R., ... Saibil, H. R. (2012). "Direct Three-Dimensional Visualization of Membrane Disruption by Amyloid Fibrils." *Proceedings of the National Academy of Sciences* **109**(50): 20455-20460.

Miller, L. M., Wang, Q., Telivala, T. P., Smith, R. J., Lanzirotti, A. and Miklossy, J. (2006). "Synchrotron-Based Infrared and X-Ray Imaging Shows Focalized Accumulation of Cu and Zn Co-Localized with β-Amyloid Deposits in Alzheimer's Disease." *Journal of Structural Biology* **155**(1): 30-37.

Miller, Y., Ma, B. and Nussinov, R. (2010). "Zinc Ions Promote Alzheimer Aβ Aggregation Via Population Shift of Polymorphic States." *Proceedings of the National Academy of Sciences* **107**(21): 9490-9495.

Millhauser, G. L. (2004). "Copper Binding in the Prion Protein." *Accounts of Chemical Research* **37**(2): 79-85.

Milojevic, J., Costa, M., Ortiz, A. M., Jorquera, J. I. and Melacini, G. (2014). "In Vitro Amyloid-β Binding and Inhibition of Amyloid-β Self-Association by Therapeutic Albumin." *Journal of Alzheimer's Disease* **38**(4): 753-765.

Milojevic, J., Esposito, V., Das, R. and Melacini, G. (2007). "Understanding the Molecular Basis for the Inhibition of the Alzheimer's Aβ-Peptide Oligomerization by Human Serum Albumin Using Saturation Transfer Difference and Off-Resonance Relaxation NMR Spectroscopy." *Journal of the American Chemical Society* **129**(14): 4282-4290.

Milojevic, J. and Melacini, G. (2011). "Stoichiometry and Affinity of the Human Serum Albumin-Alzheimer's Abeta Peptide Interactions." *Biophysical Journal* **100**(1): 183-192.

Milojevic, J., Raditsis, A. and Melacini, G. (2009). "Human Serum Albumin Inhibits Aβ Fibrillization through a "Monomer-Competitor" Mechanism." *Biophysical Journal* **97**(9): 2585-2594.

Minicozzi, V., Stellato, F., Comai, M., Serra, M. D., Potrich, C., Meyer-Klaucke, W. and Morante, S. (2008). "Identifying the Minimal Copper- and Zinc-Binding Site Sequence in Amyloid-β Peptides." *Journal of Biological Chemistry* **283**(16): 10784-10792.

Monaco, H. L. (2002). "Three-Dimensional Structure of the Transthyretin-Retinol-Binding Protein Complex." *Clinical Chemistry and Laboratory Medicine* **40**(12): 1229-1236.

Mori, T. and Inoue, Y. (2011). "Recent Theoretical and Experimental Advances in the Electronic Circular Dichroisms of Planar Chiral Cyclophanes." *Electronic and Magnetic Properties of Chiral Molecules and Supramolecular Architectures* **298**: 99-128.

Mori, T., Paris, D., Town, T., Rojiani, A. M., Sparks, D. L., Delledonne, A., ... Dickson, D. W. (2001). "Cholesterol Accumulates in Senile Plaques of Alzheimer Disease Patients and in Transgenic APPsw Mice." *Journal of Neuropathology & Experimental Neurology* **60**(8): 778-785.

Morris, M., Evans, D. A., Bienias, J. L. and Et Al. (2003). "Dietary Fats and the Risk of Incident Alzheimer Disease." *Archives of Neurology* **60**(2): 194-200.

Murakami, K., Irie, K., Morimoto, A., Ohigashi, H., Shindo, M., Nagao, M., ... Shirasawa, T. (2002). "Synthesis, Aggregation, Neurotoxicity, and Secondary Structure of Various Aβ1–42 Mutants of Familial Alzheimer's Disease at Positions 21–23." *Biochemical and Biophysical Research Communications* **294**(1): 5-10.

Mylonas, M., Krezel, A., Plakatouras, J. C., Hadjiliadis, N. and Bal, W. (2002a). "The Binding of Ni(II) Ions to Terminally Blocked Hexapeptides Derived from the Metal Binding -ESHH- Motif of Histone H2A." *Journal of the Chemical Society, Dalton Transactions*(22): 4296-4306.

Mylonas, M., Plakatouras, J. C., Hadjiliadis, N., Krężel, A. and Bal, W. (2002b). "Potentiometric and Spectroscopic Studies of the Interaction of Cu(II) Ions with the Hexapeptides $AcThrAlaSerHisHisLysNH_2$, $AcThrGluAlaHisHisLysNH_2$, $AcThrGluSerAlaHisLysNH_2$ and $AcThrGluSerHisAlaLysNH_2$, Models of C-Terminal Tail of Histone H2A." *Inorganica Chimica Acta* **339**(0): 60-70.

Nadal, R. C., Davies, P., Brown, D. R. and Viles, J. H. (2009). "Evaluation of $Copper^{2+}$ Affinities for the Prion Protein." *Biochemistry* **48**(38): 8929-8931.

Narayan, P., Meehan, S., Carver, J. A., Wilson, M. R., Dobson, C. M. and Klenerman, D. (2012a). "Amyloid-Beta Oligomers Are Sequestered by Both Intracellular and Extracellular Chaperones." *Biochemistry* **51**(46): 9270-9276.

Narayan, P., Orte, A., Clarke, R. W., Bolognesi, B., Hook, S., Ganzinger, K. A., ... Klenerman, D. (2012b). "The Extracellular Chaperone Clusterin Sequesters Oligomeric Forms of

the Amyloid-Beta(1-40) Peptide." *Nature Structural & Molecular Biology* **19**(1): 79-83.

Nielsen, H. and Hansen, T. (2000). "Localization of Human Serum Amyloid P Component and Heparan Sulfate Proteoglycan in in Vitro-Formed Aβ Fibrils." *Scandinavian Journal of Immunology* **52**(2): 110-112.

Nilsson, M. R. (2004). "Techniques to Study Amyloid Fibril Formation in Vitro." *Methods Investigating Protein Folding, Misfolding and Nonnative States: Experimental and Theoretical Methods* **34**(1): 151-160.

Nixon, R. A. (2007). "Autophagy, Amyloidogenesis and Alzheimer Disease." *Journal of Cell Science* **120**(23): 4081-4091.

Noguchi, A., Matsumura, S., Dezawa, M., Tada, M., Yanazawa, M., Ito, A., ... Hoshi, M. (2009). "Isolation and Characterization of Patient-Derived, Toxic, High Mass Amyloid β-Protein (Aβ) Assembly from Alzheimer Disease Brains." *Journal of Biological Chemistry* **284**(47): 32895-32905.

Notkola, I., Sulkava, R., Pekkanen, J., Erkinjuntti, T., Ehnholm, C., Kivinen, P., ... Nissinen, A. (1998). "Serum Total Cholesterol, Apolipoprotein E Epsilon 4 Allele, and Alzheimer's Disease." *Neuroepidemiology* **17**: 14-20.

Noy, D., Solomonov, I., Sinkevich, O., Arad, T., Kjaer, K. and Sagi, I. (2008). "Zinc-Amyloid β Interactions on a Millisecond Time-Scale Stabilize Non-Fibrillar Alzheimer-Related Species." *Journal of the American Chemical Society* **130**(4): 1376-1383.

Nunomura, A., Honda, K., Takeda, A., Hirai, K., Zhu, X., Smith, M. A. and Perry, G. (2006). "Oxidative Damage to RNA in Neurodegenerative Diseases." *Journal of Biomedicine & Biotechnology* **2006**(3): 82323.

O'Boyle, N. M., Tenderholt, A. L. and Langner, K. M. (2008). "cclib: A Library for Package-Independent Computational Chemistry Algorithms." *Journal of Computational Chemistry* **29**(5): 839-845.

O'Nuallain, B., Shivaprasad, S., Kheterpal, I. and Wetzel, R. (2005). "Thermodynamics of Aβ(1−40) Amyloid Fibril Elongation." *Biochemistry* **44**(38): 12709-12718.

O'Nuallain, B., Williams, A. D., Westermark, P. and Wetzel, R. (2004). "Seeding Specificity in Amyloid Growth Induced by Heterologous Fibrils." *Journal of Biological Chemistry* **279**(17): 17490-17499.

Office for National Statistics (2011). Deaths Registered in England and Wales in 2010, by Cause.

Orfei, M., Alcaro, M. C., Marcon, G., Chelli, M., Ginanneschi, M., Kozlowski, H., ... Messori, L. (2003). "Modeling of Copper (II) Sites in Proteins Based on Histidyl and Glycyl Residues." *Journal of Inorganic Biochemistry* **97**(3): 299-307.

Ősz, K., Nagy, Z., Pappalardo, G., Di Natale, G., Sanna, D., Micera, G., ... Sóvágó, I. (2007). "Copper(II) Interaction with Prion Peptide Fragments Encompassing Histidine Residues within and Outside the Octarepeat Domain: Speciation, Stability Constants and Binding Details." *Chemistry – A European Journal* **13**(25): 7129-7143.

Pace, C. N., Fu, H. L., Fryar, K. L., Landua, J., Trevino, S. R., Shirley, B. A., ... Grimsley, G. R. (2011). "Contribution of Hydrophobic Interactions to Protein Stability." *Journal of Molecular Biology* **408**(3): 514-528.

Paik, S. R., Shin, H. J., Lee, J. H., Chang, C. S. and Kim, J. (1999). "Copper(II)-Induced Self-Oligomerization of Alpha-Synuclein." *Biochemical Journal* **340 (Pt 3)**: 821-828.

Pall, H. S., Blake, D. R., Gutteridge, J. M., Williams, A. C., Lunec, J., Hall, M. and Taylor, A. (1987). "Raised Cerebrospinal-Fluid Copper Concentration in Parkinson's Disease." *The Lancet* **330**(8553): 238-241.

Paravastu, A. K., Leapman, R. D., Yau, W.-M. and Tycko, R. (2008). "Molecular Structural Basis for Polymorphism in Alzheimer's β-Amyloid Fibrils." *Proceedings of the National Academy of Sciences* **105**(47): 18349-18354.

Parthasarathy, S., Long, F., Miller, Y., Xiao, Y., Mcelheny, D., Thurber, K., ... Ishii, Y. (2011). "Molecular-Level Examination of Cu^{2+} Binding Structure for Amyloid Fibrils of 40-Residue Alzheimer's Beta by Solid-State NMR Spectroscopy." *Journal of the American Chemical Society* **133**(10): 3390-3400.

Pasternak, S. H., Callahan, J. W. and Mahuran, D. J. (2004). "The Role of the Endosomal/ Lysosomal System in Amyloid-Beta Production and the Pathophysiology of Alzheimer's Disease: Reexamining the Spatial Paradox from a Lysosomal Perspective." *Journal of Alzheimer's Disease* **6**(1): 53-65.

Pastorino, L., Ikin, A. F., Nairn, A. C., Pursnani, A. and Buxbaum, J. D. (2002). "The Carboxyl-Terminus of BACE Contains a Sorting Signal That Regulates BACE Trafficking but Not the Formation of Total Aβ." *Molecular and Cellular Neuroscience* **19**(2): 175-185.

Patel, S. U., Sadler, P. J., Tucker, A. and Viles, J. H. (1993). "Direct Detection of Albumin in Human Blood Plasma by Proton NMR Spectroscopy. Complexation of $Nickel^{2+}$." *Journal of the American Chemical Society* **115**(20): 9285-9286.

Peisach, J. and Blumberg, W. (1974). "Structural Implications Derived from the Analysis of Electron Paramagnetic Resonance Spectra of Natural and Artificial Copper Proteins." *Archives of Biochemistry and Biophysics* **165**(2): 691-708.

Peng, L., Minbo, H., Fang, C., Xi, L. and Chaocan, Z. (2008). "The Interaction between Cholesterol and Human Serum Albumin." *Protein and Peptide Letters* **15**(4): 360-364.

Pepys, M., Baltz, M. L., De Beer, F., Dyck, R., Holford, S., Breathnach, S., ... Feinstein, A. (1982). "Biology of Serum Amyloid P Component." *Annals of the New York Academy of Sciences* **389**(1): 286-298.

Perera, W. S. S. and Hooper, N. M. (2001). "Ablation of the Metal Ion-Induced Endocytosis of the Prion Protein by Disease-Associated Mutation of the Octarepeat Region." *Current Biology* **11**(7): 519-523.

Perez, R. G., Soriano, S., Hayes, J. D., Ostaszewski, B., Xia, W., Selkoe, D. J., ... Koo, E. H. (1999). "Mutagenesis Identifies New Signals for β-Amyloid Precursor Protein Endocytosis, Turnover, and the Generation of Secreted Fragments, Including Aβ42." *Journal of Biological Chemistry* **274**(27): 18851-18856.

Perrone, L., Mothes, E., Vignes, M., Mockel, A., Figueroa, C., Miquel, M.-C., ... Faller, P. (2010). "Copper Transfer from Cu–Aβ to Human Serum Albumin Inhibits Aggregation, Radical Production and Reduces Aβ Toxicity." *ChemBioChem* **11**(1): 110-118.

Pescitelli, G., Kurtan, T., Florke, U. and Krohn, K. (2009). "Absolute Structural Elucidation of Natural Products-a Focus on Quantum-Mechanical Calculations of Solid-State CD Spectra." *Chirality* **21**(1E): E181-E201.

Petitpas, I., Petersen, C. E., Ha, C.-E., Bhattacharya, A. A., Zunszain, P. A., Ghuman, J., ... Curry, S. (2003). "Structural Basis of Albumin–Thyroxine Interactions and Familial Dysalbuminemic Hyperthyroxinemia." *Proceedings of the National Academy of Sciences* **100**(11): 6440-6445.

Petkova, A. T., Ishii, Y., Balbach, J. J., Antzutkin, O. N., Leapman, R. D., Delaglio, F. and Tycko, R. (2002). "A Structural Model for Alzheimer's β-Amyloid Fibrils Based on Experimental Constraints from Solid State NMR." *Proceedings of the National Academy of Sciences* **99**(26): 16742-16747.

Petkova, A. T., Leapman, R. D., Guo, Z., Yau, W.-M., Mattson, M. P. and Tycko, R. (2005). "Self-Propagating, Molecular-Level Polymorphism in Alzheimer's β-Amyloid Fibrils." *Science* **307**(5707): 262-265.

Ponte, P., Gonzalez-Dewhitt, P., Schilling, J., Miller, J., Hsu, D., Greenberg, B., ... Fuller, F. (1988). "A New A4 Amyloid mRNA Contains a Domain Homologous to Serine Proteinase Inhibitors." *Nature* **331**(6156): 525-527.

Priller, C., Bauer, T., Mitteregger, G., Krebs, B., Kretzschmar, H. A. and Herms, J. (2006). "Synapse Formation and Function Is Modulated by the Amyloid Precursor Protein." *The Journal of Neuroscience* **26**(27): 7212-7221.

Putnam, F. W. (1975). *The Plasma Proteins 2e V1: Structure, Function, and Genetic Control*, Elsevier Science.

Qiu, W. Q., Wallack, M., Dean, M., Liebson, E., Mwamburi, M. and Zhu, H. (2014). "Association between Amylin and Amyloid-β Peptides in Plasma in the Context of Apolipoprotein E4 Allele." *PLoS ONE* **9**(2): e88063.

Raichle, M. E., Macleod, A. M., Snyder, A. Z., Powers, W. J., Gusnard, D. A. and Shulman, G. L. (2001). "A Default Mode of Brain Function." *Proceedings of the National Academy of Sciences* **98**(2): 676-682.

Raman, B., Ban, T., Yamaguchi, K.-I., Sakai, M., Kawai, T., Naiki, H. and Goto, Y. (2005). "Metal Ion-Dependent Effects of Clioquinol on the Fibril Growth of an Amyloid β Peptide." *Journal of Biological Chemistry* **280**(16): 16157-16162.

Rammes, G., Hasenjäger, A., Sroka-Saidi, K., Deussing, J. M. and Parsons, C. G. (2011). "Therapeutic Significance of NR2B-Containing NMDA Receptors and mGluR5 Metabotropic Glutamate Receptors in Mediating the Synaptotoxic Effects of β-Amyloid Oligomers on Long-Term Potentiation (LTP) in Murine Hippocampal Slices." *Neuropharmacology* **60**(6): 982-990.

Rapoport, M., Dawson, H. N., Binder, L. I., Vitek, M. P. and Ferreira, A. (2002). "Tau Is Essential to β-Amyloid-Induced Neurotoxicity." *Proceedings of the National Academy of Sciences* **99**(9): 6364-6369.

Rasia, R. M., Bertoncini, C. W., Marsh, D., Hoyer, W., Cherny, D., Zweckstetter, M., ... Fernández, C. O. (2005). "Structural Characterization of Copper(II) Binding to α-Synuclein: Insights into the Bioinorganic Chemistry of Parkinson's Disease." *Proceedings of the National Academy of Sciences* **102**(12): 4294-4299.

Raz, A. and Goodman, D. S. (1969). "The Interaction of Thyroxine with Human Plasma Prealbumin and with the Prealbumin-Retinol-Binding Protein Complex." *Journal of Biological Chemistry* **244**(12): 3230-3237.

Refolo, L. M., Pappolla, M. A., Lafrancois, J., Malester, B., Schmidt, S. D., Thomas-Bryant, T., ... Duff, K. E. (2001). "A Cholesterol-Lowering Drug Reduces β-Amyloid Pathology in a Transgenic Mouse Model of Alzheimer's Disease." *Neurobiology of Disease* **8**(5): 890-899.

Refolo, L. M., Pappolla, M. A., Malester, B., Lafrancois, J., Bryant-Thomas, T., Wang, R., ... Duff, K. (2000). "Hypercholesterolemia Accelerates the Alzheimer's Amyloid Pathology in a Transgenic Mouse Model." *Neurobiology of Disease* **7**(4): 321-331.

Reyes Barcelo, A., Gonzalez-Velasquez, F. and Moss, M. (2009). "Soluble Aggregates of the Amyloid-Beta Peptide Are Trapped by Serum Albumin to Enhance Amyloid-Beta Activation of Endothelial Cells." *Journal of Biological Engineering* **3**(1): 5-12.

Riddell, D. R., Christie, G., Hussain, I. and Dingwall, C. (2001). "Compartmentalization of β-Secretase (Asp2) into Low-Buoyant Density, Noncaveolar Lipid Rafts." *Current Biology* **11**(16): 1288-1293.

Riisøen, H. (1988). "Reduced Prealbumin (Transthyretin) in CSFof Severely Demented Patients with Alzheimer's Disease." *Acta Neurologica Scandinavica* **78**(6): 455-459.

Rival, T., Page, R. M., Chandraratna, D. S., Sendall, T. J., Ryder, E., Liu, B., ... Camargo, L. (2009). "Fenton Chemistry and Oxidative Stress Mediate the Toxicity of the β-Amyloid Peptide in a Drosophila Model of Alzheimer's Disease." *European Journal of Neuroscience* **29**(7): 1335-1347.

Roberts, G. W., Gentleman, S. M., Lynch, A., Murray, L., Landon, M. and Graham, D. I. (1994). "Beta Amyloid Protein Deposition in the Brain after Severe Head Injury:

Implications for the Pathogenesis of Alzheimer's Disease." *Journal Neurology, Neurosurgery & Psychiatry* **57**(4): 419-425.

Rönicke, R., Mikhaylova, M., Rönicke, S., Meinhardt, J., Schröder, U. H., Fändrich, M., ... Reymann, K. G. (2011). "Early Neuronal Dysfunction by Amyloid β Oligomers Depends on Activation of NR2B-Containing NMDA Receptors." *Neurobiology of Aging* **32**(12): 2219-2228.

Rózga, M. and Bal, W. (2010). "The Cu(II)/Abeta/Human Serum Albumin Model of Control Mechanism for Copper-Related Amyloid Neurotoxicity." *Chemical Research in Toxicology* **23**(2): 298-308.

Rózga, M., Kłoniecki, M., Dadlez, M. and Bal, W. (2009). "A Direct Determination of the Dissociation Constant for the Cu (II) Complex of Amyloid β 1− 40 Peptide." *Chemical Research in Toxicology* **23**(2): 336-340.

Rózga, M., Kloniecki, M., Jablonowska, A., Dadlez, M. and Bal, W. (2007a). "The Binding Constant for Amyloid Aβ40 Peptide Interaction with Human Serum Albumin." *Biochemical and Biophysical Research Communications* **364**(3): 714-718.

Rózga, M., Sokołowska, M., Protas, A. M. and Bal, W. (2007b). "Human Serum Albumin Coordinates Cu (II) at Its N-Terminal Binding Site with 1 pM Affinity." *JBIC Journal of Biological Inorganic Chemistry* **12**(6): 913-918.

Sadler, P. J., Tucker, A. and Viles, J. H. (1994). "Involvement of a Lysine Residue in the N-Terminal Ni^{2+} and Cu^{2+} Binding Site of Serum Albumins." *European Journal of Biochemistry* **220**(1): 193-200.

Saifer, A. and Goldman, L. (1961). "The Free Fatty Acids Bound to Human Serum Albumin." *Journal of Lipid Research* **2**(3): 268-270.

Sanokawa-Akakura, R., Cao, W., Allan, K., Patel, K., Ganesh, A., Heiman, G., ... Konsolaki, M. (2010). "Control of Alzheimer's Amyloid Beta Toxicity by the High Molecular Weight Immunophilin FKBP52 and Copper Homeostasis in *Drosophila*." *PLoS ONE* **5**(1): e8626.

Sarell, C. J. (2010). "The Copper-Amyloid-Beta-Peptide Complex of Alzheimer's Disease: Affinity, Structure, Fibril Formation and Toxicity" Doctoral Thesis, Queen Mary, University of London.

Sarell, C. J., Syme, C. D., Rigby, S. E. and Viles, J. H. (2009). "Copper(II) Binding to Amyloid-Beta Fibrils of Alzheimer's Disease Reveals a Picomolar Affinity: Stoichiometry and Coordination Geometry Are Independent of Abeta Oligomeric Form." *Biochemistry* **48**(20): 4388-4402.

Sarell, C. J., Wilkinson, S. R. and Viles, J. H. (2010). "Substoichiometric Levels of Cu^{2+} Ions Accelerate the Kinetics of Fiber Formation and Promote Cell Toxicity of Amyloid-Beta from Alzheimer Disease." *Journal of Biological Chemistry* **285**(53): 41533-41540.

Sastre, M., Calero, M., Pawlik, M., Mathews, P. M., Kumar, A., Danilov, V., ... Levy, E. (2004). "Binding of Cystatin C to Alzheimer's Amyloid β Inhibits in Vitro Amyloid Fibril Formation." *Neurobiology of Aging* **25**(8): 1033-1043.

Scheuner, D., Eckman, C., Jensen, M., Song, X., Citron, M., Suzuki, N., ... Younkin, S. (1996). "Secreted Amyloid Beta-Protein Similar to That in the Senile Plaques of Alzheimer's Disease Is Increased in Vivo by the Presenilin 1 and 2 and APP Mutations Linked to Familial Alzheimer's Disease." *Nature Medicine* **2**(8): 864-870.

Schwarzman, A. L., Gregori, L., Vitek, M. P., Lyubski, S., Strittmatter, W. J., Enghilde, J. J., ... Coyle, P. K. (1994). "Transthyretin Sequesters Amyloid Beta Protein and Prevents Amyloid Formation." *Proceedings of the National Academy of Sciences* **91**(18): 8368-8372.

Schwarzman, A. L., Tsiper, M., Wente, H., Wang, A., Vitek, M. P., Vasiliev, V. and Goldgaber, D. (2004). "Amyloidogenic and Anti-Amyloidogenic Properties of Recombinant Transthyretin Variants." *Amyloid* **11**(1): 1-10.

Selenica, M., Wang, X., Ostergaard-Pedersen, L., Westlind-Danielsson, A. and Grubb, A. (2007). "Cystatin C Reduces the in Vitro Formation of Soluble Aβ1-42 Oligomers and Protofibrils." *Scandinavian Journal of Clinical & Laboratory Investigation* **67**(2): 179-190.

Serot, J., Christmann, D., Dubost, T. and Couturier, M. (1997). "Cerebrospinal Fluid Transthyretin: Aging and Late Onset Alzheimer's Disease." *Journal of Neurology, Neurosurgery & Psychiatry* **63**(4): 506-508.

Seubert, P., Vigo-Pelfrey, C., Esch, F., Lee, M., Dovey, H., Davis, D., ... Swindlehurst, C. (1992). "Isolation and Quantification of Soluble Alzheimer's β-Peptide from Biological Fluids." *Nature* **359**(6393): 325-327.

Shafrir, Y., Durell, S., Arispe, N. and Guy, H. R. (2010). "Models of Membrane-Bound Alzheimer's Abeta Peptide Assemblies." *Proteins: Structure, Function, and Bioinformatics* **78**(16): 3473-3487.

Shankar, G. M., Bloodgood, B. L., Townsend, M., Walsh, D. M., Selkoe, D. J. and Sabatini, B. L. (2007). "Natural Oligomers of the Alzheimer Amyloid-β Protein Induce Reversible Synapse Loss by Modulating an NMDA-Type Glutamate Receptor-Dependent Signaling Pathway." *The Journal of Neuroscience* **27**(11): 2866-2875.

Shen, C. L. and Murphy, R. M. (1995). "Solvent Effects on Self-Assembly of Beta-Amyloid Peptide." *Biophysical Journal* **69**(2): 640-651.

Sheng, J. G., Price, D. L. and Koliatsos, V. E. (2002). "Disruption of Corticocortical Connections Ameliorates Amyloid Burden in Terminal Fields in a Transgenic Model of Aβ Amyloidosis." *The Journal of Neuroscience* **22**(22): 9794-9799.

Shin, B.-K. and Saxena, S. (2008). "Direct Evidence That All Three Histidine Residues Coordinate to Cu(II) in Amyloid-β1−16." *Biochemistry* **47**(35): 9117-9123.

Sieracki, N., Hwang, H., Lee, M., Garner, D. and Lu, Y. (2008). "A Temperature Independent pH (Tip) Buffer for Biomedical Biophysical Applications at Low Temperatures." *Chemical Communications* (7): 823-825.

Siggs, O. M., Cruite, J. T., Du, X., Rutschmann, S., Masliah, E., Beutler, B. and Oldstone, M. B. (2012). "Disruption of Copper Homeostasis Due to a Mutation of Atp7a Delays the Onset of Prion Disease." *Proceedings of the National Academy of Sciences* **109**(34): 13733-13738.

Sikorski, P., Atkins, E. D. and Serpell, L. C. (2003). "Structure and Texture of Fibrous Crystals Formed by Alzheimer's Aβ (11–25) Peptide Fragment." *Structure* **11**(8): 915-926.

Sisodia, S. S. (1992). "Beta-Amyloid Precursor Protein Cleavage by a Membrane-Bound Protease." *Proceedings of the National Academy of Sciences* **89**(13): 6075-6079.

Sleegers, K., Lambert, J. C., Bertram, L., Cruts, M., Amouyel, P. and Van Broeckhoven, C. (2010). "The Pursuit of Susceptibility Genes for Alzheimer's Disease: Progress and Prospects." *Trends in Genetics* **26**(2): 84-93.

Snyder, E. M., Nong, Y., Almeida, C. G., Paul, S., Moran, T., Choi, E. Y., ... Greengard, P. (2005). "Regulation of NMDA Receptor Trafficking by Amyloid-β." *Nature Neuroscience* **8**(8): 1051-1058.

Sokolov, Y., Kozak, J. A., Kayed, R., Chanturiya, A., Glabe, C. and Hall, J. E. (2006). "Soluble Amyloid Oligomers Increase Bilayer Conductance by Altering Dielectric Structure." *Journal of General Physiology* **128**(6): 637-647.

Solomon, A., Kåreholt, I., Ngandu, T., Winblad, B., Nissinen, A., Tuomilehto, J., ... Kivipelto, M. (2007). "Serum Cholesterol Changes after Midlife and Late-Life Cognition Twenty-One-Year Follow-up Study." *Neurology* **68**(10): 751-756.

Soto, C., Castano, E. M., Frangione, B. and Inestrosa, N. C. (1995). "The Alpha-Helical to Beta-Strand Transition in the Amino-Terminal Fragment of the Amyloid Beta-Peptide Modulates Amyloid Formation." *Journal of Biological Chemistry* **270**(7): 3063-3067.

Sparks, D. L., Scheff, S. W., Hunsaker Iii, J. C., Liu, H., Landers, T. and Gross, D. R. (1994). "Induction of Alzheimer-Like β-Amyloid Immunoreactivity in the Brains of Rabbits with Dietary Cholesterol." *Experimental Neurology* **126**(1): 88-94.

Sparks, D. L. and Schreurs, B. G. (2003). "Trace Amounts of Copper in Water Induce β-Amyloid Plaques and Learning Deficits in a Rabbit Model of Alzheimer's Disease." *Proceedings of the National Academy of Sciences* **100**(19): 11065-11069.

Spector, A. A. (1975). "Fatty Acid Binding to Plasma Albumin." *Journal of Lipid Research* **16**(3): 165-179.

Staniforth, R. A., Giannini, S., Higgins, L. D., Conroy, M. J., Hounslow, A. M., Jerala, R., ... Waltho, J. P. (2001). "Three-Dimensional Domain Swapping in the Folded and Molten-Globule States of Cystatins, an Amyloid-Forming Structural Superfamily." *The EMBO Journal* **20**(17): 4774-4781.

Stanyon, H. F., Cong, X., Chen, Y., Shahidullah, N., Rossetti, G., Dreyer, J., ... Viles, J. H. (2014a). "Developing Predictive Rules for Coordination Geometry from Visible Circular Dichroism of Copper(II) and Nickel(II) Ions in Histidine and Amide Main-Chain Complexes." *FEBS Journal* **281**(17): 3945-3954.

Stanyon, H. F., Patel, K., Begum, N. and Viles, J. H. (2014b). "Copper(II) Sequentially Loads onto the N-Terminal Amino Group of the Cellular Prion Protein before the Individual Octarepeats." *Biochemistry* **53**(24): 3934-3939.

Stanyon, H. F. and Viles, J. H. (2012). "Human Serum Albumin Can Regulate Amyloid-β Peptide Fiber Growth in the Brain Interstitium: Implications for Alzheimer Disease." *Journal of Biological Chemistry* **287**(33): 28163-28168.

Steinhoff, T., Moritz, E., Wollmer, M. A., Mohajeri, M. H., Kins, S. and Nitsch, R. M. (2001). "Increased Cystatin C in Astrocytes of Transgenic Mice Expressing the K670N-M671L Mutation of the Amyloid Precursor Protein and Deposition in Brain Amyloid Plaques." *Neurobiology of Disease* **8**(4): 647-654.

Stephens, P. J. and Harada, N. (2010). "ECD Cotton Effect Approximated by the Gaussian Curve and Other Methods." *Chirality* **22**(2): 229-233.

Stevens, R., Elmendorf, D., Gourlay, M., Stroebel, E. and Gaafar, H. (1979). "Application of Fluoroimmunoassay to Cerebrospinal Fluid Immunoglobulin G and Albumin." *Journal of Clinical Microbiology* **10**(3): 346-350.

Stine, W. B., Jr., Dahlgren, K. N., Krafft, G. A. and Ladu, M. J. (2003). "In Vitro Characterization of Conditions for Amyloid-Beta Peptide Oligomerization and Fibrillogenesis." *Journal of Biological Chemistry* **278**(13): 11612-11622.

Strati, G. L., Willett, J. L. and Momany, F. A. (2002). "A DFT/Ab Initio Study of Hydrogen Bonding and Conformational Preference in Model Cellobiose Analogs Using B3LYP/6-311++G." *Carbohydrate Research* **337**(20): 1851-1859.

Streltsov, V. A., Titmuss, S. J., Epa, V. C., Barnham, K. J., Masters, C. L. and Varghese, J. N. (2008). "The Structure of the Amyloid-β Peptide High-Affinity Copper II Binding Site in Alzheimer Disease." *Biophysical journal* **95**(7): 3447-3456.

Sunde, M., Serpell, L. C., Bartlam, M., Fraser, P. E., Pepys, M. B. and Blake, C. C. (1997). "Common Core Structure of Amyloid Fibrils by Synchrotron X-Ray Diffraction." *Journal of Molecular Biology* **273**(3): 729-739.

Syme, C. D., Nadal, R. C., Rigby, S. E. J. and Viles, J. H. (2004). "Copper Binding to the Amyloid-B (Aβ) Peptide Associated with Alzheimer's Disease: Folding, Coordination Geometry, pH Dependence, Stoichiometry, and Affinity of Aβ-(1–28): Insights from a Range of Complementary Spectroscopic Techniques." *Journal of Biological Chemistry* **279**(18): 18169-18177.

Syme, C. D. and Viles, J. H. (2006). "Solution 1H NMR Investigation of Zn^{2+} and Cd^{2+} Binding to Amyloid-Beta Peptide (Aβ) of Alzheimer's Disease." *Biochimica et Biophysica Acta (BBA) - Proteins & Proteomics* **1764**(2): 246-256.

Tabaton, M. and Tamagno, E. (2007). "The Molecular Link between Beta- and Gamma-Secretase Activity on the Amyloid Beta Precursor Protein." *Cellular & Molecular Life Sciences* **64**(17): 2211-2218.

Tackenberg, C., Grinschgl, S., Trutzel, A., Santuccione, A. C., Frey, M. C., Konietzko, U., ... Nitsch, R. M. (2013). "NMDA Receptor Subunit Composition Determines Beta-Amyloid-Induced Neurodegeneration and Synaptic Loss." *Cell Death & Disease* **4**: e608.

Talmard, C., Guilloreau, L., Coppel, Y., Mazarguil, H. and Faller, P. (2007). "Amyloid-Beta Peptide Forms Monomeric Complexes with CuII and ZnII Prior to Aggregation." *ChemBioChem* **8**(2): 163-165.

Tanzi, R. E., Mcclatchey, A. I., Lamperti, E. D., Villa-Komaroff, L., Gusella, J. F. and Neve, R. L. (1988). "Protease Inhibitor Domain Encoded by an Amyloid Protein Precursor mRNA Associated with Alzheimer's Disease." *Nature* **331**(6156): 528-530.

Teir, M. A., Ghithan, J., Darwish, S. and Abu-Hadid, M. M. (2012). "Multi-Spectroscopic Investigation of the Interactions between Cholesterol and Human Serum Albumin." *Journal of Applied Biological Sciences* **6**(3): 45-55.

Tennent, G. A., Lovat, L. B. and Pepys, M. B. (1995). "Serum Amyloid P Component Prevents Proteolysis of the Amyloid Fibrils of Alzheimer Disease and Systemic Amyloidosis." *Proceedings of the National Academy of Sciences* **92**(10): 4299-4303.

Teplow, D. B. (2006). "Preparation of Amyloid Beta-Protein for Structural and Functional Studies." *Methods in Enzymology* **413**: 20-33.

Texidó, L., Martín-Satué, M., Alberdi, E., Solsona, C. and Matute, C. (2011). "Amyloid β Peptide Oligomers Directly Activate NMDA Receptors." *Cell Calcium* **49**(3): 184-190.

Thinakaran, G., Borchelt, D. R., Lee, M. K., Slunt, H. H., Spitzer, L., Kim, G., ... Sisodia, S. S. (1996). "Endoproteolysis of Presenilin 1 and Accumulation of Processed Derivatives in Vivo." *Neuron* **17**(1): 181-190.

Tian, Y., Bassit, B., Chau, D. and Li, Y.-M. (2010). "An APP Inhibitory Domain Containing the Flemish Mutation Residue Modulates γ-Secretase Activity for Aβ Production." *Nature Structural & Molecular Biology* **17**(2): 151-158.

Török, M., Milton, S., Kayed, R., Wu, P., Mcintire, T., Glabe, C. G. and Langen, R. (2002). "Structural and Dynamic Features of Alzheimer's Aβ Peptide in Amyloid Fibrils Studied by Site-Directed Spin Labeling." *Journal of Biological Chemistry* **277**(43): 40810-40815.

Tõugu, V., Karafin, A. and Palumaa, P. (2008). "Binding of Zinc(II) and Copper(II) to the Full-Length Alzheimer's Amyloid-β Peptide." *Journal of Neurochemistry* **104**(5): 1249-1259.

Tsangaris, J. M. and Martin, R. B. (1970). "Visible Circular Dichroism of Copper (II) Complexes of Amino Acids and Peptides." *Journal of the American Chemical Society* **92**(14): 4255-4260.

Turner, P. R., O'connor, K., Tate, W. P. and Abraham, W. C. (2003). "Roles of Amyloid Precursor Protein and Its Fragments in Regulating Neural Activity, Plasticity and Memory." *Progress in Neurobiology* **70**(1): 1-32.

Tycko, R. (2000). "Solid-State NMR as a Probe of Amyloid Fibril Structure." *Current Opinion in Chemical Biology* **4**(5): 500-506.

Tycko, R. (2006). "Molecular Structure of Amyloid Fibrils: Insights from Solid-State NMR." *Quarterly reviews of biophysics* **39**(01): 1-55.

Uchida, K., Kuroki, K., Yoshino, T., Yamaguchi, R. and Tateyama, S. (1997). "Immunohistochemical Study of Constituents Other Than β-Protein in Canine Senile Plaques and Cerebral Amyloid Angiopathy." *Acta Neuropathologica* **93**(3): 277-284.

Ulmer, T. S., Bax, A., Cole, N. B. and Nussbaum, R. L. (2005). "Structure and Dynamics of Micelle-Bound Human α-Synuclein." *Journal of Biological Chemistry* **280**(10): 9595-9603.

Urbanc, B., Cruz, L., Le, R., Sanders, J., Ashe, K. H., Duff, K., ... Hyman, B. T. (2002). "Neurotoxic Effects of Thioflavin S-Positive Amyloid Deposits in Transgenic Mice and Alzheimer's Disease." *Proceedings of the National Academy of Sciences* **99**(22): 13990-13995.

Uversky, V. N., Li, J. and Fink, A. L. (2001). "Metal-Triggered Structural Transformations, Aggregation, and Fibrillation of Human α-Synuclein: A Possible Molecular Link between Parkinson′s Disease and Heavy Metal Exposure." *Journal of Biological Chemistry* **276**(47): 44284-44296.

Valensin, D., Migliorini, C., Valensin, G., Gaggelli, E., La Penna, G., Kozlowski, H., ... Messori, L. (2011). "Exploring the Reactions of β-Amyloid (Aβ) Peptide 1–28 with AlIII and FeIII Ions." *Inorganic Chemistry* **50**(15): 6865-6867.

Van Dam, D. and De Deyn, P. P. (2006). "Drug Discovery in Dementia: The Role of Rodent Models." *Nature Reviews Drug Discovery* **5**(11): 956-970.

Varley, P. G. (1994). Chapter 15: Fluorescence Spectroscopy. *Microscopy, Optical Spectroscopy, and Macroscopic Techniques*. C. Jones, B. Mulloy and A. H. Thomas. Totowa, NJ, Humana Press Inc. **22:** 203-218.

Vassar, R., Bennett, B. D., Babu-Khan, S., Kahn, S., Mendiaz, E. A., Denis, P., ... Citron, M. (1999). "β-Secretase Cleavage of Alzheimer's Amyloid Precursor Protein by the Transmembrane Aspartic Protease BACE." *Science* **286**(5440): 735-741.

Vatassery, G., Quach, H., Smith, W., Benson, B. and Eckfeldt, J. (1991). "A Sensitive Assay of Transthyretin (Prealbumin) in Human Cerebrospinal Fluid in Nanogram Amounts by ELISA." *Clinica Chimica Acta* **197**(1): 19-25.

Veerhuis, R., Van Breemen, M., Hoozemans, J., Morbin, M., Ouladhadj, J., Tagliavini, F. and Eikelenboom, P. (2003). "Amyloid β Plaque-Associated Proteins C1q and SAP Enhance the Aβ1–42 Peptide-Induced Cytokine Secretion by Adult Human Microglia in Vitro." *Acta Neuropathologica* **105**(2): 135-144.

Vetrivel, K. S. and Thinakaran, G. (2010). "Membrane Rafts in Alzheimer's Disease Beta-Amyloid Production." *Biochimica et Biophysica Acta (BBA) - Molecular and Cell Biology of Lipids* **1801**(8): 860-867.

Viles, J. H. (2012). "Metal Ions and Amyloid Fiber Formation in Neurodegenerative Diseases. Copper, Zinc and Iron in Alzheimer's, Parkinson's and Prion Disease." *Coordination Chemistry Reviews* **256**(19): 2271-2284.

Viles, J. H., Cohen, F. E., Prusiner, S. B., Goodin, D. B., Wright, P. E. and Dyson, H. J. (1999). "Copper Binding to the Prion Protein: Structural Implications of Four Identical Cooperative Binding Sites." *Proceedings of the National Academy of Sciences* **96**(5): 2042-2047.

Viles, J. H., Klewpatinond, M. and Nadal, R. C. (2008). "Copper and the Structural Biology of the Prion Protein." *Biochemical Society Transactions* **36**(Pt 6): 1288-1292.

Vinters, H., Nishimura, G., Secor, D. L. and Pardridge, W. (1990). "Immunoreactive A4 and Gamma-Trace Peptide Colocalization in Amyloidotic Arteriolar Lesions in Brains of Patients with Alzheimer's Disease." *The American Journal of Pathology* **137**(2): 233.

Wadsworth, J., D. F., Hill, A., F., Joiner, S., Jackson, G., S., Clarke, A., R. and Collinge, J. (1999). "Strain-Specific Prion-Protein Conformation Determined by Metal Ions." *Nature Cell Biology* **1**(1): 55-59.

Walsh, D. M., Hartley, D. M., Kusumoto, Y., Fezoui, Y., Condron, M. M., Lomakin, A., ... Teplow, D. B. (1999). "Amyloid β-Protein Fibrillogenesis: Structure and Biological Activity of Protofibrillar Intermediates." *Journal of Biological Chemistry* **274**(36): 25945-25952.

Walsh, D. M., Klyubin, I., Fadeeva, J. V., Cullen, W. K., Anwyl, R., Wolfe, M. S., ... Selkoe, D. J. (2002). "Naturally Secreted Oligomers of Amyloid Beta Protein Potently Inhibit Hippocampal Long-Term Potentiation in Vivo." *Nature* **416**(6880): 535-539.

Walsh, D. M., Lomakin, A., Benedek, G. B., Condron, M. M. and Teplow, D. B. (1997). "Amyloid Beta-Protein Fibrillogenesis. Detection of a Protofibrillar Intermediate." *Journal of Biological Chemistry* **272**(35): 22364-22372.

Walter, E. D., Chattopadhyay, M. and Millhauser, G. L. (2006). "The Affinity of Copper Binding to the Prion Protein Octarepeat Domain: Evidence for Negative Cooperativity." *Biochemistry* **45**(43): 13083-13092.

Wang, C., Liu, L., Zhang, L., Peng, Y. and Zhou, F. (2010). "Redox Reactions of the α-Synuclein−Cu^{2+} Complex and Their Effects on Neuronal Cell Viability." *Biochemistry* **49**(37): 8134-8142.

Wardell, M., Wang, Z., Ho, J. X., Robert, J., Ruker, F., Ruble, J. and Carter, D. C. (2002). "The Atomic Structure of Human Methemalbumin at 1.9 Å." *Biochemical and Biophysical Research Communications* **291**(4): 813-819.

Watt, N. T., Taylor, D. R., Kerrigan, T. L., Griffiths, H. H., Rushworth, J. V., Whitehouse, I. J. and Hooper, N. M. (2012). "Prion Protein Facilitates Uptake of Zinc into Neuronal Cells." *Nature Communications* **3**: 1134.

Wei, L., Chen, Z. and Min, W. (2012). "Stimulated Emission Reduced Fluorescence Microscopy: A Concept for Extending the Fundamental Depth Limit of Two-Photon Fluorescence Imaging." *Biomedical Optics Express* **3**(6): 1465-1475.

Wei, L., Walker, L. C. and Levy, E. (1996). "Cystatin C Icelandic-Like Mutation in an Animal Model of Cerebrovascular β-Amyloidosis." *Stroke* **27**(11): 2080-2085.

Weil, J. A. and Bolton, J. R. (2007). *Electron Paramagnetic Resonance: Elementary Theory and Practical Applications*, John Wiley & Sons.

Wells, M. A., Jelinska, C., Hosszu, L. L. P., Craven, C. J., Clarke, A. R., Collinge, J., ... Jackson, G. S. (2006). "Multiple Forms of Copper (II) Co-Ordination Occur Throughout the Disordered N-Terminal Region of the Prion Protein at pH 7.4." *Biochemical Journal* **400**(3): 501-510.

Westermark, P., Wernstedt, C., Wilander, E., Hayden, D. W., O'brien, T. D. and Johnson, K. H. (1987). "Amyloid Fibrils in Human Insulinoma and Islets of Langerhans of the Diabetic Cat Are Derived from a Neuropeptide-Like Protein Also Present in Normal Islet Cells." *Proceedings of the National Academy of Sciences* **84**(11): 3881-3885.

Westmark, C. J. (2013). "What's HAPPening at Synapses? The Role of Amyloid β-Protein Precursor and β-Amyloid in Neurological Disorders." *Molecular Psychiatry* **18**(4): 425-434.

Whitmer, R., Sidney, S., Selby, J., Johnston, S. C. and Yaffe, K. (2005). "Midlife Cardiovascular Risk Factors and Risk of Dementia in Late Life." *Neurology* **64**(2): 277-281.

Wollmer, M. A. (2010). "Cholesterol-Related Genes in Alzheimer's Disease." *Biochimica et Biophysica Acta (BBA) - Molecular and Cell Biology of Lipids* **1801**(8): 762-773.

Wood, S. J., Maleeff, B., Hart, T. and Wetzel, R. (1996). "Physical, Morphological and Functional Differences between pH 5.8 and 7.4 Aggregates of the Alzheimer's Amyloid Peptide Abeta." *Journal of Molecular Biology* **256**(5): 870-877.

Wood, S. P., Oliva, G., O'hara, B. P., White, H. E., Blundell, T. L., Perkins, S. J., ... Pepys, M. B. (1988). "A Pentameric Form of Human Serum Amyloid P Component: Crystallization, X-Ray Diffraction and Neutron Scattering Studies." *Journal of Molecular Biology* **202**(1): 169-173.

Wright, J. A., Wang, X. and Brown, D. R. (2009). "Unique Copper-Induced Oligomers Mediate Alpha-Synuclein Toxicity." *The FASEB Journal* **23**(8): 2384-2393.

Wu, J., Anwyl, R. and Rowan, M. J. (1995). "β-Amyloid Selectively Augments NMDA Receptor-Mediated Synaptic Transmission in Rat Hippocampus." *NeuroReport* **6**(17): 2409-2413.

Wyatt, A. R., Yerbury, J. J., Berghofer, P., Greguric, I., Katsifis, A., Dobson, C. M. and Wilson, M. R. (2011). "Clusterin Facilitates in Vivo Clearance of Extracellular Misfolded Proteins." *Cellular & Molecular Life Sciences* **68**(23): 3919-3931.

Wyatt, A. R., Yerbury, J. J., Poon, S. and Wilson, M. R. (2009). "Therapeutic Targets in Extracellular Protein Deposition Diseases." *Current Medicinal Chemistry* **16**(22): 2855-2866.

Xiao, Z. and Wedd, A. G. (2010). "The Challenges of Determining Metal-Protein Affinities." *Natural Product Reports* **27**(5): 768-789.

Yamamoto, K., Shimada, H., Koh, H., Ataka, S. and Miki, T. (2013). "Serum Levels of Albumin-Amyloid Beta Complexes Are Decreased in Alzheimer's Disease." *Geriatrics & Gerontology International*.

Yamin, G., Glaser, C. B., Uversky, V. N. and Fink, A. L. (2003). "Certain Metals Trigger Fibrillation of Methionine-Oxidized Alpha-Synuclein." *Journal of Biological Chemistry* **278**(30): 27630-27635.

Yan, L.-M., Velkova, A. and Kapurniotu, A. (2014). "Molecular Characterization of the Hetero-Assembly of β-Amyloid Peptide with Islet Amyloid Polypeptide." *Current Pharmaceutical Design* **20**(8): 1182-1191.

Yan, L.-M., Velkova, A., Tatarek-Nossol, M., Andreetto, E. and Kapurniotu, A. (2007). "IAPP Mimic Blocks Aβ Cytotoxic Self-Assembly: Cross-Suppression of Amyloid Toxicity of Aβ and IAPP Suggests a Molecular Link between Alzheimer's Disease and Type II Diabetes." *Angewandte Chemie International Edition* **46**(8): 1246-1252.

Yang, D. T., Joshi, G., Cho, P. Y., Johnson, J. A. and Murphy, R. M. (2013). "Transthyretin as Both a Sensor and a Scavenger of β-Amyloid Oligomers." *Biochemistry* **52**(17): 2849-2861.

Yang, F., Bian, C., Zhu, L., Zhao, G., Huang, Z. and Huang, M. (2007). "Effect of Human Serum Albumin on Drug Metabolism: Structural Evidence of Esterase Activity of Human Serum Albumin." *Journal of Structural Biology* **157**(2): 348-355.

Yankner, B. A., Lu, T. and Loerch, P. (2008). "The Aging Brain." *Annual Review of Pathology* **3**: 41-66.

Yerbury, J. J., Poon, S., Meehan, S., Thompson, B., Kumita, J. R., Dobson, C. M. and Wilson, M. R. (2007). "The Extracellular Chaperone Clusterin Influences Amyloid Formation and Toxicity by Interacting with Prefibrillar Structures." *The FASEB Journal* **21**(10): 2312.

You, H., Tsutsui, S., Hameed, S., Kannanayakal, T. J., Chen, L., Xia, P., ... Zamponi, G. W. (2012). "Aβ Neurotoxicity Depends on Interactions between Copper Ions, Prion

Protein, and N-Methyl-D-Aspartate Receptors." *Proceedings of the National Academy of Sciences* **109**(5): 1737-1742.

Younan, N. D., Klewpatinond, M., Davies, P., Ruban, A. V., Brown, D. R. and Viles, J. H. (2011). "Copper(II)-Induced Secondary Structure Changes and Reduced Folding Stability of the Prion Protein." *Journal of Molecular Biology* **410**(3): 369-382.

Younan, N. D., Sarell, C. J., Davies, P., Brown, D. R. and Viles, J. H. (2013). "The Cellular Prion Protein Traps Alzheimer's Aβ in an Oligomeric Form and Disassembles Amyloid Fibers." *The FASEB Journal* **27**(5): 1847-1858.

Zagorski, M. G. and Barrow, C. J. (1992). "NMR Studies of Amyloid Beta-Peptides: Proton Assignments, Secondary Structure, and Mechanism of an Alpha-Helix----Beta-Sheet Conversion for a Homologous, 28-Residue, N-Terminal Fragment." *Biochemistry* **31**(24): 5621-5631.

Zagorski, M. G., Yang, J., Shao, H., Ma, K., Zeng, H. and Hong, A. (1999). "Methodological and Chemical Factors Affecting Amyloid Beta Peptide Amyloidogenicity." *Methods in Enzymology* **309**: 189-204.

Zatta, P., Zambenedetti, P., Stella, M. P. and Licastro, F. (2002). "Astrocytosis, Microgliosis, Metallothionein-I-II and Amyloid Expression in High Cholesterol-Fed Rabbits." *Journal of Alzheimer's Disease* **4**(1): 1-9.

Zhang, S., Iwata, K., Lachenmann, M. J., Peng, J. W., Li, S., Stimson, E. R., ... Lee, J. P. (2000). "The Alzheimer's Peptide A Beta Adopts a Collapsed Coil Structure in Water." *Journal of Structural Biology* **130**(2-3): 130-141.

Zhu, H., Wang, X., Wallack, M., Li, H., Carreras, I., Dedeoglu, A., ... Qiu, W. Q. (2014). "Intraperitoneal Injection of the Pancreatic Peptide Amylin Potently Reduces Behavioral Impairment and Brain Amyloid Pathology in Murine Models of Alzheimer's Disease." *Molecular Psychiatry*.